



LAWRENCE
LIVERMORE
NATIONAL
LABORATORY

JOWOG 32Mat: Conference Proceedings Part 1

daniel orlikowski, John Heidrich

May 11, 2010

JOWOG 32 Mat
Livermore, CA, United States
January 25, 2010 through January 29, 2010

Disclaimer

This document was prepared as an account of work sponsored by an agency of the United States government. Neither the United States government nor Lawrence Livermore National Security, LLC, nor any of their employees makes any warranty, expressed or implied, or assumes any legal liability or responsibility for the accuracy, completeness, or usefulness of any information, apparatus, product, or process disclosed, or represents that its use would not infringe privately owned rights. Reference herein to any specific commercial product, process, or service by trade name, trademark, manufacturer, or otherwise does not necessarily constitute or imply its endorsement, recommendation, or favoring by the United States government or Lawrence Livermore National Security, LLC. The views and opinions of authors expressed herein do not necessarily state or reflect those of the United States government or Lawrence Livermore National Security, LLC, and shall not be used for advertising or product endorsement purposes.

JOWOG 32MAT



**January 25-29, 2010
Conference Proceedings Part 1 of 2
Monday-Wednesday**

**Bld. 132 Auditorium
Livermore, CA**

LLNL • LANL • SNL • AWE

This work performed under the auspices of the U.S. Department of Energy by Lawrence
Livermore National Laboratory under Contract DE-AC52-07NA27344.

JOWOG 32MAT Conference Agenda January 25-29, 2010

MONDAY, January 25

07:45 Formalities Visitor Badges, etc.
Office West Badge

08:15 M. Dunning Welcome, Bldg 132
J. Heidrich Auditorium

Session 1: EOS I

Session Chairman: *Chris Robinson*

09:30 *Geoff Cox* UK.01
EOS for Titanium

10:00 BREAK

Session 2: EOS II & Model Assessment I

Session Chairman: *Lorin Benedict*

10:30 *Steven McGuire* UK.02
EOS for Vanadium

11:00 *Michael Prime* LA.02
Comparison of Beryllium EOS & Constitutive Models with Recent Shock D

12:00 LUNCH

16:30 CLOSE

TUESDAY, January 26

08:20 Formalities

Session 4: EOS IV

Session Chairman: *Carl Greeff*

09:30 *Eric Chisolm* LA.04
Recent Advances In Vibration-Transit
Theory of Liquids

10:00 BREAK

Session 5: EOS V & Dynamic Experiments I

Session Chairman: *Eric Chisolm*

11:00 *Jim Belak* LL.06
Phase-Field Modeling of Coring
in Pu Alloys

11:30 *Jeremy Millett* UK.05
On the Behavior of Body Centered Cubic Metals
During One-Dimensional Shock Loading

12:00 LUNCH

Session 6: Dynamic Experiments II

Session Chairman: *Jean-Paul Davis*

13:30 *Jon Eggert* LL.07
Laser-Induced Ramp Compression of Tantalum
and Iron to Over 300 Gpa: EOS & X-Ray
Diffraction

14:00 *Matthew Cotton* UK.06
EOS & Spall Data for Ta-2.5% W

14:30 *Jeremy Millett* UK.07
Response of Aluminum Alloys to Shock Loading

15:00 BREAK

15:30 Discussion Session

EOS Test Problem: Comparison of
Lab's EOSs (30 min.)

(Discussion Leader: *Chris Robinson*)

EOS Theory: Phases, Future Directions (60 min.)

(Discussion Leader: *Lorin Benedict*)

17:00 CLOSE

WEDNESDAY, January 27

08:20 Formalities

Session 7: Dynamic Experiments III

Session Chairman: *Frank Cherne*

09:00 *Jean-Paul Davis* SN.01
Update on Multi-Megabar Ramp Compression at Z

10:00 BREAK

Session 8: Strength & Damage I

Session Chairman: *Brian Jensen*

11:00 *Scott Alexander* SN.02
New Strength Data on Aluminum to 160 GPa

11:30 LUNCH

15:00 Discussion Sessions

MaRIE: (Discussion Leaders:

Curt Bronkhorst & Franz Freibert)

2007 Strength & Damage Test Problems

(Discussion Leader: *James Turner*)

16:30 CLOSE

18:30 Conference Banquet - Zyphyr Grill & Bar*

19:00 Dinner Served

*Directions:

• Exit South-East Gate/Go straight on East Avenue/Turn right onto
South Livermore/Turn left onto First Street/Zephyr Grill
& Bar located on right hand side next to Vine Cinema

JOWOG 32MAT Conference Agenda January 25-29, 2010

THURSDAY, January 28

08:50 Formalities

Session 10: STRENGTH & DAMAGE III

Session Chairman: *Davis Tonks*

09:00 *Gareth Owen* UK.09

Assessment of the Self Consistent Technique
on the Determination of the Shear Strength
of Shocked Metal Targets

09:30 *Bryan Reed* LL.11
Extracting Plastic Flow Properties from
Shock Velocity

10:00 BREAK

Session 11: STRENGTH & DAMAGE IV

Session Chairman: *Bryan Reed*

12:00 LUNCH

Session 12: STRENGTH & MULTISCALE MODELING I

Session Chairman: *Curt Bronkhorst*

13:30 *Thomas Canfield* LA.09
Damage Modeling with Void Evolution

14:00 *Roger Minich* LL.13
Spall & Melt Kinetics

14:30 *Ellen Cerreta* LA.10
Influence of Microstructure on Materials
Modeling

15:00 BREAK

Session 13: STRENGTH & MULTISCALE MODELING II

Session Chairman: *Bill Blumenthal*

15:30 *Curt Bronkhorst* LA.11
Modeling the Grain Scale Microstructural
Evolution of Metallic Polycrystals

16:00 *Tom Arsenlis* LL.14
Multiscale Models for the Dynamic Strength
of Ta and V

16:30 CLOSE

FRIDAY, January 29

08:20 Formalities

Session 14: MULTISCALE MODELING & FRICTION I

Session Chairman: *Jeremy Millett*

08:30 *Franz Freibert* LA.12
Pu Microstructures & Thermal Physical Properties

09:00 *Stewart Stirk* UK.10
Investigations of Dynamic Dry Friction at Obliquely
Shocked Metal Interfaces

10:00 BREAK

10:30 Discussion Session

Multiscale Models & Anisotropic Models
(Discussion Leader: *Nigel Park*)

11:30 LUNCH

12:30 Summary of Discussion Sessions
DAC

Bruce Baer (10 min.)

EOS Test Problem

Chris Robinson (10 min.)

EOS Theory Phases & Future Direction

Lorin Benedict (10 min.)

MaRIE

Curt Bronkhorst & Franz Freibert (10 min.)

Strength & Damage Test Problems

James Turner (10 min.)

Multiscale Models & Anisotropic Model

Nigel Park (10 min.)

13:30 Final Remarks

13:45 Executive Meeting

*Chris Robinson, James Hammerberg,
Tracy Vogler, John Heidrich, Daniel Orlikowski*



JOWOG 32MAT

January 25-29, 2010
(Conference Agenda)
Bld. 132 Auditorium

Conference Banquet
Wednesday, 6:30 PM
Zephyr Grill & Bar
1736 First Street
Livermore, CA
(925) 961-1000

LLNL • LANL • SNL • AWE

JOWOG 32MAT



January 25, 2010
Monday



An EoS for Titanium

Geoffrey Cox

+44 1189826197

Outline

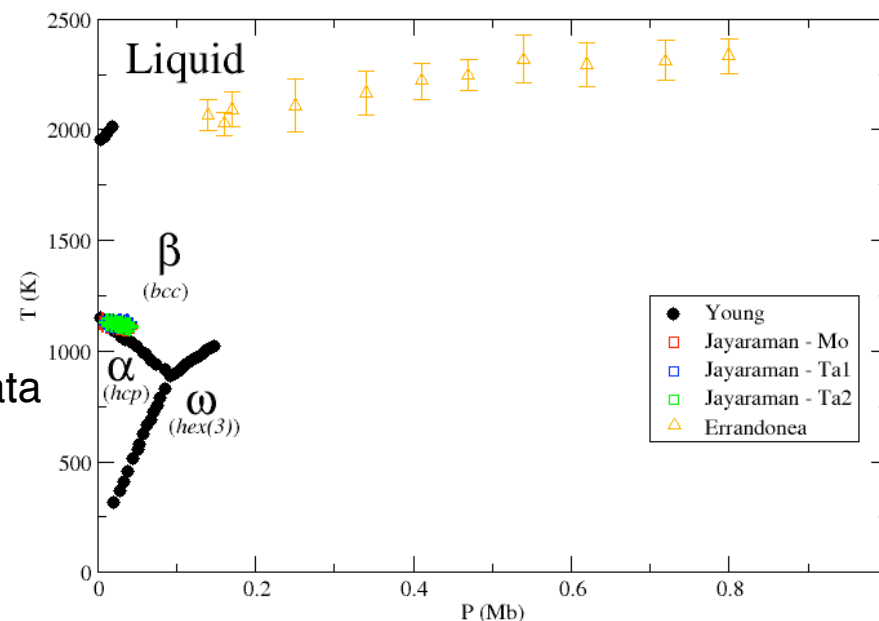
- Introduction
- Data Review
- EoS Review
- New EoS
 - Multiphase
 - Development issues
 - Final version
- Comparisons with data and other EoSs
- Future plans for Ti-6Al-4V

Introduction

- Ti-6Al-4V used in some simulations
 - Want to improve our material model
 - Want a physics based equation of state for Ti-6Al-4V
 - Need a test suite
 - Need a review of EoS data
 - Need a pure Ti PBE as starting point
 - Empirical based adjustment to get alloy EoS
 - Need a data review and test suite
 - More data available than alloy

Summary of Ti Data Available

- Phase boundary data
 - 3 solid phases
 - Low pressures
 - Lots of uncertainty
 - Melt data
 - Slope of phase boundary at RP
 - Possible dynamic melt on release data
- Hugoniot up to 140 Mb, though bulk below 3 Mb
 - $\alpha \rightarrow \omega$ causes unstable shock
 - $\omega \rightarrow \beta$ no evidence of wave splitting
- RT Isothermal compression data up to 2.2 Mb
 - $\alpha \rightarrow \omega \rightarrow \delta(?)$
- RP isobaric data from 0 K to 6000 K
 - $\alpha \rightarrow \beta \rightarrow \text{Liquid}$





Pure Ti EoS Review

- Two available in EoS package
 - “Balmoral” EoS
 - Steinberg Compendium
 - Analytic EoS fit to Hugoniot
 - Single phase
 - Steinberg has a melt curve
- No pure Ti EoS for Maw Ti-6Al-4V EoS
 - Maw based parameters on Ti-6Al-4V data only
 - Issues with scaling
 - Derived strength model also

Pure Ti EoS Review

- Greeff et al., JAP, 90(5) pp2221 (2001)
 - Generated via FREE code
 - α , ω phases for Ti
 - So far only generated over small range
- Kerley, Sandia Report
 - Parameters for α , ω , β , and liquid phases for Ti
 - However, model differs slightly from what's in SOLICE
 - TFD match allows extrapolation to large densities
 - Different electron model
 - Also the β parameters change at high pressure
 - To match high pressure RT measurements

Pure Ti EoS Review

- Of the EoSs currently available
 - No physics based EoS in EoS package
 - No multiphase EoS in EoS package
 - Kerley only multiphase EoS with liquid parameters
- Requirements
 - Temperatures 0-32 eV
 - EoS up to densities of 29 g/cc
 - Physics based



Initial stage

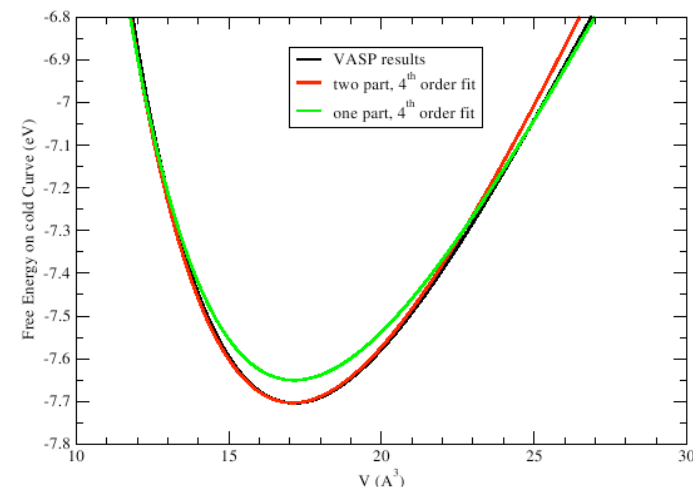
- Problems
 - FREE EoS has negative C_V issues at low temperatures
 - So minimum temperature larger than zero
 - High temp approximation used for lattice vibrations
 - Cold curves from Kerley have negative K_T around 13 g/cc
 - Remember no TFD match in SOLICE
 - Cannot use β and liquid phases
 - Bercegeay cold curve parameters give negative K_T around 13 g/cc
 - Cannot use α , ω phases up to large densities
 - Need to try something new to extend EoS to large enough density

VASP *ab-initio* cold curve calculation for β

- GGA PAW pseudopotentials
- PW91 functional of Perdew and Wang
- Fermi-Dirac smearing used ($T=300\text{K}$)
- Converged
 - 2 meV at maximum density ($6.5\rho_0$)
 - 0.5meV at minimum density ($0.5\rho_0$)
- Fit B-M equation
 - $E = E_0 + 9V_0K_0\left(\frac{f^2}{2} + a_1\frac{f^3}{3} + a_2\frac{f^4}{4} + \dots\right)$
 - Two part fit
 - Around V_0 better
 - Worse for $V>21.5\text{\AA}^3$

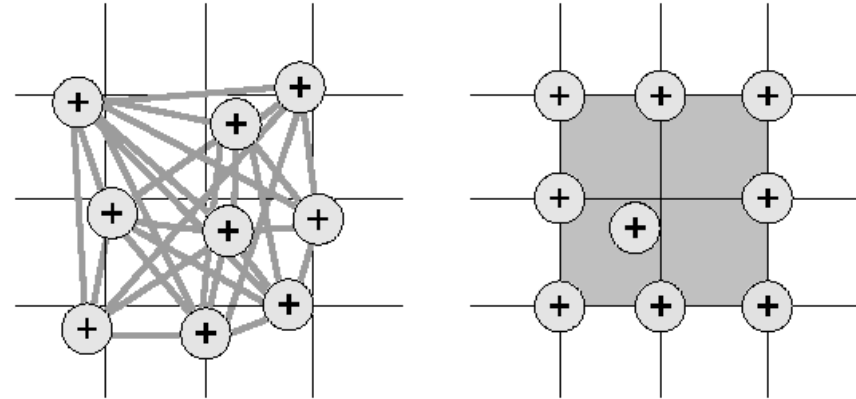
Lattice	Grid	E_{aug} (eV)	E_{val} (eV)	[core] valence states
<i>bcc</i>	Monkhorst-Pack 32x32x32	1650	550	[Ne]3s ² 3p ⁶ 3d ² 4s ²

B-M	One part fit	Two part fit
V_0 (\AA^3)	17.14	17.09
E_0 (eV)	-7.6502	-7.7030
K_0 (GPa)	94.94	105.7
a_1	-0.9543	-1.1797
a_2	0.9514	1.0891



Thermal contribution for β phase

- Mean field model for ions
 - Cold curve used to calculate mean field
 - Pairwise interactions assumed with smearing approximation
 - Central “wanderer” decoupled from fixed nearest neighbours
 - All particles in solid behave in same way
 - Obtain Einstein expression for solid ions
- Thomas-Fermi model used for electrons
- Parameter free



Liquid phase

- Fluid perturbation theory used
 - $F_{IL} = F_{IG} + F_{HS} + \Delta F_{SS} + \Delta U$
 - F_{IG} relation known
 - F_{HS} use Kerley expression for hard sphere
 - ΔF_{ss} use Ross expression
 - ΔU
 - Kerley expression for hard sphere radial distribution
 - Pair interaction term obtained from cold curve
 - Continuous change to Mie Potential at $V=V_0$
- Thomas-Fermi model used for electrons
- Parameter free
- Correction to G_L to obtain correct RP melt

New EoS

PHASE	COLD CURVE	THERMAL IONS	THERMAL ELECTRONS
β	DFT	Mean Field	Thomas-Fermi
Liquid	-	Fluid Perturbation	Thomas-Fermi

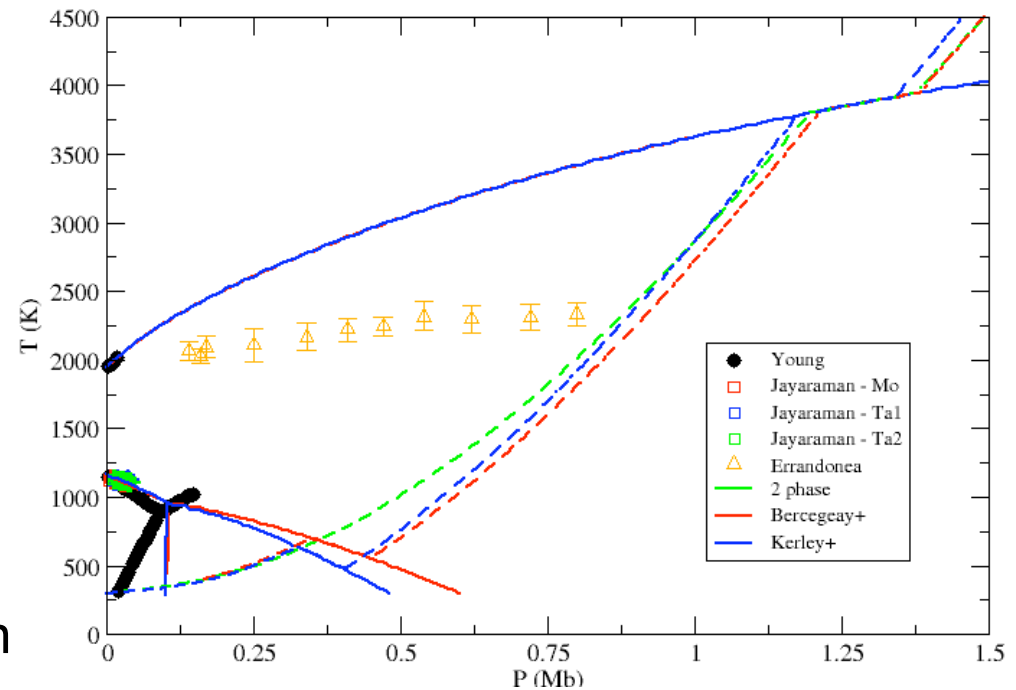
- α, ω phases
 - Are they needed?
 - Final goal is an EoS for Ti-6Al-4V
 - 2 phase
 - Could an existing model be used for these phases?
 - Kerley+
 - Cold curve inferred
 - Debye model for lattice vibrations
 - Bercegeay+
 - Models same as β
 - Could try empirical method?
 - Little data for ω phase

What about strength?

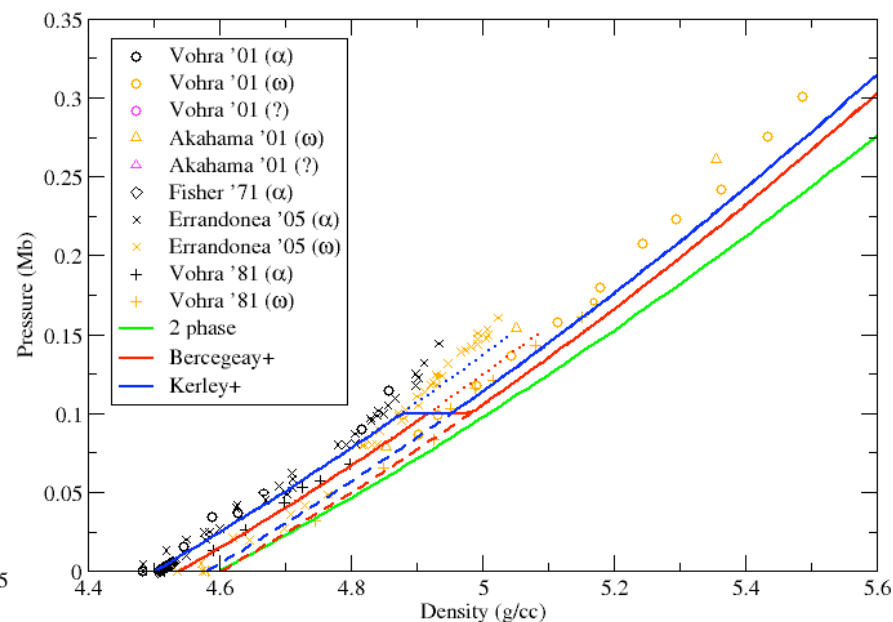
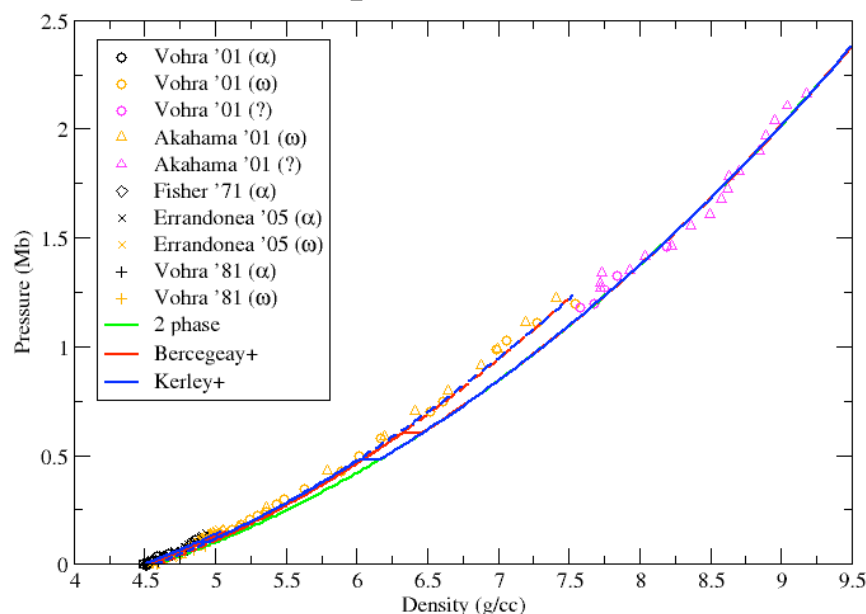
- In the following calculations strength is not included
- Current modelling limitations
 - Melt temperature only output in solid-liquid cases
 - G and Y currently not separated
 - Phase dependent G
 - MSG or CPR
- Hugoniot calculation using a simple constant G and Y model
 - Performed part way through development
 - Made Hugoniot a little stiffer which improved fit slightly
 - A more thorough investigation is required

Phase Diagram

- Same melt for all, as expected
- Kerley+ boundary conditions are α - β and α - ω
 - RP $\alpha \rightarrow \beta$ from data
 - Triple point mentioned in Kerley report
 - RT $\alpha \rightarrow \omega$ at 0.1 Mb
- Bercegeay+ just used same boundary conditions
- Really want $\omega \rightarrow \beta$ RT transition at around 1.2 Mb

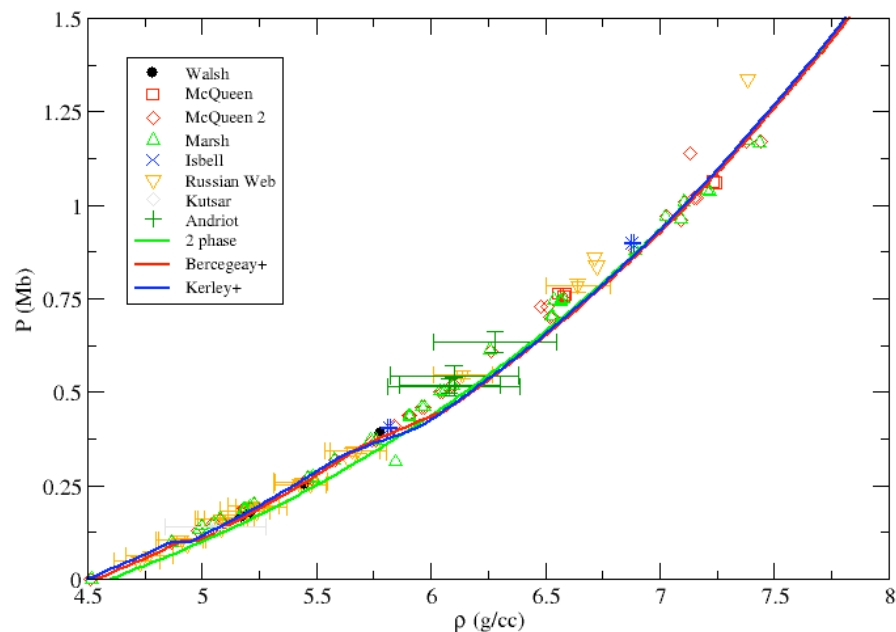
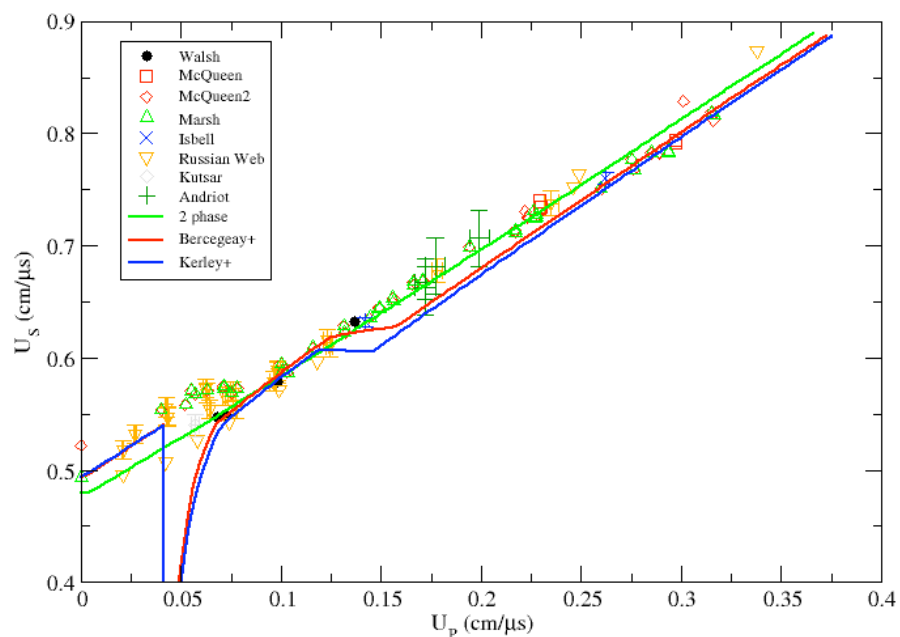


RT compression



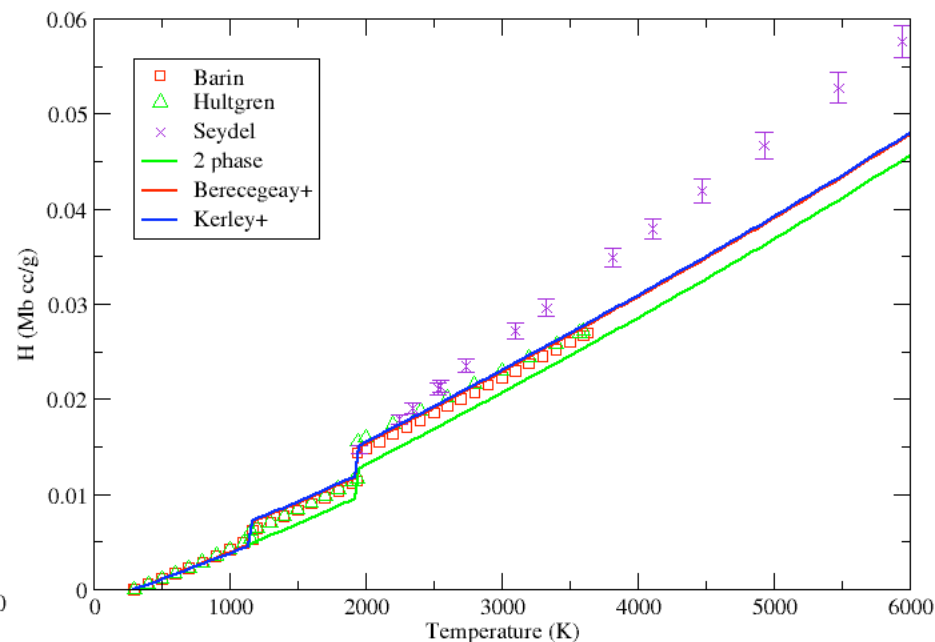
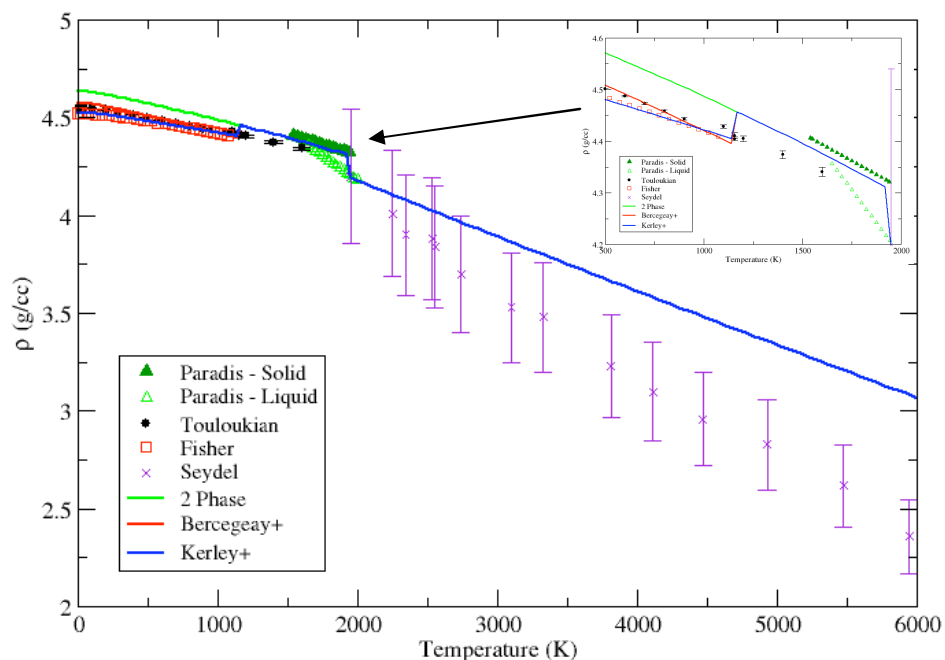
- Good agreement at high pressures
- Poor for 2 phase at low pressures
- $\omega \rightarrow \beta$ too low
- For α , ω phases Kerley shows best agreement

Low Pressure Hugoniot



- **Us-Up**
 - $\alpha \rightarrow \omega$ transition improves it
 - $\omega \rightarrow \beta$ makes it worse
 - Kerley+ becomes unstable
 - Could fixing RT $\alpha \rightarrow \omega$ transition pressure help?

RP Isobar



- Contradictory density data
- Kerley+/Bercegeay+
 - Density improved at low temperatures
 - $\alpha \rightarrow \beta$ sees larger increase in enthalpy that is not seen in the data
 - $\beta \rightarrow \text{Liquid}$ enthalpy change matches data

The story so far

- New β , liquid phases
 - Physics based
 - Only ones capable of reaching densities needed
 - Poor match to data in α , ω region
 - Thus more than 2 phases are needed
 - Questions about β phase density at RP
- α , ω phases
 - Kerley looks the best against the data
 - Pressure for $\omega \rightarrow \beta$ transition at RT is too low
 - $\omega \rightarrow \beta$ transition has made Hugoniot agreement worse

New Boundary Condition

- Moved α - ω to lower pressure at RT
 - Large uncertainty
 - Small increase in range of ω phase
 - Made Hugoniot poor
 - Note that no kinetics model in use
- Specify ω - β boundary instead of α - ω
 - ω phase as stable RTP phase
- Raised temperature of triple point
 - RT $\omega \rightarrow \beta$ now at reasonable pressure
 - Hugoniot improved
 - RP latent heat of $\alpha \rightarrow \beta$ too large

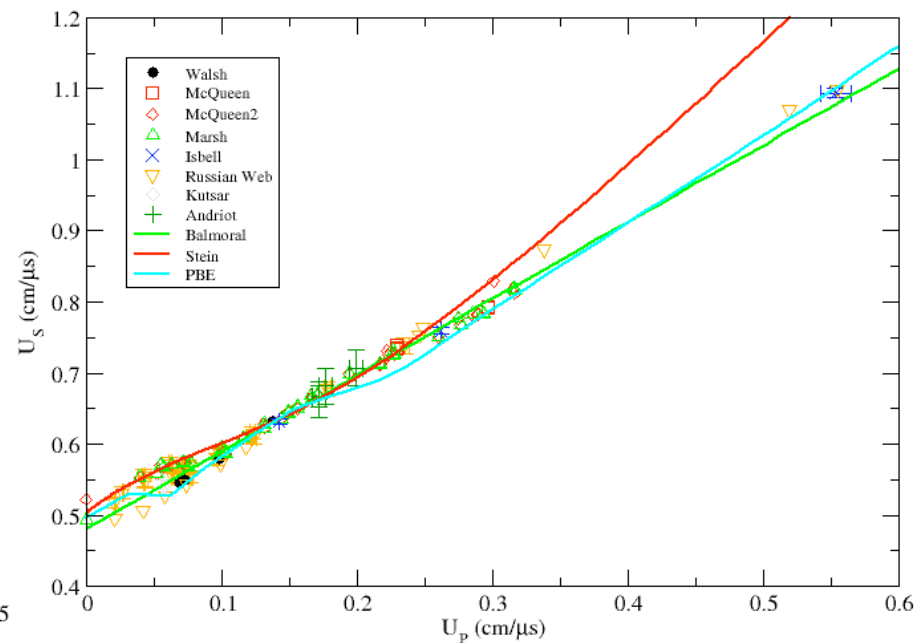
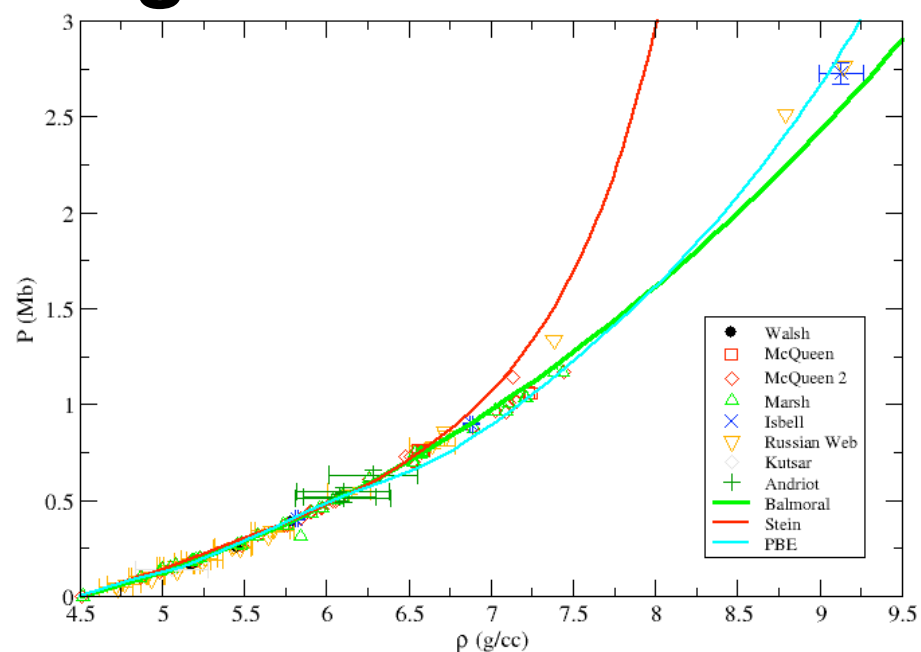
Investigation into RP $\alpha \rightarrow \beta$ transition

- ΔS , ΔV , and $\frac{dT}{dP}$ data inconsistent
 - Various connotations tried
 - Triple point temperature too low if ΔS in agreement with data
- Tried empirical model for α , ω phases
 - Could adjust parameters to influence $\frac{d^2T}{dP^2}$
 - $$\frac{d^2T}{dP^2} = (\beta_2 V_2 - \beta_1 V_1) \frac{2T}{\Delta H} \frac{dT}{dP} + \left(\frac{V_1}{K_{T1}} - \frac{V_2}{K_{T2}} \right) \frac{T}{\Delta H} + (C_{P1} - C_{P2}) \frac{1}{\Delta H} \left(\frac{dT}{dP} \right)^2$$
 - If $\frac{dT}{dP} \rightarrow 0$ then sensitive to bulk modulus
 - If $\frac{dT}{dP} \rightarrow \infty$ then sensitive to heat capacities
 - Large adjustments needed
 - Fit to data became poor
 - Too much freedom with ω phase

Final Decision

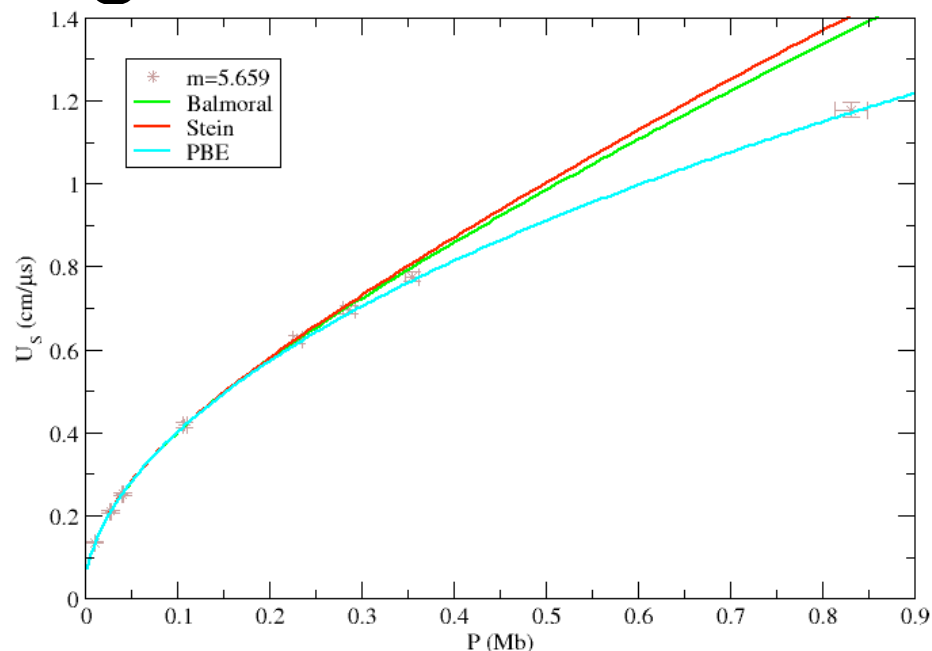
- Use Kerley parameters for α , ω phases
- Keep $\alpha \rightarrow \omega$ RT transition at 0.1 Mb
- Accept incorrect ΔS at RP $\alpha \rightarrow \beta$ transition
- Raised TP temperature to get correct $\omega \rightarrow \beta$ at RT
- So how does it compare to our existing EoS?

Hugoniot



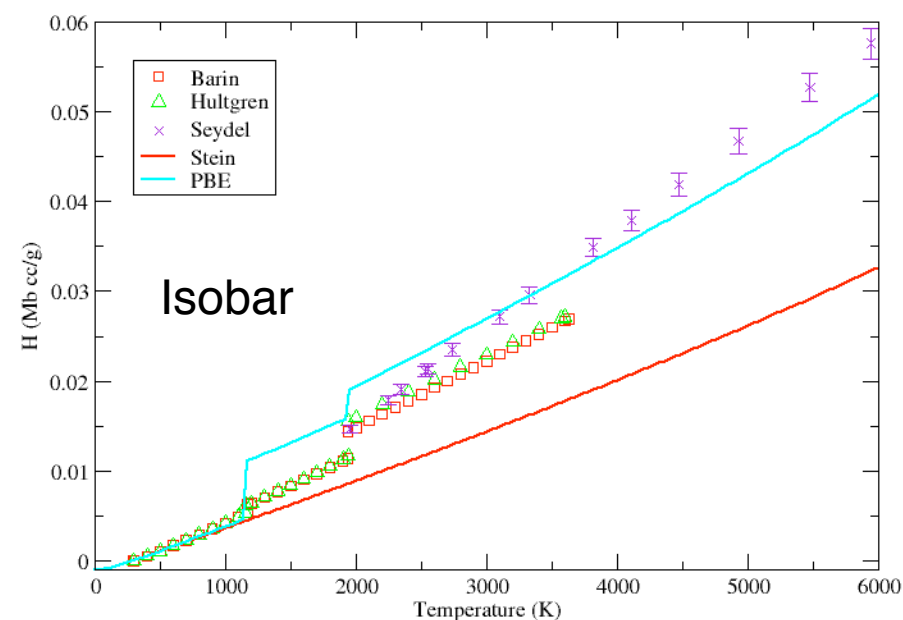
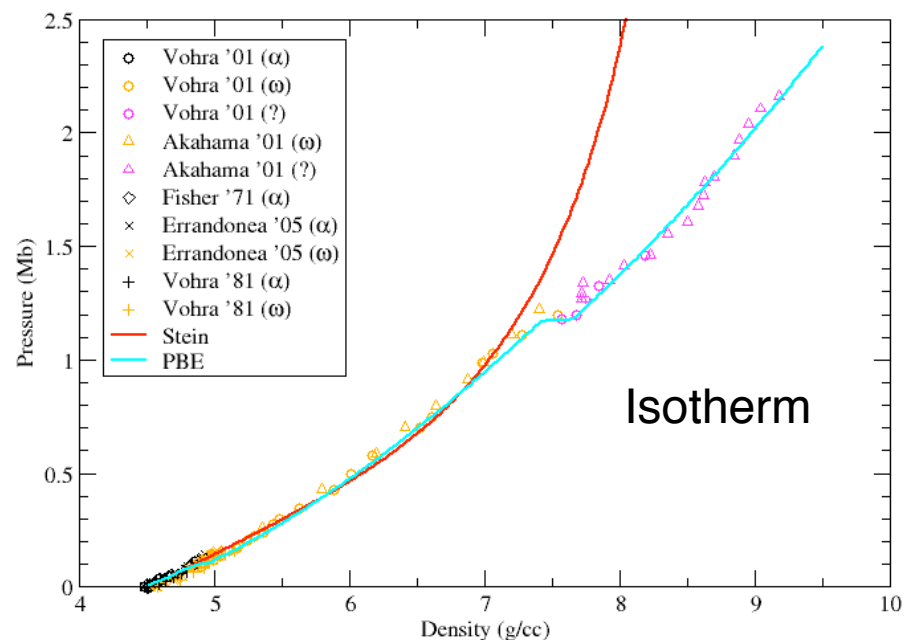
- Stein poor for $P > 1.5$ Mb
- Balmoral is good
- PBE is good
 - $\alpha \rightarrow \omega$ unstable
 - $\omega \rightarrow \beta$ stable

Porous Hugoniot



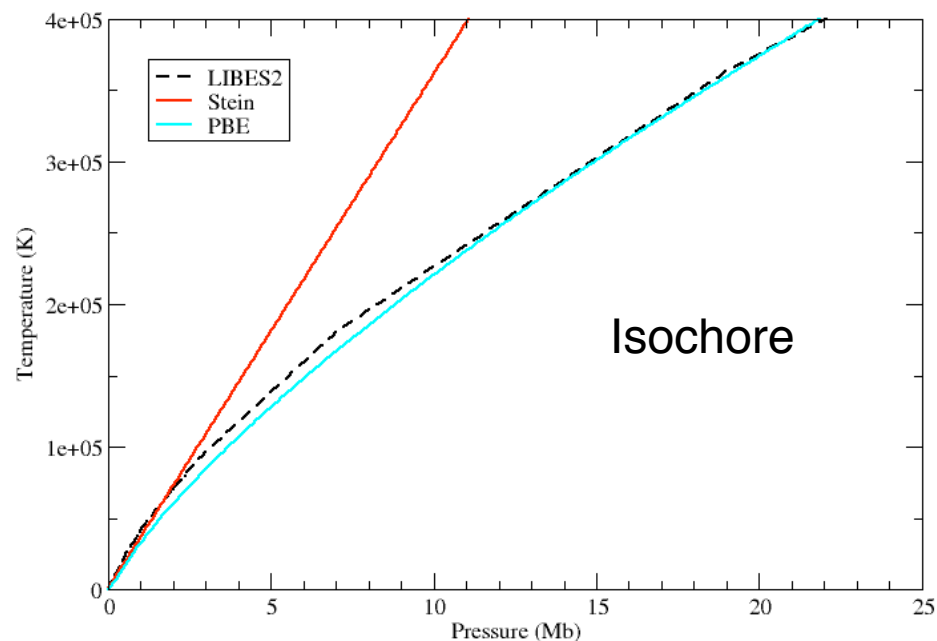
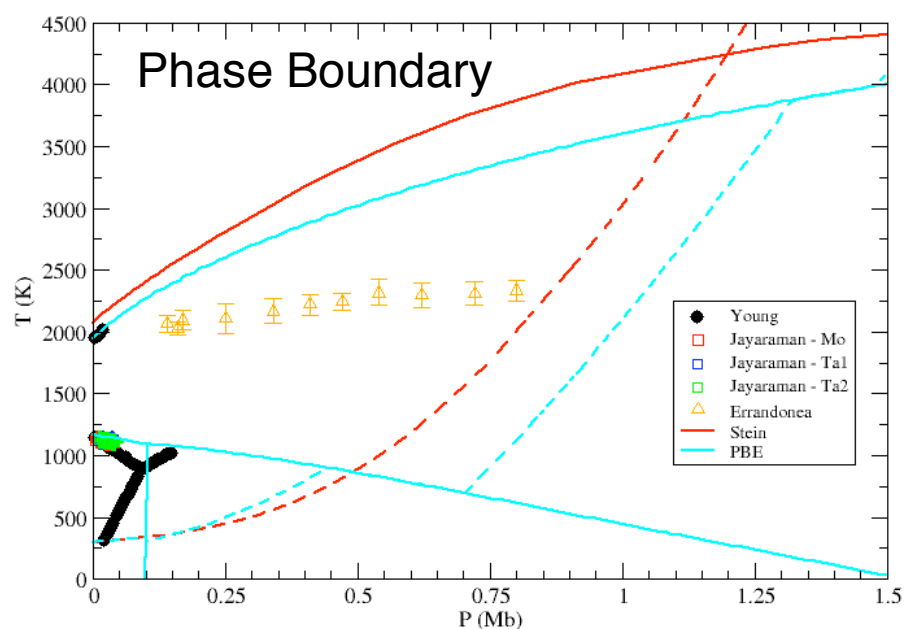
- Snowplough porosity model used
- No wave splitting seen in data from porous samples
- In calculation temperature increase causes $\alpha \rightarrow \beta$ instead of $\alpha \rightarrow \omega$
 - No wave splitting seen
- PBE model agrees with data in most extreme case

Other Comparisons



- Balmoral has no temperature
- Stein has poor isotherm
- PBE mostly good but large ΔH for $\alpha \rightarrow \beta$ at RP

Other Comparisons



- Small difference in shock melt between 2 EoS
- Good agreement between PBE and LIBES2

Future Plans for Ti-6Al-4V

- Use Ti PBE as starting point
 - Empirical adjustment
 - e.g. Pb4Sb, Ta-W
 - Density scale VASP cold curve
 - Need to consider Ti-6Al-4V phase boundary
 - Data quite limited
 - RP melting temperature
 - RT $\alpha \rightarrow \omega$ transition
 - Keep Ti α , ω phases?
 - Similar density scaling
 - Adjust boundary conditions
 - Or use Kerley parameters for α Ti-6Al-4V phase?
 - Possible criticism of scaling assumptions
 - Difference here is that the starting point is a multiphase EoS
- Use available Ti-6Al-4V data for validation

Conclusions

- Review of experimental data completed
- New Physics based EoS for Ti
 - α , ω , β , and liquid phases
 - Good agreement with data overall
 - Improvement over existing EoS
- Basis of plans for Ti-6Al-4V



Progress Towards an EoS for Vanadium

Stephen McGuire

+44 1189826786

Outline

- Introduction
- Data Review
- EoS Review
- New EoS
- Comparison with data and other EoS
- Conclusions

Introduction

- Vanadium is a good fire resistant material
- Improve the current material model
- “Balmoral” EoS
 - Analytic EoS fit to Hugoniot
 - No temperature
 - No melt curve
- Use physics based EoS
 - Better predictive capabilities
 - Temperature and melt curve calculated

Data Review

- Hugoniot up to 4 Mb
 - 5 data sets
- RT Isothermal compression data up to 0.8 Mb
 - 2 data set
- RP isobaric data up to 4000 K
 - 4 data sets
- Phase boundary data
 - Solid - liquid phase transition
 - Melt data
 - Slope of phase boundary near RP
 - 2 data sets with conflicting results

EoS Review

- 1 available in EoS package
 - “Balmoral” EoS
 - Analytic EoS fit to Hugoniot
 - Single phase
- 1 from Steinberg compendium
 - Single phase
 - Melt curve available
- 2 from Sesame library 2550,2551
 - Single phase
 - No melt curve

Physics Based EoS

- Combination of a classical pair potential and simplified quantum mechanical approaches used to create a PBE.
- The vanadium EoS was modelled using two phases; a solid phase and a liquid phase
- The solid Helmholtz free energy, F , was calculated as a sum of three components, a cold curve internal energy, E_c , a lattice component, F_{ion} , and an electron component, F_{elec}

$$F(\rho, T) = E_c(\rho) + F_{ion}(\rho, T) + F_{elec}(\rho, T)$$

- The liquid phase was modelled using a hybrid of the CRIS and Ross liquid models

Solid Phase

- The cold curve model used in this work was a third order Birch-Murnaghan model

$$E_c = 9 \frac{K_c}{\rho_c} \sum_{n=0}^n \frac{a_n}{(n+2)} f^{n+2} + E_0$$

- The lattice vibrations were described using the standard Debye model

$$F_{ion}(\rho, T) = \frac{9}{8} Nk\theta_D + 9NkT \left(\frac{T}{\theta_D} \right)^3 \int_0^{\theta_D} x^2 \ln(1 - e^{-x}) dx$$

- The electron contribution to the solid phase was described using the free electron (FE) model

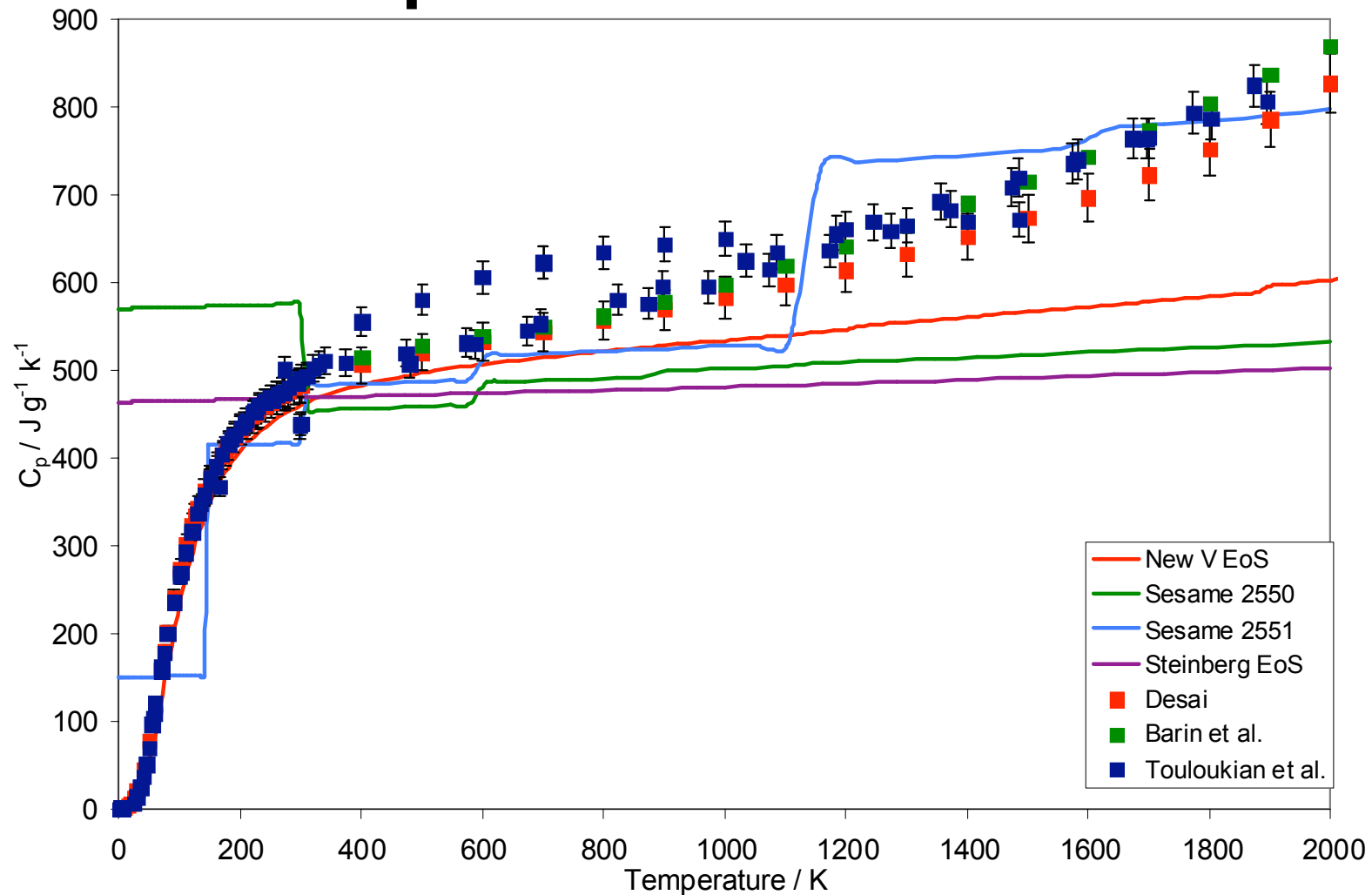
$$F_{elec}(\rho, T) = -\frac{1}{4} N \frac{(\pi kT)^2}{\varepsilon_f}$$



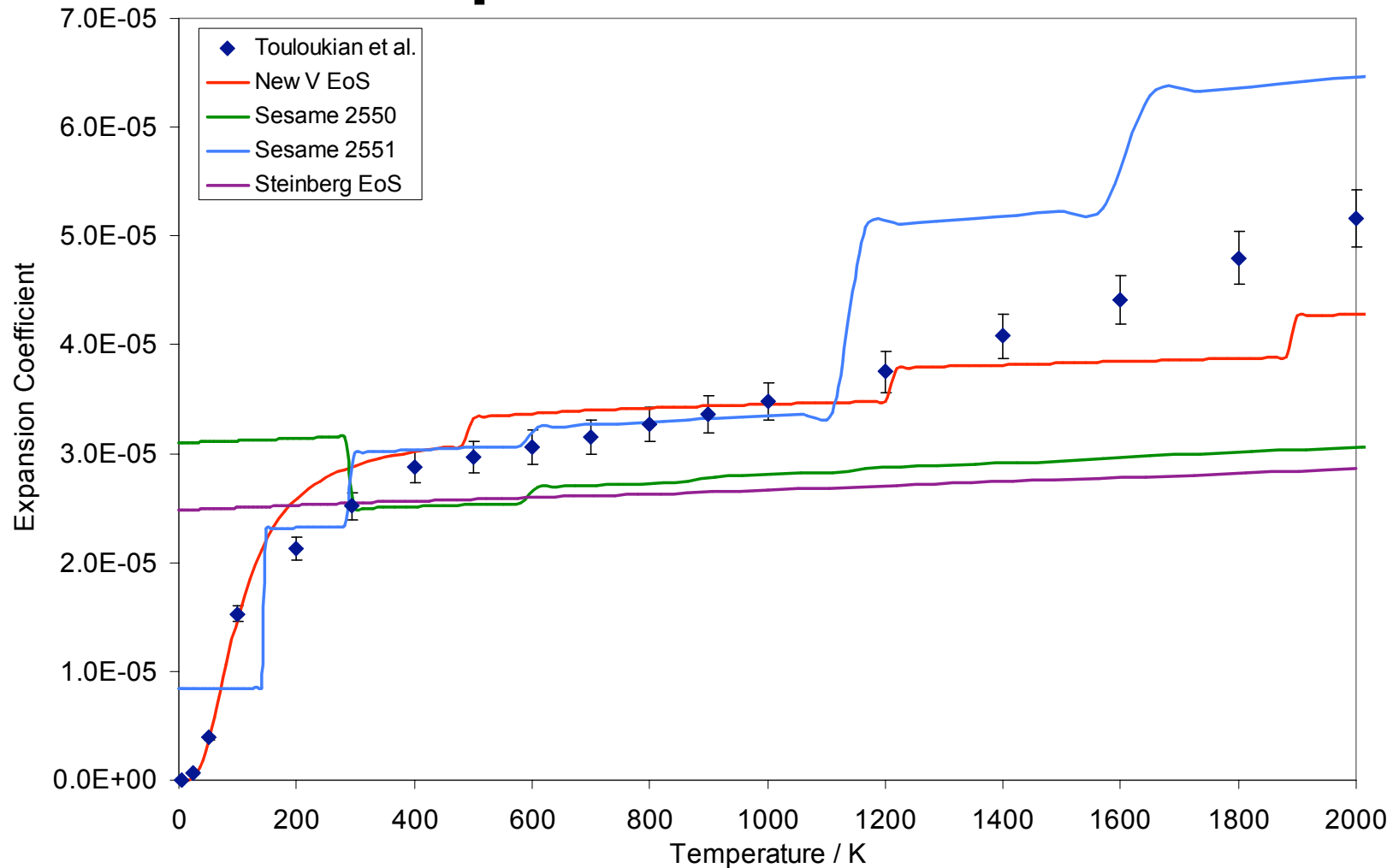
Liquid Phase

- Fluid perturbation theory was used to model the liquid phase
- The liquid model used in this work is a hybrid of the CRIS and Ross liquid models.
- In the CRIS and Ross models the atoms are treated as rigid spheres but corrections are applied to soften the hard sphere interaction.
- Additional correction terms, to the pressure, ΔP , the entropy, ΔS , and the energy, ΔE , in the liquid model, are used to match the calculated melt curve to a point on the experimental melt curve

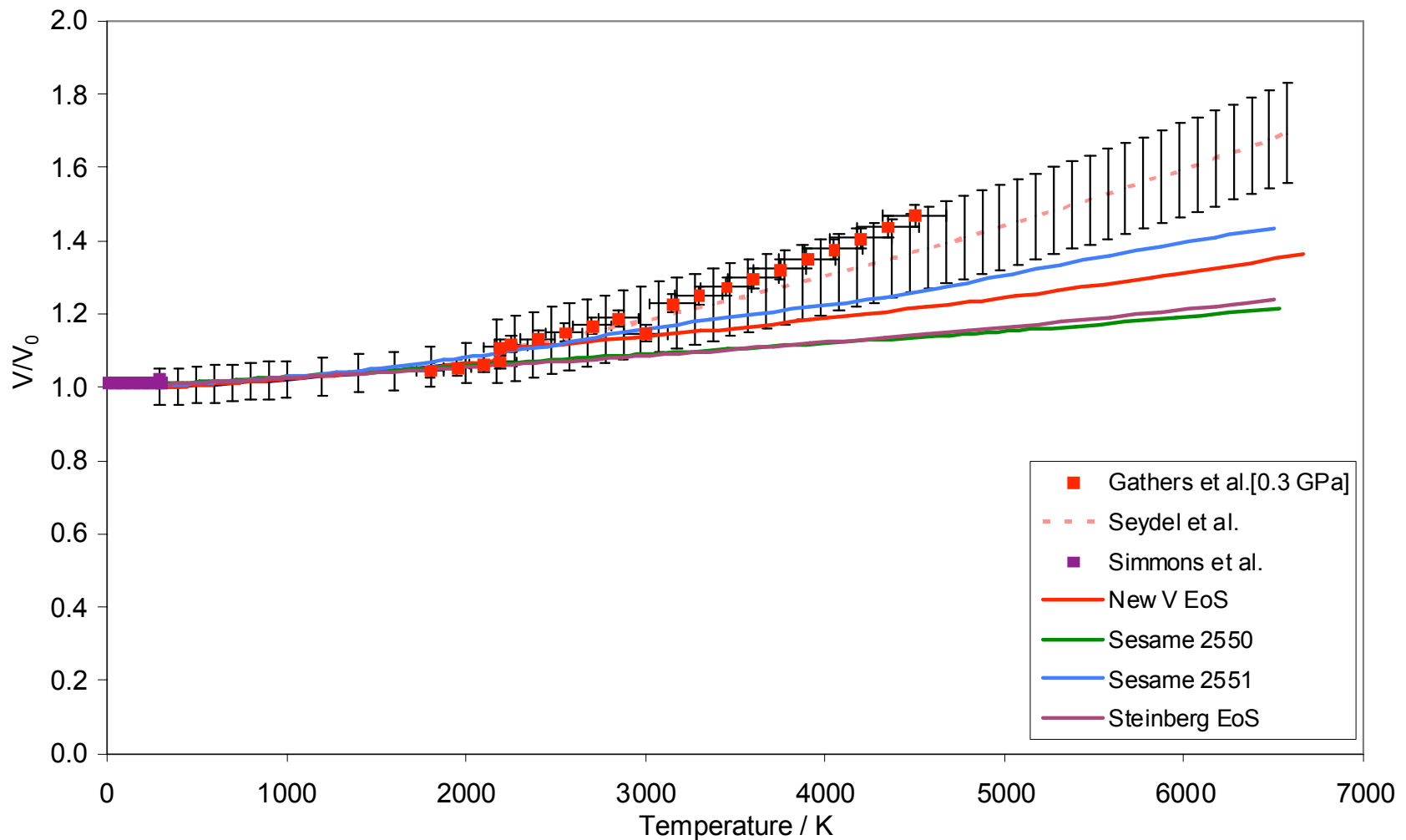
RP Isobar – Specific Heat



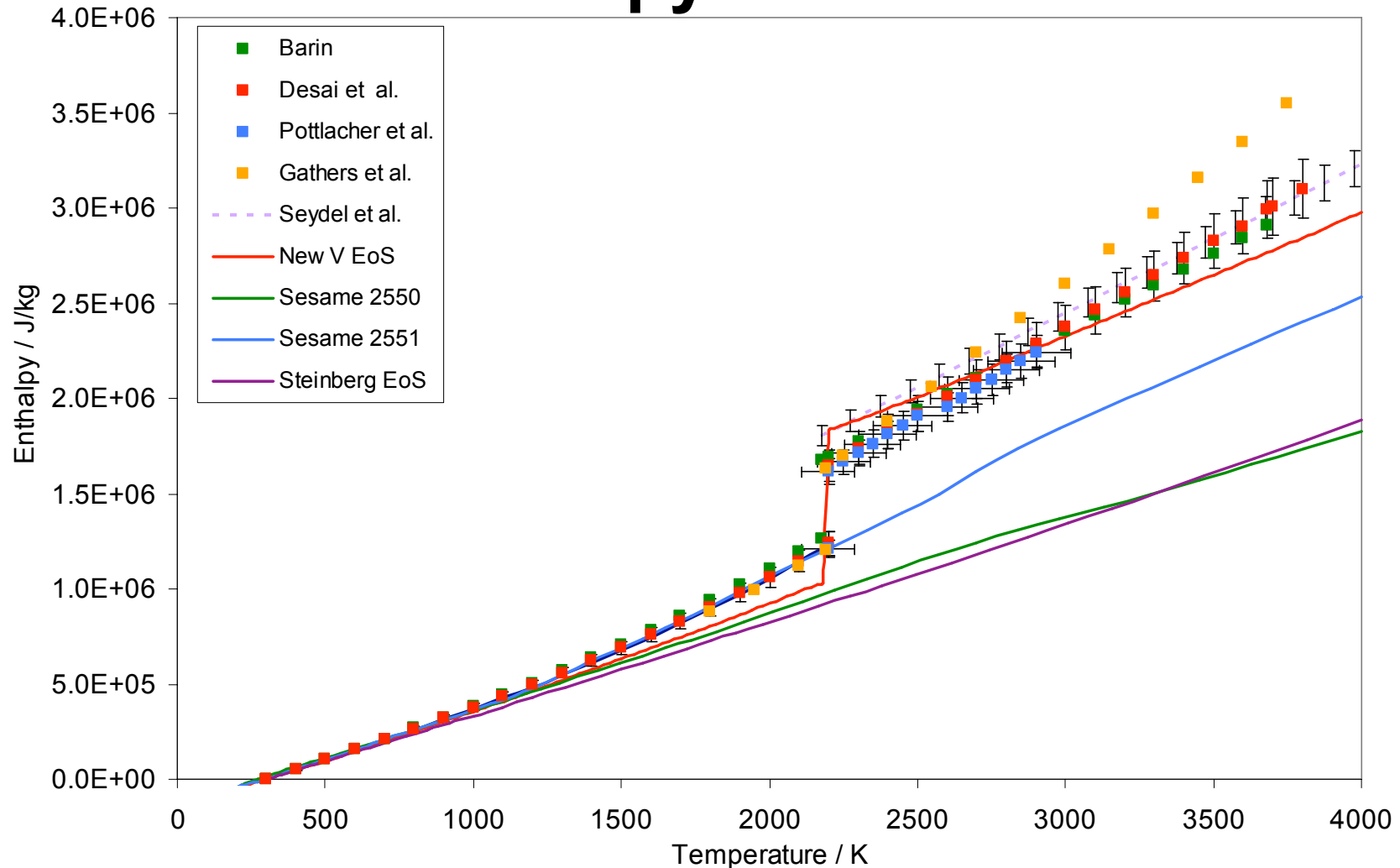
RP Isobar – Expansion Coefficient



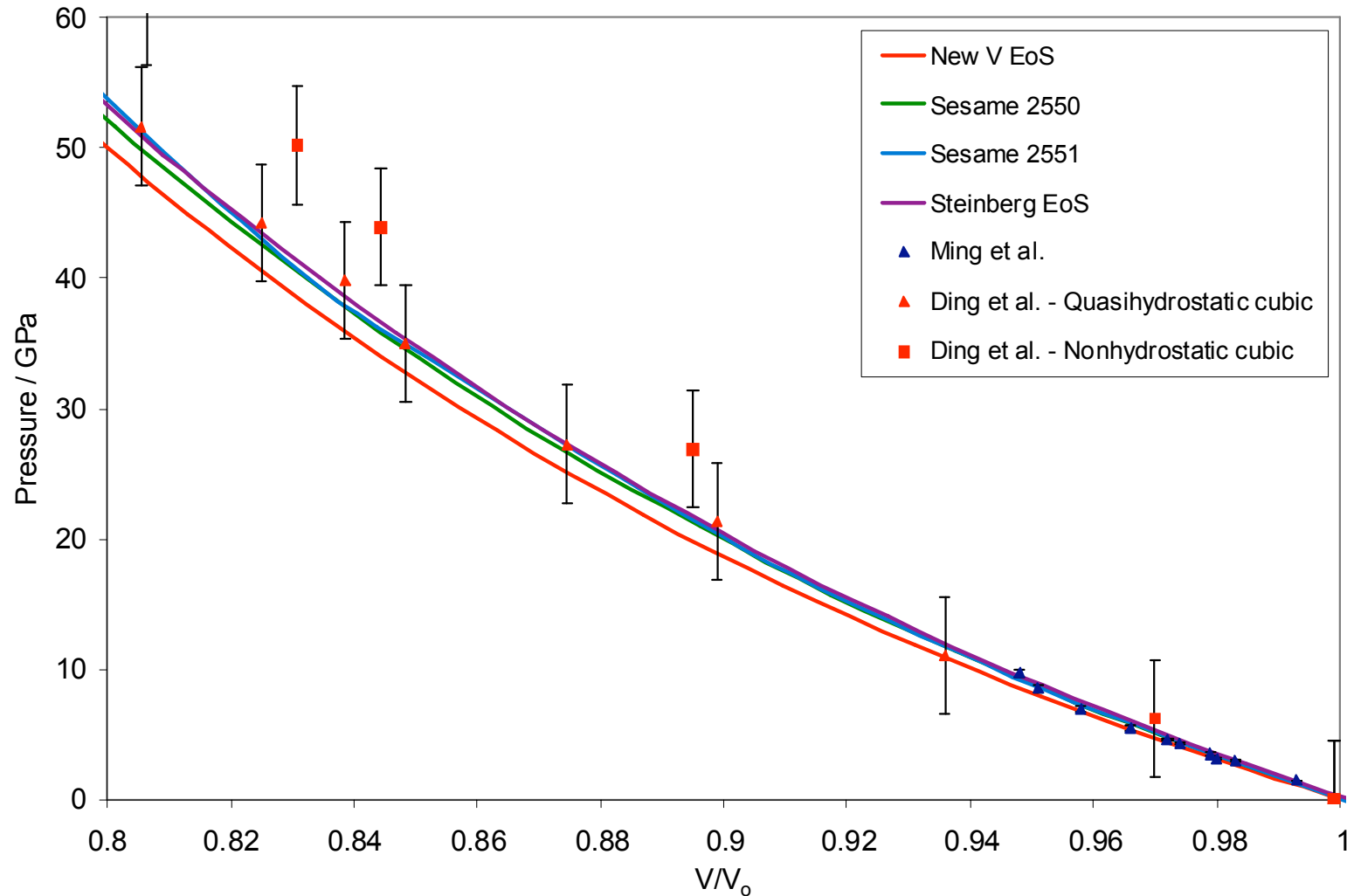
RP Isobar – Specific Volume



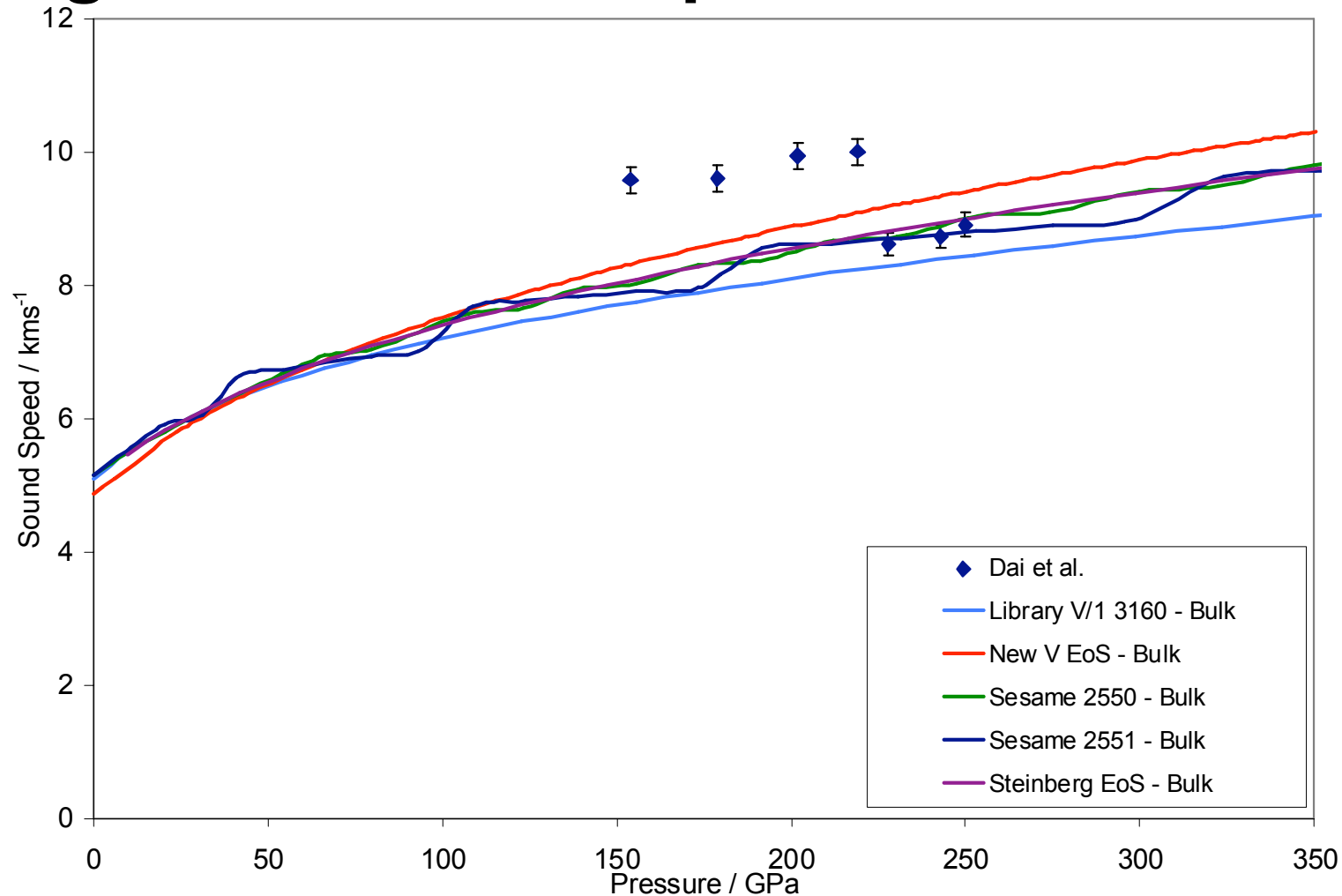
RP Isobar – Enthalpy



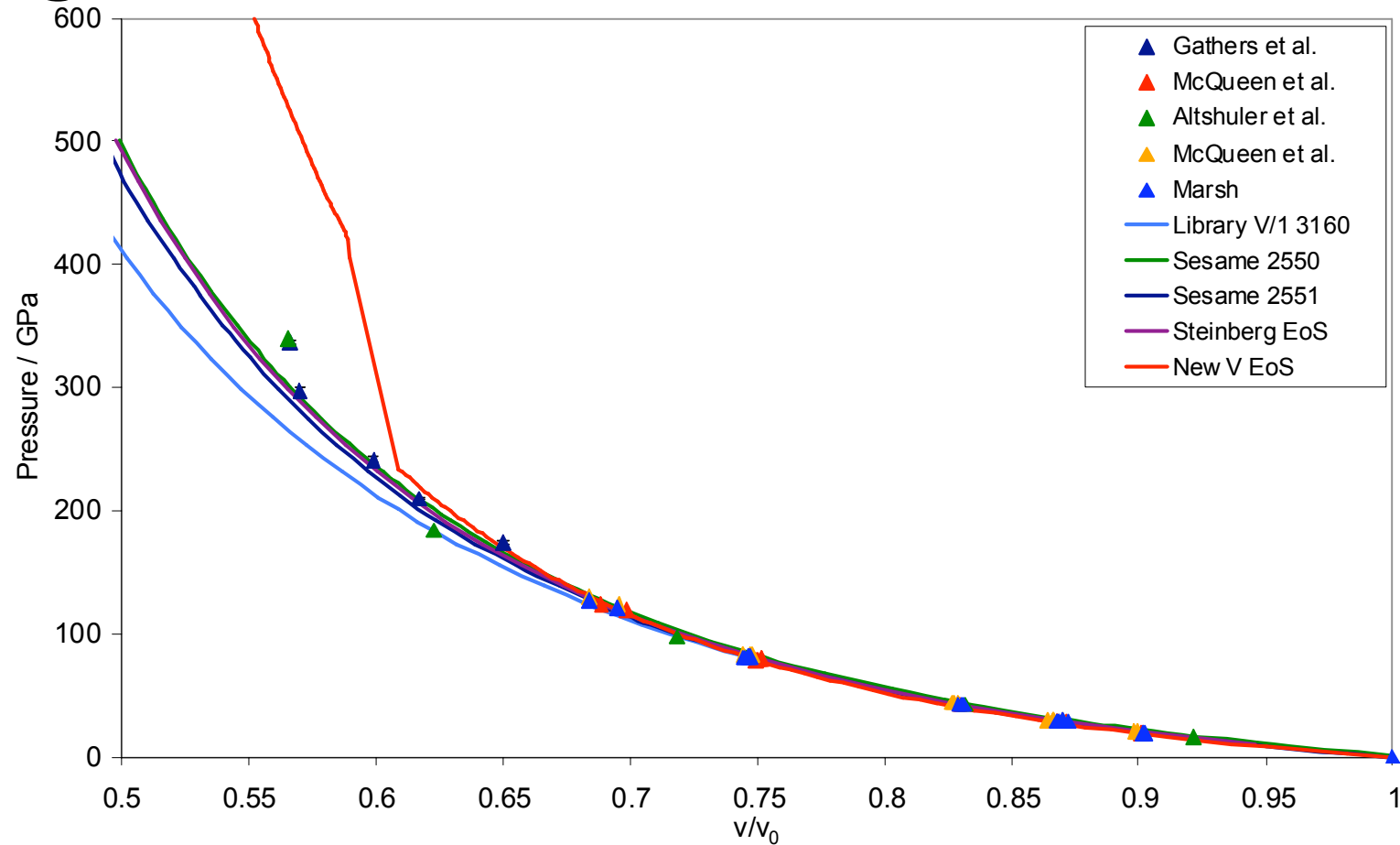
RT Isotherm



Hugoniot – Sound Speed



Hugoniot



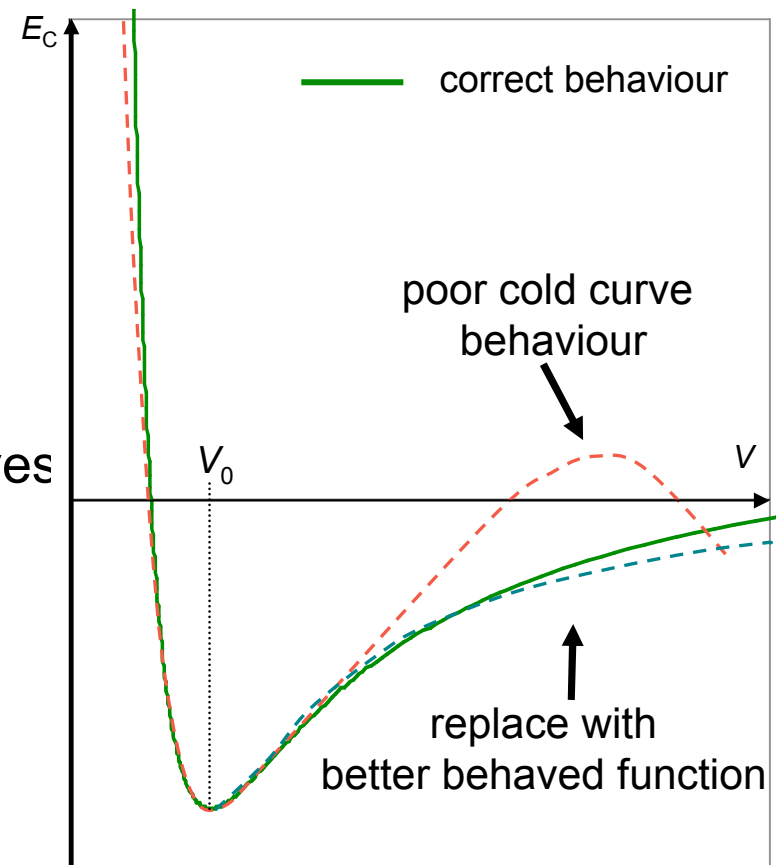
- problem due to the inadequacy of the cold curve representation

Cold Curve – Compression & Tension

- The Birch-Murnaghan cold curve is designed for use in compression
 - Iterative method used to determine cold curve parameters, V_0 , K_0, K'_0, E_0
- Poor behaviour at low density behaviour ($E \rightarrow 0$, as $\rho \rightarrow 0$)
 - for solids this is not a problem – past tensile limit
 - for liquids this is a problem – interactions must vanish for $\rho \rightarrow 0$
- Cold curves which have good behaviour at low density, e.g. Lennard-Jones, are poor in compression

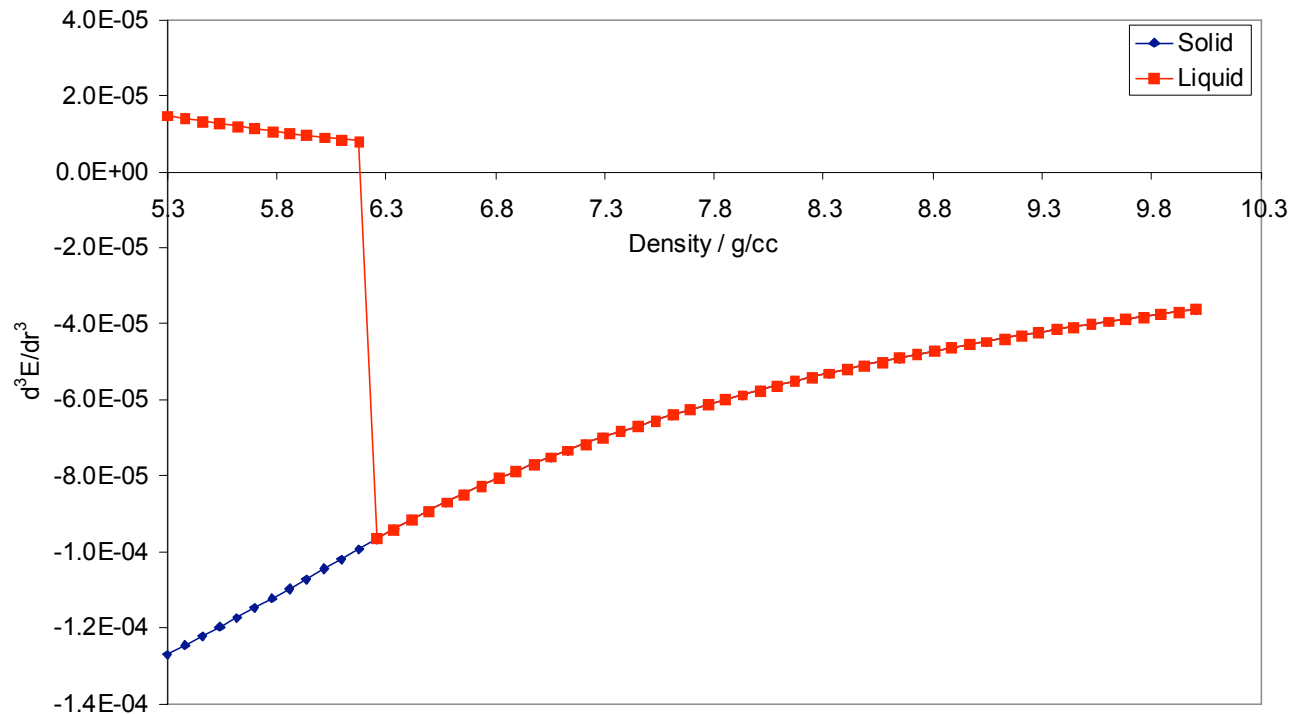
“Fixing” the cold curve

- To enable the liquid model to work the cold curve is modified in the tension region
 - replaced by Lennard-Jones type function for $V > V_0$
 - so that thermodynamic properties are continuous at V_0 the derivatives of the compression and tension curves must be made continuous to third order
 - no flexibility in shape of tension cold curve
- For several materials this approach has been adequate Pb, Pb-Sb, Ta, Be



Cold Curve Derivatives

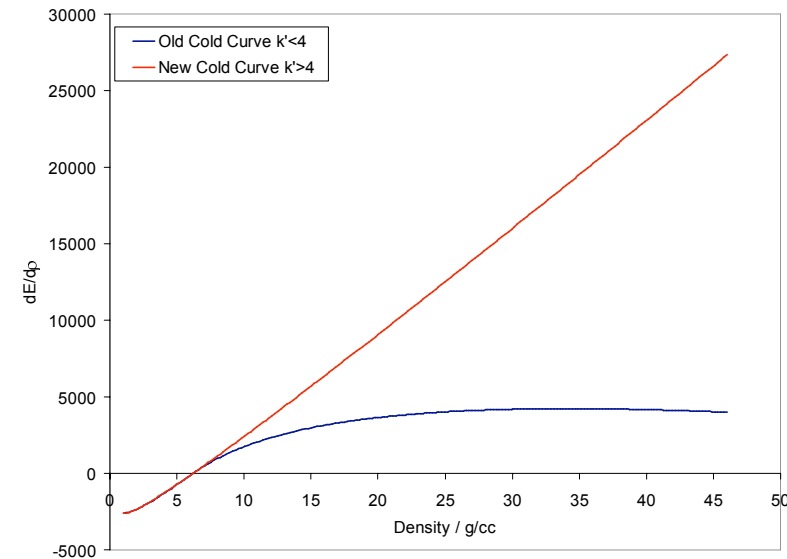
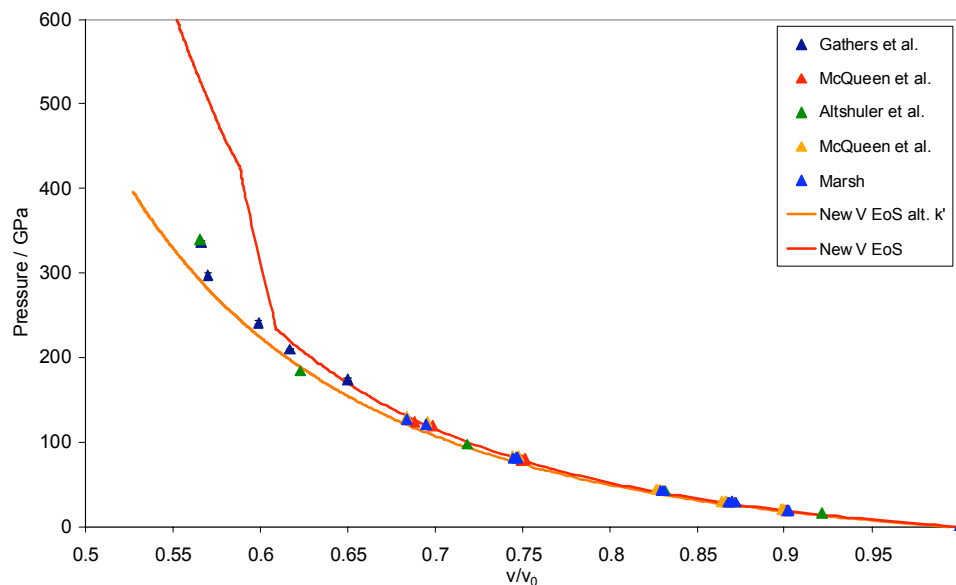
- Choice of cold curve parameters, V_o , K_o , K'_o , E_o resulted in cold curve derivatives which are non-continuous.



- Varying cold curve parameter, K'_o , produced better fit to the data.

Cold Curve Modifications

- Alternative cold curve parameters improved fit to Hugoniot and other experimental data.



- K'_0 less than four resulted in a shallow cold curve which had a limited temperature and density range.
- Other cold curve functions were also ineffective resulting in either limited range or poor behaviour.
- Alternative cold curve function is being created.

Future Plans

- Propose to use Augmented Stabilised Jellium model¹ (DFT) to create a cold curve.
- Use DFT to model a simple metal with
 - allow for ion core overlap - corrects high pressure behaviour
 - recognises that electron gas will become non-uniform in expansion - corrects expansion behaviour
- An analytic function can be constructed for the cold curve in terms of E_0 , V_0 , K_0 , K_0'

1. Alchagirov, *et al.* Phys. Rev B, 224115 (2001)

Conclusions

- Compute an EoS for vanadium.
- Good match to data on
 - RP Isobar
 - RT Isotherm
- Poor Hugoniot behaviour
 - Poor cold curve representation
- Work currently ongoing to create an alternative cold curve with correct behaviour.

UNCLASSIFIED

Comparison of Beryllium EOS & Constitutive Models with Recent Shock Data

Michael Prime, W-13

Chris D. Adams, DE-9

Shuh-Rong Chen , William R. Blumenthal, MST-8

James D. Johnson, Sven P. Rudin, Scott Crockett, T-1



**JOWOG 32MAT, January 25-29, 2010,
Livermore, CA**

This document deemed Unclassified by
____R. Liljestrand _____(DC)



Operated by Los Alamos National Security, LLC for NNSA

UNCLASSIFIED

LA-UR-10-00166/W-13-10-0002U



Goals

- **We now have flyer plate wave profiles on pedigreed S-200F Beryllium**
- **See how our best EOS and constitutive models perform on this data**
 - Such data was not used in model calibration
- **Not looking at failure modeling even though these are spall tests**

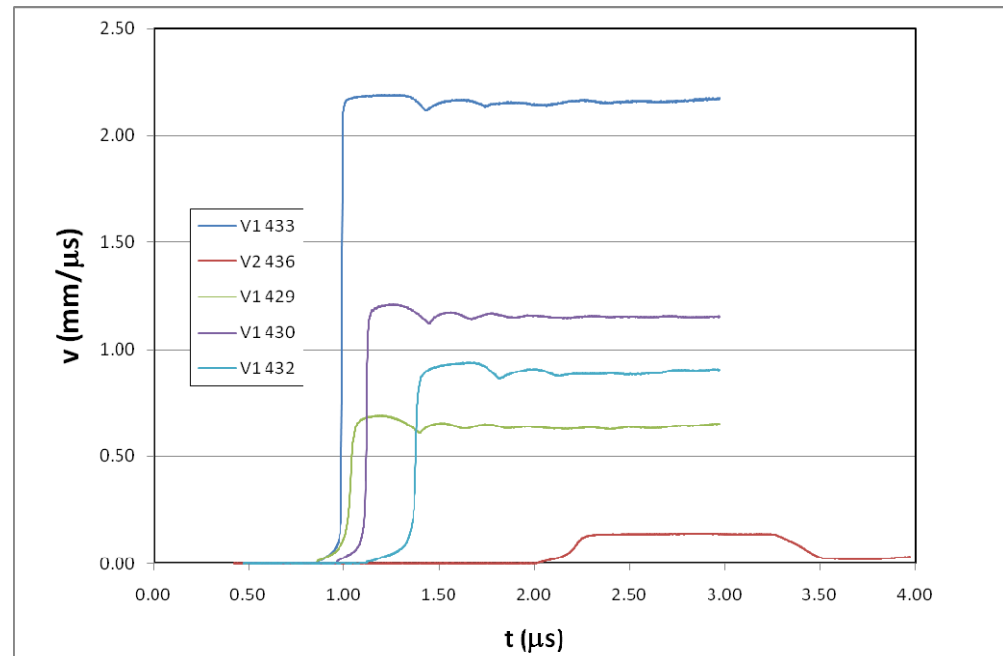
Outline

- **Data**
- **Models:**
 - Hydro
 - Materials
 - Mesh refinement and convergence
- **Compare to simulations**
- **Examine plastic strain and strain rate regimes**
- **Conclusions**

Data

“EOS and Spall Behavior of S200F Beryllium,” C.D. Adams, W.W. Anderson, G.T. Gray III, W.R. Blumenthal, C.T. Owens, F.J. Freibert, J.M. Montoya, P.J. Contreras, 16th APS Topical Conference on Shock Compression of Condensed Matter, June 28–July 3 2009; Nashville, Tennessee. LA-UR-09-05055

- + 1 shot since then
- 4 spall shots 56 – 193 kbar
- 1 windowed shot ~ 20 kbar



Slide 4

Data timing

- **First 2 shots required time shift *by experimentalist***
 - For Be impactors only, had to measure assembly in the box at TA55
 - Difficult to measure impactor runout accurately
 - Undersized impactor – so piezo pins hit ring, not impact surface
 - Measured longitudinal and shear sound speed before experiments
 - Adjusted impact time to make elastic precursor wave speed match longitudinal sound speed
 - 12 ns for 429
 - 23 ns for 430
 - Would do symmetric impact differently in future to avoid issue
- **No adjustments to other 3 shots**
- **No other times shifts used in comparing simulations to data**

Expected shock heating and plastic strain

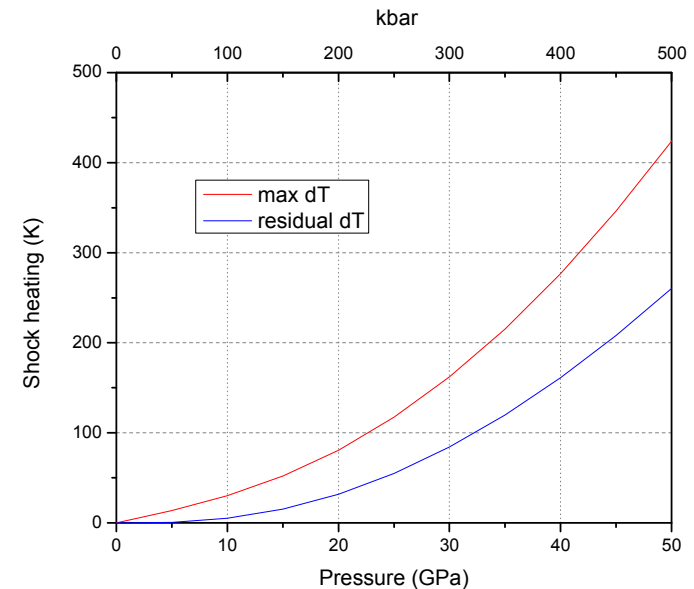
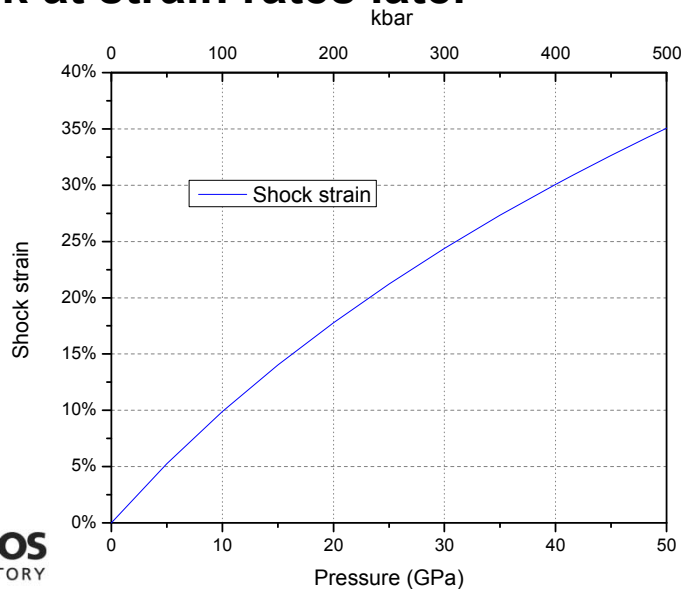
■ Upper bound plastic strain

- From linear U_s - U_p , deviatoric strength not considered – we have elasticity
- For full loading-unloading cycle – we don't fully unload

■ Lower bound on heating

- Plastic work heating can be similar magnitude
- Still will be less than 200K under 200 kbar

■ Will look at strain rates later



Slide 6

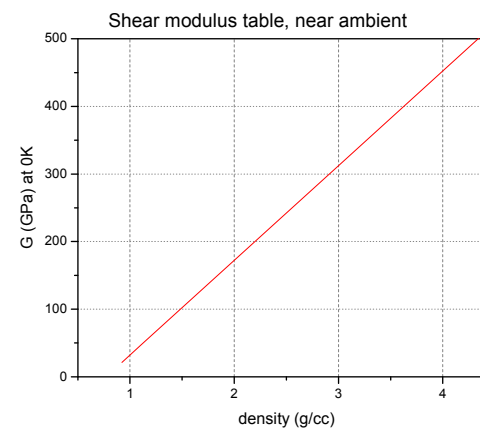
Hydro model

- 1D Lagrangian model in Flag
- Contact surfaces between flyer-target and target-window
- Will discuss zone size

Material model - Be

■ Latest Sesame table

- 2024 (September 2006) (export controlled)
- Linear Us-Up fit to higher P Hugoniot data and extrapolated back to intercept
 - Avoids having strength contributions the shock data effect the derived cold curve
- Has a consistent melt table, but no shear modulus table
- Had shear modulus table (Leonid Burakovsky, T-1) added in
 - So used developmental EOS number 92024
 - (G table makes negligible difference in these simulations)



Material model – PTW Fits for Be

■ Preston-Tonks-Wallace strength

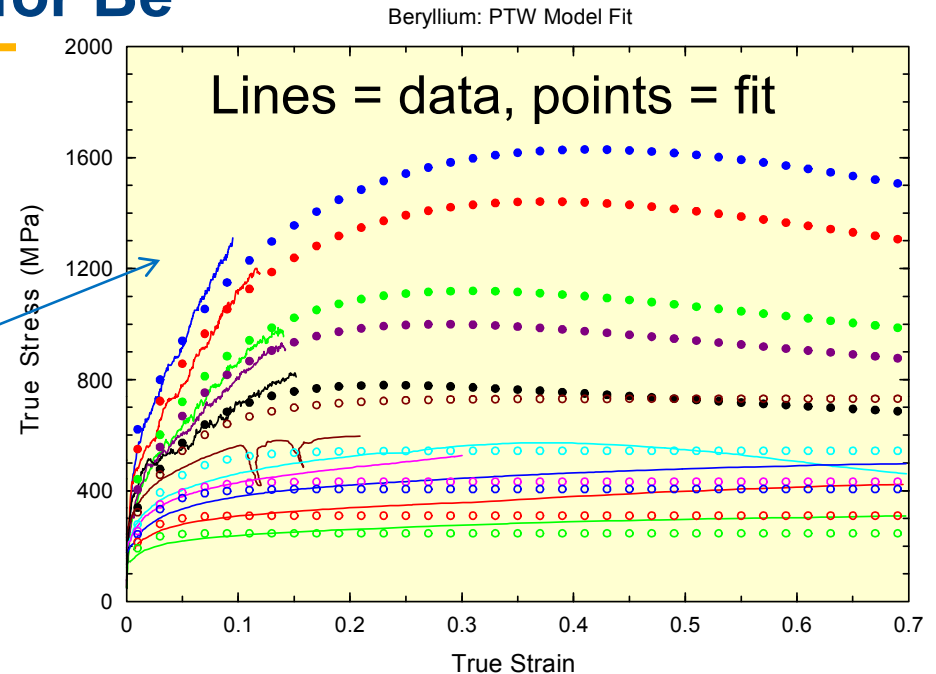
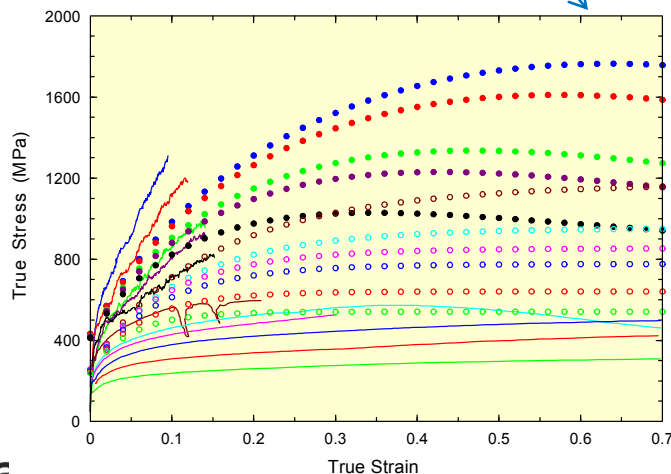
- Preston, DL; Tonks, DL; Wallace, DC, "Model of plastic deformation for extreme loading conditions," *J. Applied Physics*, **93**(1), p.211-220, 2003.

■ MST-8 (Shuh-Rong Chen) fit

- Newer high rate data

■ Original Dean Preston Fit

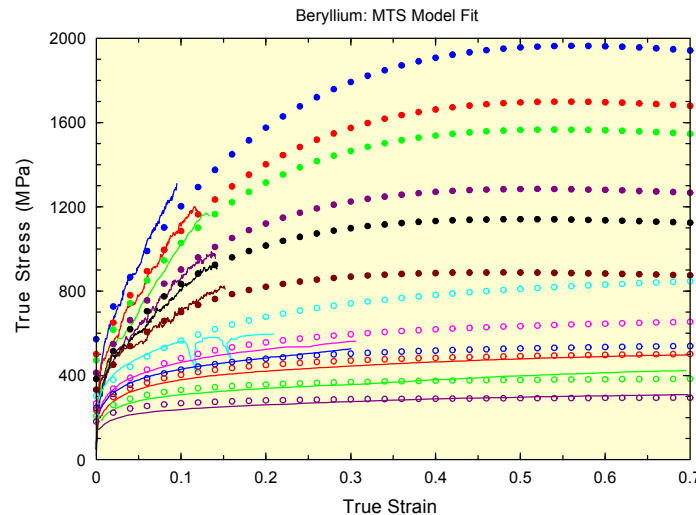
- Older Montoya data



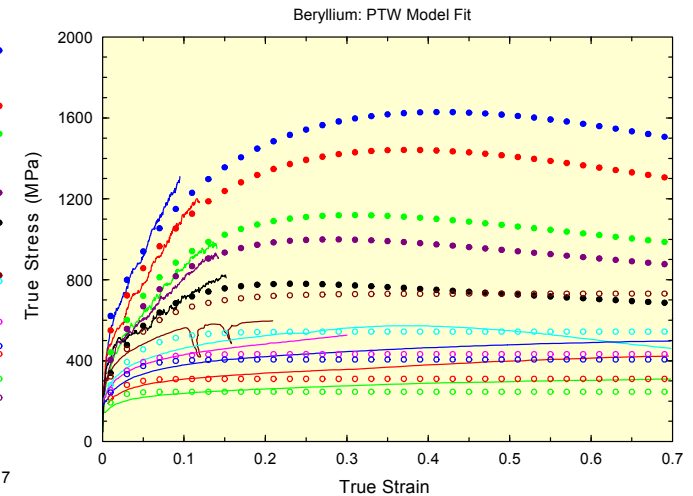
- | | |
|---------------------|---------------|
| 1 : BeHP-196303.txt | 77K; 3000/s |
| 2 : Bed-50353.txt | 223K; 3500/s |
| 3 : Bed20373.txt | 473K; 3700/s |
| 4 : Bed30393.txt | 573K; 3900/s |
| 5 : Bed50433.txt | 773K; 4300/s |
| 6 : Bef200c1.txt | 473K; 1/s |
| 7 : Bef300c1.txt | 573K; 1/s |
| 8 : Bef200c1e-3.txt | 473K; 0.001/s |
| 9 : Bef400c1.txt | 673K; 1/s |
| 10 : Bef500c1.txt | 773K; 1/s |
| 11 : Bef600c1.txt | 873K; 1/s |

MTS Fit

- **Mechanical Threshold Stress**
- **MTS fit looks similar to PTW**
 - In low strain region of interest
- **Made some compromises to match new high-rate data and old low-rate data**
- **New high-rate branch of MTS not used**



— 77 K; 3000 /s
 — 223 K; 3500 /s
 — 298 K; 3500 /s
 — 473 K; 3700 /s
 — 573 K; 3900 /s
 — 773 K; 4300 /s
 — 473 K; 1 /s
 — 573 K; 1 /s
 — 473 K; 0.001 /s
 — 673 K; 1 /s
 — 773 K; 1 /s
 — 873 K; 1 /s
 • MTS: 77 K; 3000 /s; adiabatic
 • MTS: 223 K; 3500 /s; adiabatic
 • MTS: 298 K; 3500 /s; adiabatic
 • MTS: 473 K; 3700 /s; adiabatic
 • MTS: 573 K; 3900 /s; adiabatic
 • MTS: 773 K; 4300 /s; adiabatic
 • MTS: 473 K; 1 /s
 • MTS: 573 K; 1 /s
 • MTS: 473 K; 0.001 /s
 • MTS: 673 K; 1 /s
 • MTS: 773 K; 1 /s
 • MTS: 873 K; 1 /s



1 : BeHP-196303.txt
 2 : BeD-50353.txt
 3 : BeD20373.txt
 4 : BeD30393.txt
 5 : BeD50433.txt
 6 : BeF200c1.txt
 7 : BeF300c1.txt
 8 : BeF200c1e-3.txt
 9 : BeF400c1.txt
 10 : BeF500c1.txt
 11 : BeF600c1.txt
 — 77K; 3000/s
 — 223K; 3500/s
 — 473K; 3700/s
 — 573K; 3900/s
 — 773K; 4300/s
 — 473K; 1/s
 — 573K; 1/s
 — 473K; 0.001/s
 — 673K; 1/s
 — 773K; 1/s
 — 873K; 1/s

Make your bets: do you think one will be better? Will they work well?

Other materials - Sapphire

■ Sapphire (flyer shot 432)

- Gruneisen, Linear Us-Up in elastic regime
 - LM Barker, RE Hollenbach, “Shock-Wave Studies of PMMA, Fused Silica, and Sapphire,” *Journal of Applied Physics* (1970) **41**(10), 4208
 - $C = 11.19$ km/s, $s = 1.0$
 - Elastic to 120 kbar
 - P in shot 432: 77 kbar
- Sesame 7411 for alumina is fit to higher P data, not accurate in this regime
 - In the literature, used for Sapphire at higher pressures

Other materials - Tantalum

- **Tantalum (shot 433)**
- **Sesame 3520 (export controlled)**
- **PTW (Preston-Tonks-Wallace) strength**
 - Parameters from Shuh-Rong Chen, MST-8, LANL, April 2004
- **Pmin strength at 75 kbar**
 - In 433, Ta does not hit tension until after target separates

Other materials – Quartz and LiF

■ Z-cut quartz flier shot 436

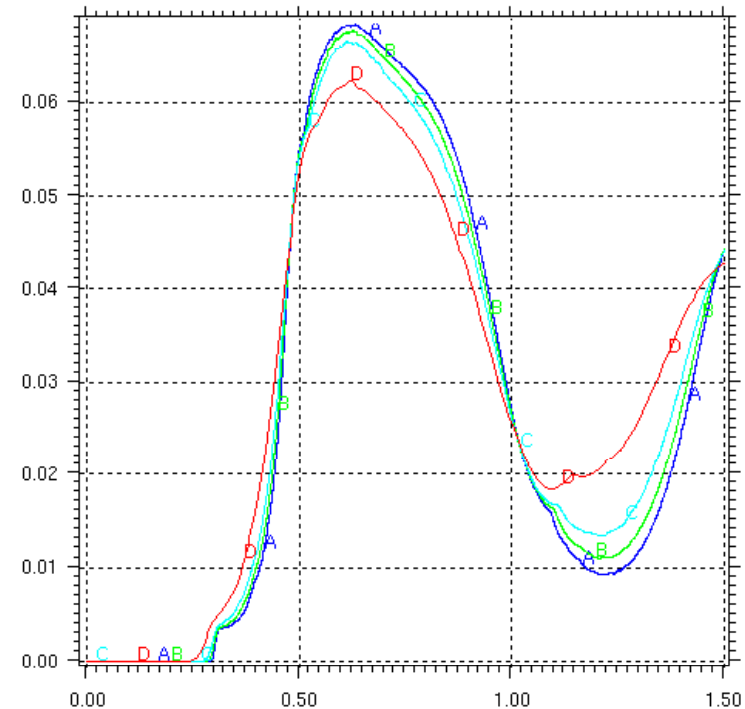
- Gruneisen with quadratic U_s-U_p
 - Jones, SC; Gupta, YM, “Refractive index and elastic properties of z-cut quartz shocked to 60 kbar,” *Journal of Applied Physics*; 2000; **88**(10), p.5671-9
 - $C=6.319$ km/sec. $S_1=1.20$, $S_2=0.82$
 - DE-9 used $C = 6.36$, $S_1=1.36$, $S_2=0$ in their analysis

■ LiF window shot 436

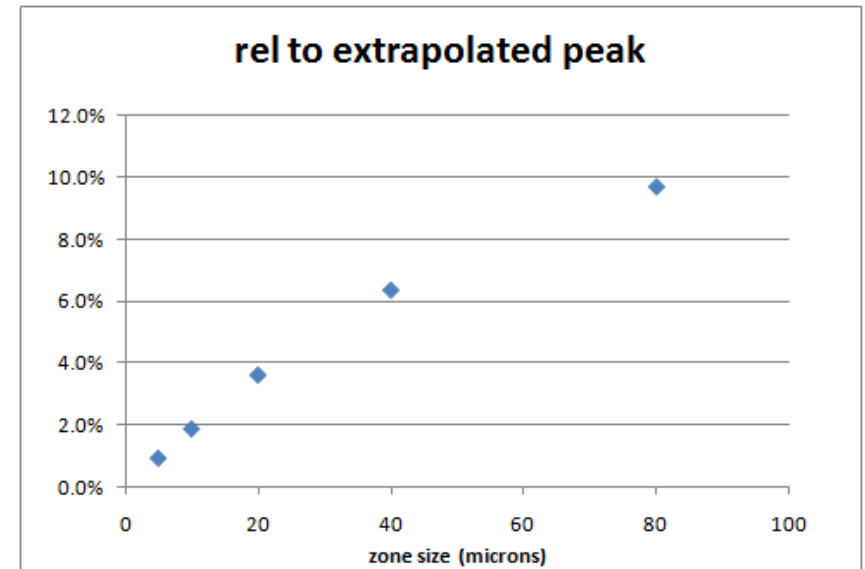
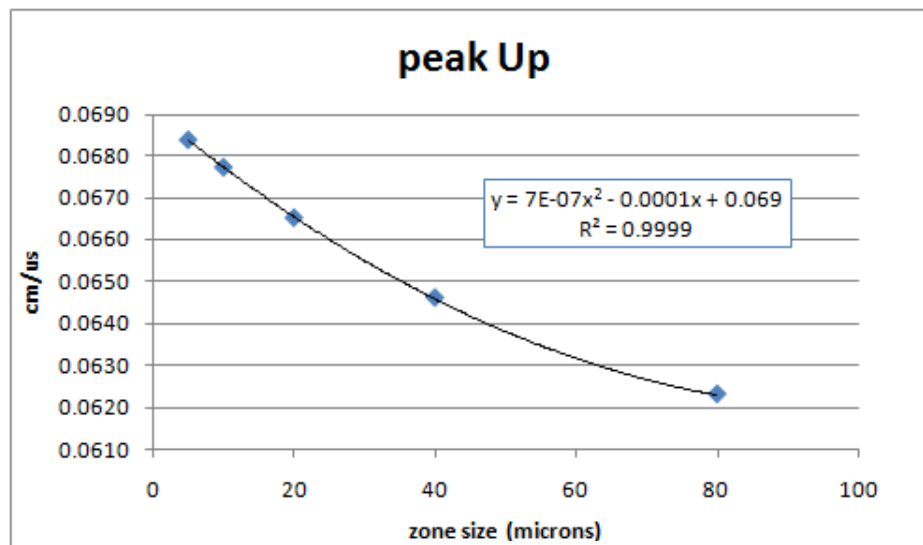
- Sesame 7271

Mesh refinement

- **Shot 429**
 - 56 kbar Be-Be
- **Zone sizes 80 μm , 40, 20, 10 ,5**
- **PTW strength**
- **Good convergence**



Convergence



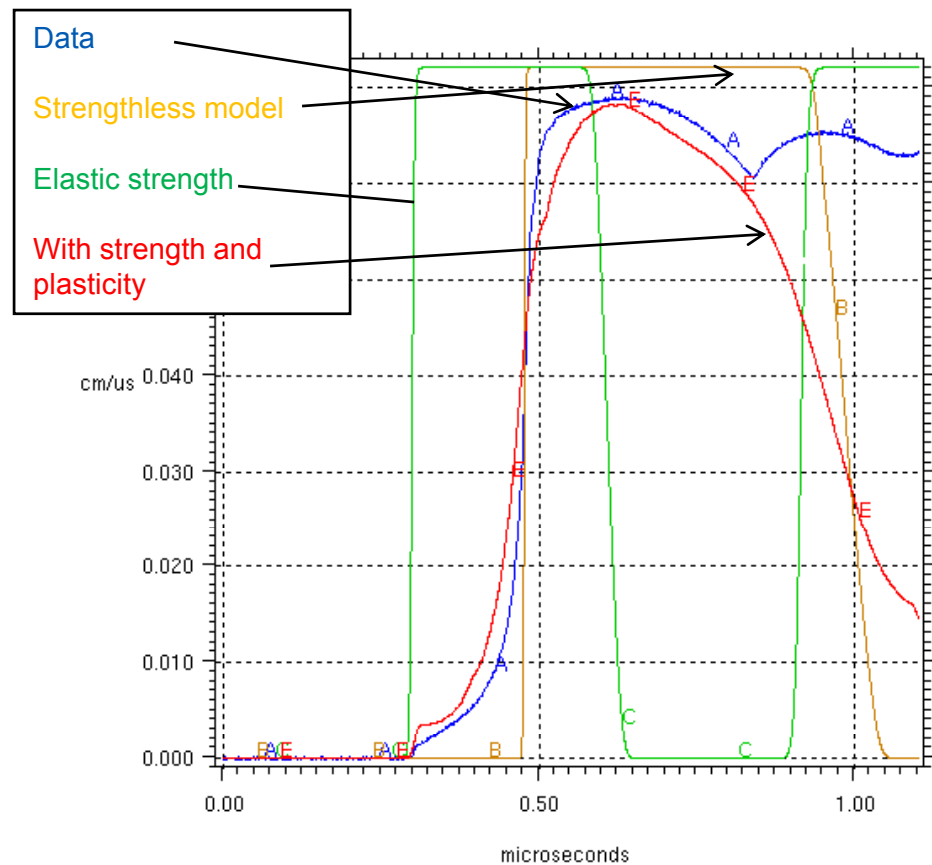
- At 20 μm , peak Up is 4% below converged value
- 1% at 5 μm
- *All results in this talk at 5 μm zoning unless noted*

Outline

- **Data**
- **Models:**
 - Hydro
 - Materials
 - Mesh refinement and convergence
- **Compare to simulations**
- **Examine plastic strain and strain rate regimes**
- **Conclusions**

Example

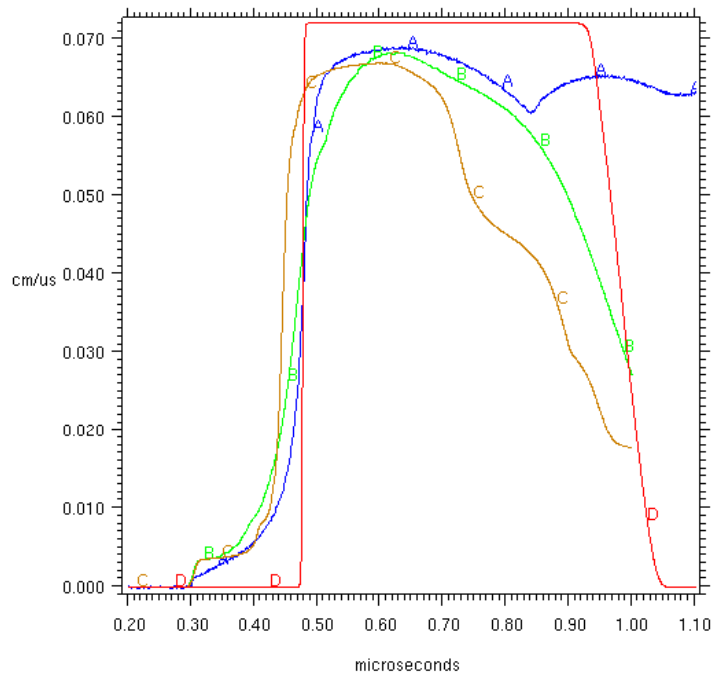
- Before we discuss details, get oriented
- Shot 429
 - Be on Be spall
 - Peak pressure 56 kbar
- Large strength effects
- Remember, not modeling spall



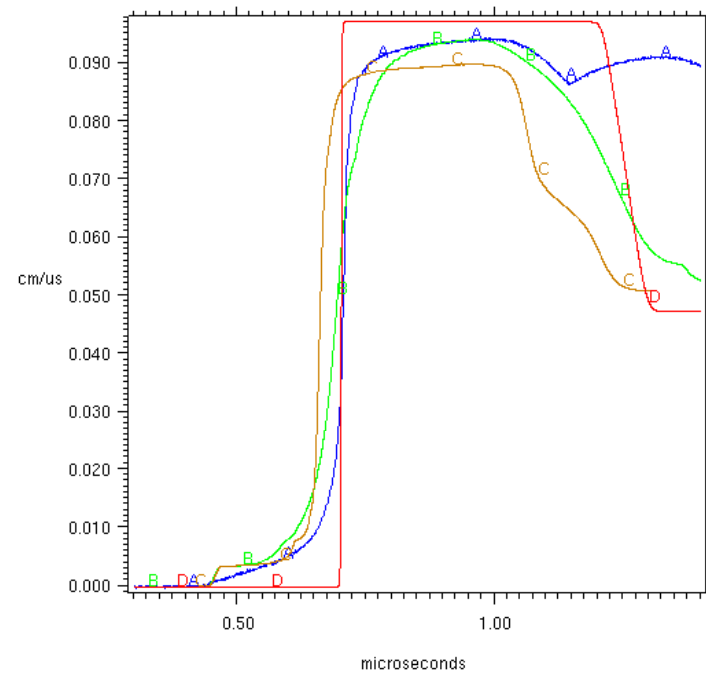
Compare wave profiles – low P spall

- A is data, B is PTW (MST-8), C is MTS, D is no deviatoric strength

429 – 56 kbar Be-Be



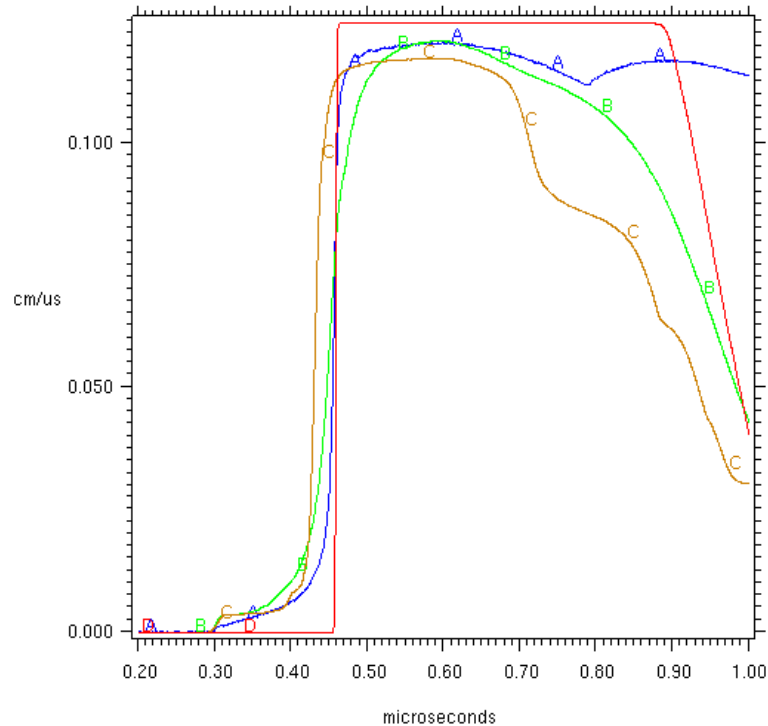
432 – 77 kbar Sapphire-Be



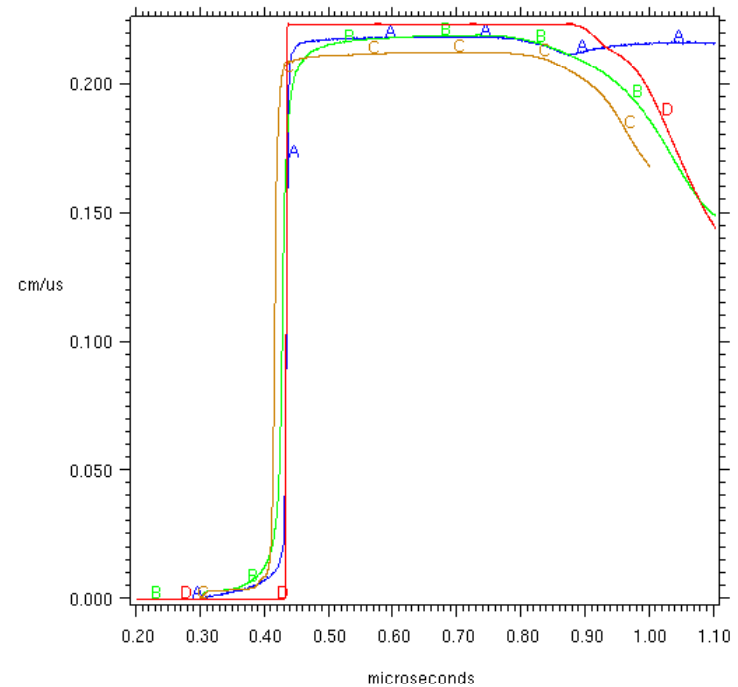
Higher P spall

- A is data, B is PTW, C is MTS, D is no deviatoric strength

430 – 100 kbar Be-Be

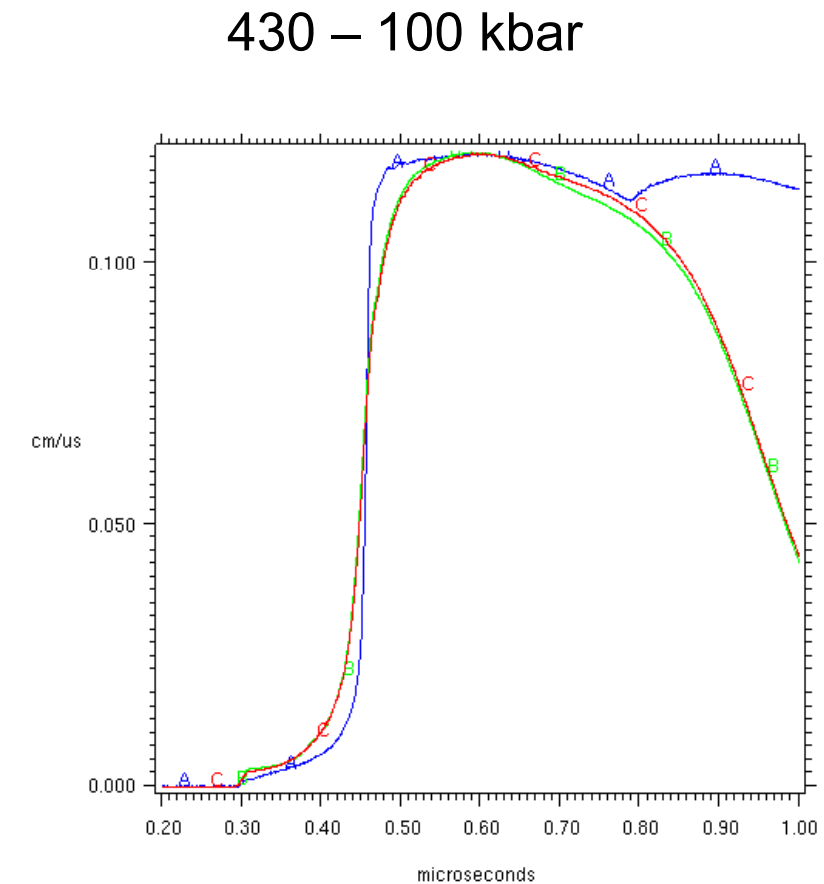


433 – 193 kbar Ta-Be



Compare different PTW fits

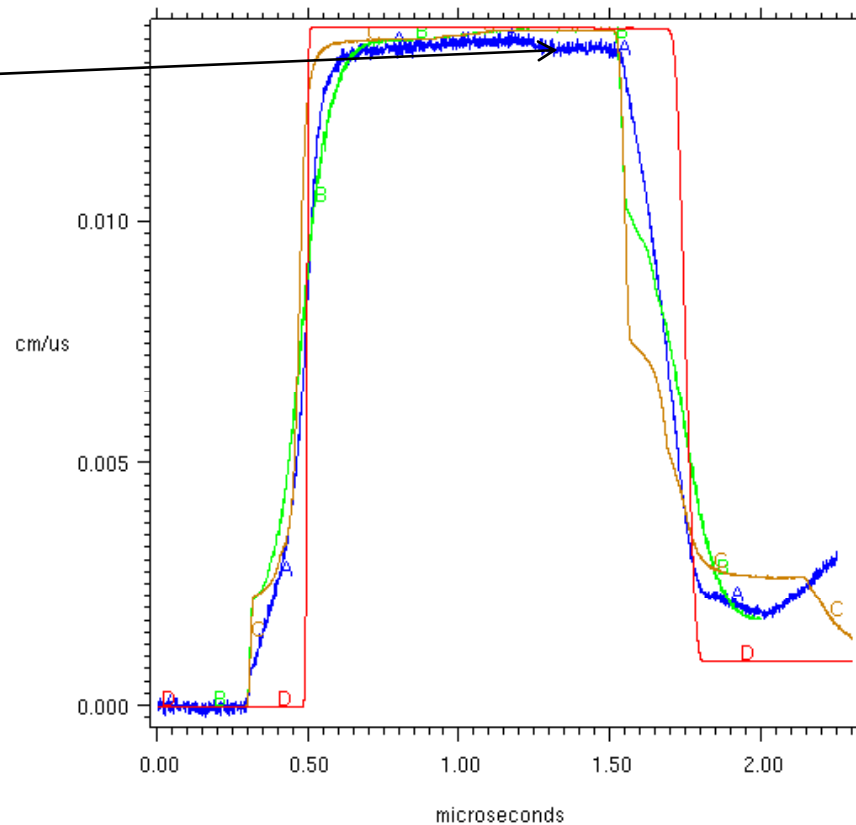
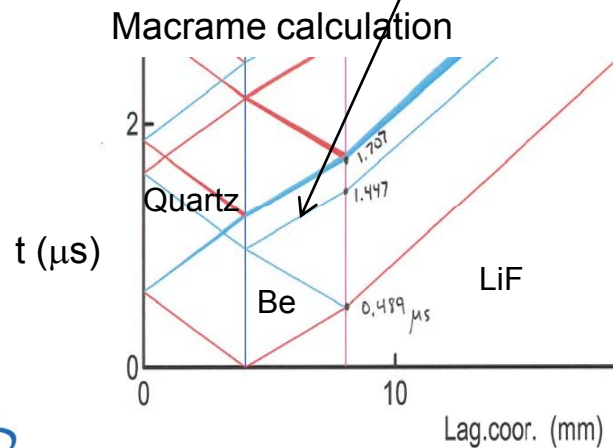
- **A = data**
- **B = MST-8 PTW fit**
- **C = Dean Preston**
- **So no significant difference between different PTW fits**



Low P EOS

- **A is data, B is PTW, C is MTS, D is no deviatoric strength**
- **Data shows slight release off of the Quartz-Be surface**
 - No strength calculation shows it barely
 - Strength calculations show re-shock instead

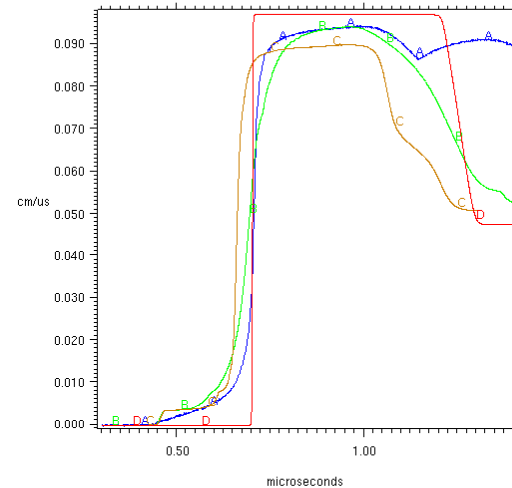
436 – 20 kbar – Quartz – Be - LiF



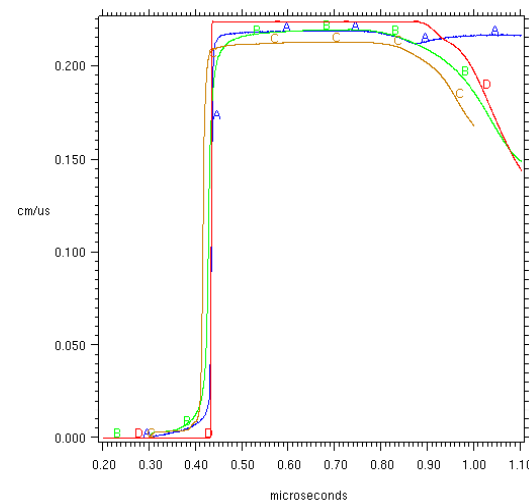
Observations

- **Model precursor too sharp**
 - Stress relaxation by twinning ?
- **MTS giving early shock arrival and low Up**
- **PTW giving too shallow of a slope on the rise**
 - And too much corner rounding
 - MTS better
- **Release coming in early**
 - Until highest P shot and PTW
- **MTS has much larger reverse yielding effect**
- **Constitutive models could be improved**
 - To match, would need some combination of changes to initial yield and strain and rate hardening
 - Lets examine further ...

432 – 77 kbar



433 – 193 kbar



Slide 22

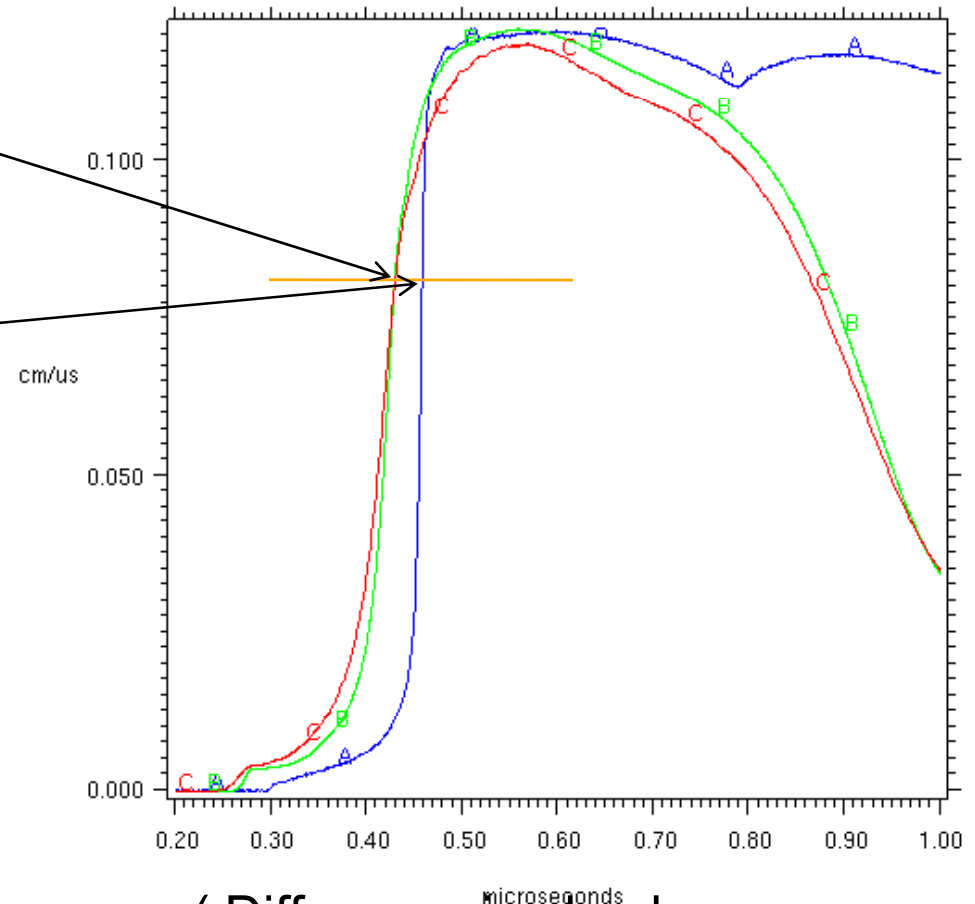
Outline

Next

- Quantify some differences
- Examine strain and strain rate regimes
- Look at differences between MTS and PTW in appropriate regimes

Compare sims to data – “shock speed” U_b

- **Use crossover point in 20 μm and 5 μm meshes**
 - Fairly mesh independent
- **Take experimental arrival time at same velocity**
- **Divide by target thickness for shock speed**
- **This is *not* conventional shock speed**
 - Modified for code/data comparison
 - Call it U_b for bulk arrival

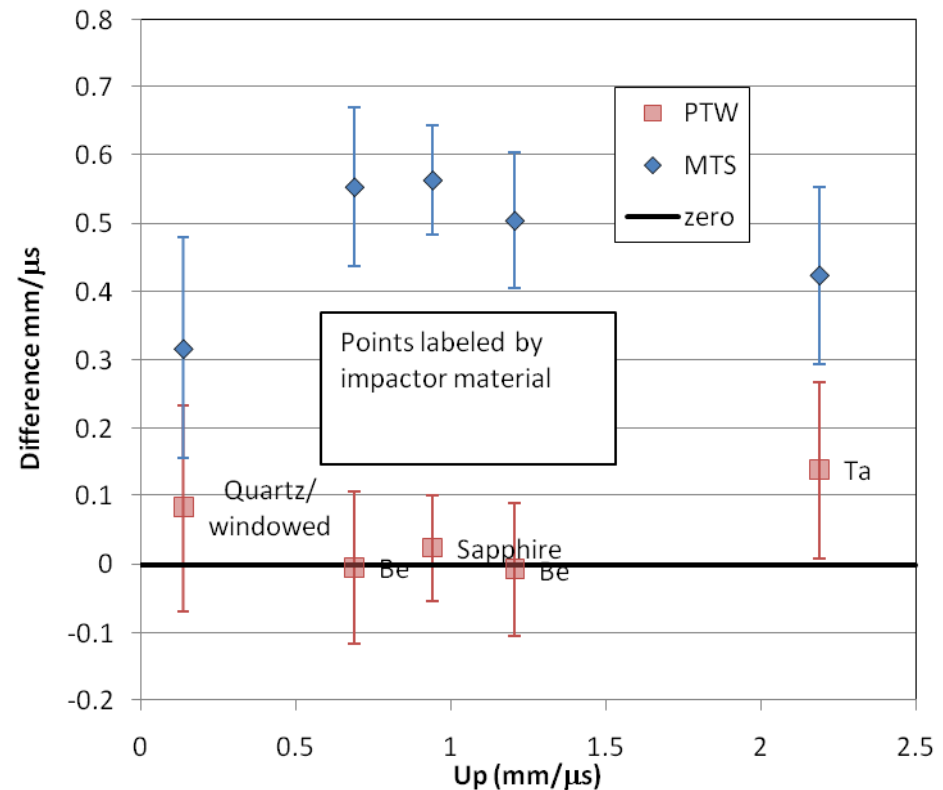


(Difference in shock arrival times exaggerated)

Slide 24

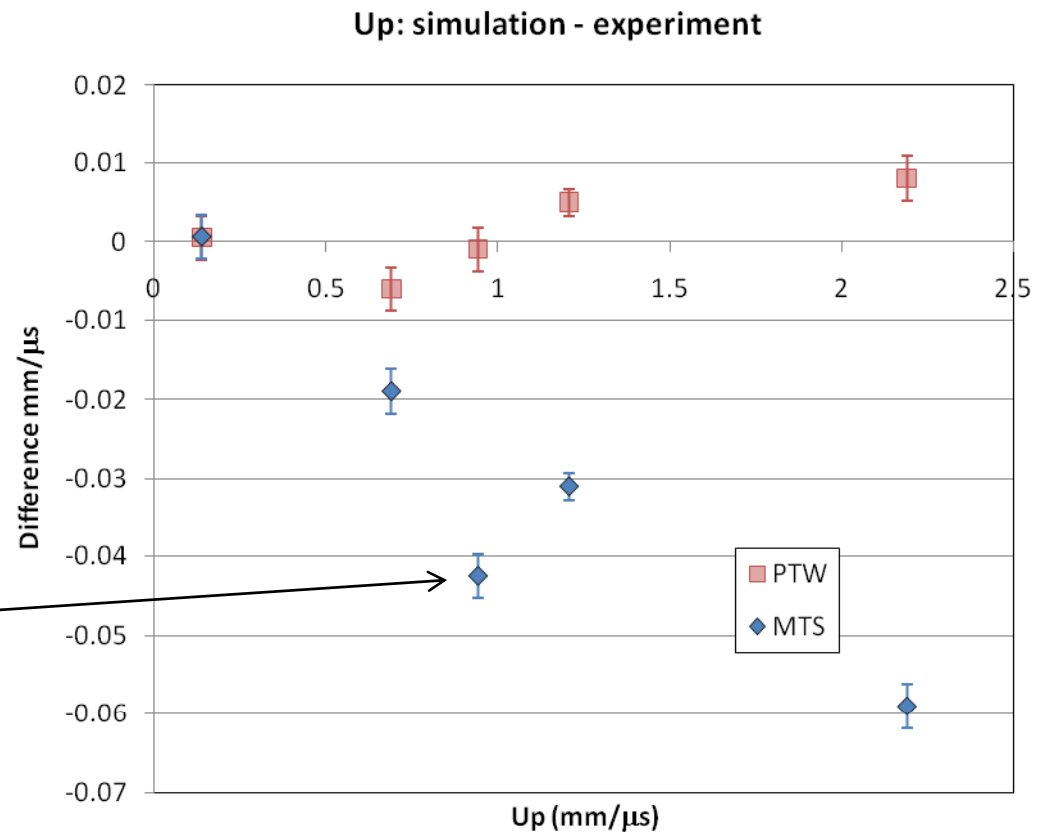
Compare “shock speed”

- $(U_b)_{\text{simulation}} - (U_b)_{\text{experiment}}$
- Error bars from uncertainty in experimental impact times
- PTW model generally within uncertainty of expt'l data
 - Trending slightly early
- MTS model giving significantly early arrival



Compare particle speed

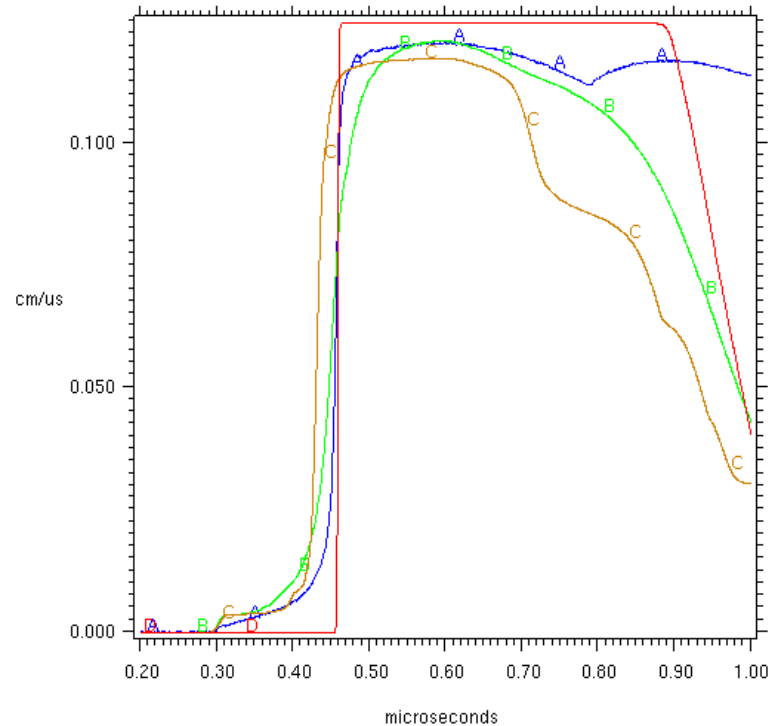
- $(U_p)_{\text{simulation}} - (U_p)_{\text{experiment}}$
- **PTW model close to expt'l data**
 - No trend
- **MTS model giving significantly low U_p**
 - Magnitude increases with increasing pressure
 - 3 spall shots are 2.8% low
 - Sapphire shot is 4.5% low



Some differences not yet quantified

- **Slope of shock rise**
 - MTS is better
- **Corner rounding**
 - MTS seems better

430 – 100 kbar Be-Be



Look at strain/strain-rate regime in Be

- **Use simulations**

- Since Be loading is rampy, it is reasonable to numerically look at rates during shock

- **Sample multiple locations in Be target for strain and strain rate**

- Equivalent (Von Mises) plastic strain
- Rate thereof

- **Look at lowest (56 kbar) and highest (193 kbar) pressure spall shots**

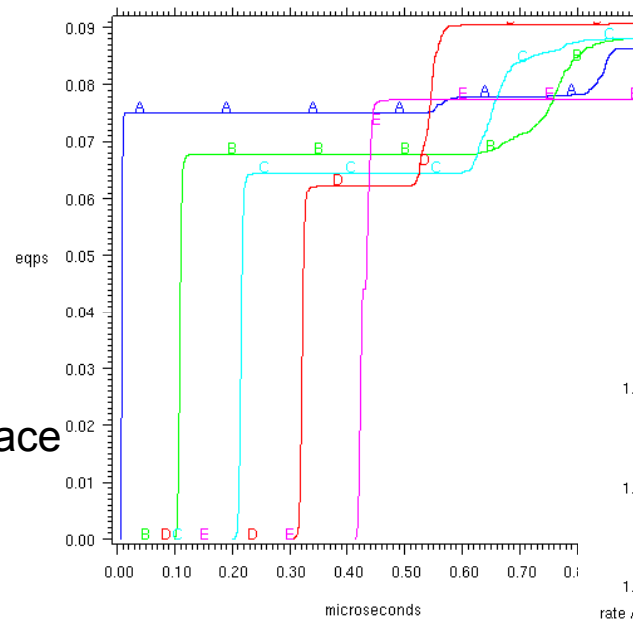
- EOS shot has only ~ 0.5 % plastic strain

Strain and strain rate – 193 kbar (433)

■ PTW

■ Plastic strains

- A near flyer
- B = $\frac{1}{4}$ point
- C = midpoint
- D = $\frac{3}{4}$ point
- E near free surface



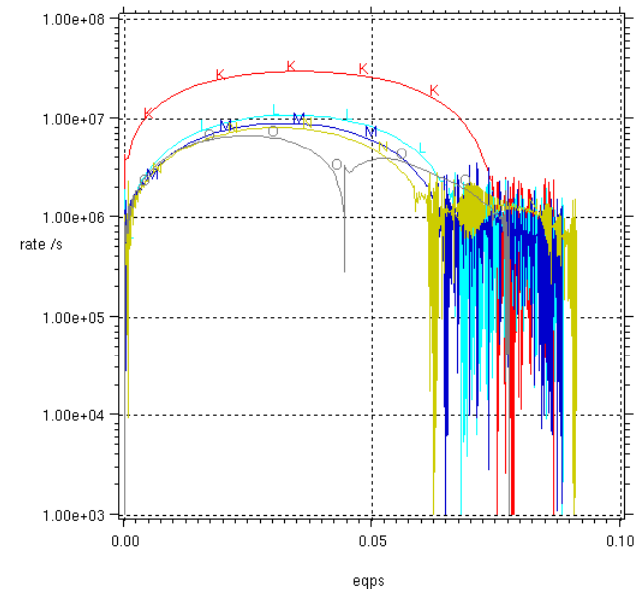
5 μm zone, PTW

■ Strain rate plotted vs. strain (remove time)

- K near flyer
- O near free surface

■ $\sim 10^7$ /sec during shock

■ $\sim 10^6$ during release

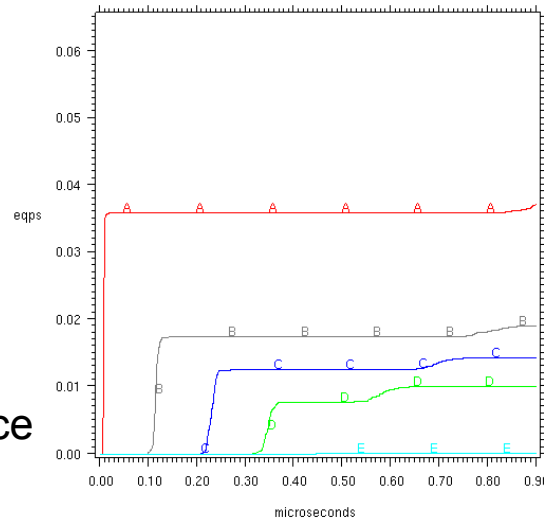


Strain and strain rate – 56 kbar (429)

■ PTW

■ Plastic strains

- A near flyer
- B = $\frac{1}{4}$ point
- C = midpoint
- D = $\frac{3}{4}$ point
- E near free surface



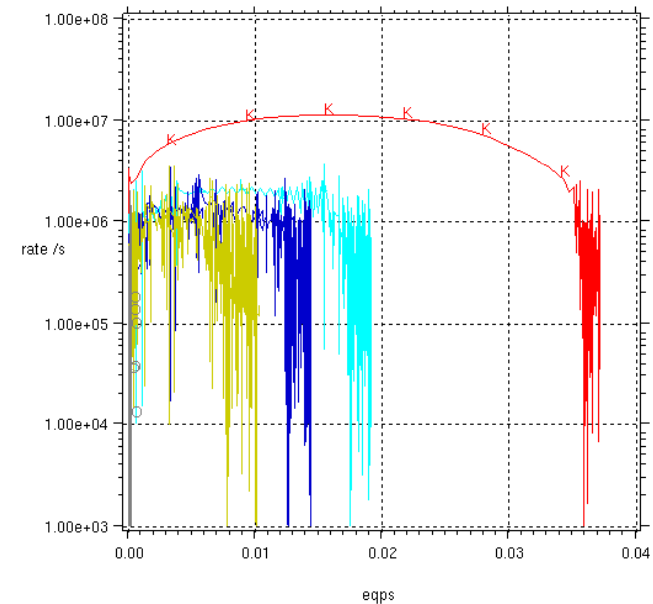
5 μm zone, PTW

■ Strain rate plotted vs. strain (remove time)

- K near flyer
- O near free surface

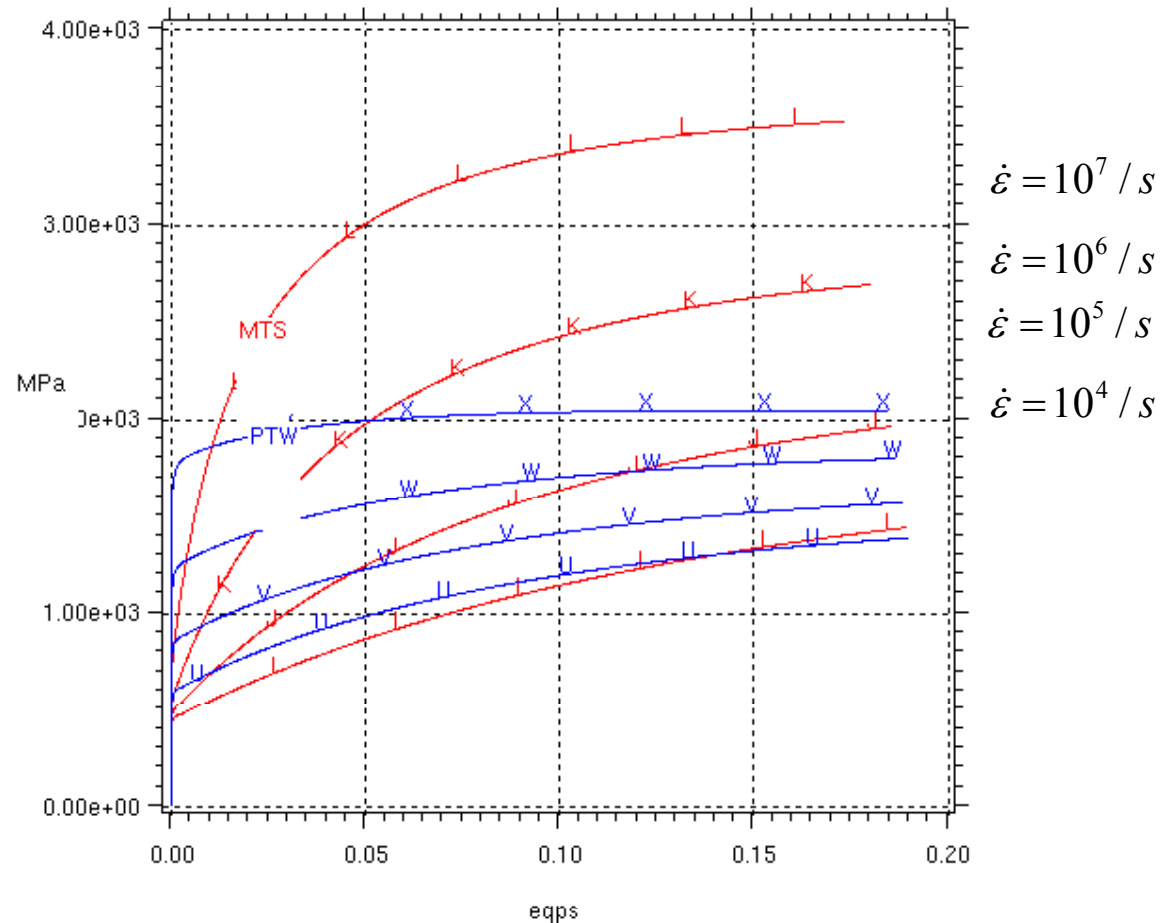
■ $\sim 10^7 - 10^6$ /sec during shock

■ $\sim 10^6$ during release



Constitutive models in appropriate regimes

- **PTW** and **MTS**
- **Adiabatic starting at 298 K**
- **Only plotted to 20% strain**
- $\bar{\sigma}(\bar{\varepsilon}_p)$
- **PTW has more rate sensitivity for initial yield**
- **MTS shows increasing strain hardening at higher rates**



Conclusions

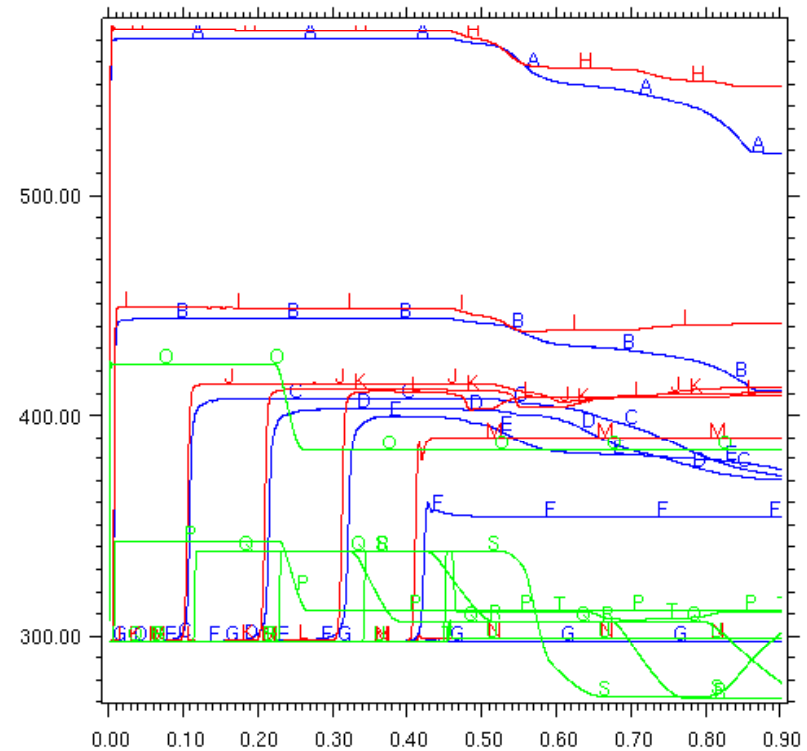
- **Sesame 2024 agrees quite well with this shock data at pressures below 200 kbar**
- **MTS and PTW constitutive models agree with different aspects of the data**
- **Currently, PTW + 2024 gives best overall agreement**
- **Better fits possible**
 - Can use the information to inform high-rate extrapolation without deviating from known material science
- **Better models likely require adding physics to constitutive models**
 - E.g, twinning
- **Incomplete**
 - Quantify other comparisons (e.g., loading slope)
 - Understand in models why MTS is reverse yielding more

End

- Backup slides after this

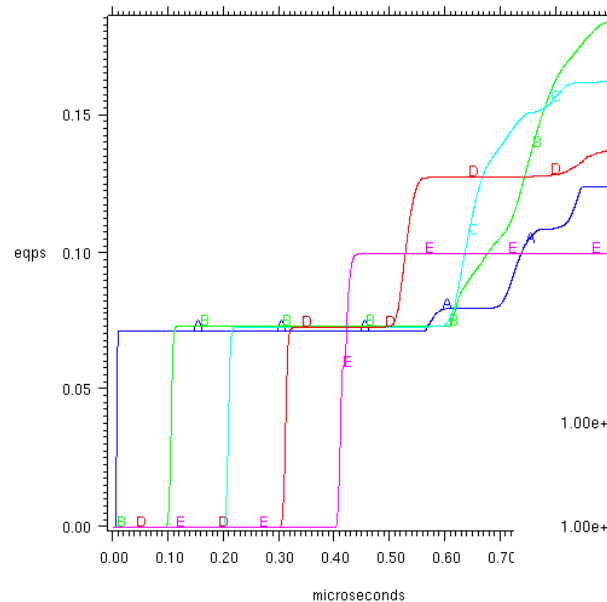
Heating

- Shot 433
- Zones
 - 10 from interface
 - $\frac{1}{4}$, $\frac{1}{2}$, $\frac{3}{4}$,
 - 10 from end
- MTS
- PTW
- No Strength
- Lots of plastic heating

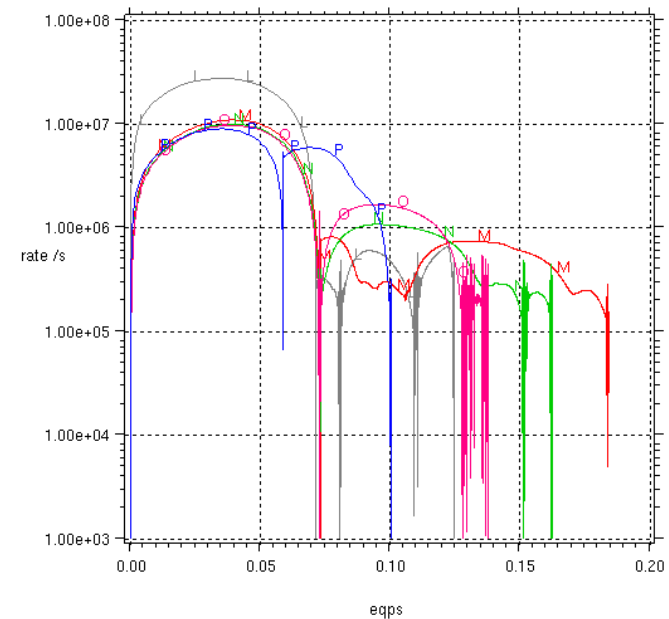


Strain and strain rate – 194 kbar (433)

- **MTS**
- **Plastic strains**
 - A near flyer
 - B = $\frac{1}{4}$ point
 - C = midpoint
 - D = $\frac{3}{4}$ point
 - E near free surface

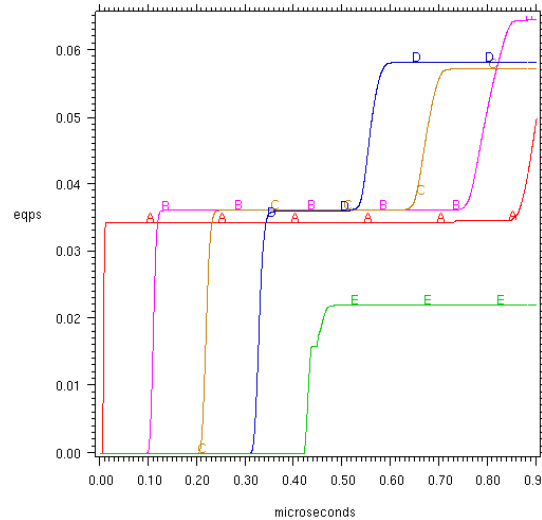


- **Strain rate plotted vs. strain (remove time)**
 - L near flyer
 - P near free surface
- **$\sim 10^7$ /sec during shock**
- **$\sim 5 \times 10^5$ during release**



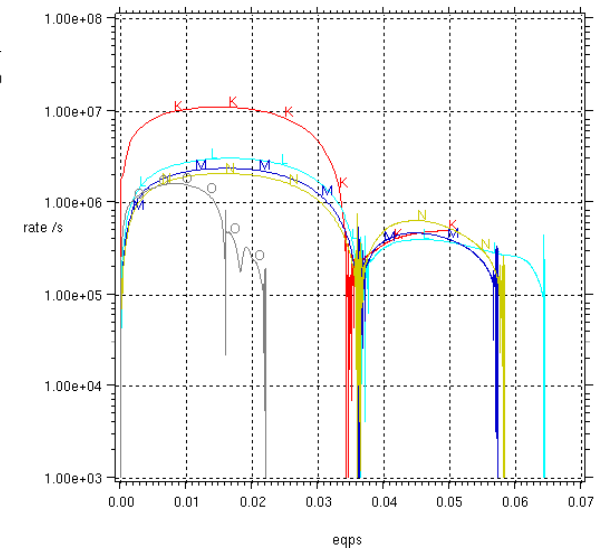
Strain and strain rate – 56 kbar (429)

- **MTS**
- **Plastic strains**
 - A near flyer
 - B = $\frac{1}{4}$ point
 - C = midpoint
 - D = $\frac{3}{4}$ point
 - E near free surface



5 μm zone, MTS

- **Strain rate plotted vs. strain (remove time)**
 - K near flyer
 - O near free surface
- **$\sim 10^6 - 10^7$ /sec during shock**
- **$\sim 10^5 - 10^6$ during release**



JOWOG 32MAT



January 26, 2010
Tuesday

Recent developments in the V-T theory of liquids

Eric Chisolm

Theoretical Division, LANL

JOWOG32Mat, Jan 25-29 2010, LLNL

Outline

- Review of V-T theory
- The transit contribution to liquid free energy
- Model for self-intermediate scattering function

What is V-T theory?

- Goal: An analytically tractable Hamiltonian formulation describing the motion of atoms in a liquid

What is V-T theory?

- Goal: An analytically tractable Hamiltonian formulation describing the motion of atoms in a liquid
- Postulate: Many-body potential surface is dominated by ***random*** valleys
 - All have the same statistical properties as $N \rightarrow \infty$

What is V-T theory?

- Goal: An analytically tractable Hamiltonian formulation describing the motion of atoms in a liquid
- Postulate: Many-body potential surface is dominated by **random** valleys
 - All have the same statistical properties as $N \rightarrow \infty$
- Strategy: Divide the problem into a dominant, simple piece and a smaller, complicated piece
 - In gases, free motion + interactions
 - In crystals, harmonic motion + anharmonicity
 - In liquids, **vibrations** in one valley + **transits** between valleys

UNCLASSIFIED

Transit contribution to liquid free energy

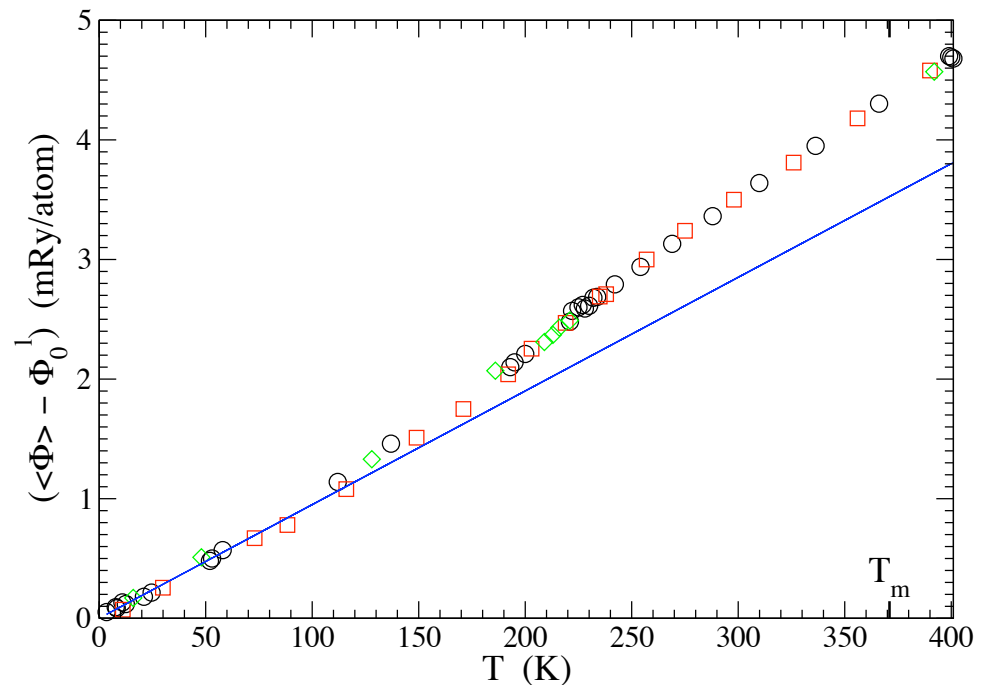
arXiv:0912.4285

Configurational entropy

- Previously, we've asserted w^N random valleys
- This contributes excess entropy $k_B \ln w$ per atom
- Set $\ln w = 0.8$ to explain entropy of melting

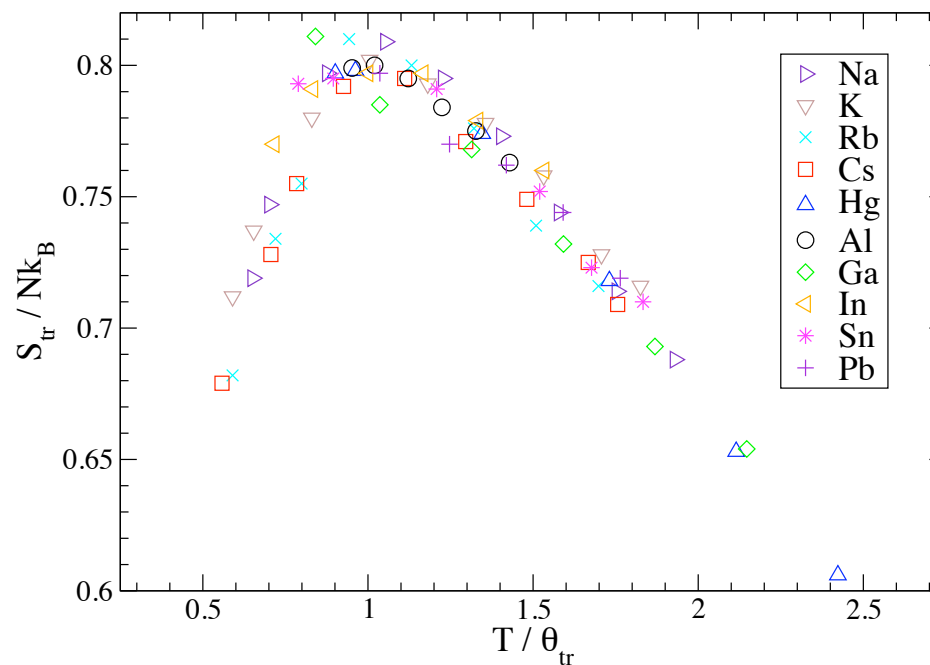
Configurational entropy

- Previously, we've asserted w^N random valleys
- This contributes excess entropy $k_B \ln w$ per atom
- Set $\ln w = 0.8$ to explain entropy of melting
- But what about this?
- Excess entropy due to this energy difference completely accounts for entropy of melting
- $\ln w$ must be much less than 0.8



Transit entropy data

- Let's neglect $\ln w$ for the moment and model the rest
- Experimental data for ten liquids show this result:



Phys Rev E **79**, 051201 (2009)

- Note a scaling temperature that is not T_m

The picture

- What do regions between the potential valleys look like?
 - At energies below $k_B T_m$, openings between valleys begin to appear
 - At energies much higher than $k_B T_m$, surface has repulsive “pillars” where particles approach each other
 - Between, ridges form between valleys which stretch up to the sides of the pillars

The picture

- What do regions between the potential valleys look like?
 - At energies below $k_B T_m$, openings between valleys begin to appear
 - At energies much higher than $k_B T_m$, surface has repulsive “pillars” where particles approach each other
 - Between, ridges form between valleys which stretch up to the sides of the pillars
- We suggest that the first feature contributes to low-temperature transits (up to roughly T_m), and the middle one to higher-temperature transits (liquid-gas transition)
- Let's model the first feature

The model

- Let the transit surfaces have an average energy ϵ_λ in the direction of normal mode λ ; then the configurational partition function per mode is

$$Q_\lambda(T) = \int_{-\infty}^{\infty} \exp\left(-\frac{1}{2}\beta M \omega_\lambda^2 q_\lambda^2\right) dq_\lambda + \left(\int_{-c_\lambda}^{-b_\lambda} + \int_{b_\lambda}^{c_\lambda}\right) \exp(-\beta \epsilon_\lambda) dq_\lambda$$

The model

- Let the transit surfaces have an average energy ϵ_λ in the direction of normal mode λ ; then the configurational partition function per mode is

$$Q_\lambda(T) = \int_{-\infty}^{\infty} \exp\left(-\frac{1}{2}\beta M \omega_\lambda^2 q_\lambda^2\right) dq_\lambda + \left(\int_{-c_\lambda}^{-b_\lambda} + \int_{b_\lambda}^{c_\lambda}\right) \exp(-\beta \epsilon_\lambda) dq_\lambda$$

- Making various substitutions and setting ϵ_λ same for all modes,

$$\begin{aligned} Z_{\text{tr}}(T) &= [1 + h(T)]^{3N}, \\ h(T) &= \mu \sqrt{\beta \epsilon} \exp(-\beta \epsilon) \end{aligned}$$

The model

- To set μ and ϵ , require entropy to have a maximum of $0.8 k_B/\text{atom}$ at $T=\theta_{\text{tr}}$:

$$\mu = 0.53221, \quad \epsilon = 1.26452 k_B \theta_{\text{tr}}$$

The model

- To set μ and ϵ , require entropy to have a maximum of $0.8 k_B/\text{atom}$ at $T=\theta_{\text{tr}}$:

$$\mu = 0.53221, \quad \epsilon = 1.26452 k_B \theta_{\text{tr}}$$

- Now everything is a function not of $\beta\epsilon$ but of T/θ_{tr}

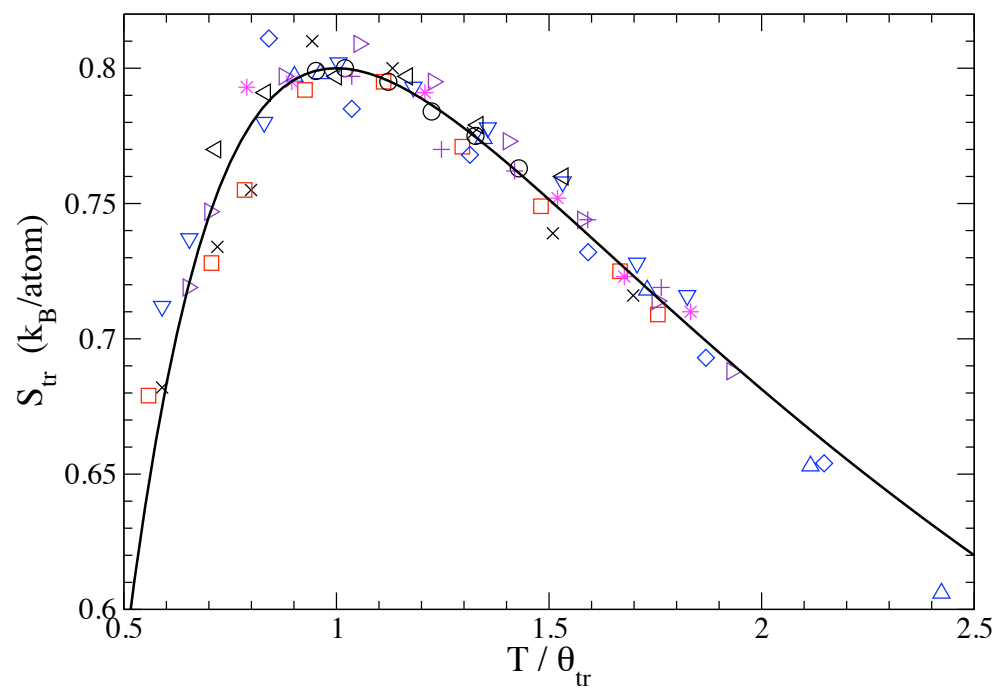
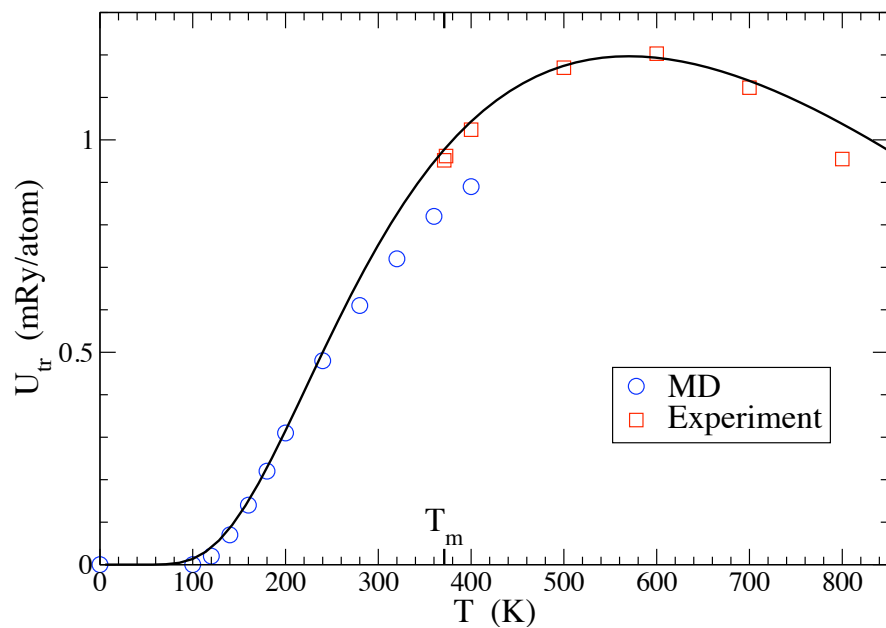
$$F_{\text{tr}} = -3Nk_B T \ln [1 + h]$$

$$U_{\text{tr}} = 3Nk_B T \left(\beta\epsilon - \frac{1}{2} \right) \frac{h}{1 + h}$$

$$S_{\text{tr}} = 3Nk_B \left[\ln [1 + h] + \left(\beta\epsilon - \frac{1}{2} \right) \frac{h}{1 + h} \right]$$

$$C_{\text{tr}} = 3Nk_B \frac{h}{1 + h} \left[\frac{(\beta\epsilon - \frac{1}{2})^2}{(1 + h)} - \frac{1}{2} \right].$$

Comparison with data



Results and further work

- Data suggest that transit entropy varies as a scaled temperature
- We have a model for “low-temperature” transits with that property; it matches data
- Some questions remain:
 - Are there w^N valleys? What's w ?
 - Can one calculate θ_{tr} from first principles? How?
 - What about high-temperature transits?

UNCLASSIFIED

The self-intermediate scattering function

Phys Rev E **78**, 041205 (2008)

The self-intermediate scattering function

- The intermediate scattering function is used to calculate scattering cross sections in the Born approximation

$$F(q, t) = \frac{1}{N} \left\langle \sum_{K,L} e^{-i\mathbf{q} \cdot (\mathbf{r}_K(t) - \mathbf{r}_L(0))} \right\rangle$$

- The self ($K=L$) part displays different physics from the distinct part and is easier to handle theoretically

$$F^s(q, t) = \frac{1}{N} \left\langle \sum_K e^{-i\mathbf{q} \cdot (\mathbf{r}_K(t) - \mathbf{r}_K(0))} \right\rangle$$

The vibrational contribution

- We decompose atoms' positions as

$$\mathbf{r}_K(t) = \mathbf{R}_K + \mathbf{u}_K(t)$$

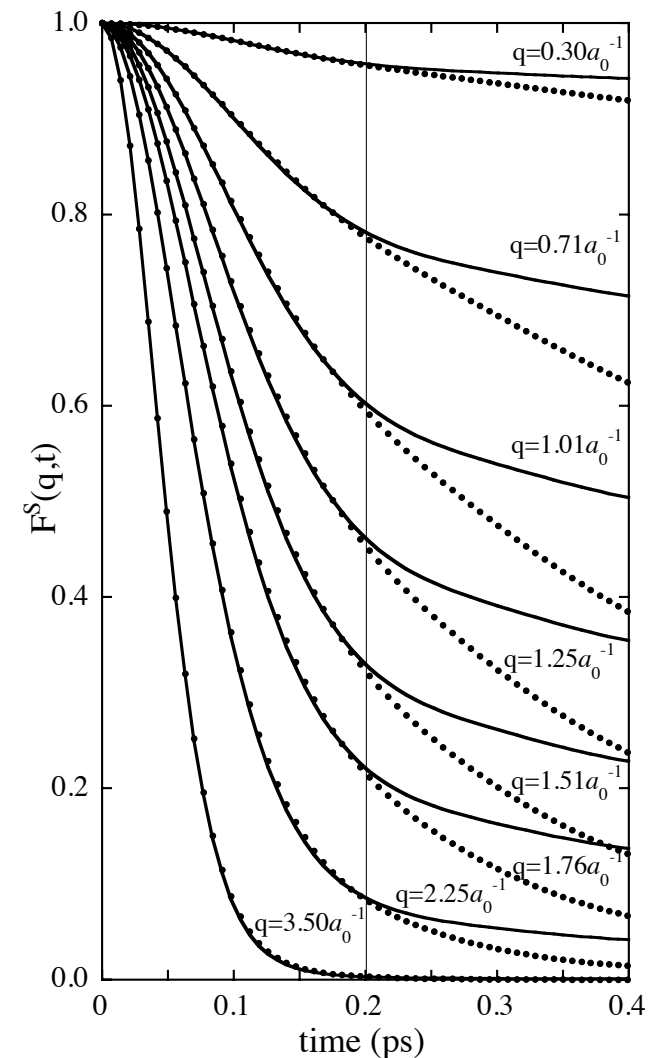
- \mathbf{R}_K has no time dependence, \mathbf{u}_K vibrates harmonically

The vibrational contribution

- We decompose atoms' positions as

$$\mathbf{r}_K(t) = \mathbf{R}_K + \mathbf{u}_K(t)$$

- \mathbf{R}_K has no time dependence, \mathbf{u}_K vibrates harmonically
- Dots are MD, lines are vibrational calculation
- They agree over a wide q range to the same time
- Vibrations capture most of the short-time motion



Including transits

- We considered a random walk model for transits
- The parameters are a rate ν and a step size δR

Including transits

- We considered a random walk model for transits
- The parameters are a rate ν and a step size δR
- The full expression is

$$F^s(q, t) = F_{vib}^s(q, t)D(q, t)$$

$$D(q, t) = \begin{cases} 1 & \text{for } t \leq \tau_c \\ e^{-\gamma(q)(t-\tau_c)} & \text{for } t \geq \tau_c \end{cases}$$

$$\gamma(q) = \nu \left[1 - \frac{\sin q\delta R}{q\delta R} \right]$$

Including transits

- We considered a random walk model for transits
- The parameters are a rate ν and a step size δR
- The full expression is

$$F^s(q, t) = F_{vib}^s(q, t)D(q, t)$$

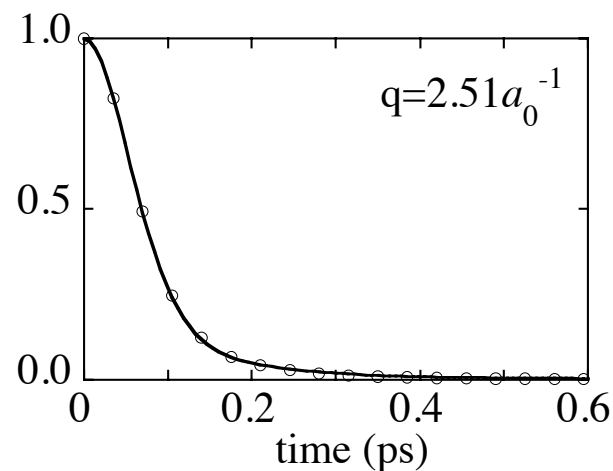
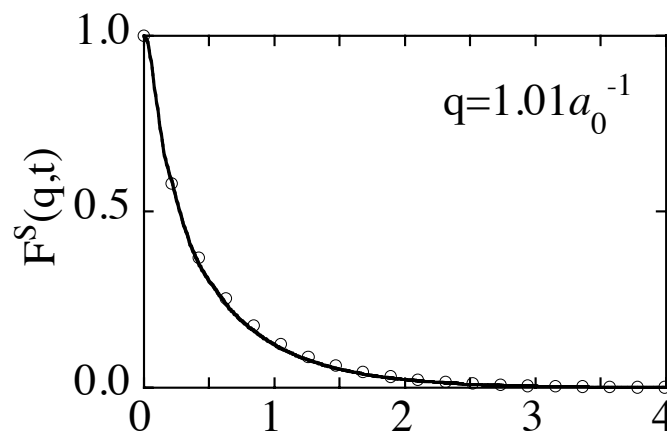
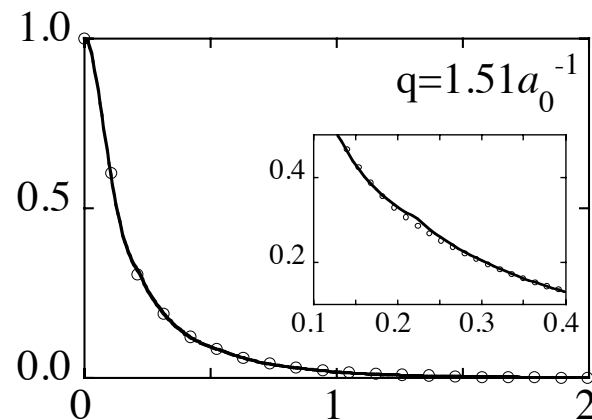
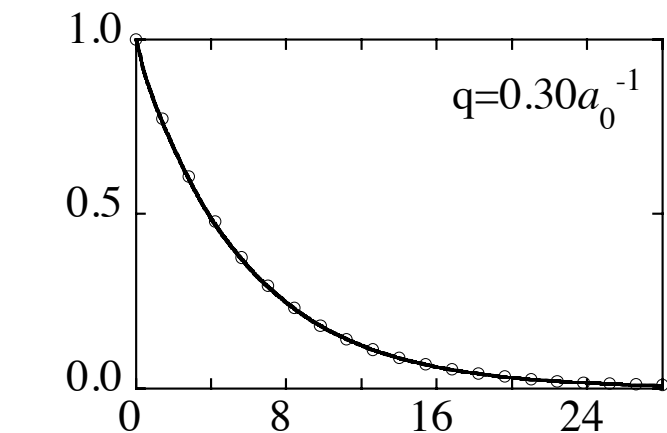
$$D(q, t) = \begin{cases} 1 & \text{for } t \leq \tau_c \\ e^{-\gamma(q)(t-\tau_c)} & \text{for } t \geq \tau_c \end{cases}$$

$$\gamma(q) = \nu \left[1 - \frac{\sin q\delta R}{q\delta R} \right]$$

- This model has the correct free ($q \rightarrow 0$) and hydrodynamic ($q \rightarrow \infty$) limits

Comparison with MD

- At various q , the model compares well with MD



Results and further work

- $F^s(q,t)$ is the self part of a correlation function that describes scattering
- Its vibrational approximation describes early-time behavior very well
- Adding random walk model for transits covers behavior at all times and limits in q
- Some questions remain:
 - How does one calculate the parameters from first principles?
 - Can transit random walk model be connected to transit treatment of free energy?
 - What about the distinct part?

Collaborators

LANL:

Duane Wallace

Giulia De Lorenzi-Venneri

Nicolas Bock

Travis B. Peery

Universidad Austral de Chile, Valdivia, Chile:

Erik Holmström

Raquel Lizárraga

Special thanks:

Carl W. Greeff

Brad C. Clements



UNCLASSIFIED

Lawrence Livermore National Laboratory



Phase Field Modeling of Coring in Pu alloys

**James Belak, Milo Dorr, Jean-luc Fattebert, Michael Wickett,
and Patrice Turchi**

JOWOG 32MAT Conference, January 25-29, 2010

Livermore, CA, USA

“Nothing can be learned as to the physical world save by observation and experiment, or by mathematical deductions from data so obtained.” - P.G. Tait

“Art (simulation) is the lie that helps us see the truth.” - Picasso

This work was performed under the auspices of the U.S. Department of Energy by Lawrence Livermore National Laboratory under Contract DE-AC52-07NA27344..

UNCLASSIFIED

LLNL-PRES-425756

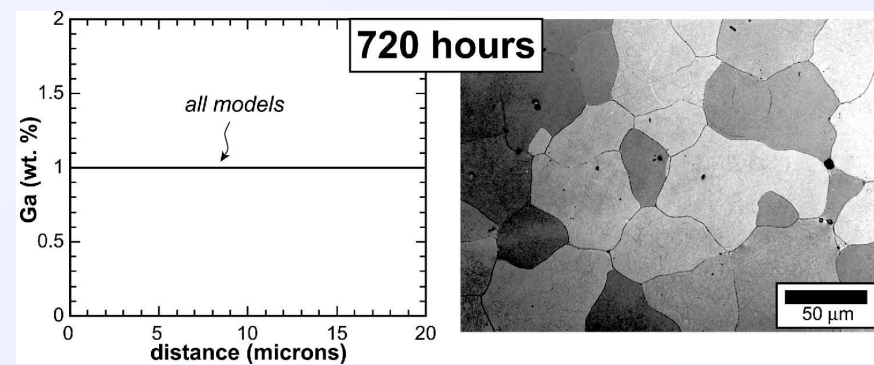
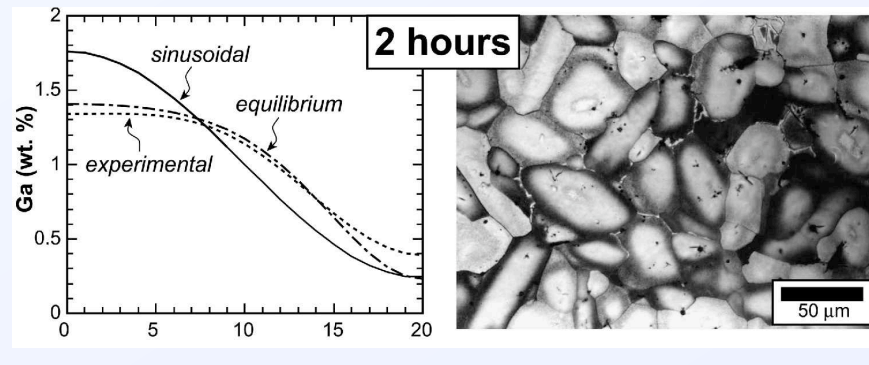
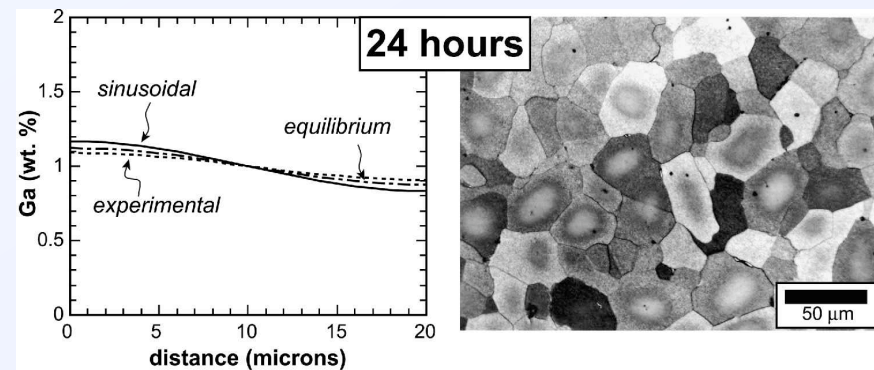
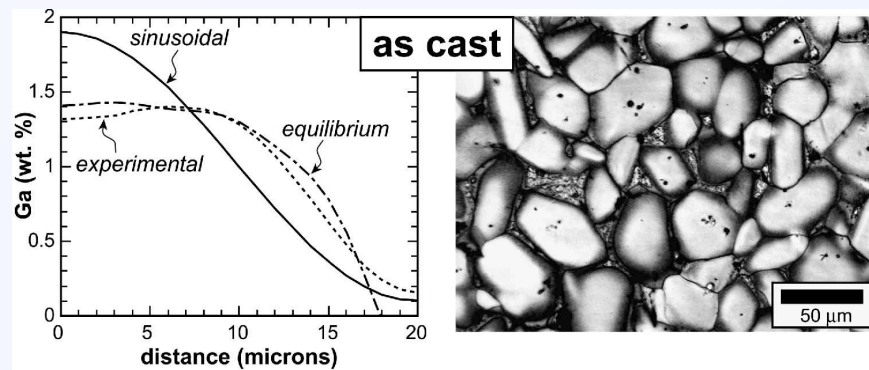
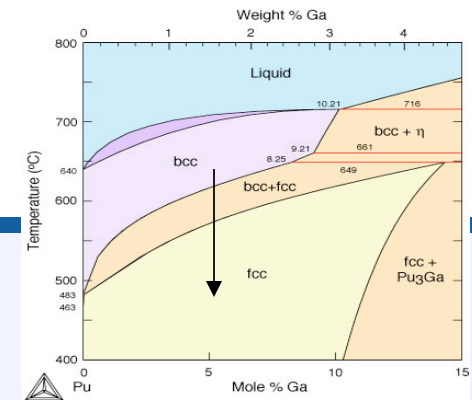
Outline: Phase-field modeling

- The Problem
- Phase-field modeling
 - What is it? Crystallography!
 - Input: Alloy Phase Diagram and Species Mobility
 - Examples: Coarsening, Coring in PuGa alloys, Bubbles
- Conclusion



UNCLASSIFIED

The lower diffusivity in the FCC phase results in an inhomogeneous alloy distribution (Coring)



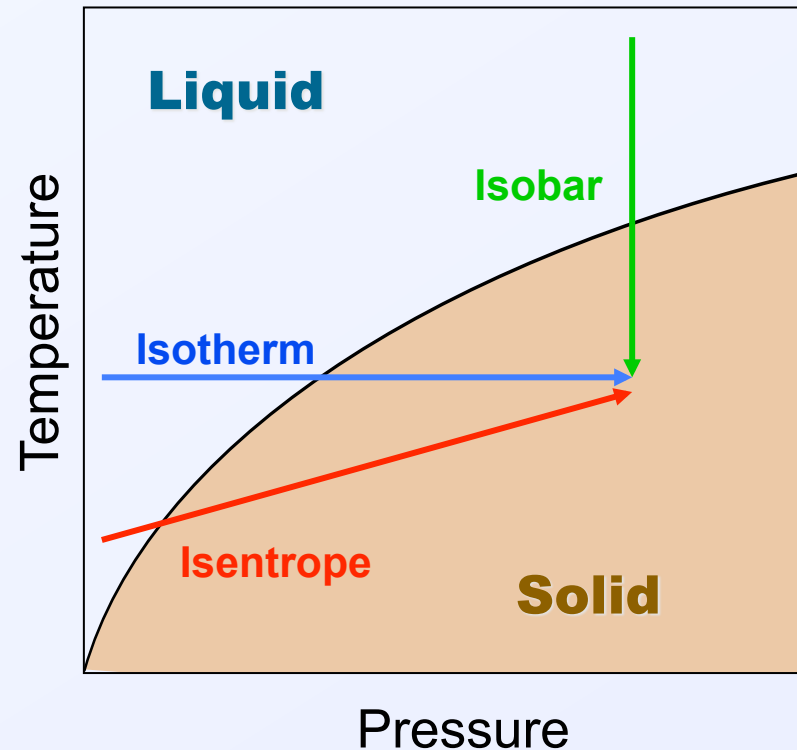
Ref: J. Mitchell, F. Gibbs, T. Zocco, and R. Pereyra, "Modeling of Structural and Compositional Homogenization of Plutonium-1 Weight Percent Gallium Alloys," *Metall. Mater. Trans. A*, 2001, vol. 32A, pp. 649-59.



Pressure driven solidification of metals

Explicitly model the details of the solidification process

- Extend highly successful molecular dynamics (MD) results to longer times and larger lengths
- Determine structure and stability of metals under dynamic loading conditions
- Identify relevant time scales (from ps to μ s) for solidification
- Locate non-equilibrium phase boundaries
- Describe rate and path dependence of approach to final structure

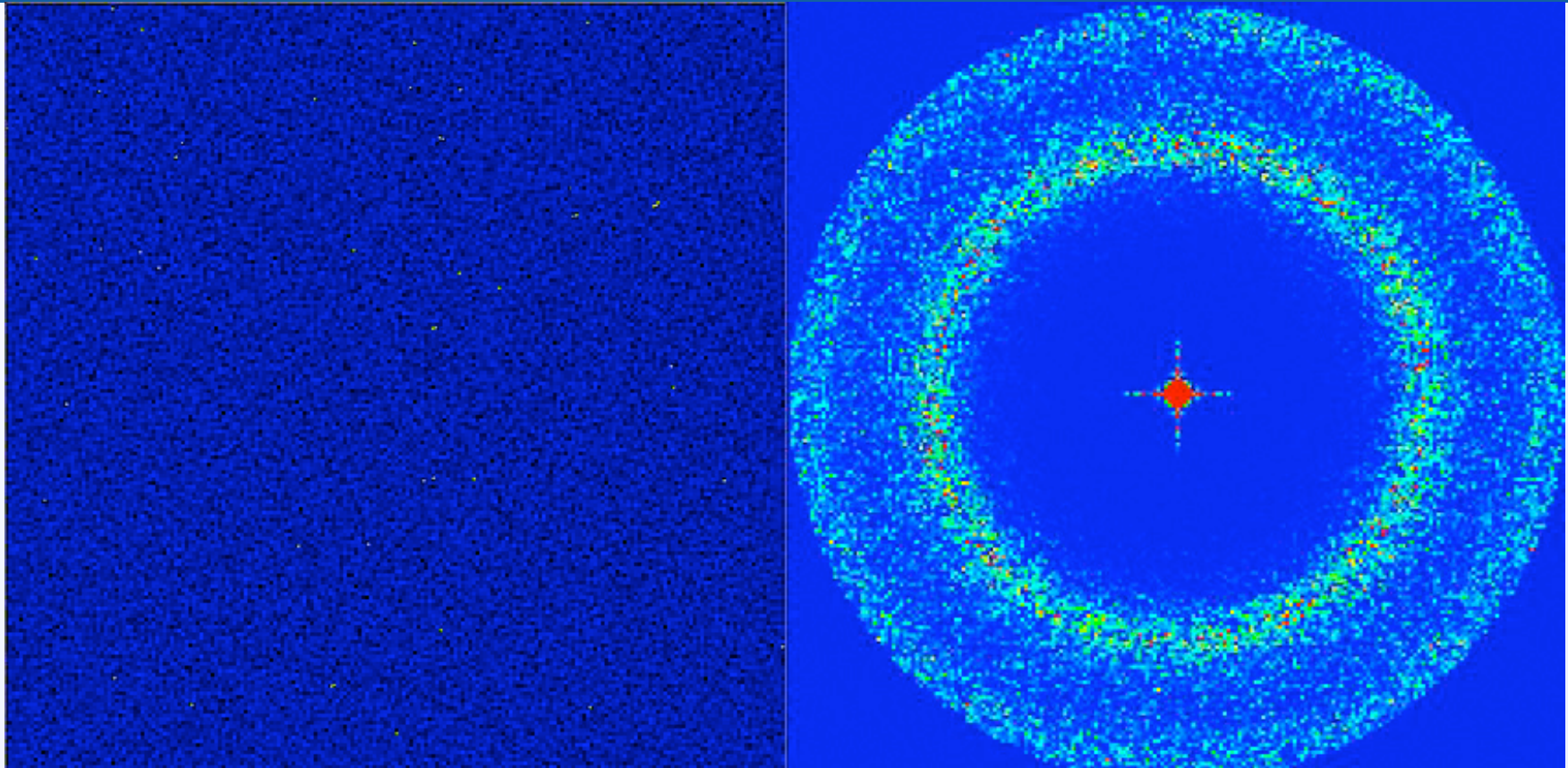


- ➡ Corroborate details with experiments where possible
- ➡ Condense results into phenomenological models which can be incorporated into hydrocodes



UNCLASSIFIED

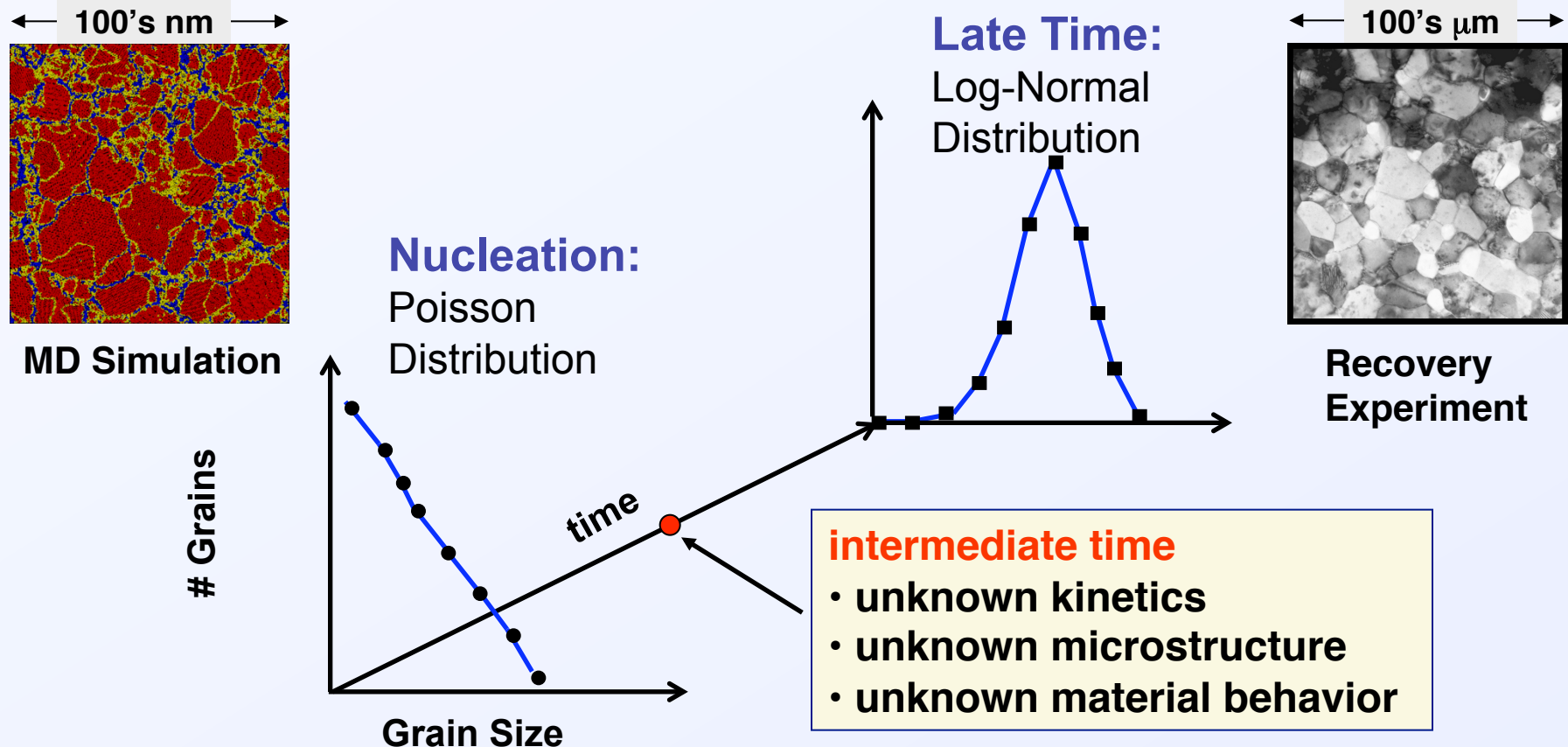
Molecular Dynamics (MD) are now large enough to model the initiation of realistic microstructure



Simulations suggest novel in situ x-ray scattering experiments using emerging sources such as LCLS



MD will not get us to the hydrodynamic time of interest

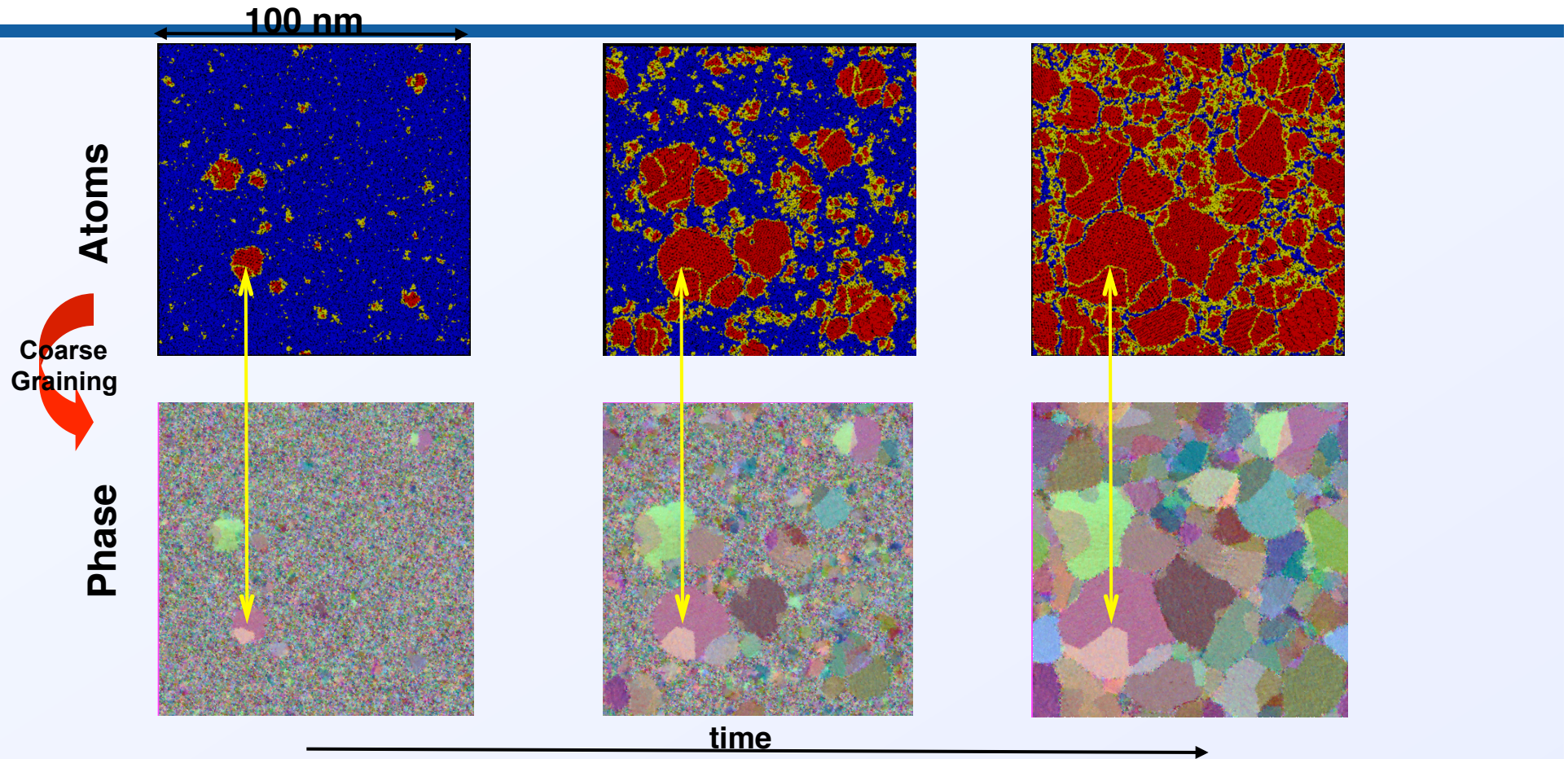


Phase-field modeling (PFM) will propagate MD nucleation results onto hydrodynamic length- and time-scales



UNCLASSIFIED

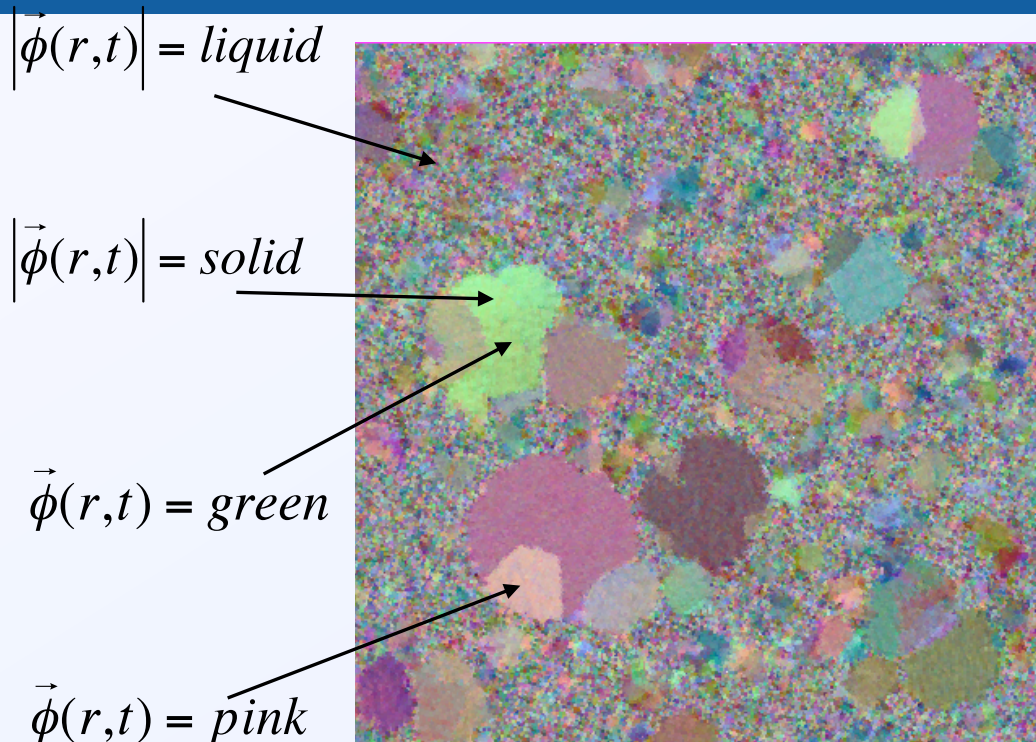
Propagate the phase order parameter using the molecular dynamics



New Multi-scale Paradigm: Phase Field Model and MD simulations that **overlap** in time and space



What is Phase Field modeling? - PFM



Thermodynamic representation of phase (or “color”) everywhere

- Each color represents a different value of the phase field $\vec{\phi}$ (solid orientation)
- Free energy describes how colors interact and evolve
- Accuracy depends on fidelity of physics in the equations

Evolution Equations

$$F(P,T) = \int dx \left\{ |\nabla \vec{\phi}|^2 + f(\vec{\phi}, P, T) + \dots \right\}$$

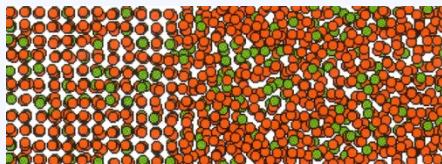
$$\frac{\partial \vec{\phi}}{\partial t} = -\Gamma \frac{\delta F}{\delta \vec{\phi}} + \text{noise}$$



What is Phase Field modeling? Basic Equations

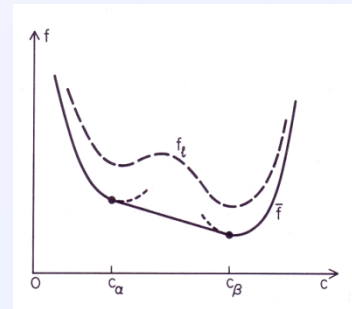
Phase Field modeling is time-dependent Ginzburg-Landau theory

Solid Liquid

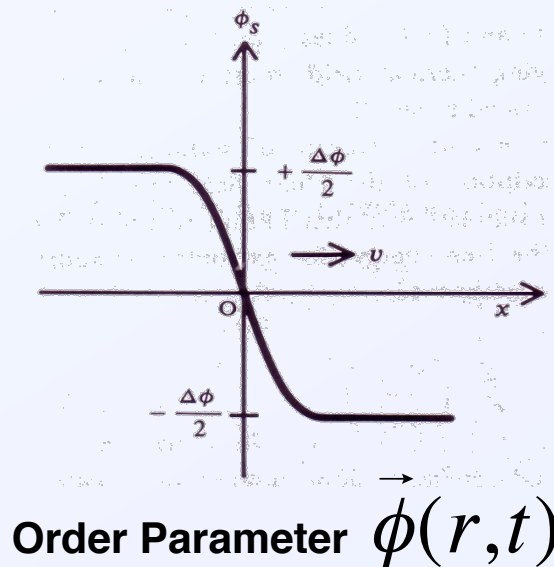


$$F(\phi) = \int dx \left[\frac{1}{2} |\nabla \phi|^2 + f(\phi, P, T) + f_{GB}(\nabla \theta) + f_{el} \right]$$

Total Free Energy of multi-phase material



Local Free Energy Density $f(\phi) \approx \phi(1 - \phi)(1 + \phi)$



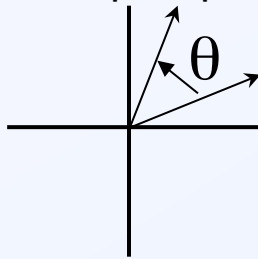
$$\frac{\partial \phi}{\partial t} = -\Gamma(-\nabla^2)^a \frac{\delta F}{\delta \phi} + noise$$

Kinetic Equation with Thermal Noise



Quaternions are used extensively to represent rotations, e.g. in computer graphics (games)

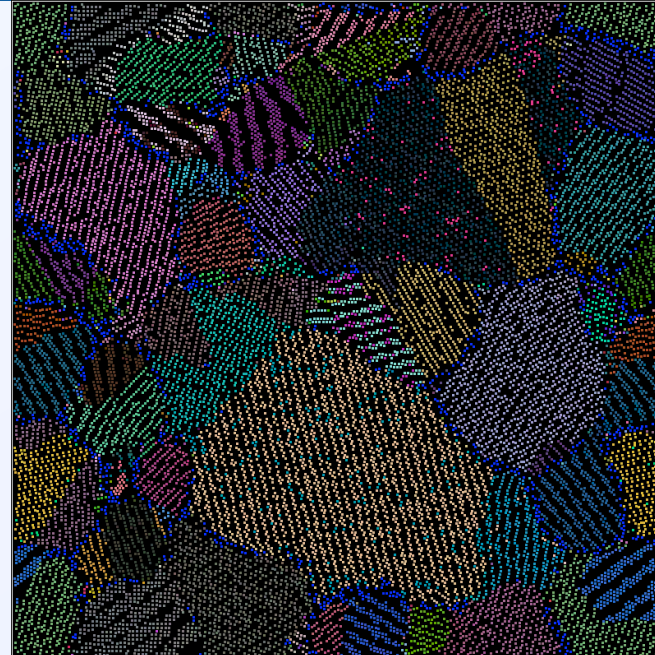
Complex numbers have the form, $a + ib$, and multiplying by $e^{i\theta}$ produces rotation by an angle θ in the complex plane



Quaternions have the form, $a + ib + jc + kd$, where $i^2=j^2=k^2=ijk=-1$. A rotation about the unit vector \hat{n} by an angle θ can be computed using the unit quaternion:

$$(s, v) = \left(\cos\left(\frac{\theta}{2}\right), \hat{n} \sin\left(\frac{\theta}{2}\right) \right)$$

We assign to each atom a quaternion that best represents the local value of the Q6 order parameter with the smallest rotation from a reference unit cell.



D. Richards

The associated quaternion enables quick calculation of the rotation between two misoriented grains (c.f. Reed et.al Acta Cryst. (2004) A60, 263-277)



What does a crystallographic-aware phase-field model of polycrystal solidification look like?

Pusztai et al., have proposed a 3D quaternion-based phase-field model

- Represents crystal orientation with quaternion order parameter
- Quaternions are widely used to analyze crystallography of polycrystal interfaces
- Quaternion algebra is fast, efficient, avoids singularities, ...

Free Energy

$$F = \int \left[\frac{\varepsilon_\phi^2}{2} |\nabla \phi|^2 + f(\phi, c, T) + HT[1 - p(\phi)] \left(\sum_i (\nabla q_i)^2 \right)^{1/2} \right] d^3r$$

Evolution

$$\frac{\partial q_i}{\partial t} = -M_q \frac{\delta F}{\delta q_i} + \xi_i = M_q \left[\nabla \cdot \left(D \frac{\nabla q_i}{|\nabla q_i|} \right) - 2\lambda q_i \right] + \xi_i$$

Where q_i is the quaternion order parameter, M_q is the associated mobility and ξ is the fluctuation in q .

We have implemented the Pusztai model in our 3D AMR code

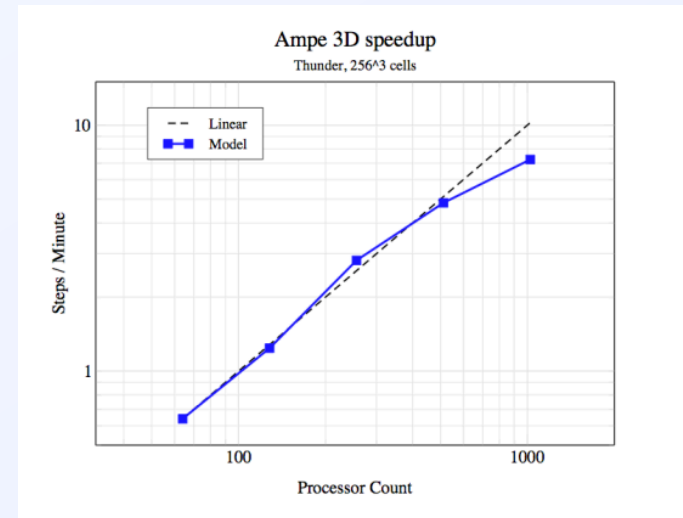
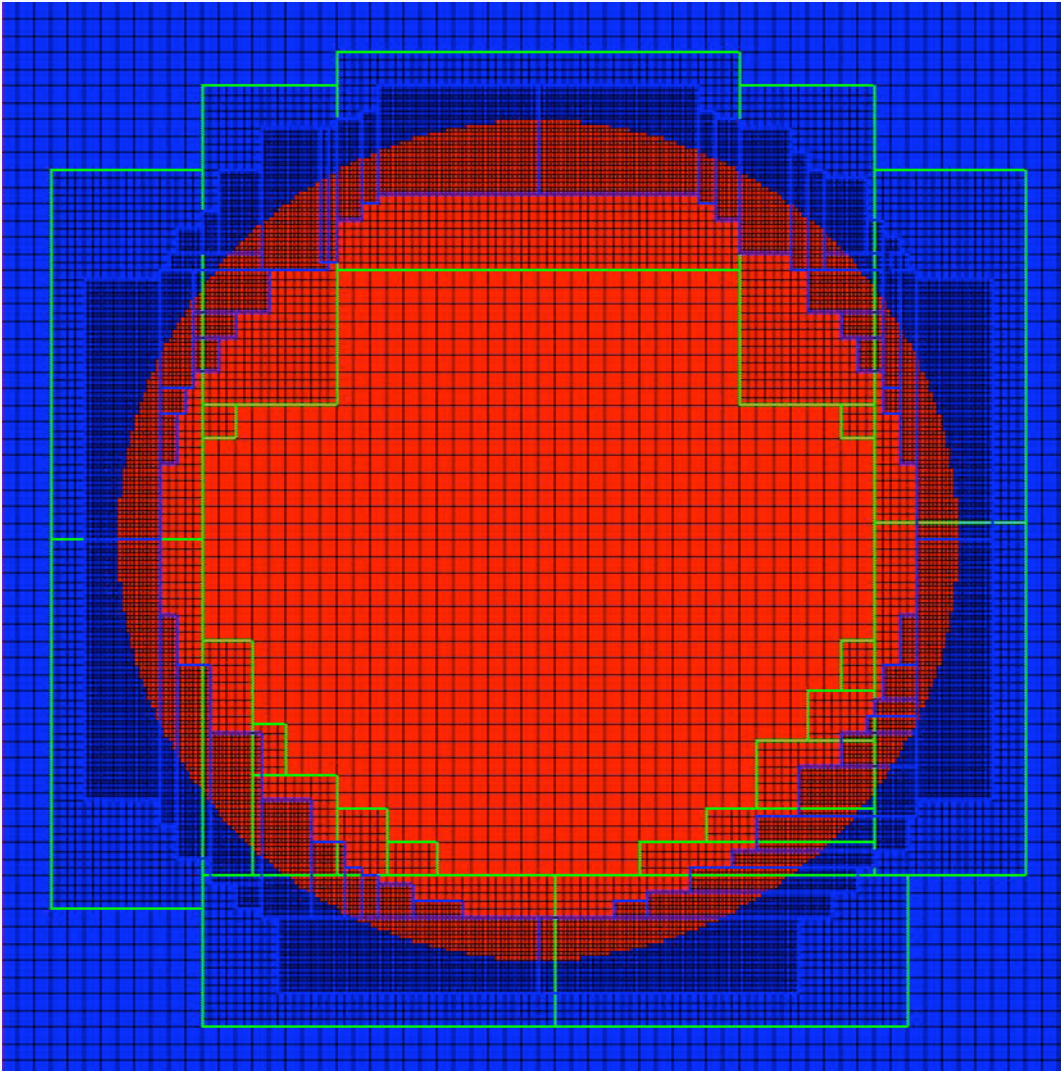
- Enhance energy functional to represent energetics of grain boundaries
- Crystal symmetry aware quaternion mathematics
- Extend energy functional to include elasticity and alloy concentration

Refs: T. Pusztai, G. Bortel, and L. Granasy, "Phase field theory of polycrystalline solidification in three dimensions," Europhys. Lett, 71 (2005) 131-137; R. Kobayoshi and J.A Warren, "Modeling the formation and dynamics of polycrystals in 3D," Physica A 356 (2005) 127-132.



UNCLASSIFIED

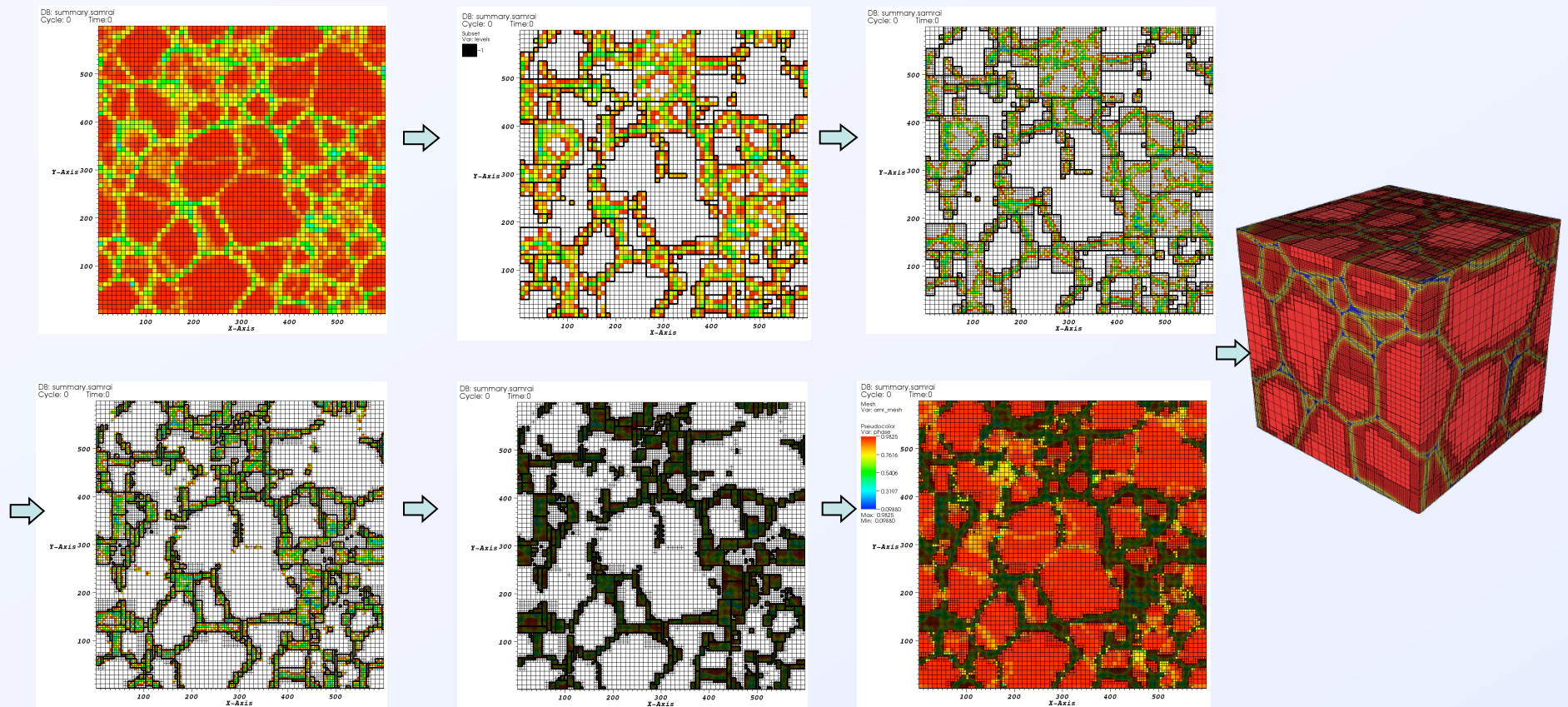
Model Problem: Single Spherical Grain (2D with scalar order-parameter)



We obtain strong scalability to thousands of processors by leveraging LLNL's investment in parallel computing (e.g. SAMRAI)

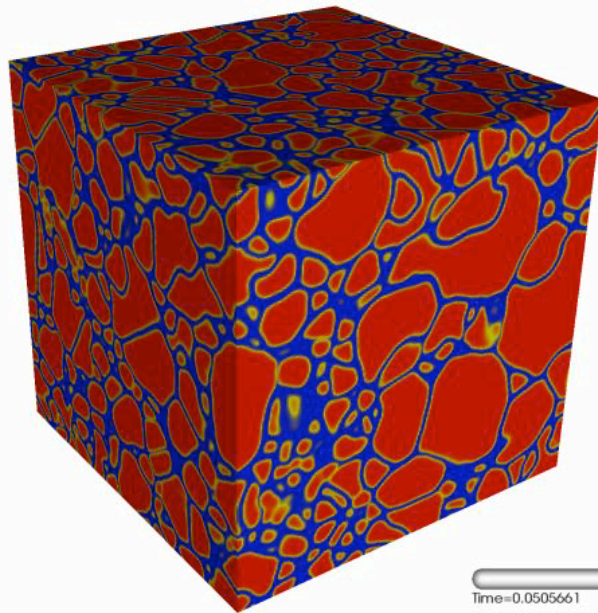
UNCLASSIFIED

Representation of MD Data onto the AMR Grid Hierarchy - 2D example

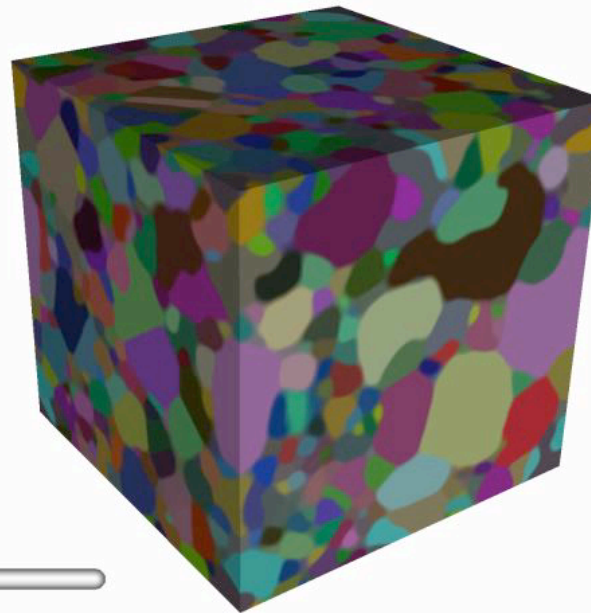


UNCLASSIFIED

MD nucleated microstructure onto the micro-second hydro time-scale with the crystallographic quaternion model

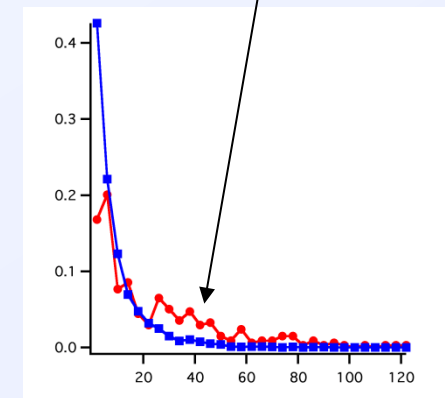


Phase Order Parameter



Quaternion Order Parameter

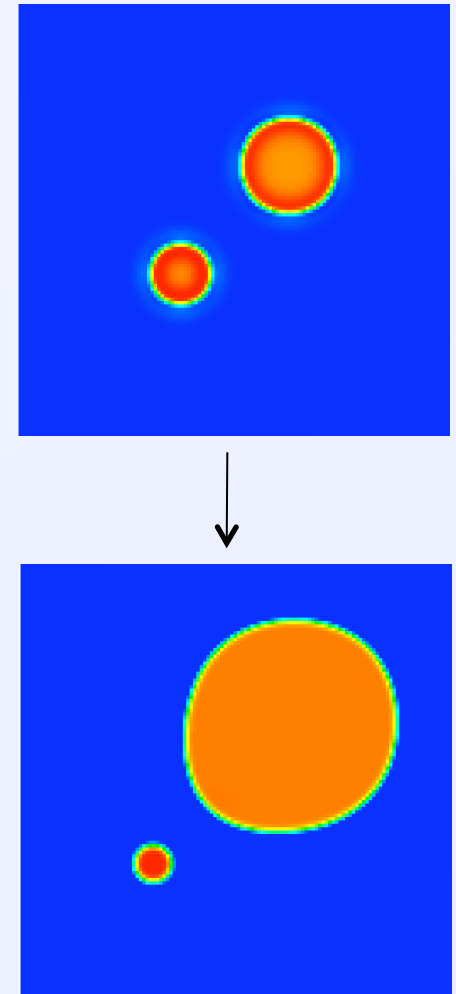
Growth of large grains
Blue: MD nucleation
Red: Phase-field evolution



While significant grain coarsening has occurred on the microsecond scale, the microstructure is far from log-normal

At the meso-scale each phase is spatially resolved and diffusion is solved through the evolving multi-phase microstructure

- Need to know:
 - Validated representation of alloy phase diagram and thermodynamic driving forces
 - Validated multi-species concentration-dependent mobilities in each phase (diffusivities) – both ambient and irradiation enhanced
 - Validated representation of internal boundary mobility – both inter-phase and inter-grain
 - Validated representation of phase nucleation – the phase-field uses this as input
 - Effects of microstructure (grain boundaries, dislocations, pores, cracks, ...) in species migration



CALPHAD is a Phenomenological Approach to Thermodynamics characterized by Models, Gibbs Energy Functions, and the concept of Lattice Stability

Gibbs Energy for Unary Phases

$${}^0G_i^\phi(T) - H_i^{SER}(298.15K) = a + bT + cT \ln(T) + d_2T^2 + d_3T^3 + d_{-1}T^{-1} + d_nT^n$$

Gibbs Energy of a Line Compound

$$G^{A_mB_n}(T) = \sum_i c_i {}^0G_i^{SER}(T) + a + bT + \dots$$

Gibbs Energy for Multi-component Phases

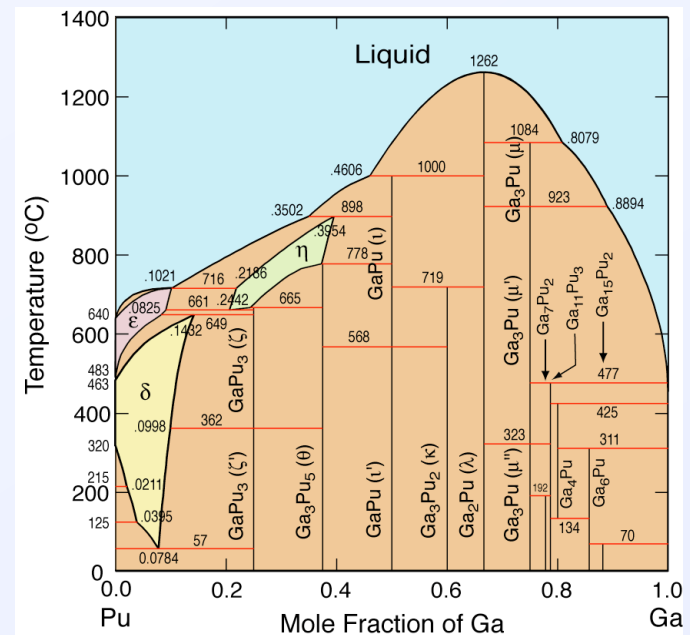
$$G^\phi(\{c_i\}, T) = {}^{ref}G^\phi(\{c_i\}, T) + {}^{ideal}G^\phi(\{c_i\}, T) + {}^{xs}G^\phi(\{c_i\}, T)$$

$${}^{ref}G^\phi(\{c_i\},T)=\sum_i c_i^0 G_i^\phi(T)$$

$$^{ideal}G^\phi(\{c_i\},T) = RT \sum_i c_i \ln c_i$$

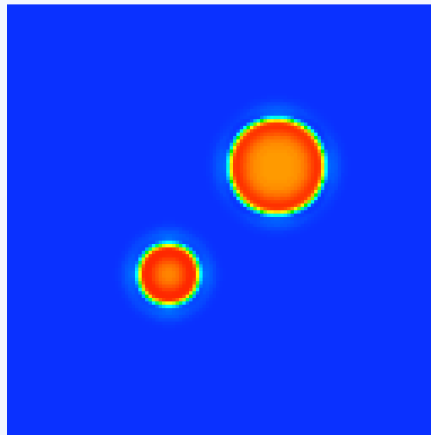
$${}^{xs}G^{\phi}(\{c_i\},T)=\sum_{i,j>i}c_ic_j\sum_{p=0}^n{}^pL_{ij}^{\phi}(T)(c_i-c_j)^p$$

$${}^pL_{ij}^\phi = {}^pa_{ij}^\phi + {}^pb_{ij}^\phi T + \dots$$

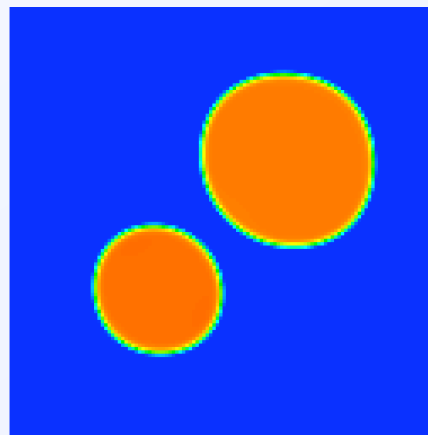


Ref. P. E. A. Turchi, L. Kaufman, S. Zhou, and Z.-K. Liu,
"Thermodynamics and Kinetics of Transformations in Pu-
based Alloys," J. Alloys and Comp, 444-445 (2007) 28-35.

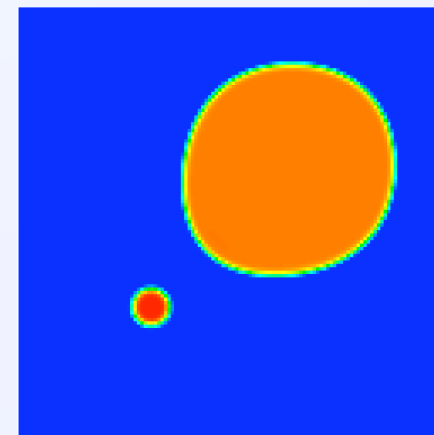
Coring in PuGa alloys



t=0.01 sec



t=6.95 sec



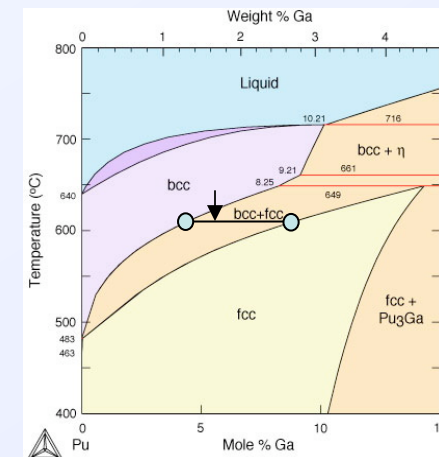
t=37.9 sec

6.4 microns

$$\frac{d}{dt}c = \nabla \cdot D(c, \phi) \nabla c + \nabla \cdot D(c, \phi) h'(\phi) (c_l - c_s) \nabla \phi$$

We have implemented the concentration model of Kim et al. (1999) in our quaternion PFM code and **validated** our code with the published simulations on Pu-Ga of Hu et al. (2007).

- Non-equilibrium phase fraction growth
- Explicit grain orientation prevents coalescence
- Late time Ostwald ripening

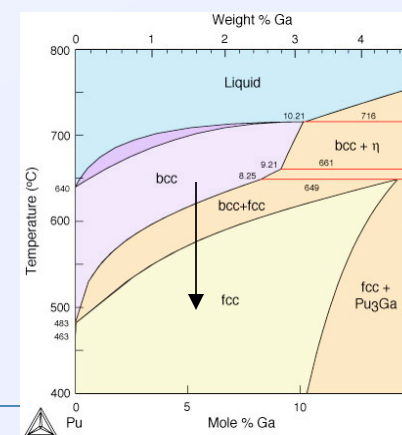
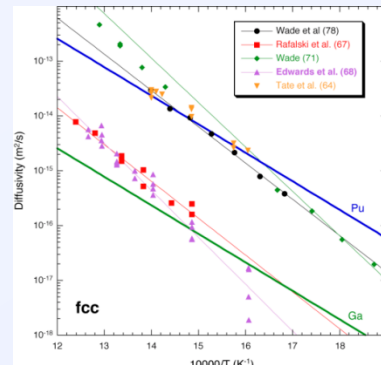
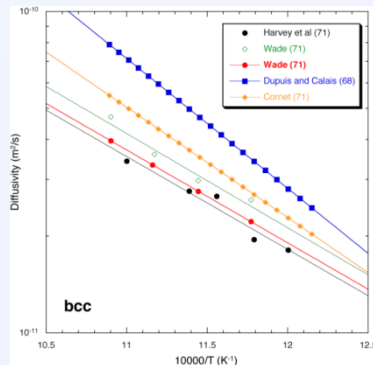
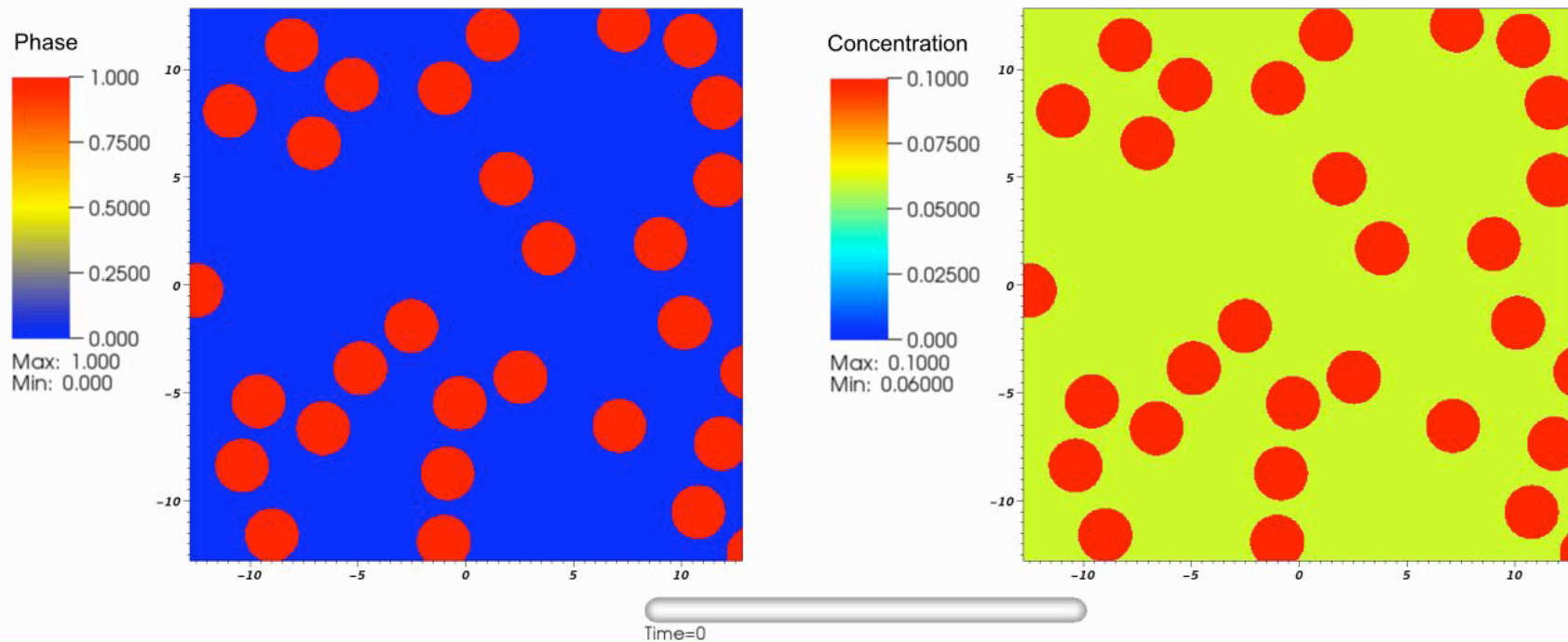


CALPHAD Alloy Phase Diagram



Coring in Alloys (e.g., bcc \rightarrow fcc)

Thermodynamic driving force & Diffusion (here $D^{\text{bcc}} \gg D^{\text{fcc}}$)



Bubbles - Equations

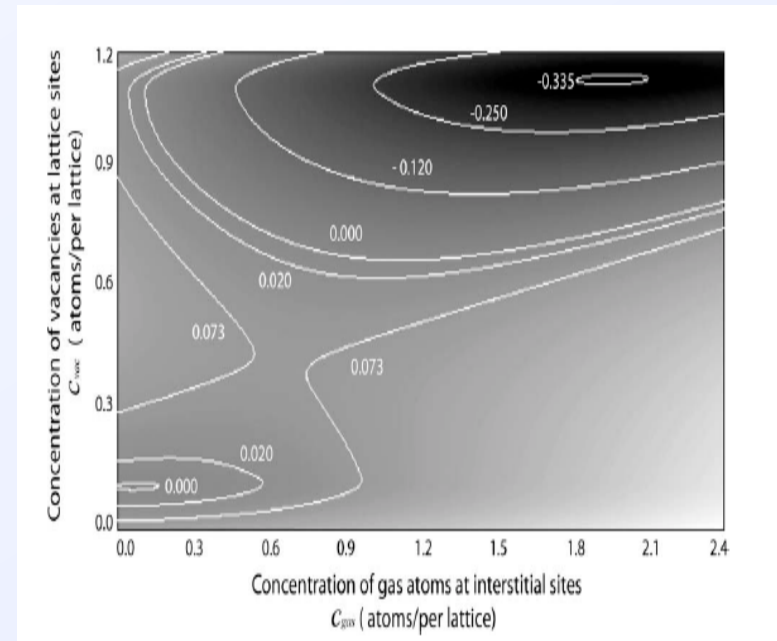
Recently, Shenyang Hu (PNNL, JNM 2009) proposed the phase-field model for bubble formation

$$F = \int (F(c_{gas}, c_{vac}) + \kappa_{gas} |\nabla c_{gas}|^2 + \kappa_{vac} |\nabla c_{vac}|^2 + F_{elastic}) dV$$

$$F(c_{gas}, c_{vac}) = f_{vac}(c_{vac}^4 + Ac_{vac}^3 + Bc_{vac}^2 + Cc_{vac} + D) + f_{gas}(c_{gas} - c_{gas}^0) + E(c_{gas} - c_{gas}^0)(c_{vac} - c_{vac}^0)$$

$$\frac{\partial c_{g/v}}{\partial t} = \nabla \cdot M_{g/v} \nabla \frac{\delta E(c_g, c_v)}{\delta c_{g/v}(r, t)} + \dot{g}_{g/v}(r, t)$$

$$M_{g/v} = M_{g/v}^0 (1 + f(|\nabla \phi|, c_v(r, t)))$$



Paul C. Millett^a, Dilpuneet S. Aidhy^b, Tapan Desai^a, Simon R. Phillpot^b, Dieter Wolf^a^aMaterials Science Department, Idaho National Laboratory, Idaho Falls, USA^bDepartment of Materials Science and Engineering, University of Florida, Gainesville, USA

Grain-boundary source/sink behavior for point defects: An atomistic simulation study

Dedicated to Professor Dr. Günter Gottstein on the occasion of his 65th birthday

$D_v = 0.021 \text{ nm}^2/\text{ps}$, Millet, IJMR, 2009

$\text{BFV} = 6.4 \times 10^{-11} \text{ m}^3 / \text{m}^2$,

Svindclerman, JMS, 2006

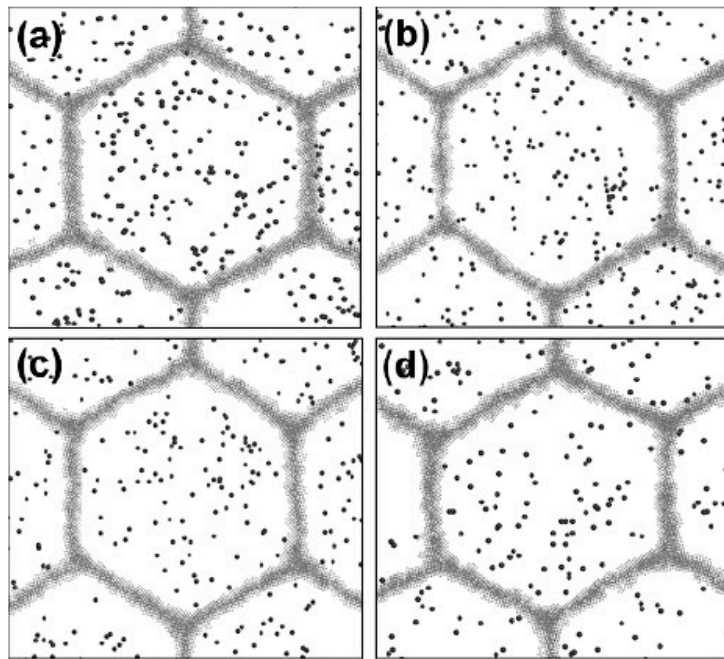


Fig. 6. Progressive snapshots of the vacancy population in a single grain of the over-saturated sample taken at (a) $t = 0$ ps, (b) $t = 72$ ps, (c) $t = 205$ ps, and (d) $t = 1025$ ps (see also Fig. 3). The initial vacancy concentration is twice that at equilibrium. The evolution is quantified in the upper curve of Fig. 5.

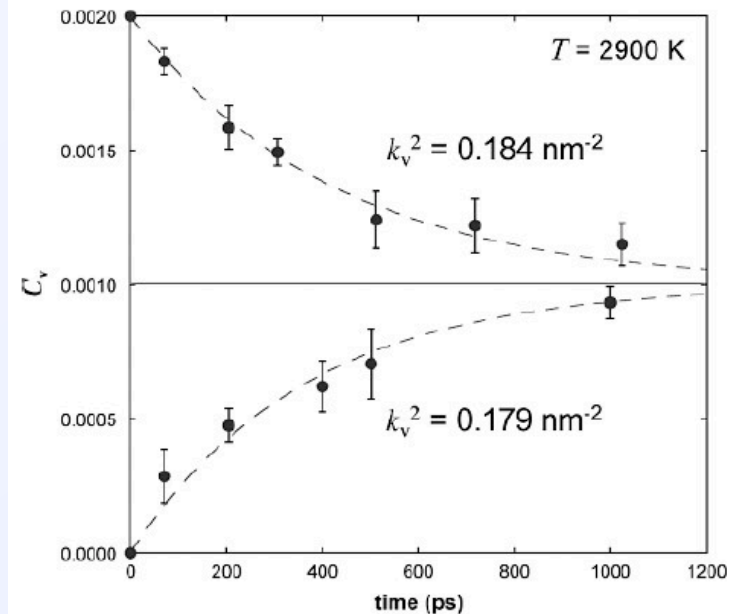
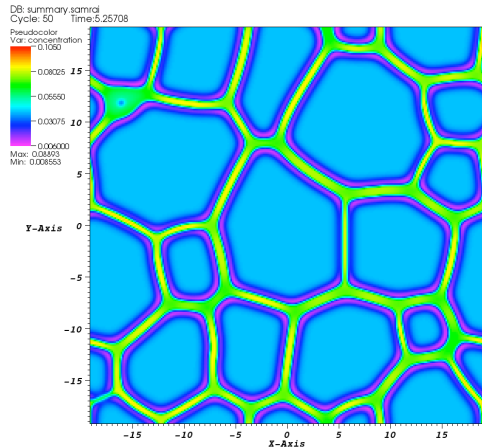


Fig. 5. Evolution of the vacancy concentration in the under- and over-saturated nanocrystalline structures at $T = 2900$ K (see Figs. 3 and 6). In both cases c_v evolves exponentially towards equilibrium concentration of $c_v^{\text{eq}} = (1 \pm 0.1) \times 10^{-3}$. The dashed lines represent fits to Eq. (4), yielding the GB sink and source strengths of $k_v^2 = 0.184 \text{ nm}^{-2}$ and $k_v^2 = 0.179 \text{ nm}^{-2}$, respectively.

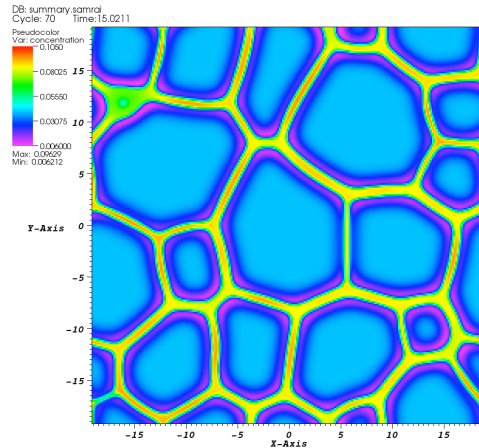
Redistribution of the vacancies to the GBs, parameters from Millet's MD study of hi T Mo

UNCLASSIFIED



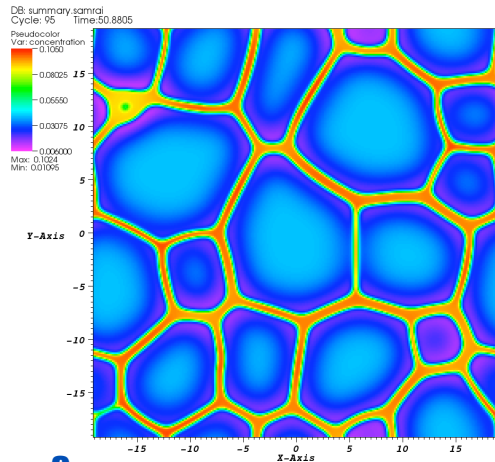
1

user: wickett
Thu Jul 23 16:51:33 2009



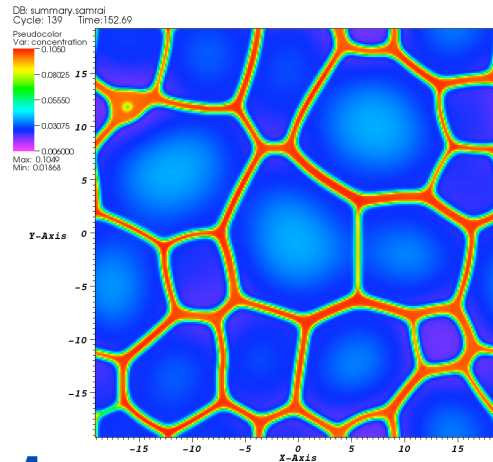
2

user: wickett
Thu Jul 23 16:51:42 2009



3

user: wickett
Thu Jul 23 16:52:04 2009



4

user: wickett
Thu Jul 23 16:52:12 2009

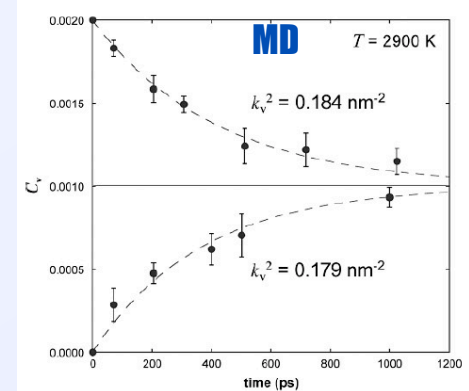
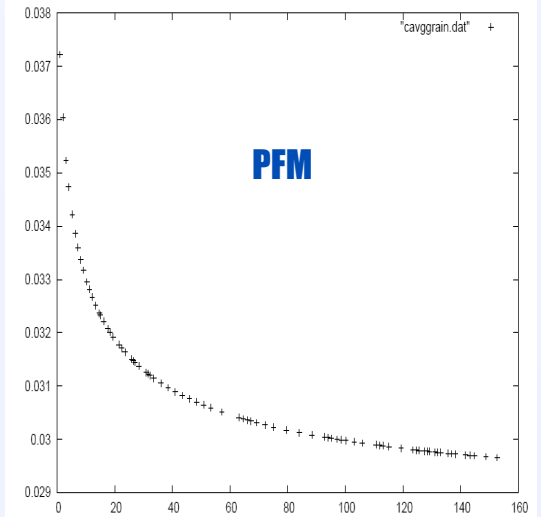
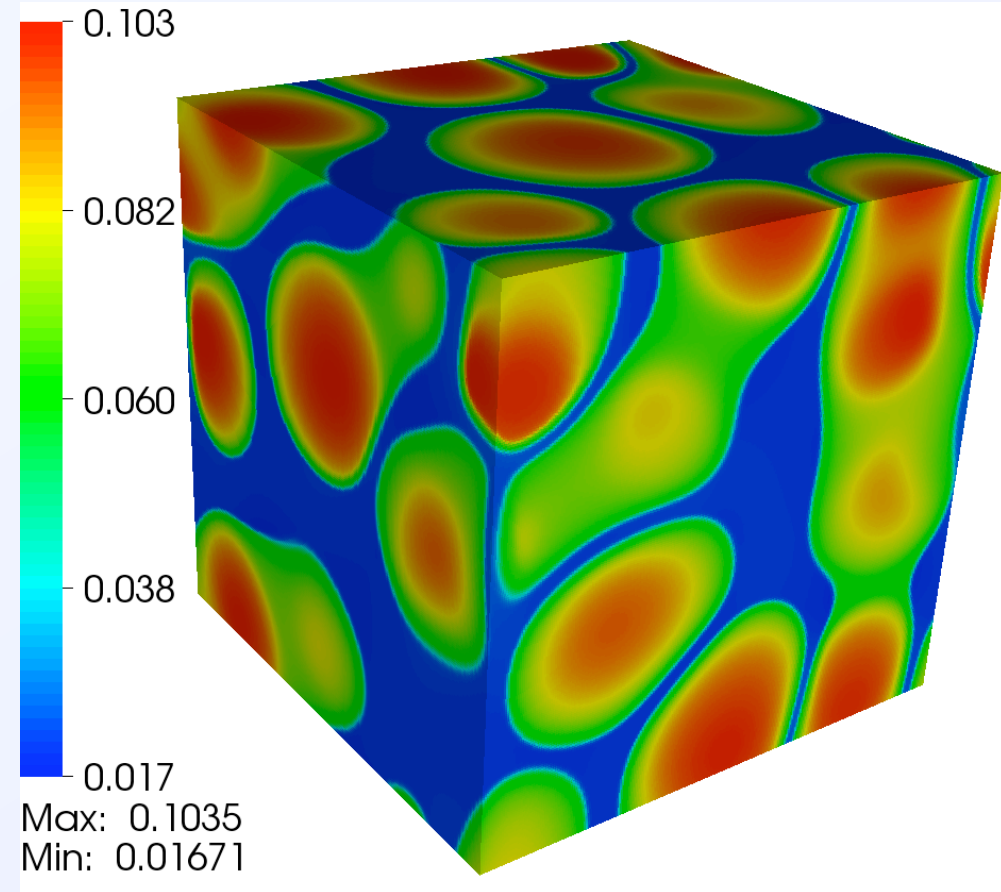


Fig. 5. Evolution of the vacancy concentration in the under- and over-saturated nanocrystalline structures at $T = 2900 \text{ K}$ (see Figs. 3 and 6). In both cases C_v evolves exponentially towards equilibrium concentration of $C_v^{\text{eq}} = (1 \pm 0.1) \times 10^{-3}$. The dashed lines represent fits to Eq. (4), yielding the GB sink and source strengths of $k_v^2 = 0.184 \text{ nm}^{-2}$ and $k_v^2 = 0.179 \text{ nm}^{-2}$, respectively.



Conclusions:

Phase-field modeling offers the prospect to understand microstructure development following phase-transformation in the presence of diffusing alloy and other species.



UNCLASSIFIED

Thank you for your attention!





The Response of Aluminium Alloys to Shock Loading – Shear Strength and Microstructural Development

Jeremy Millett

jeremy.millett@awe.co.uk

www.awe.co.uk



Co-Authors

- Neil Bourne
 - AWE, Aldermaston
- Ming Chu, Ian Jones
 - Dept. Met. Mat / Centre for Electron Microscopy,
University of Birmingham
- Rusty Gray
 - MST-8, Los Alamos National Laboratory
- Gareth Appleby-Thomas
 - Cranfield Defence and Security

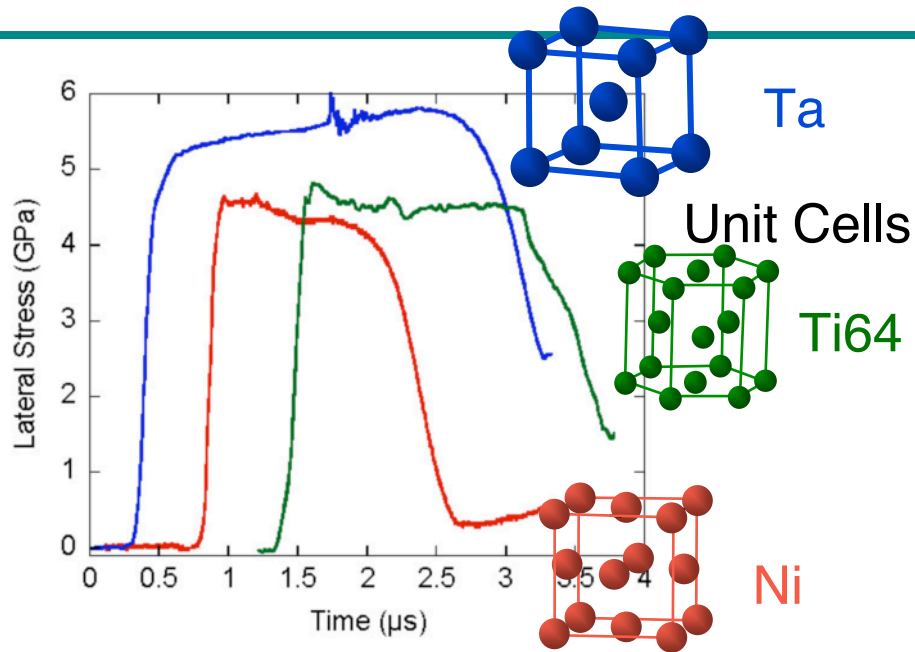


Shock Loading Experiments

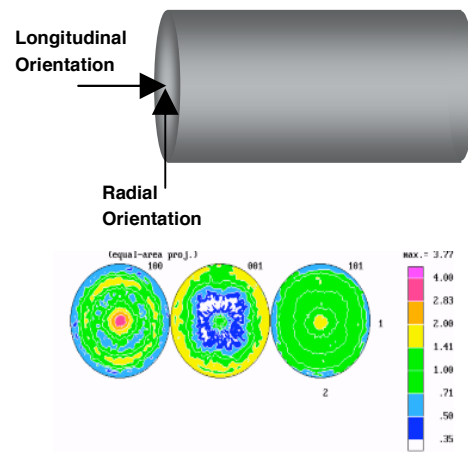
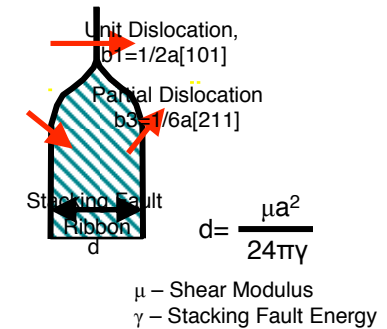
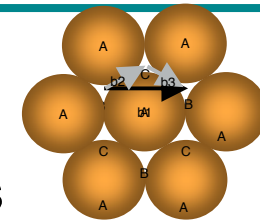
- Time resolved
 - Measurement of shock profiles (stress, velocity *etc*)
 - Observation of waves via high-speed photography, flash x-ray, proton radiography *etc*
- Time integrated
 - Post-mortem analysis of shocked samples
 - Microstructure, chemistry, mechanical properties
 - Loading + Pulse Duration + Release
- Major assumption
 - Sample is semi-infinite



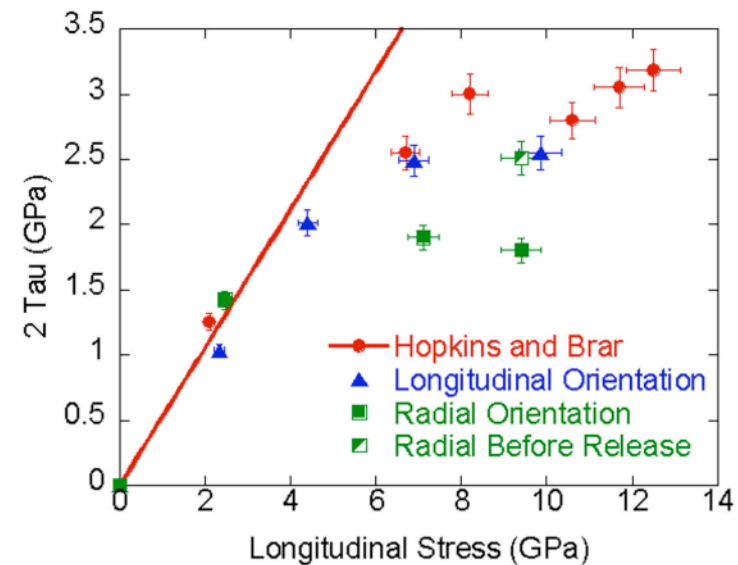
Introduction



Stacking fault Energy - FCCs

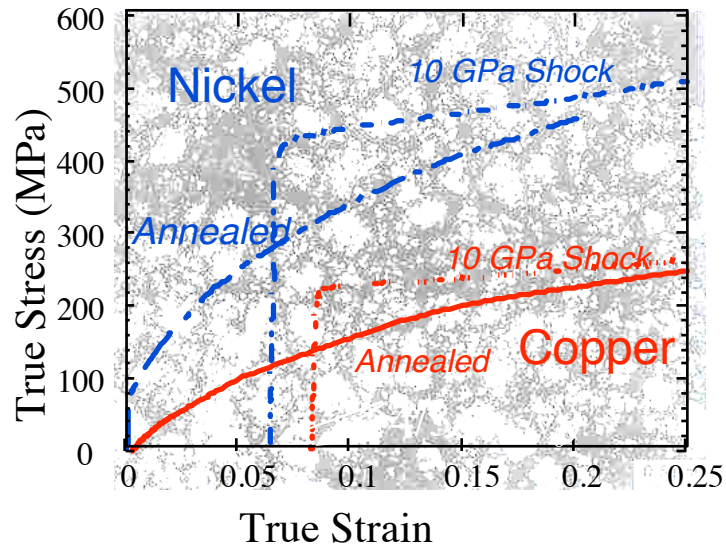


Anisotropy - Ti64

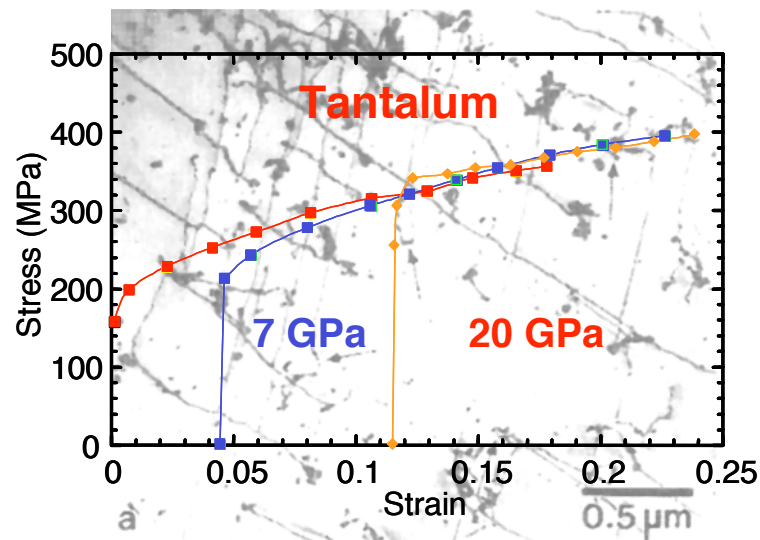




Post Shock Properties



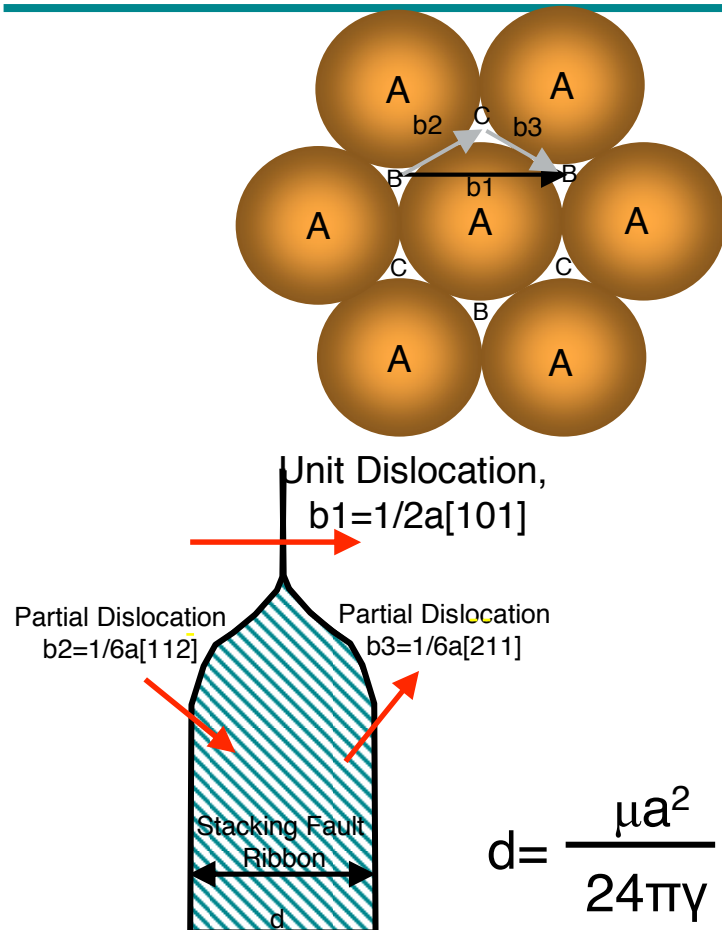
- High stacking fault FCCs show hardening behind shock front. Recovered samples show greater hardness compared to as-received material – dislocation generation – cells



- BCCs show softening behind shock front. No hardening in recovered samples compared to as-received material – motion of existing dislocations



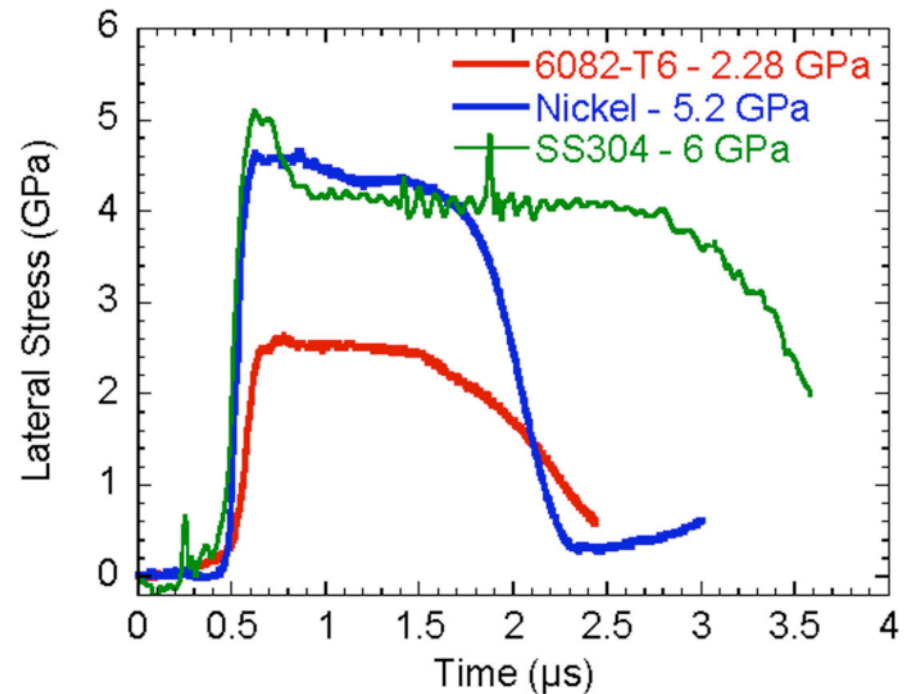
Variations Within FCC Lattice



Extended dislocation on (111) plane

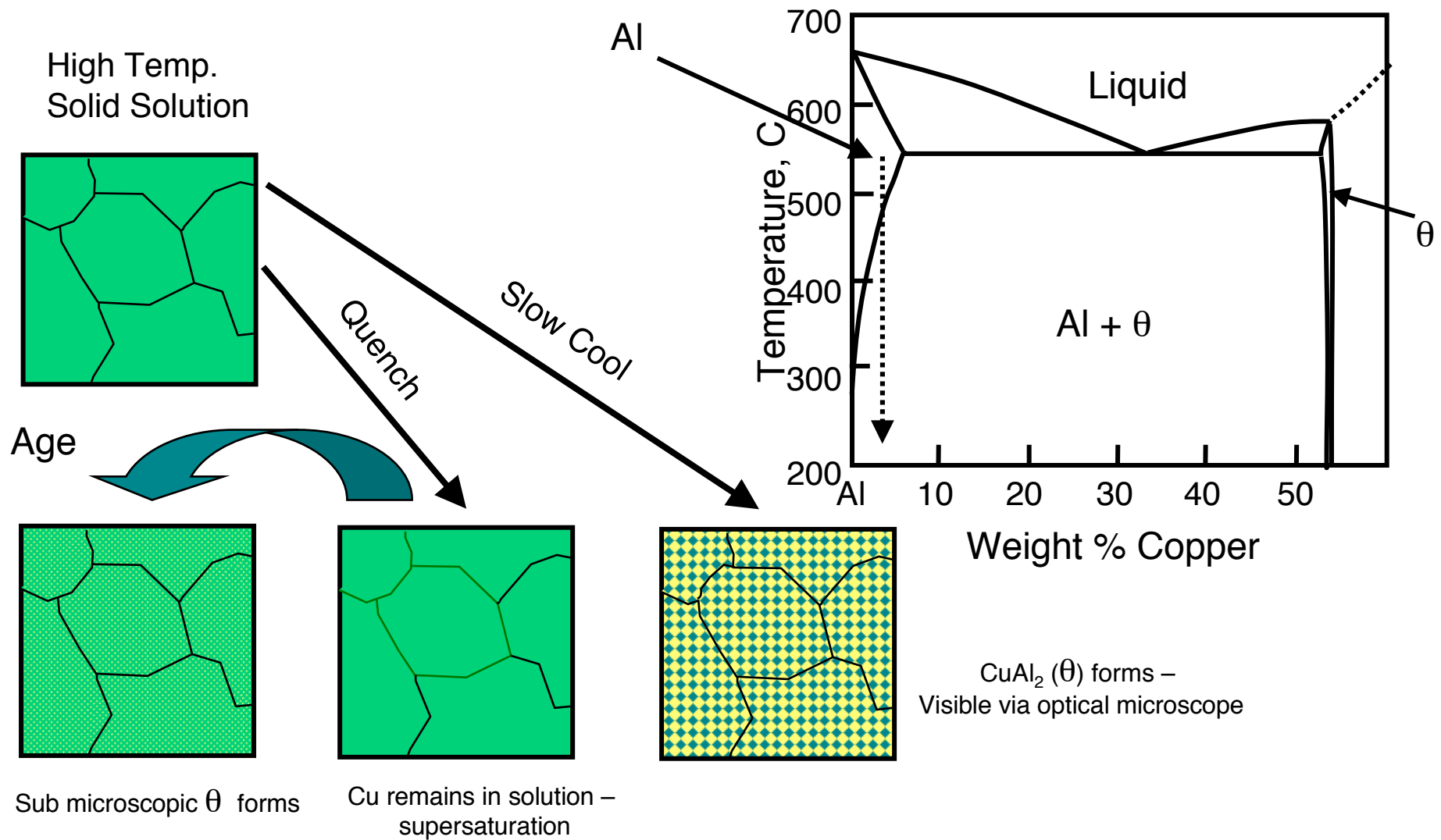
μ – Shear Modulus

γ – Stacking Fault Energy





Age Hardening



- **Al-6061**
 - Solution treated 550°C 3 hours, water quench (T0)
 - Stored at -18°C to prevent RT aging
 - Solution treated-Aged 180°C 8 hours, air cool (T6)
- **Al 5083-H32**
 - 20% Cold Work
- **Al 6082-T6 As-Received off the Shelf**

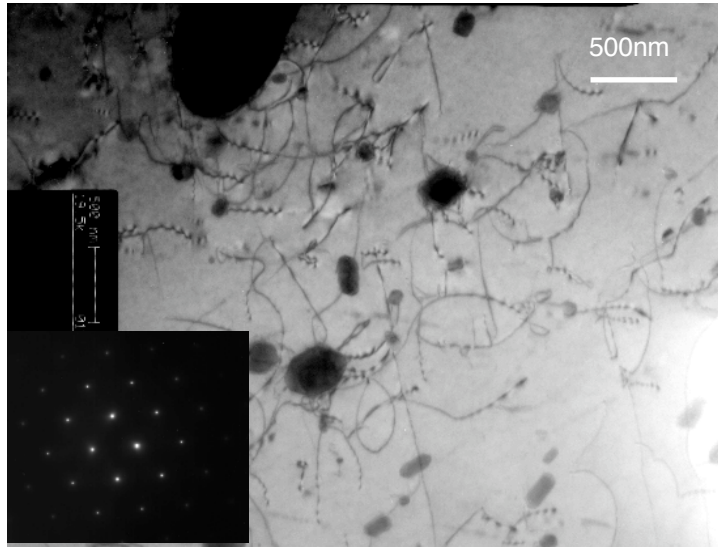
Chemical composition (wt%)

6061								
Si	Fe	Cu	Mn	Mg	Cr	Zn	Ti	Al
0.4 - 0.8	0.7	0.15 - 0.4	0.15	0.8 - 1.2	0.04 - 0.35	0.25	0.15	bal
5083								
0.4	0.4	0.1	0.4-1.0	4.0-4.9	0.05-0.25	0.25	0.15	bal
6082								
0.7-1.3	0.5	0.1	0.4-1.0	0.6-1.2	0.25	0.2	0.1	bal

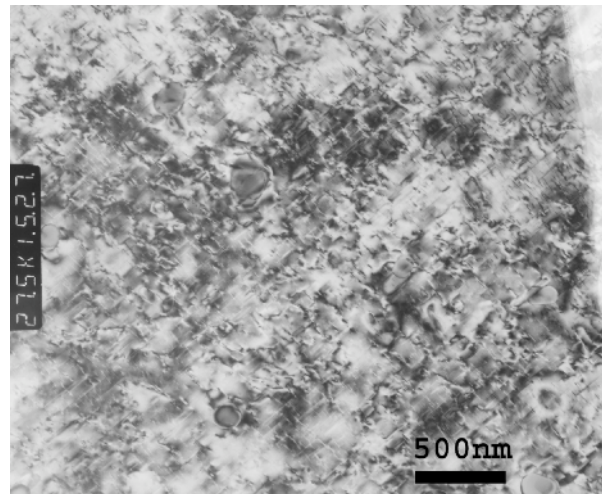
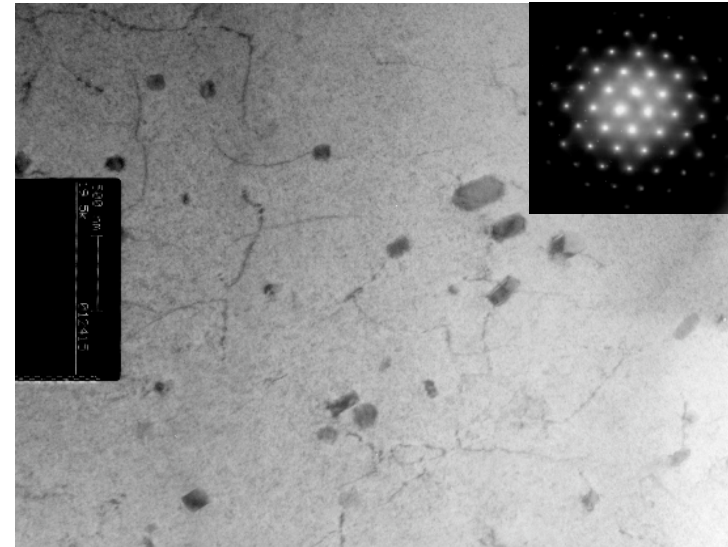


As-Received Al-6061 Microstructure

6061 T0



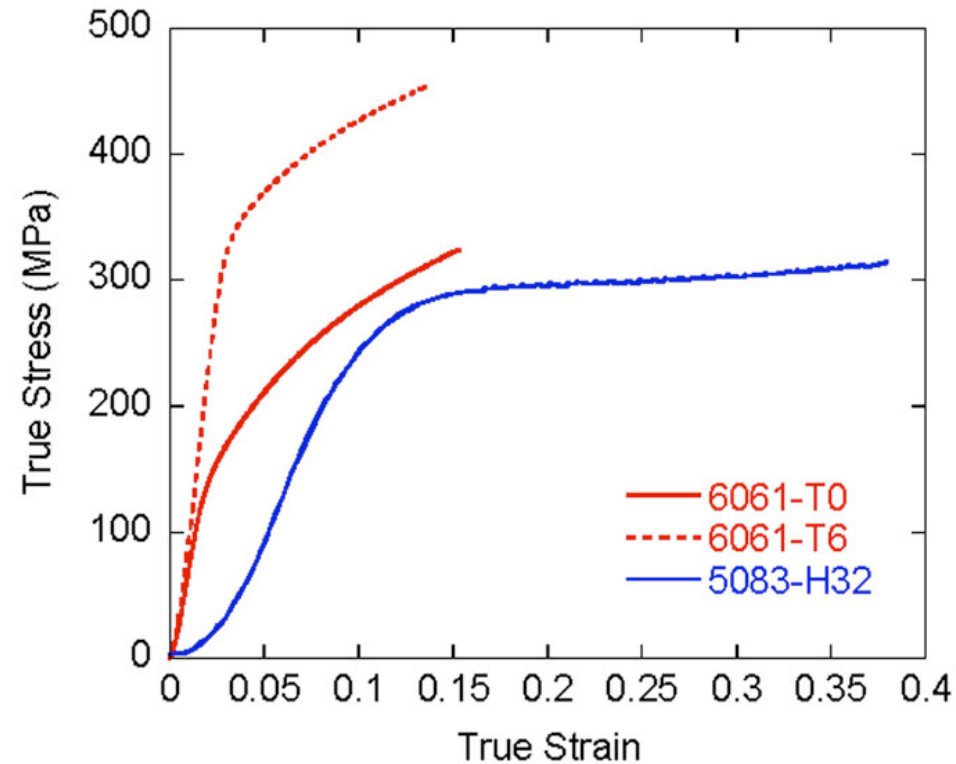
6061 T6



5083-H32



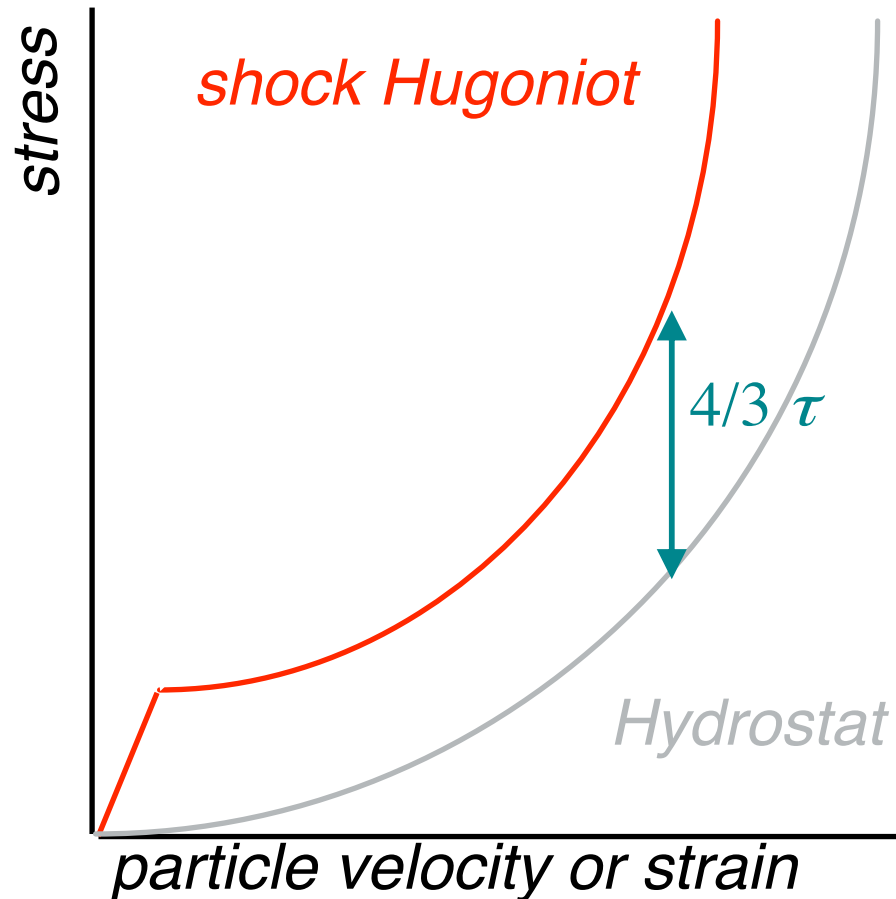
As-Received Properties



	c_L (mm μs^{-1})	c_S (mm μs^{-1})	ρ_0 (g cc $^{-1}$)	ν
6061	6.32	3.15	2.70	0.34
5083-H32	6.32	3.11	2.67	0.34
6082-T6	6.32	3.15	2.70	0.34



Measurement of Shear Strength



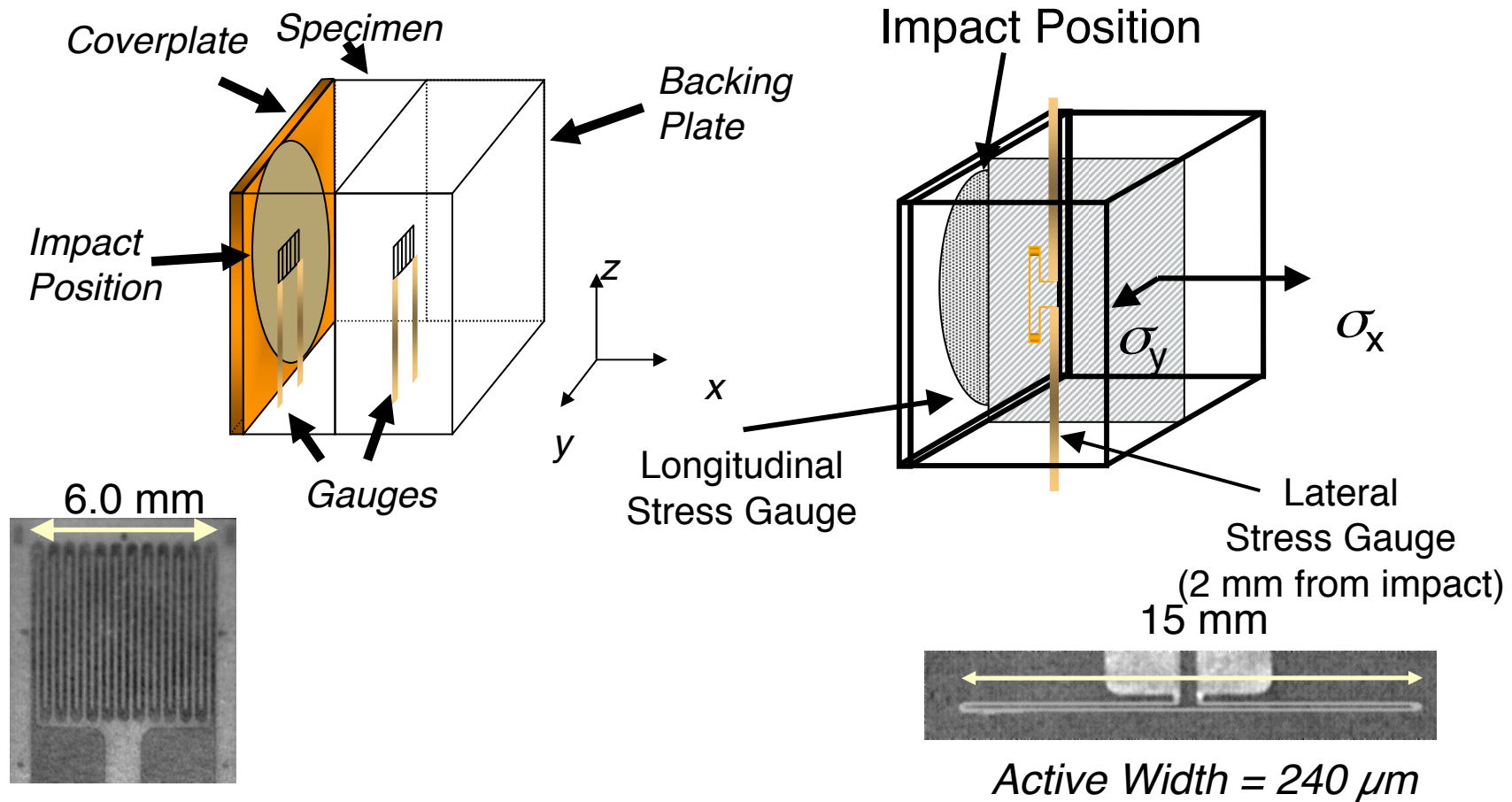
- **Shear stress** indication of a materials ballistic performance.
- Traditionally measured as offset of Hugoniot from hydrostat - theoretically derived.

BUT

- $2\tau = \sigma_x - \sigma_y$
- Can be deduced by directly measuring orthogonal components of stress



Specimens and Gauges



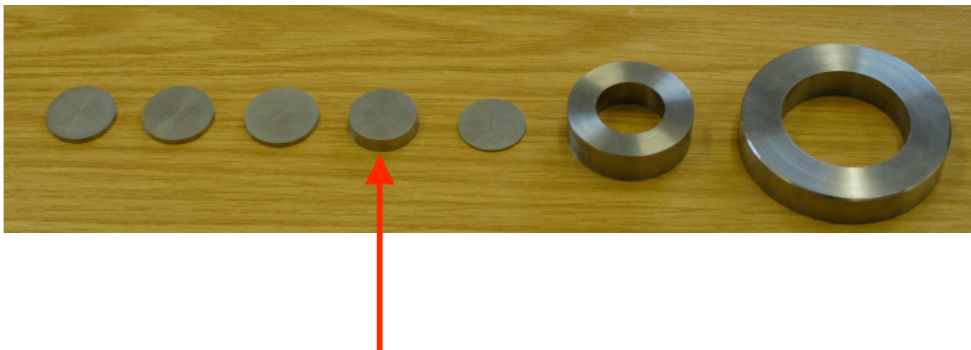


Recovery Fixture



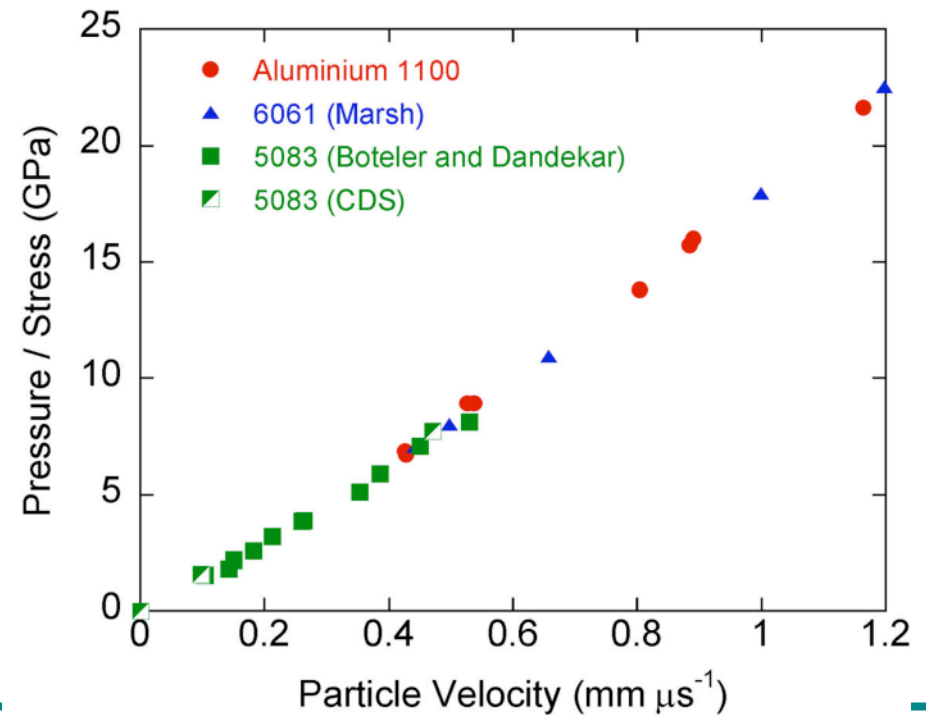
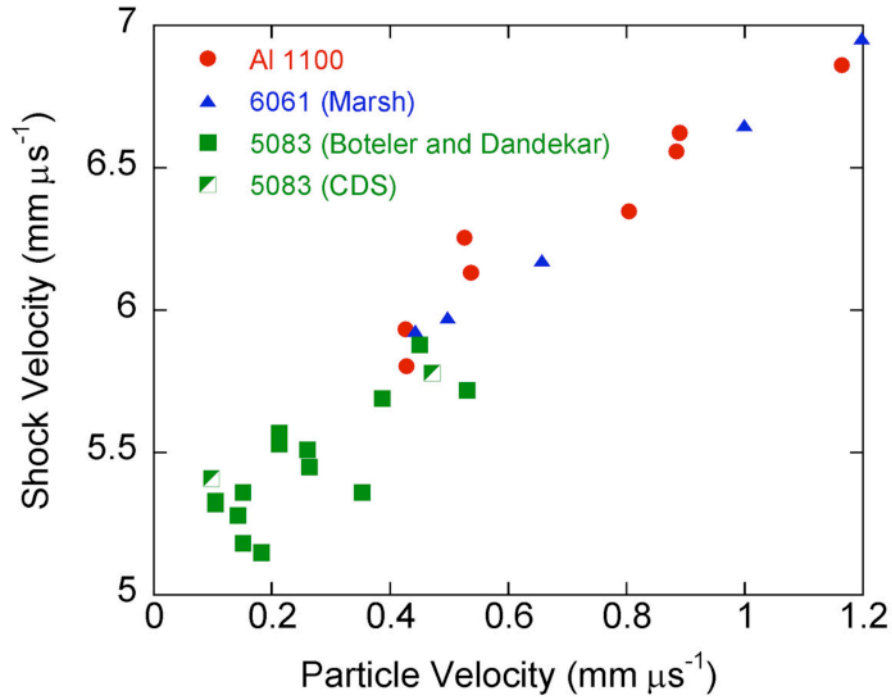
- Input shock needs to see monolithic specimen
- Releases need to see interfaces to be trapped
- Machining tolerances $\pm 2 \mu\text{m}$
- Each specimen takes 2 weeks to make

*Bourne and Gray Proc. R. Soc. A **461** 3297 (2005)*



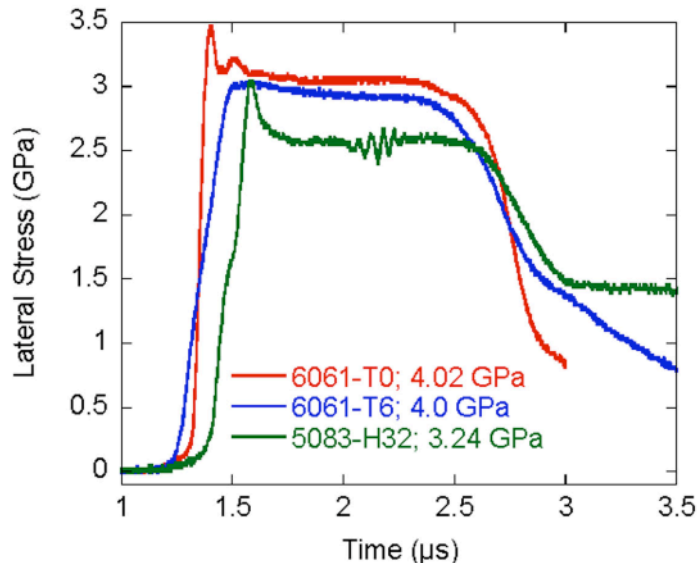
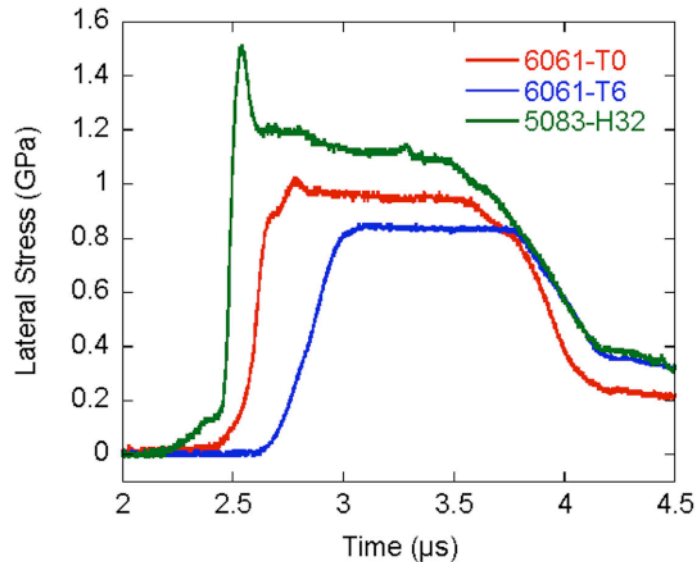


Aluminium Alloys EoS





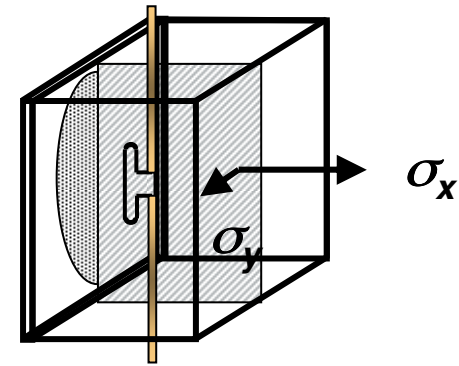
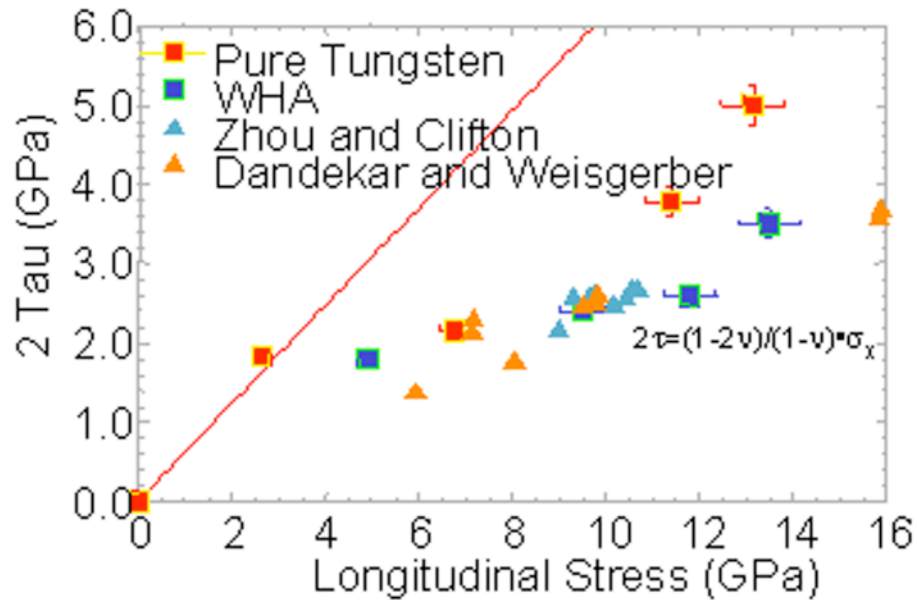
Lateral Stress Histories in 6061



- T0 traces higher amplitude than T6
 - To be expected as T6 is stronger
- T0 reach steady stress level faster than T6
 - Single phase material – dislocations move and interact faster without interference from intermetallic particles
- T0 has faster rise times than T6
 - Less interference from intermetallics
- 5083 lower strength than 6061
- Hardening behind shock front lower at higher stresses
 - Higher initial dislocation density



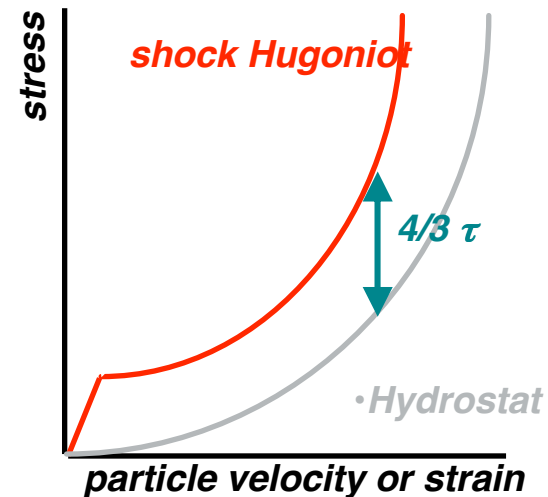
Agreement with Other Techniques ?



J. Appl. Phys. 86 (1999) 6702



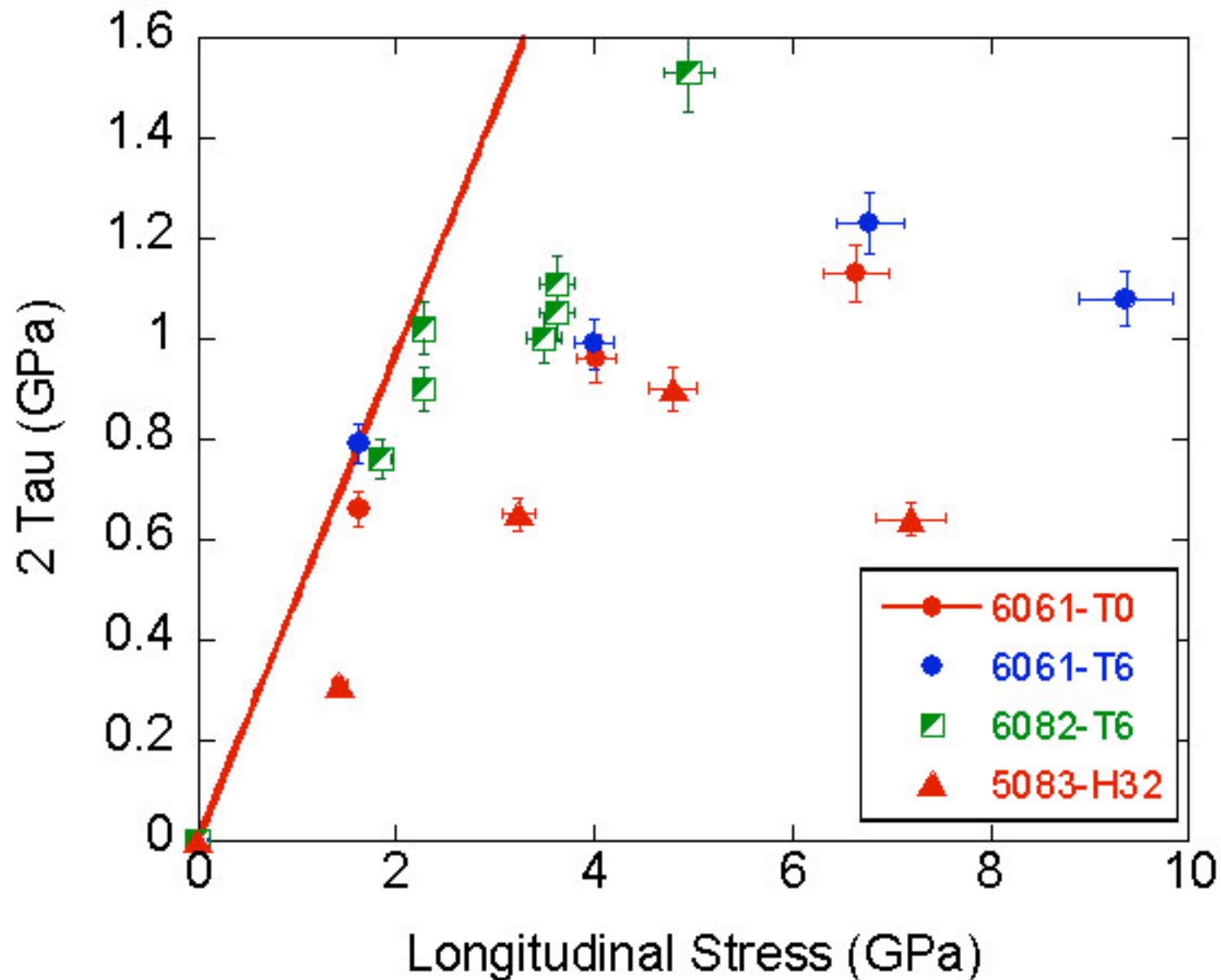
Inclined Impact (Pressure Shear)
Zhou and Clifton



Offset of Hugoniot from Hydrostat
Dandekar and Weisgerber



Shear strengths in aluminium alloys





Cross Comparison



Inclined Impact

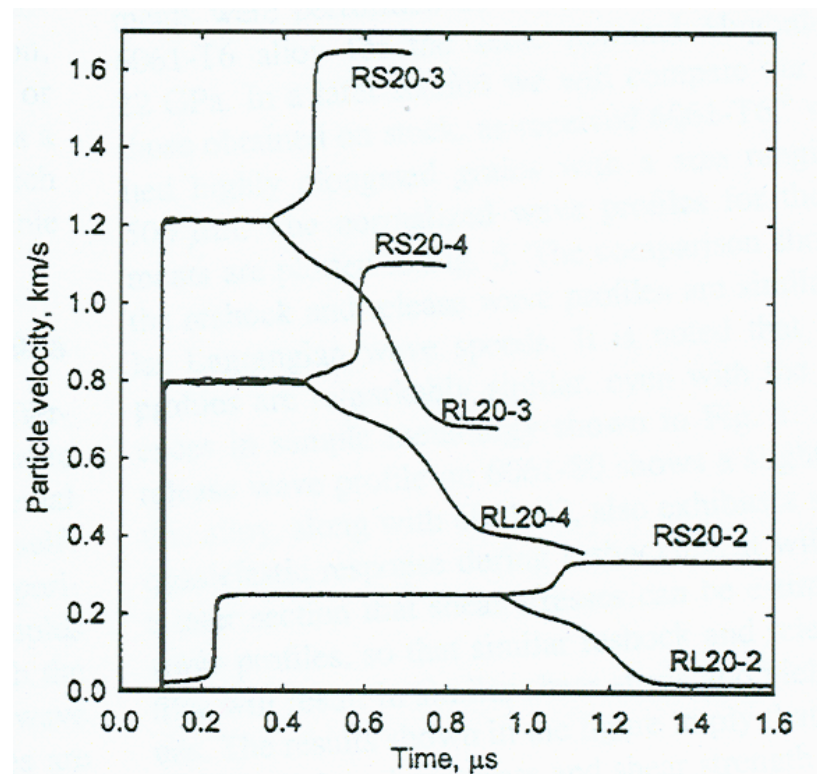
Yadav et al.

Acta Mat. Met. **43** 4453 (1995)

Load Unload – Load Reload

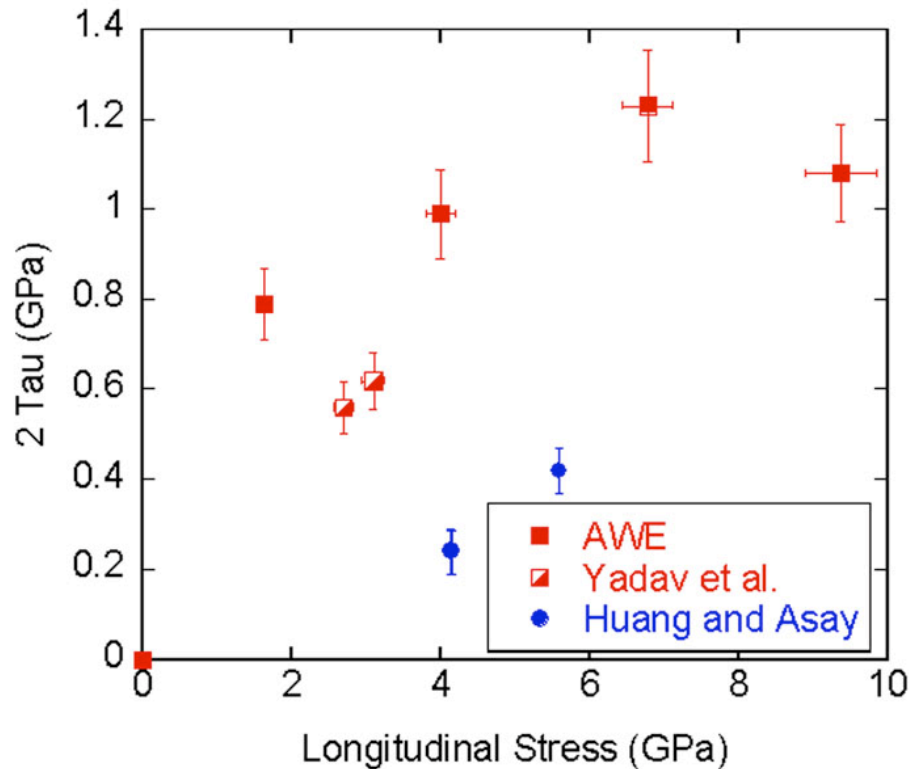
Huang and Asay

J. Appl. Phys. **98** 033524 (2005)





Cross Comparison (6061-T6)



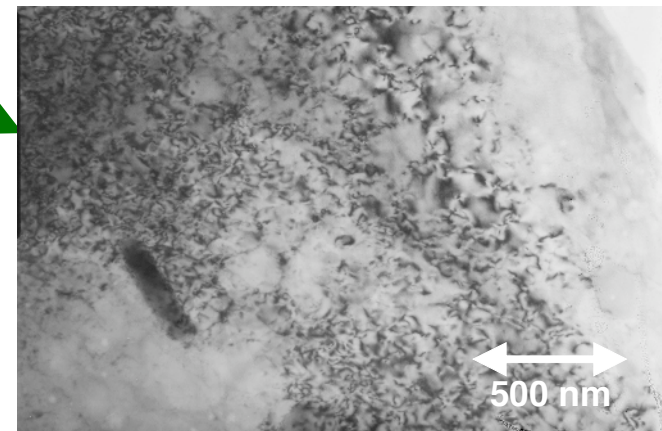
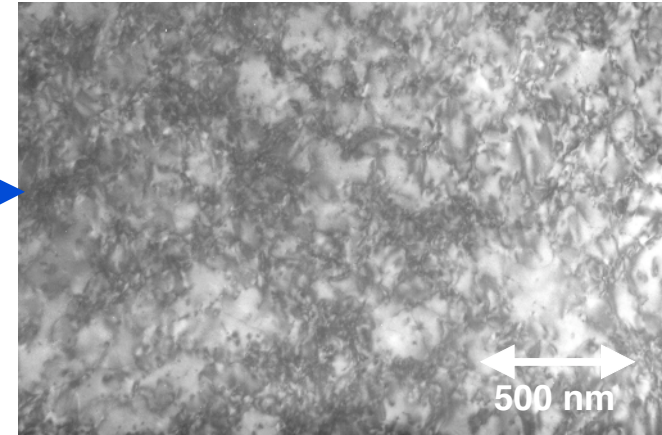
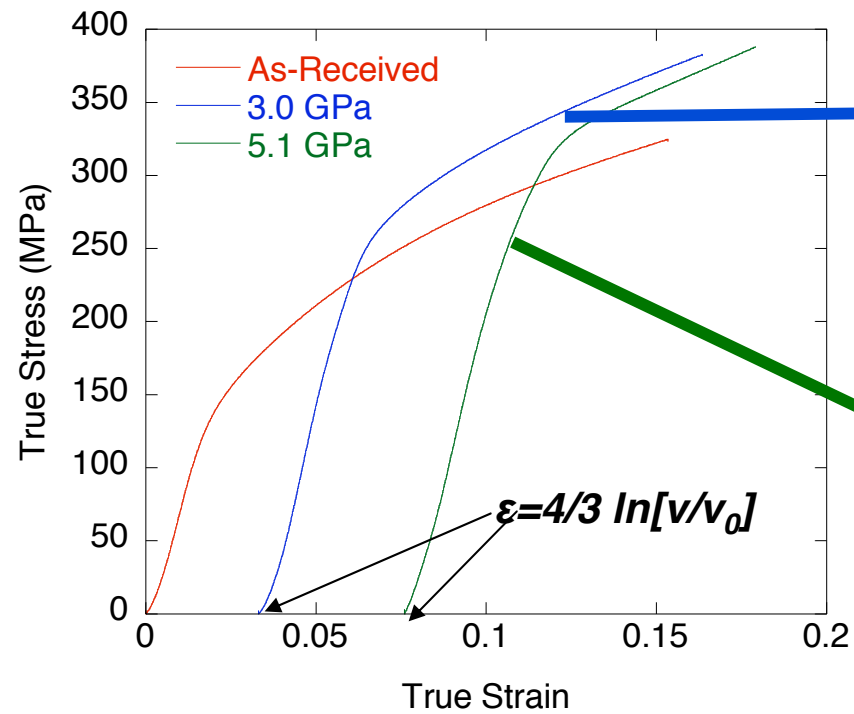
- Different techniques give different shear strengths
- Lateral gauges and load-unload load-reload nominally same material
- Yadav *et al.* very large Mg_2Si size – Overaged?
 - 2 μm
- High particle spacing – reduced strength

$$\tau = \frac{\alpha \mu b}{L}$$

μ - Shear Modulus
 b - Burger's vector
 L - particle spacing
 α - constant

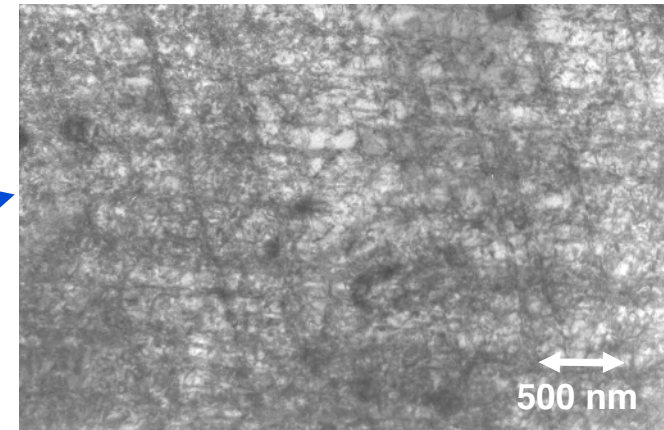
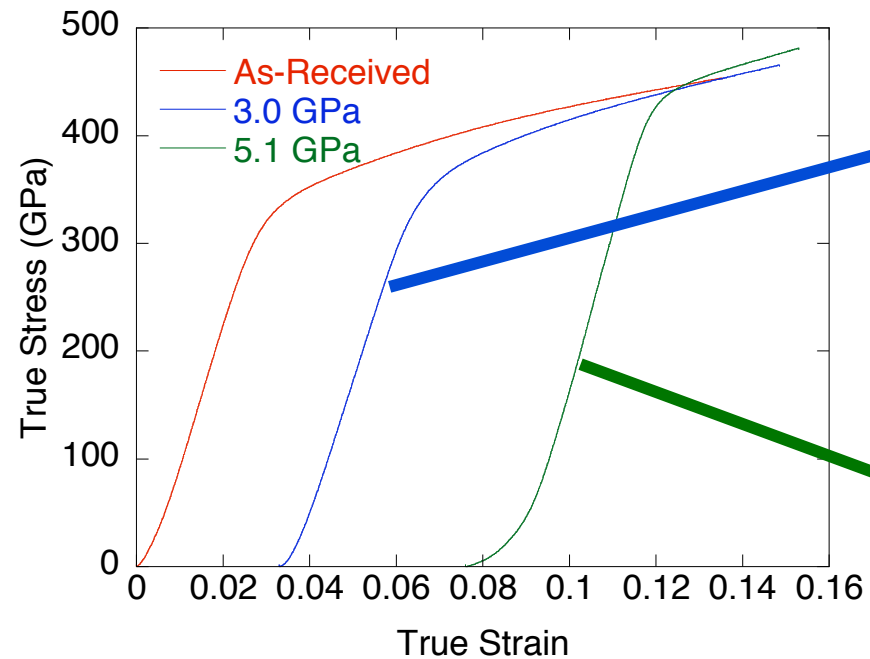


Post Shock Response: T0



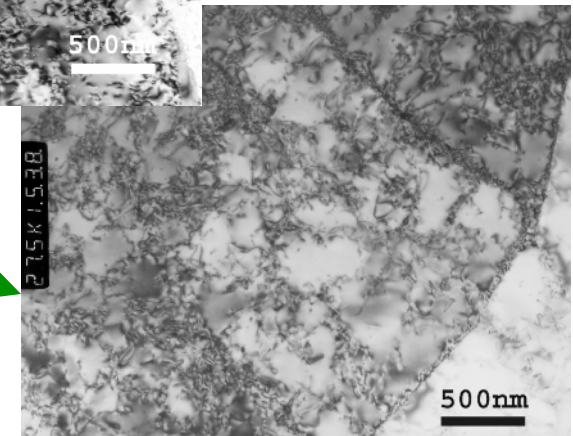
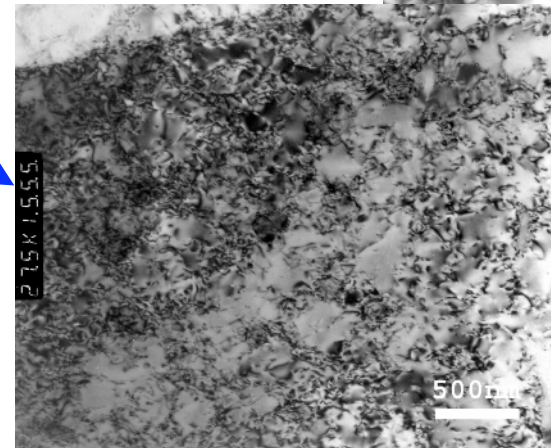
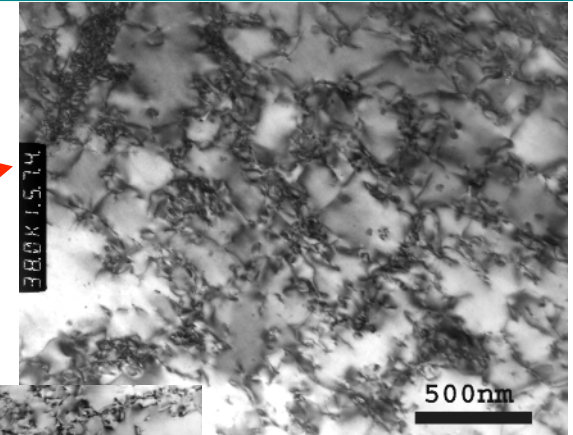
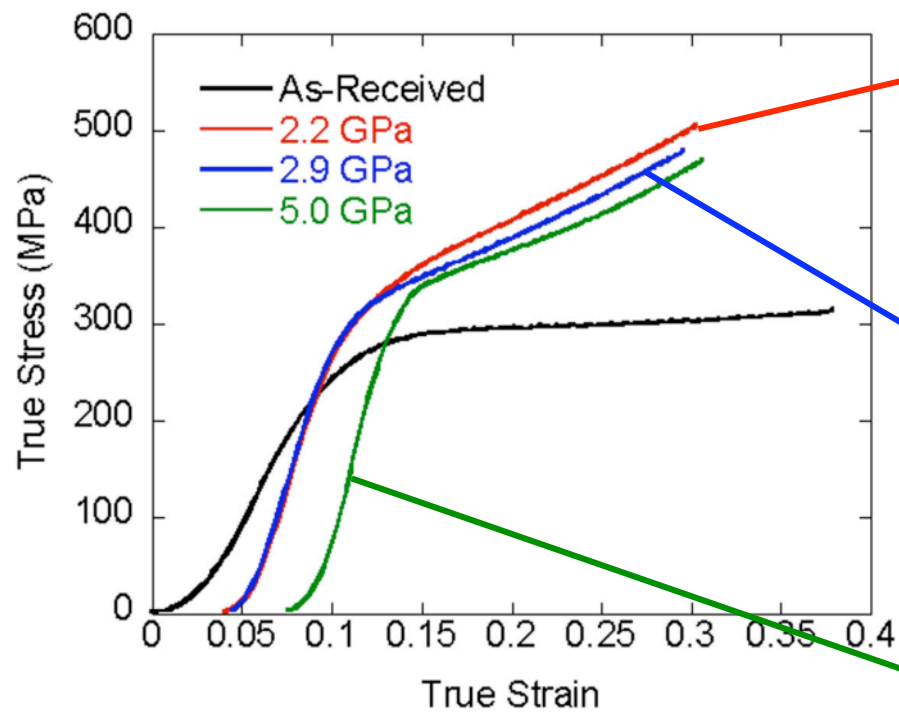


Post Shock Response: T6





Post Shock 5083-H32





Conclusions

- Lateral stress traces show differences in amplitude and shape according to heat treatment and composition
 - Small strength increase from T0 to T6
 - T0 shows faster rise and equilibration behind shock
 - Flatter in 5083-H32
- Recovered microstructures vary according to heat treatment
 - T0 – dislocation cells; T6 – mixture of random dislocations and planar arrays; 5083-H32 – dislocation cells
- Recovered mechanical response varies according to heat treatment
 - T0 – enhanced hardening; T6 no enhanced hardening; 5083-H32 – enhanced hardening
 - Work hardening in shocked T0 and 5083-H32 may be evidence of post shock dislocation recovery

Jowog-32, 2010



LLNL

January 26, 2009

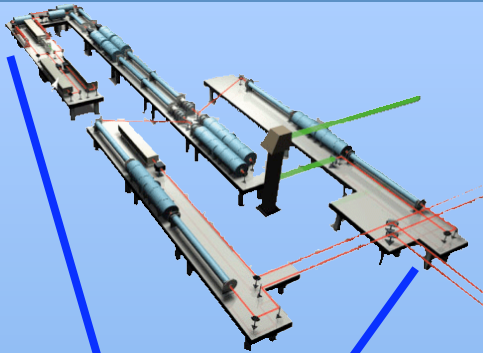
**Laser-induced ramp
compression of tantalum and
iron to over 300 Gpa: EOS and
x-ray diffraction**

Jon H. Eggert

**Marina Bastea, Dave Braun, Don Fujino, Ryan Rygg,
Raymond Smith, Jim Hawreliak, Damien Hicks, Gilbert Collins**

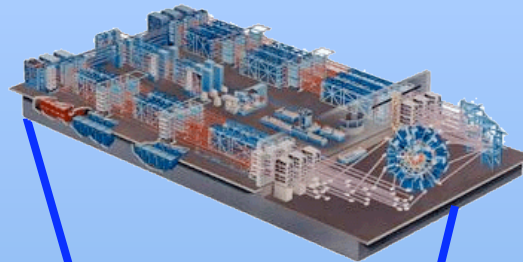
IM-385940-3

Laser Facilities



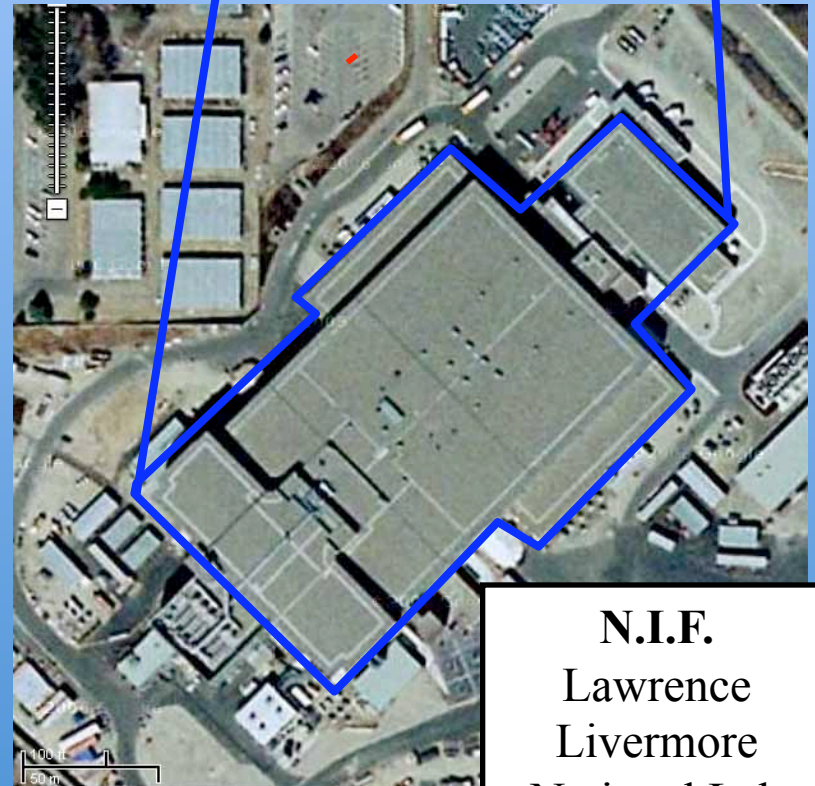
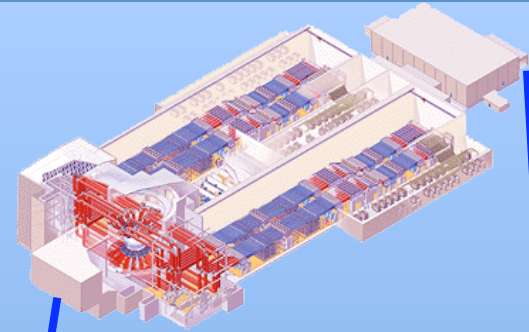
Janus
Lawrence
Livermore
National Lab
(CA)

2 beam
1 kJ



Omega
University of
Rochester (NY)

60 Beams
30 kJ



N.I.F.
Lawrence
Livermore
National Lab

192 Beams, 2 MJ

100 meters

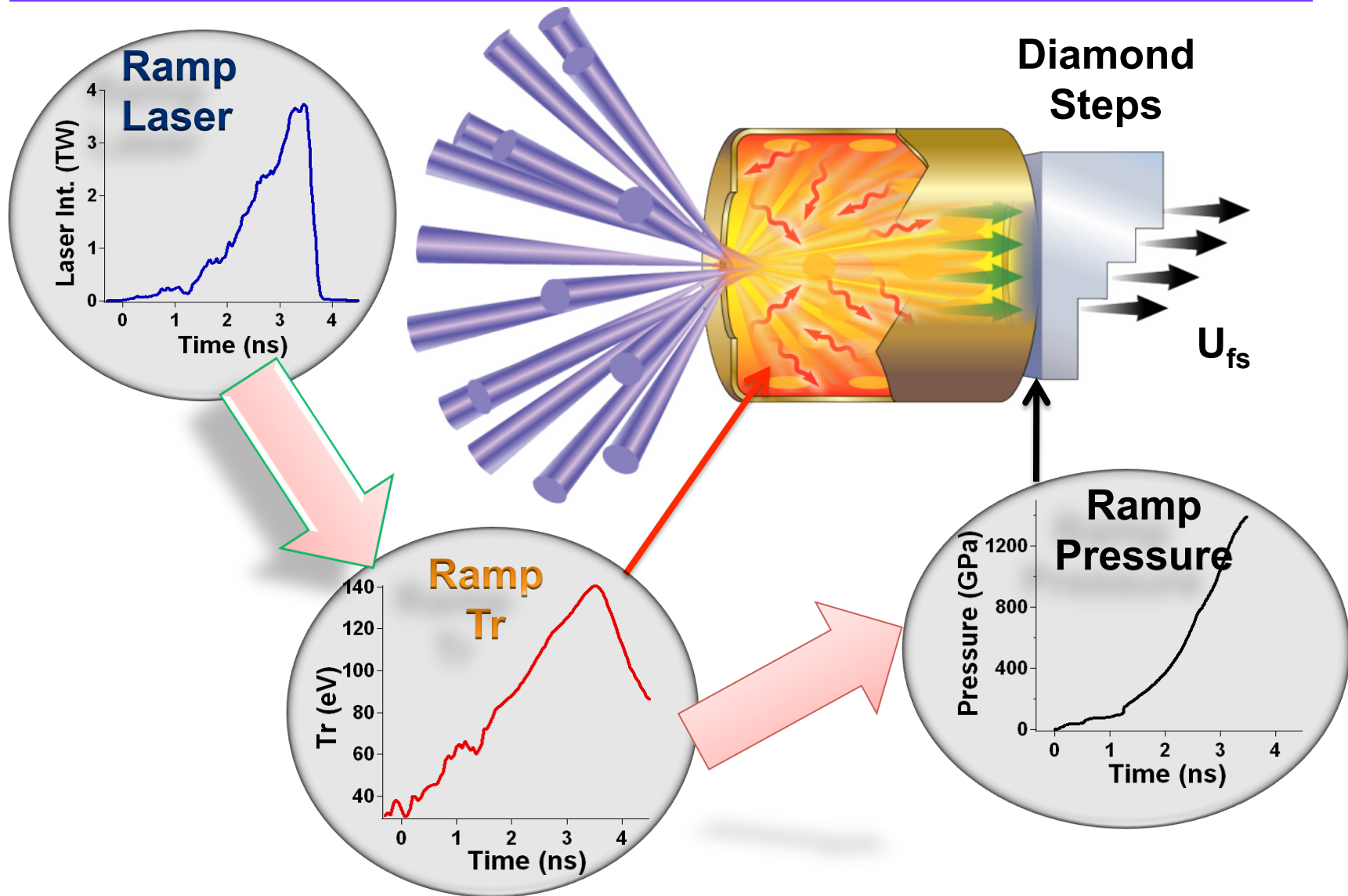
Outline



Laser-Driven Ramp Compression Experiments

- **Introduction**
- **Ramp-Compression EOS on Tantalum to 320 GPa**
 - Cold Sample
 - Absolute Stress-Strain
- **X-ray Diffraction on Iron to 470 GPa**
 - Far Above Shock Melting on Hugoniot
 - Still Solid
 - Consistent with HCP
- **On to NIF . . .**

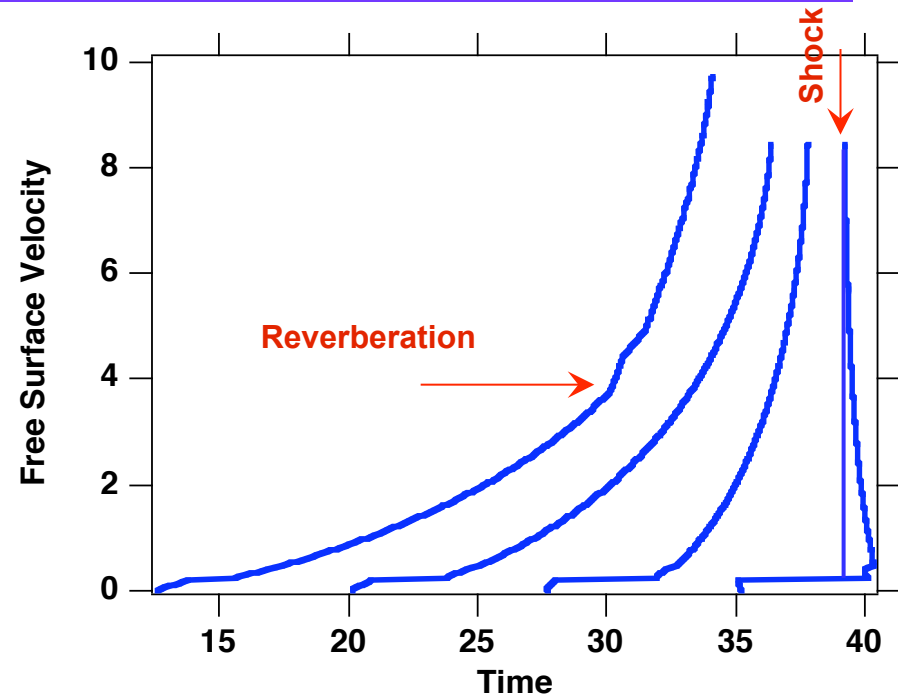
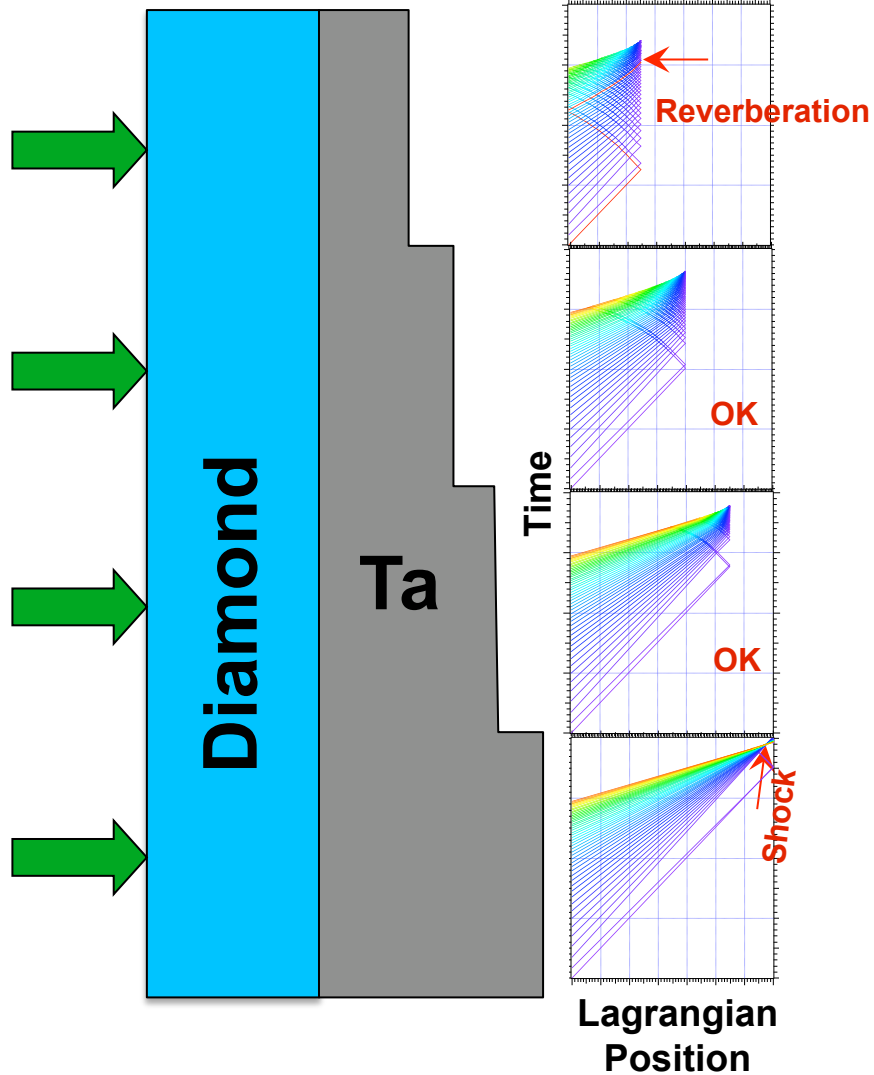
We ramp compressed diamond to 1500 GPa



Apply this drive to Tantalum

Ramp-Wave EOS

--Design Requirements--

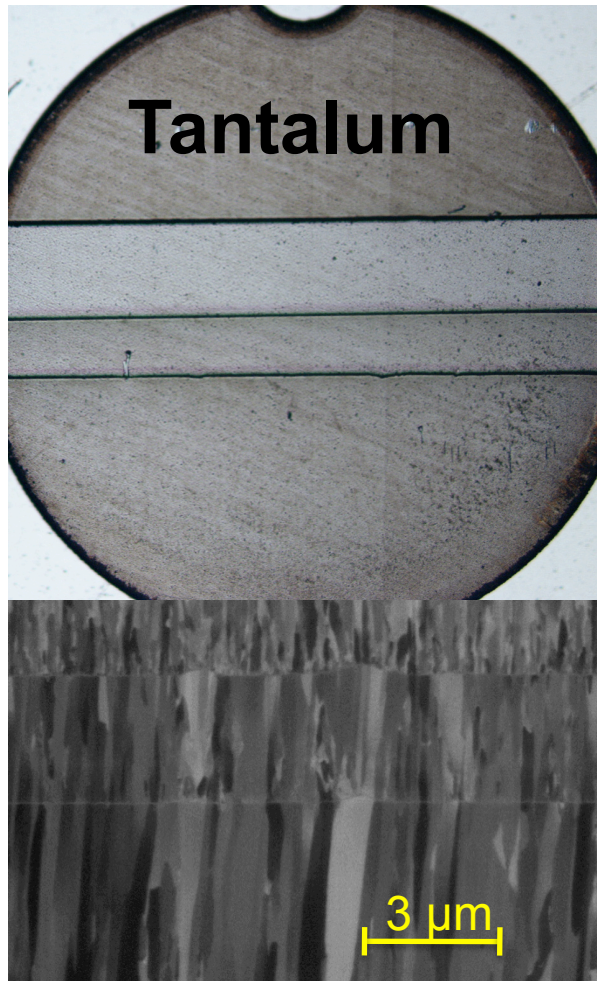


No reverberation

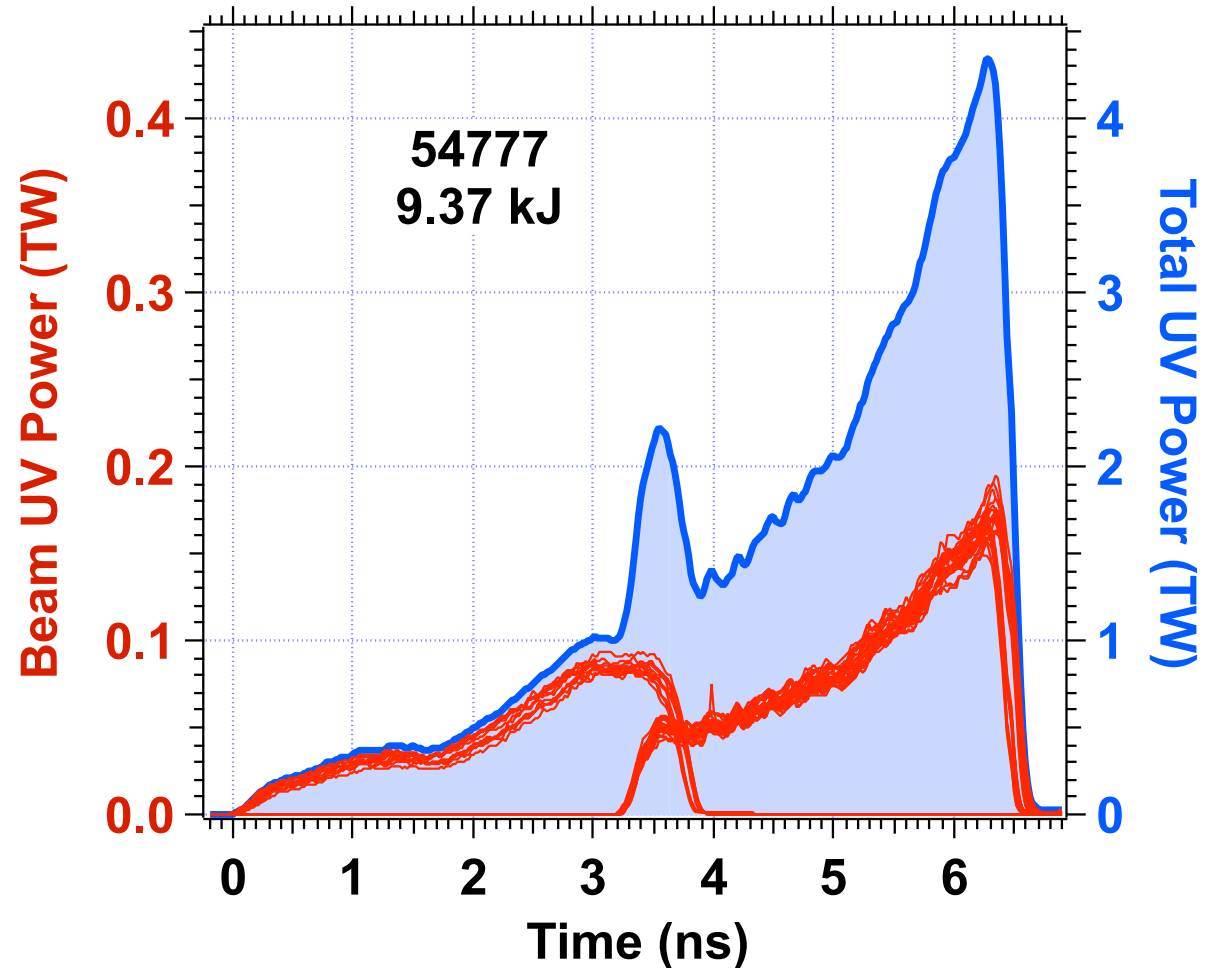
--and--

No Shock.

Target Metrology and Pulse Shape



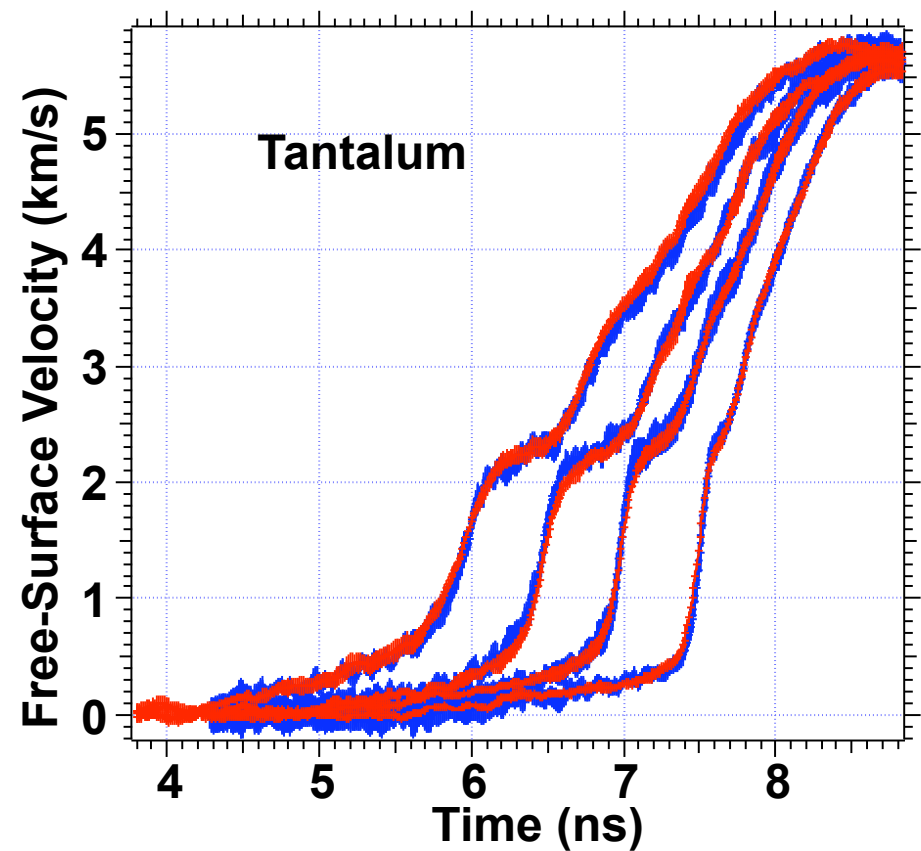
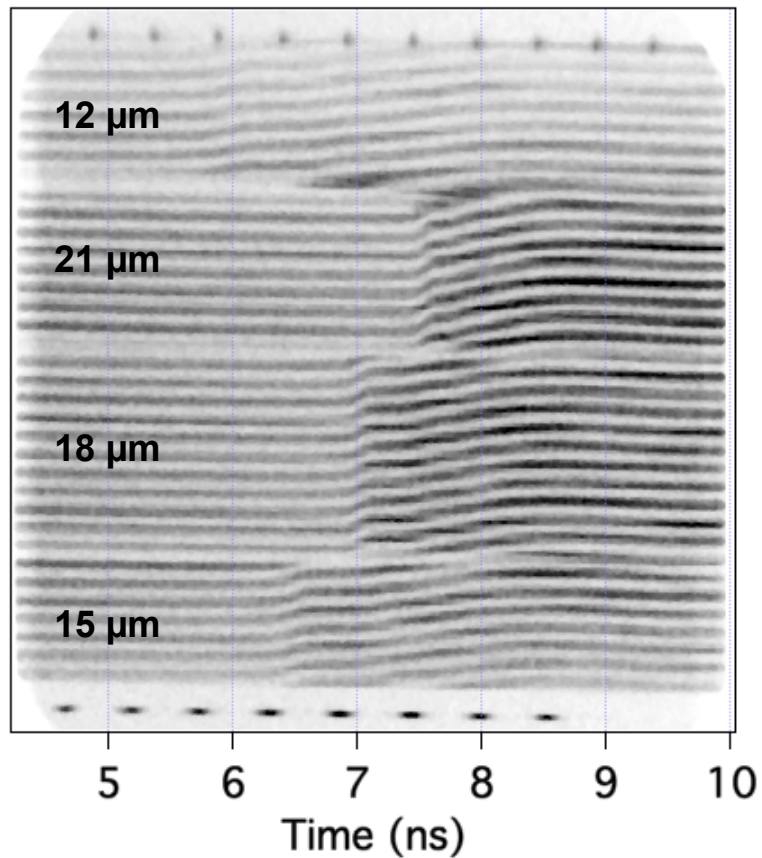
$d_A = 11.24 \pm 0.5 \mu\text{m}$
 $d_B = 13.83 \pm 0.5 \mu\text{m} - 2.59 \mu\text{m}$
 $d_C = 16.54 \pm 0.5 \mu\text{m} - 2.71 \mu\text{m}$
 $d_D = 19.35 \pm 0.5 \mu\text{m} - 2.81 \mu\text{m}$



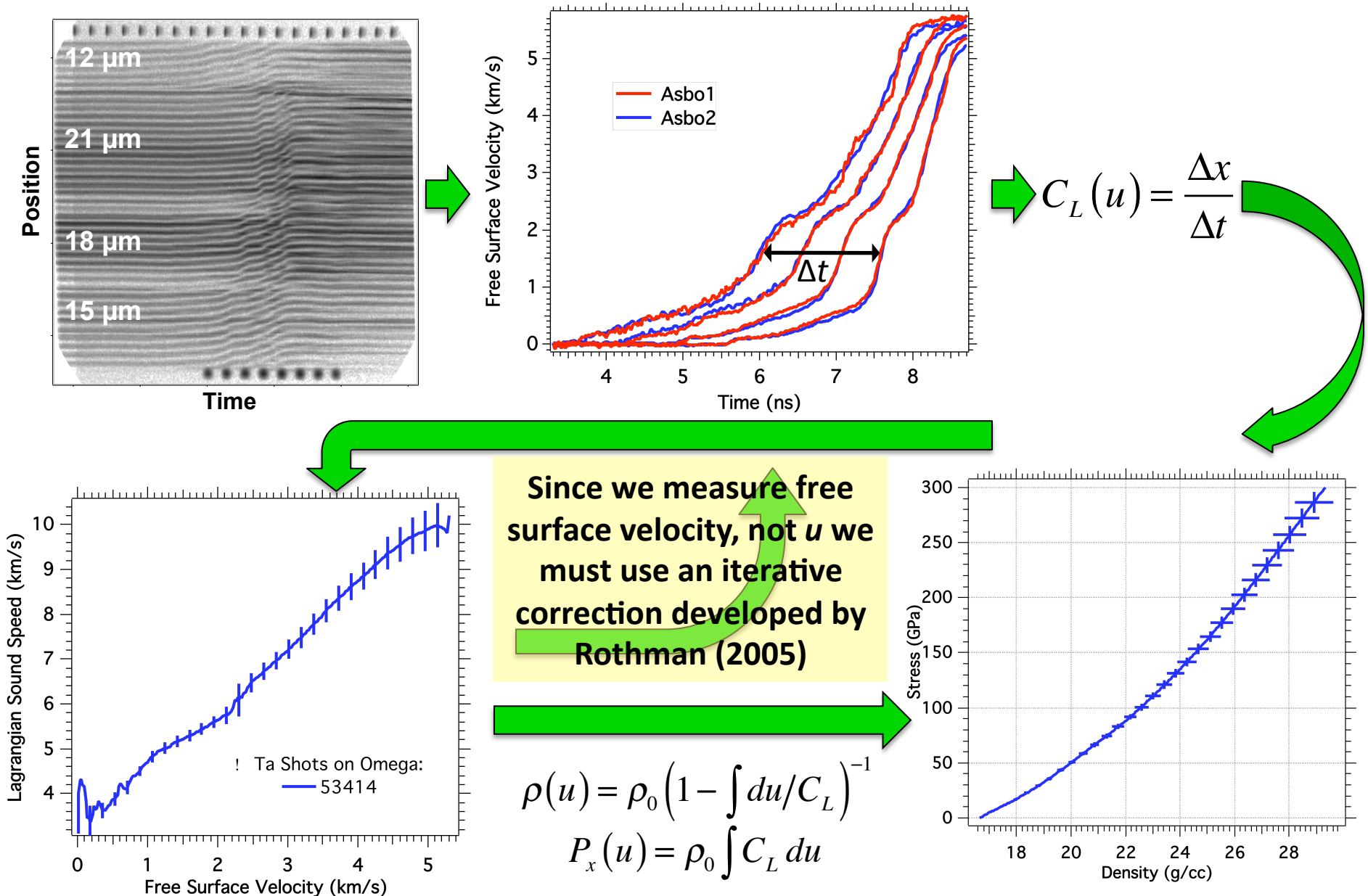
Tantalum deposition: Paul Mirkarimi
and Kerry Bettencourt.

VISAR Wave Profiles

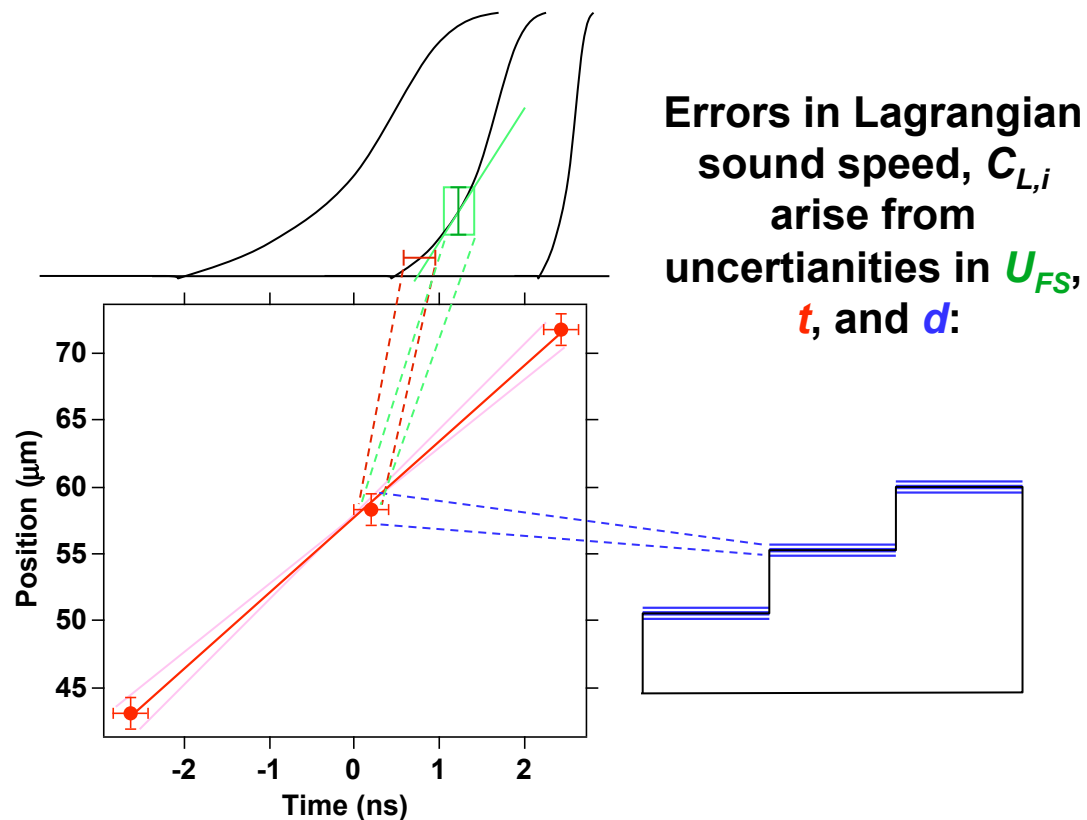
Shot 54777



We collect data using a line visar and use an iterative Lagrangian Analysis (Rothman, et al., (2005))



We propagate uncertainties throughout the iterative analysis



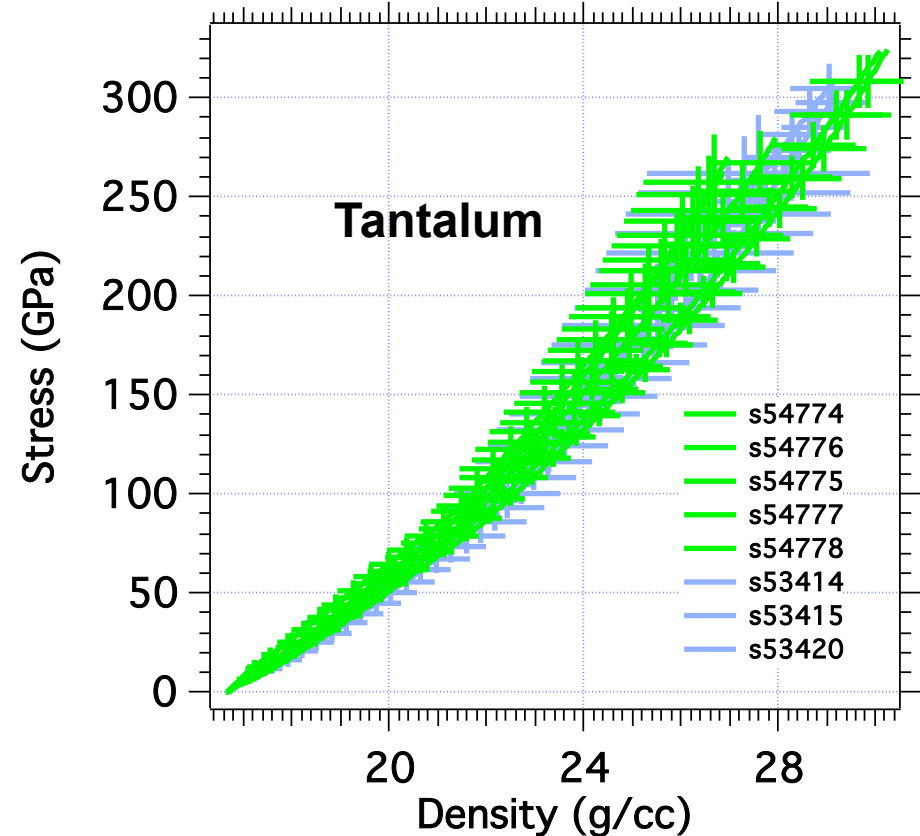
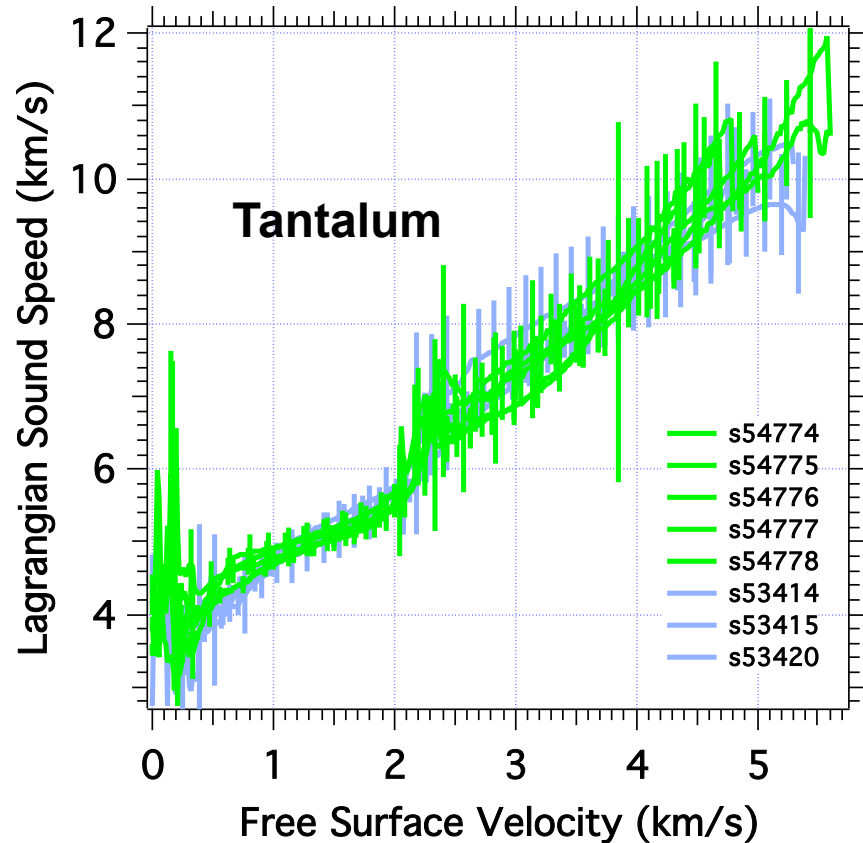
Dominant uncertainties are *not* independent as a function of U_{FS} (e.g. thickness, streak camera warping, visar laser speckle). Thus the errors propagate linearly to strain and stress:

$$\delta \varepsilon_j = \Delta U p \left(\frac{\rho}{\rho_0} \right)^2 \sum_{i=0}^j \frac{\delta C_{L,i}}{C_{L,i}^2}$$

$$\delta P(U p_j) = \rho_0 \Delta U p \sum_{i=0}^j \delta C_{L,i}$$

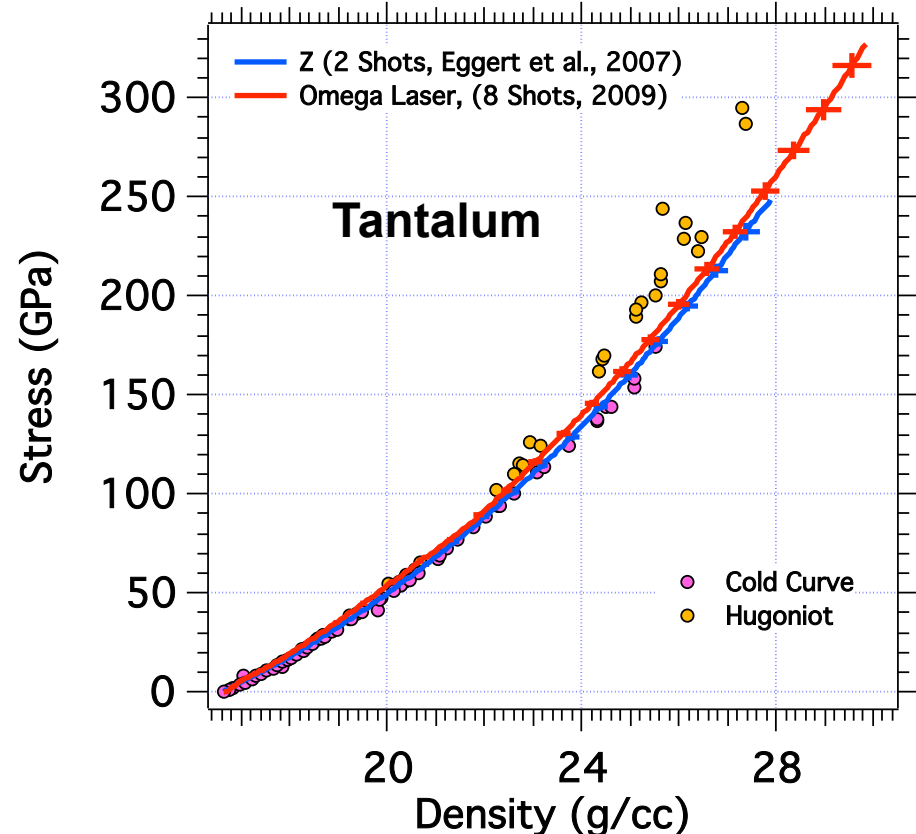
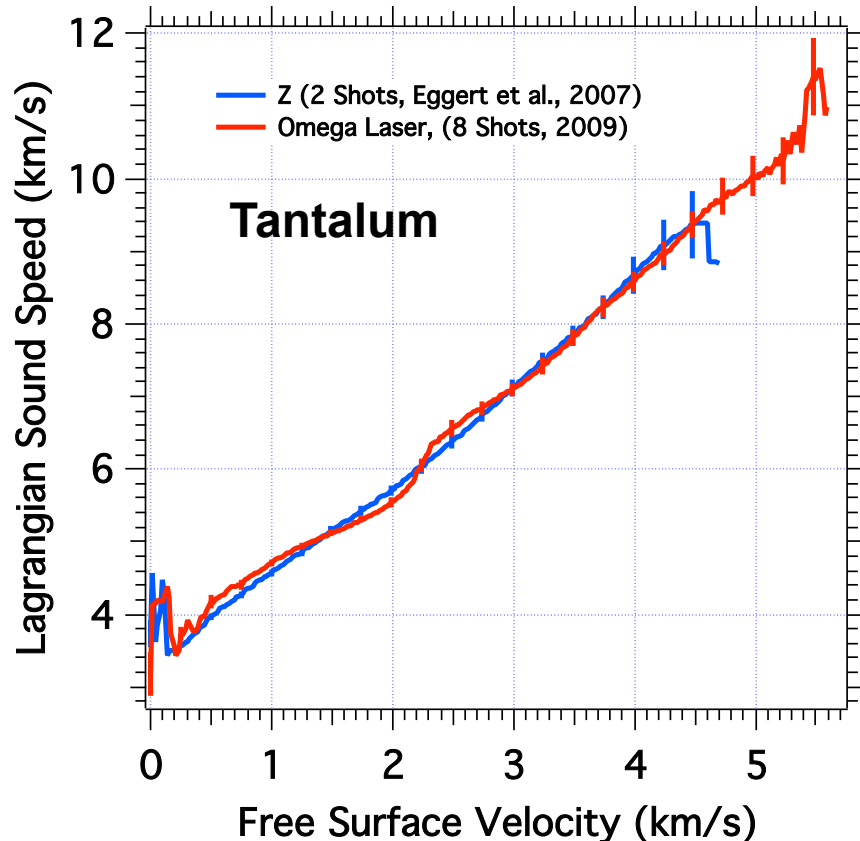
Uncertainties continue to grow at high pressure.

8 Shots—Highly Consistent Results



8 Shots on the Omega Laser in 2009
100% Data Return

Averaging All Laser Shots

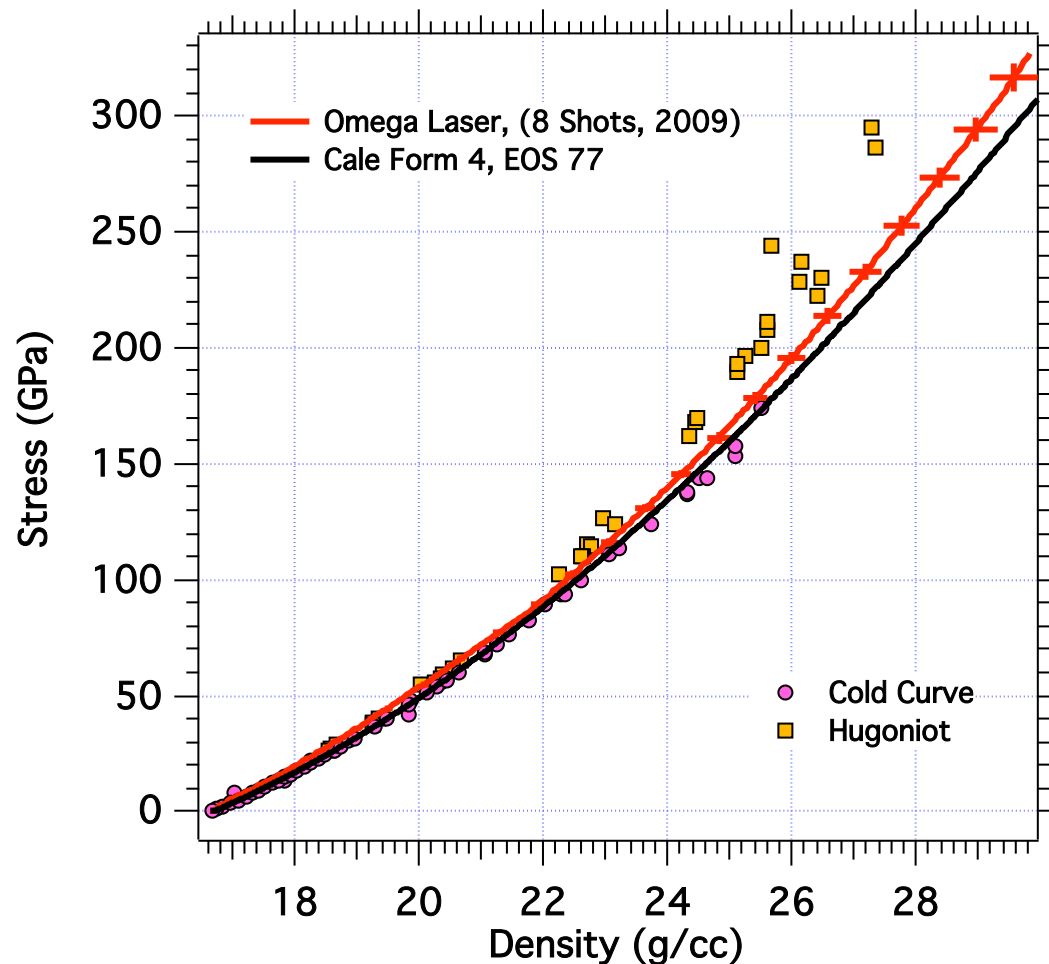


Ramp Compression Tantalum Equation of State

- Stress-density on 8 shots to over 300 GPa.
- Very consistent with previous Z shots.

Next Year: NIF experiments to 500 GPa and more . . .

To Estimate Plastic Work Heating We Estimate Deviatoric Stress or “Strength”

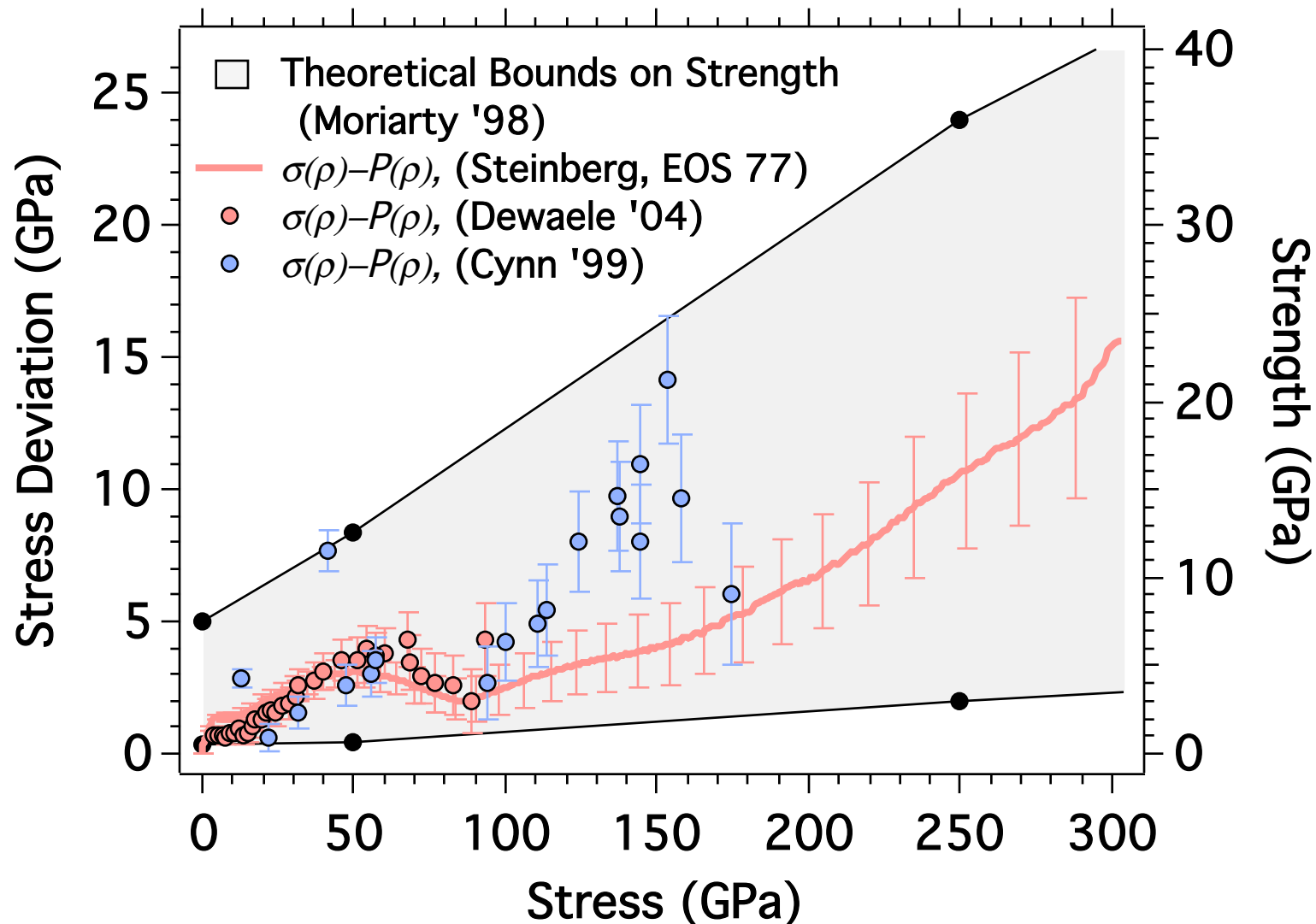


We equate the deviatoric stress with the strength,

$$Y = \frac{3}{4} [\sigma(\rho) - P(\rho)]$$

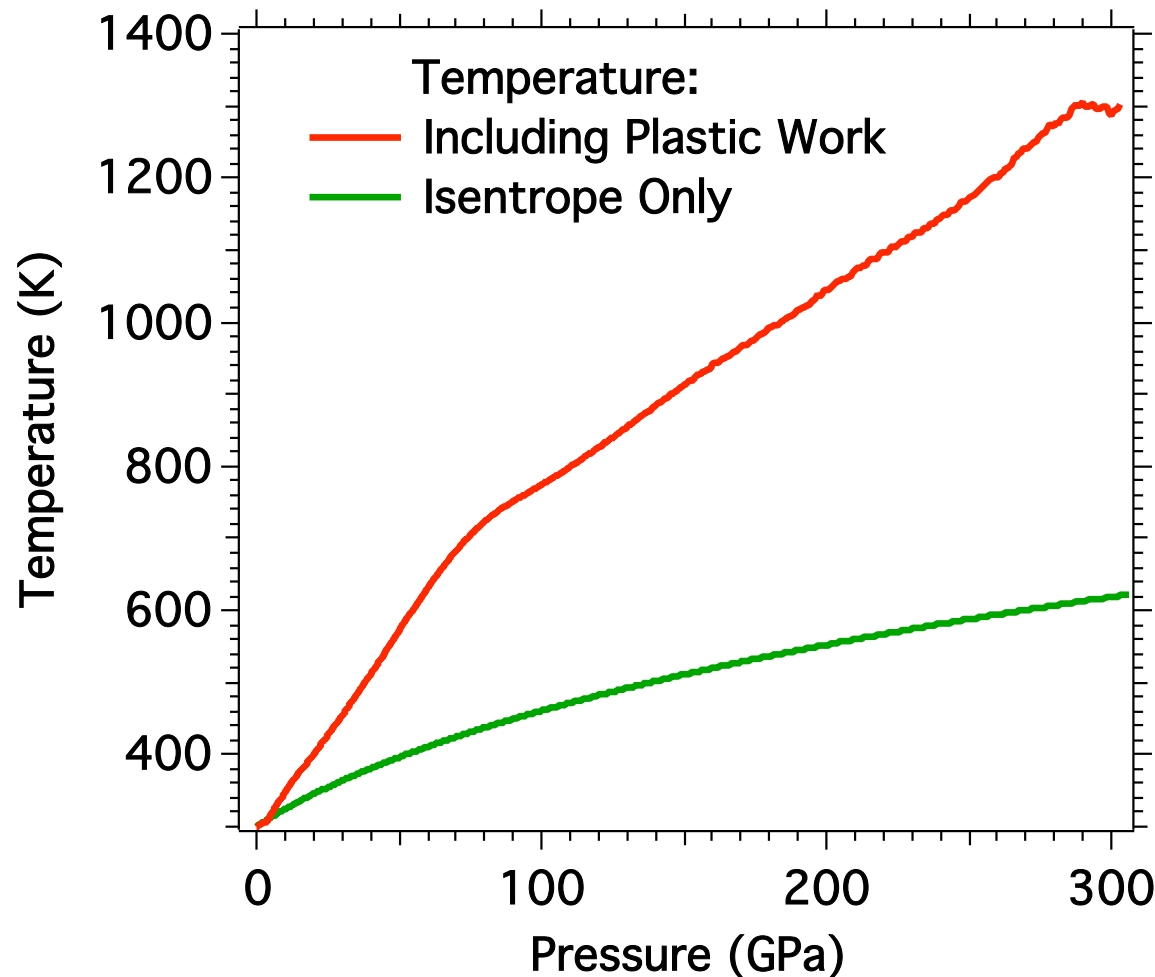
For simplicity, we will compare our with CALE Form 4, EOS 77, and with two sets of DAC isothermal EOS measurements:

Estimate of Strength Used to Calculate Plastic-Work Heating.



Data falls within theoretical bounds on strength. (Moriarty, 1998)

We Estimate the Temperature due to Plastic-Work Heating



Assuming Dulong-Petite limit for specific heat. Iterative approach used to correct strength for thermal pressure.

Future Directions



- **We are currently working to compress Iron to 300 GPa at Omega.**
- **Analysis that accounts for kinetics.**
- **Separation of EOS and strength.**
- **Determination of crystal structure.**
- **Temperature determination.**

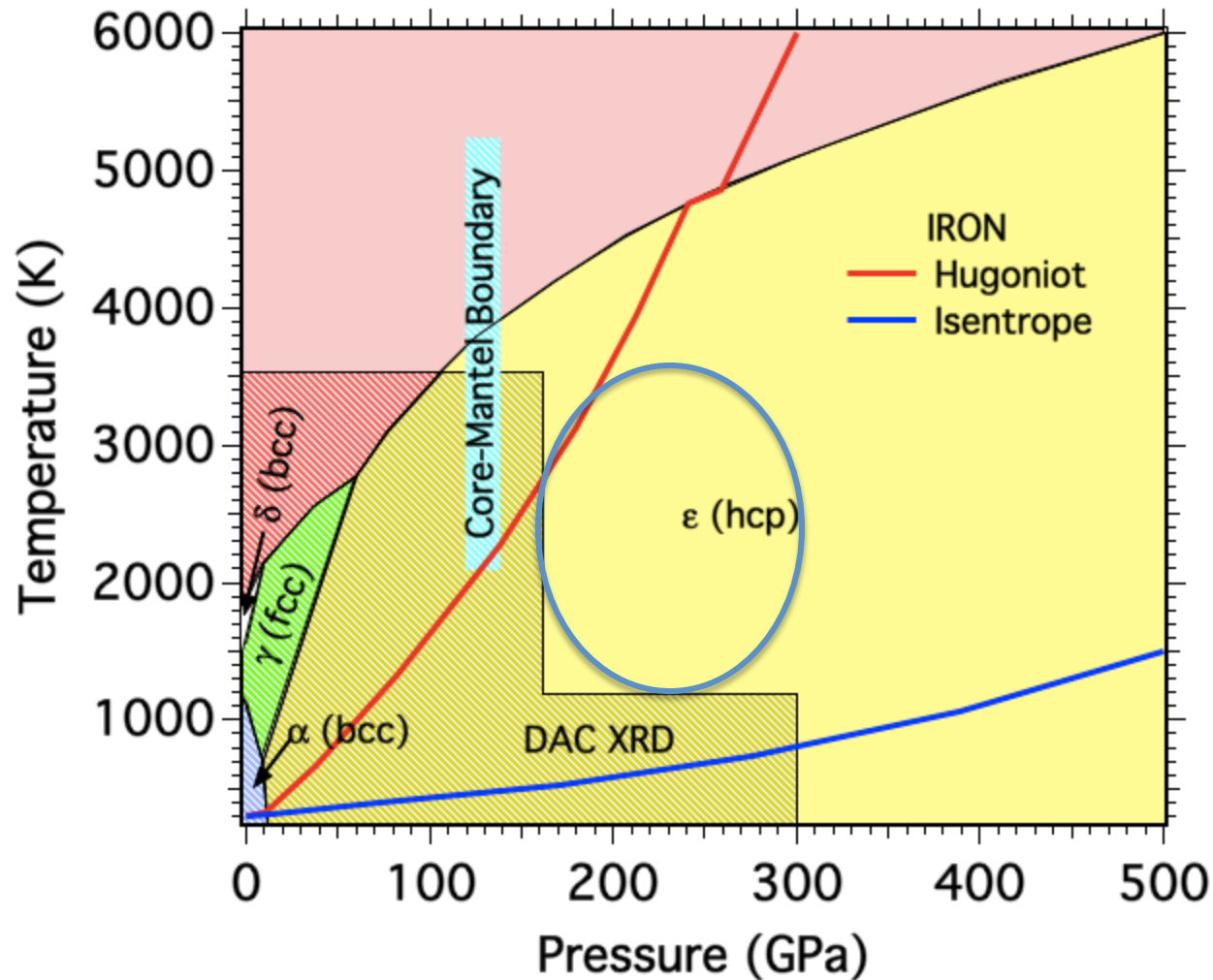
X-Ray Diffraction



- **Diffraction -- Most direct way to determine crystal structure**
- **Laser Drive -- Ideal for X-ray diagnostics**
- **Ramp Compression -- limits shock heating, very high pressures in solid phase.**

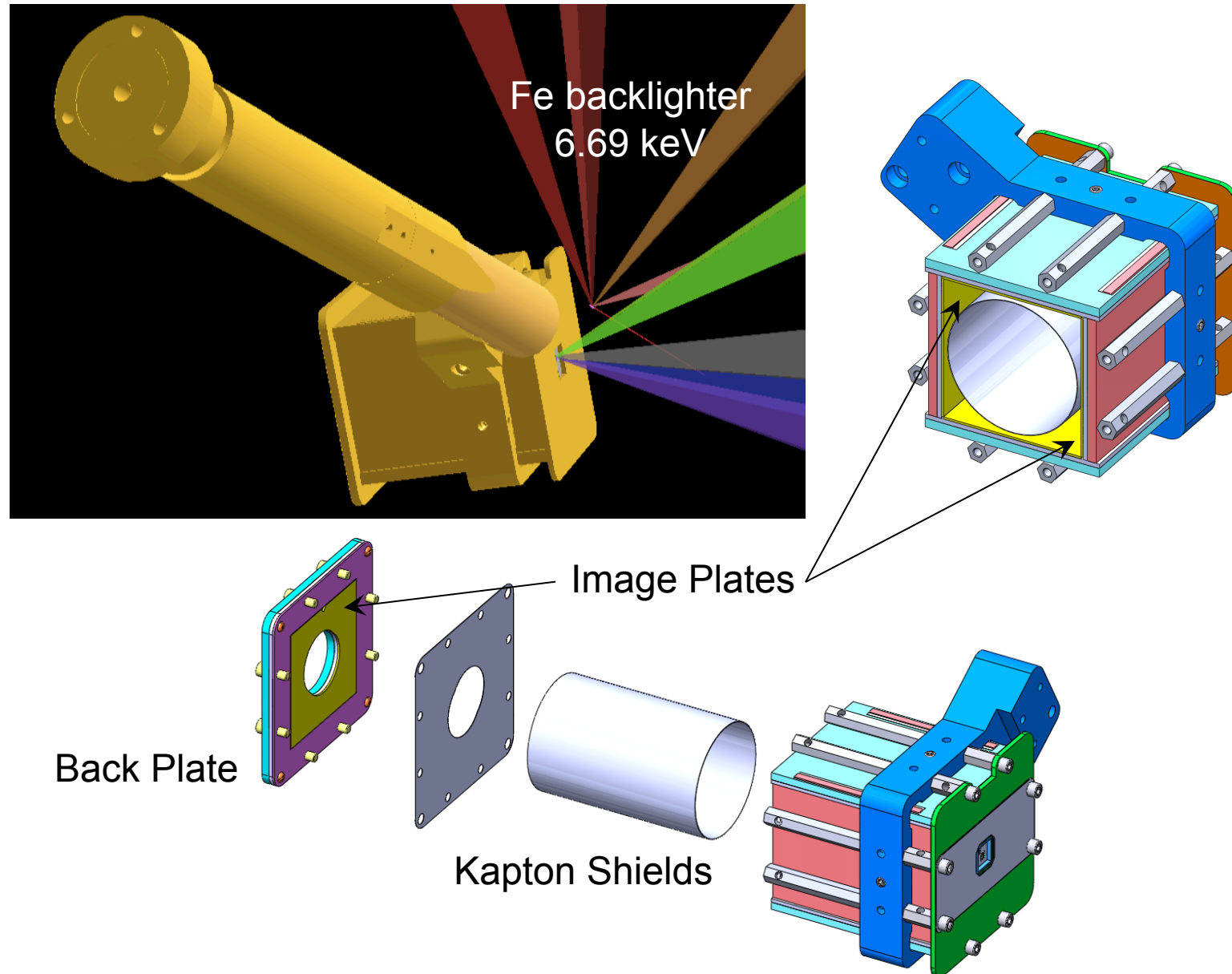


Iron Phase Diagram

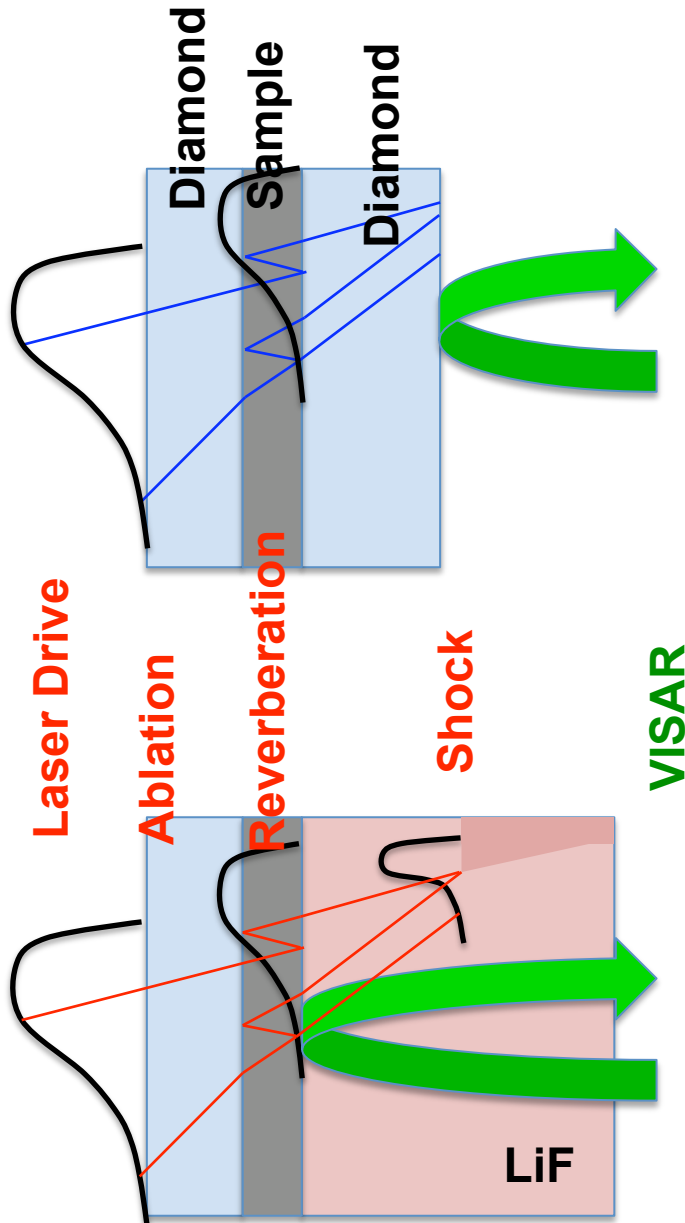


- Diffraction above the shock melting pressure?

X-Ray Diffraction at Omega Laser



Sandwich Ramp-Compression



As long as the sample is hydrodynamically thin, P and u at the LiF or Diamond interface is the same as in sample

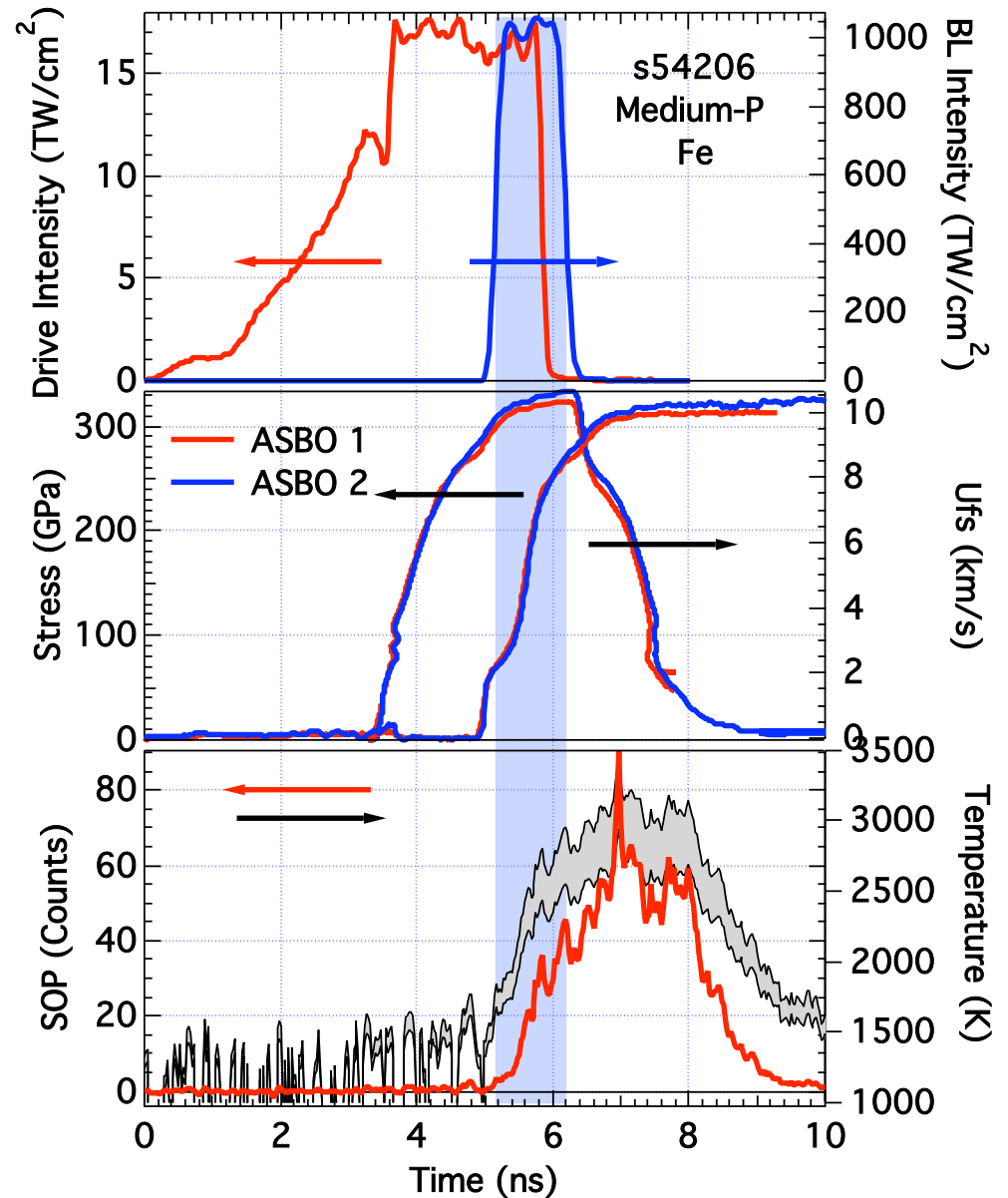
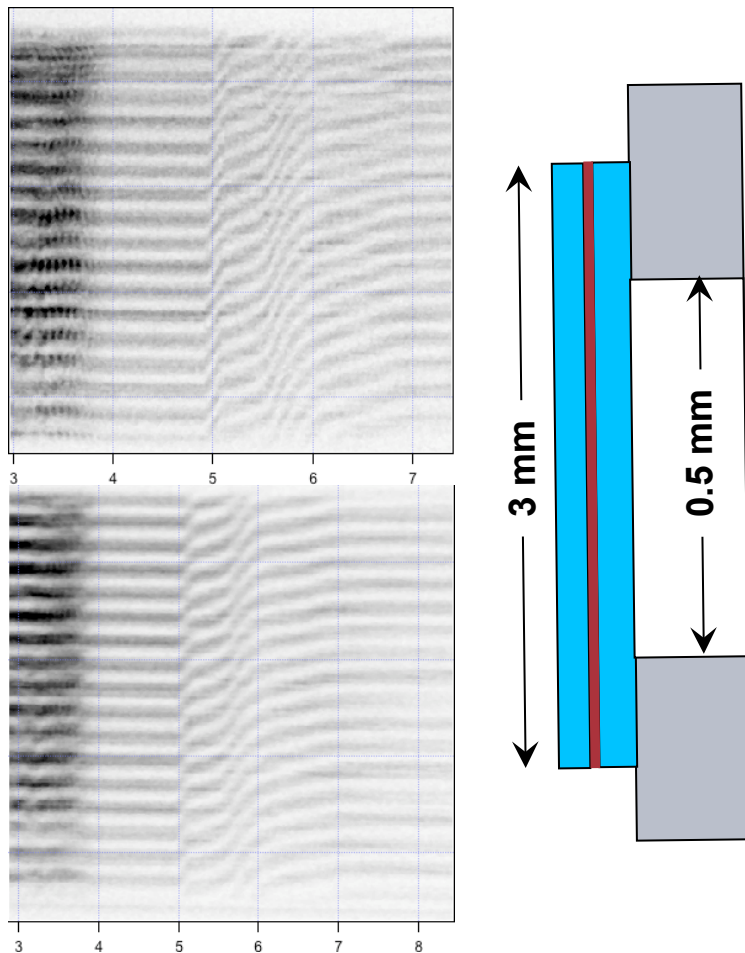
If we know the EOS of LiF or Diamond we can find the Pressure in the sample using the VISAR diagnostic

Proof of principle already demonstrated for XRD and XAFS on iron

Using this target design, we believe we can ramp compress samples to ~30 Mbar, Hold the state for several ns, Determine the pressure, and Make a measurement.

XRD, XAFS, XANES, Reflectivity, . . .
Temperature remains the most important parameter that we do not know how to measure.

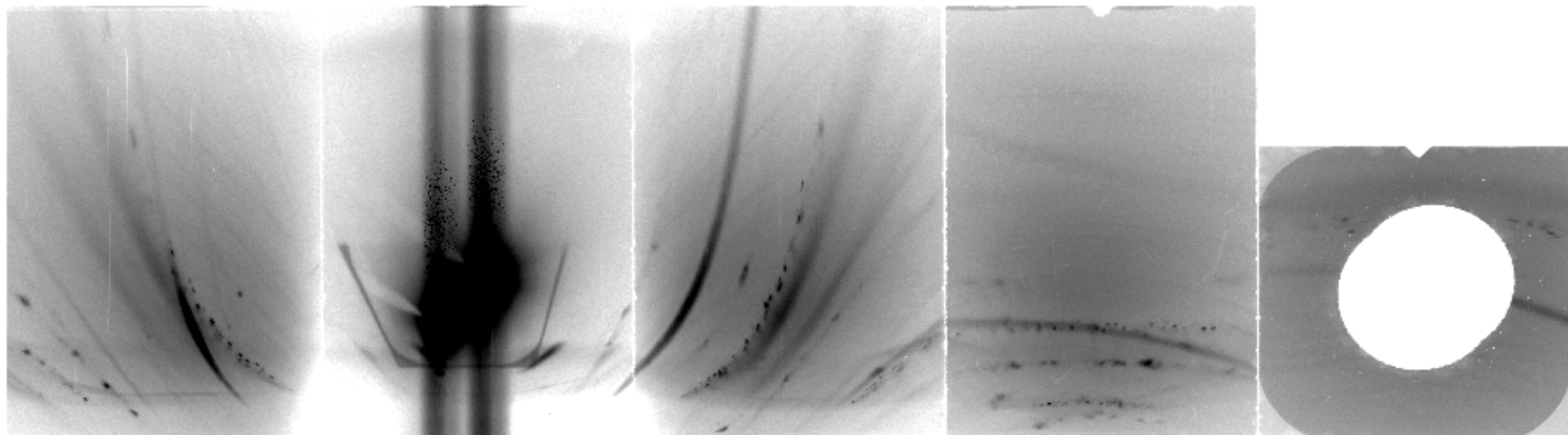
s54206, Fe



Strain rate is very high, $\sim 10^8 \text{ s}^{-1}$.
Looks like temperature is low.
What does diffraction look like?

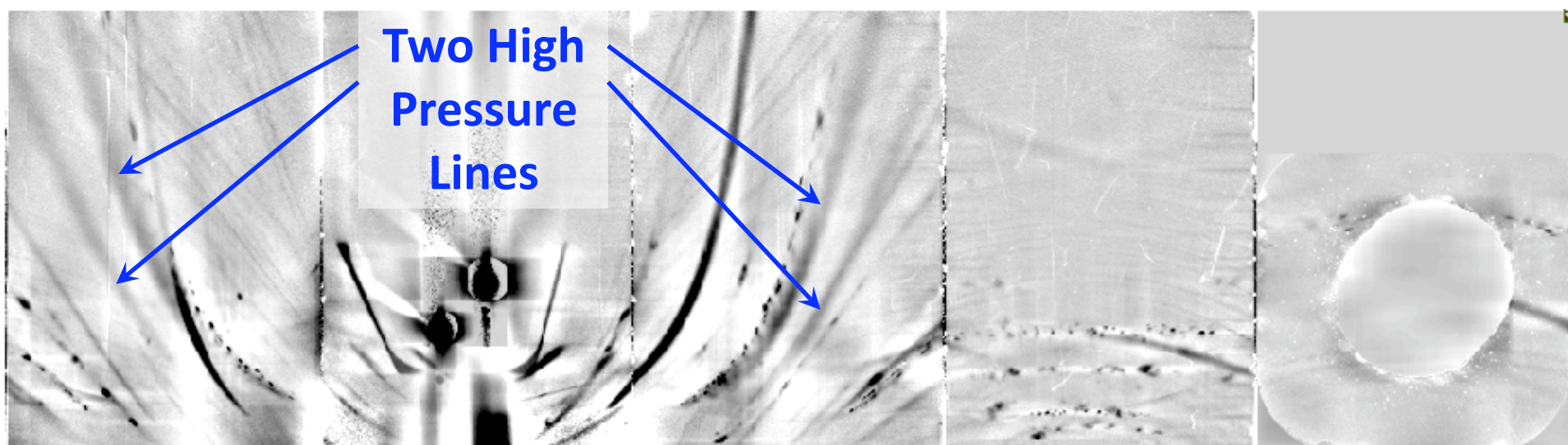
Shot 54203

$$P = 185^{+6}_{-17} \text{ GPa}$$

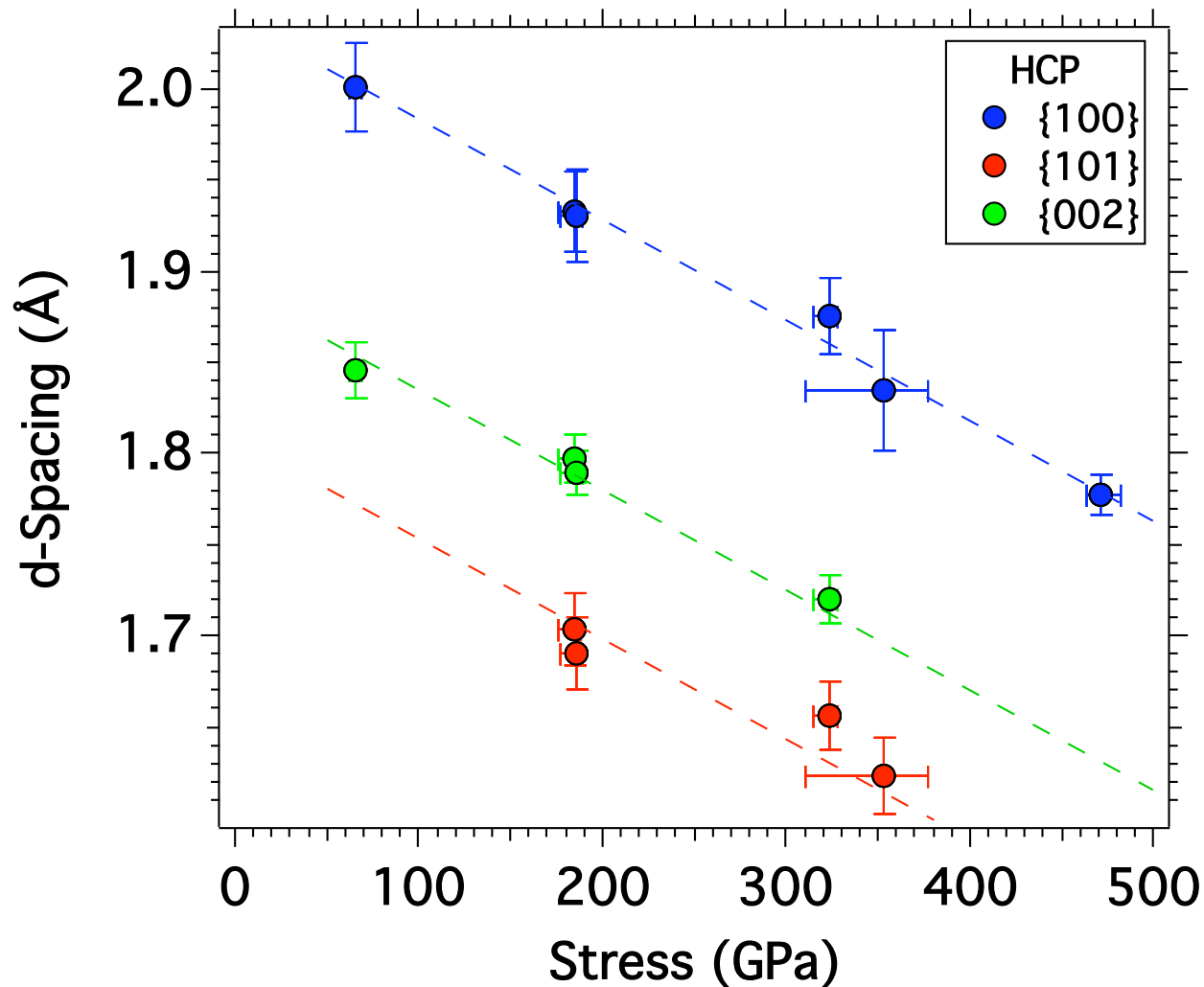


Raw Data ↑

↓ Wavelet-FT Background Subtraction

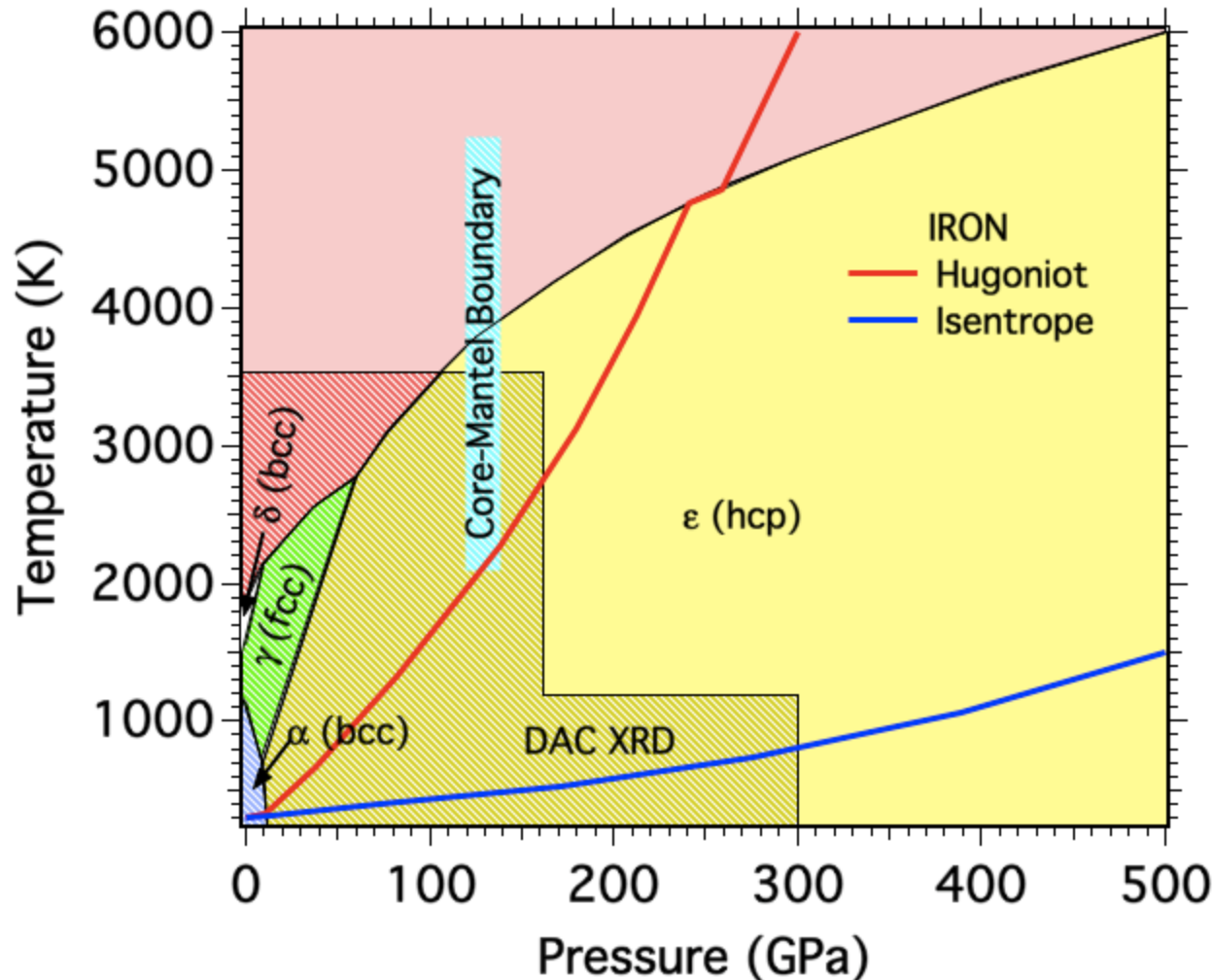


We see 2 strong, 1 weak reflections.



We will *assume* a structure and fit.

Likely Structures: HCP (variable c/a), FCC

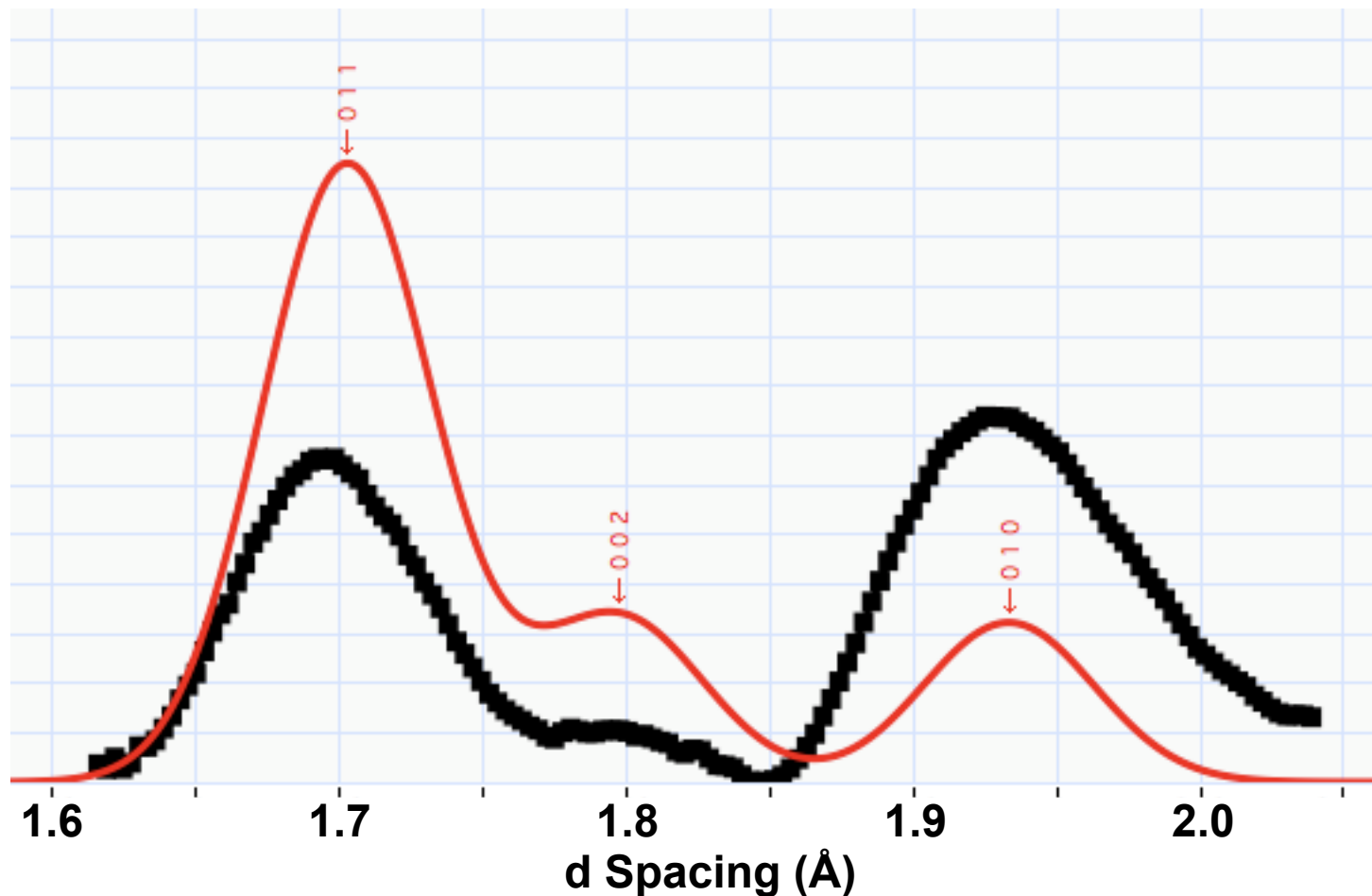


Guided by static experiments, potential structures are hcp with $c/a=1.61$ and fcc. (Ma, et al. 2004)

Previous shock experiments on single crystals found hcp ($c/a=1.73$) (Kalantar, et al. 2005)

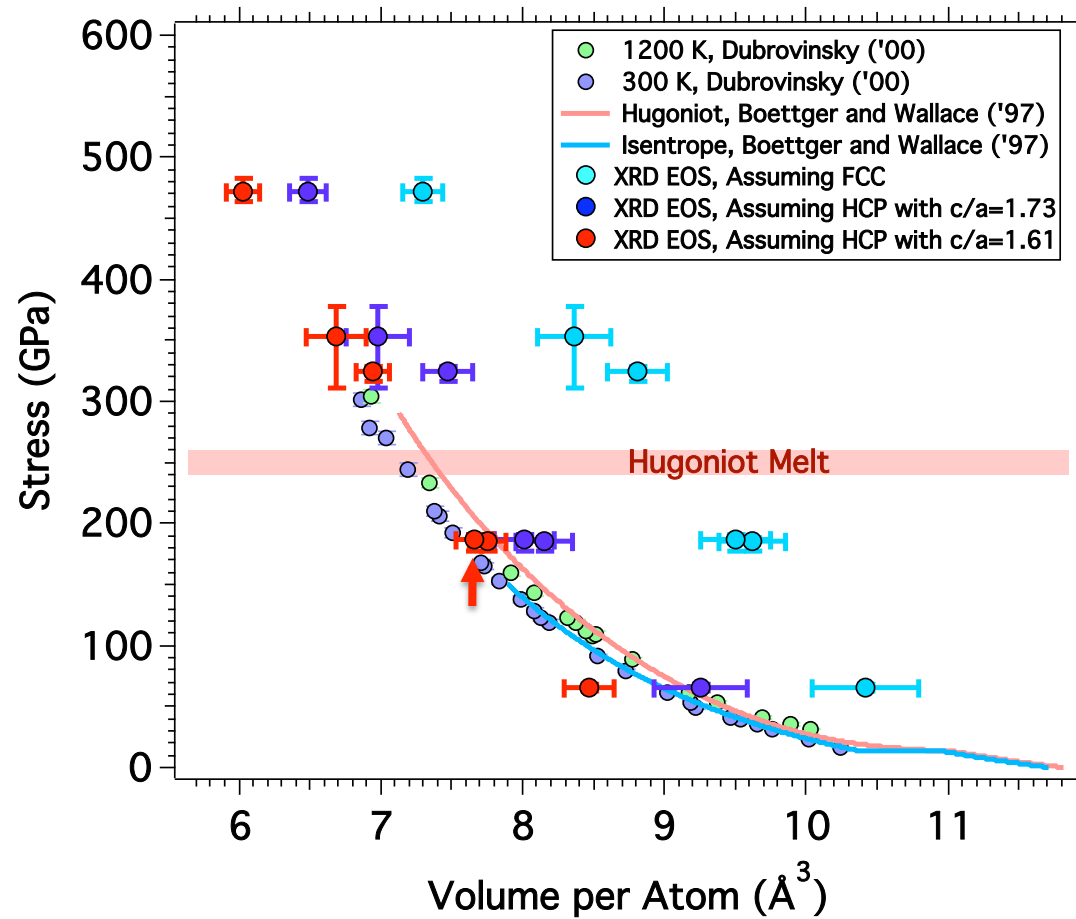
Best Fit Assuming HCP, $c/a = 1.61$

As observed in DAC experiments



Triplet, peak positions fit well for this shot, but significant basal texture required to get agreement with doublet structure observed.

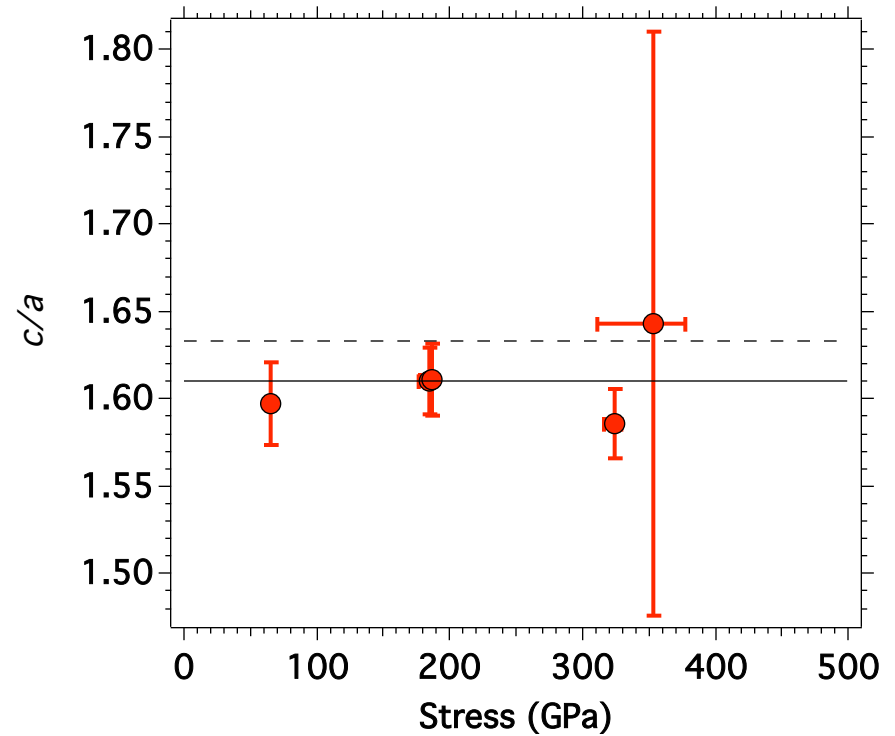
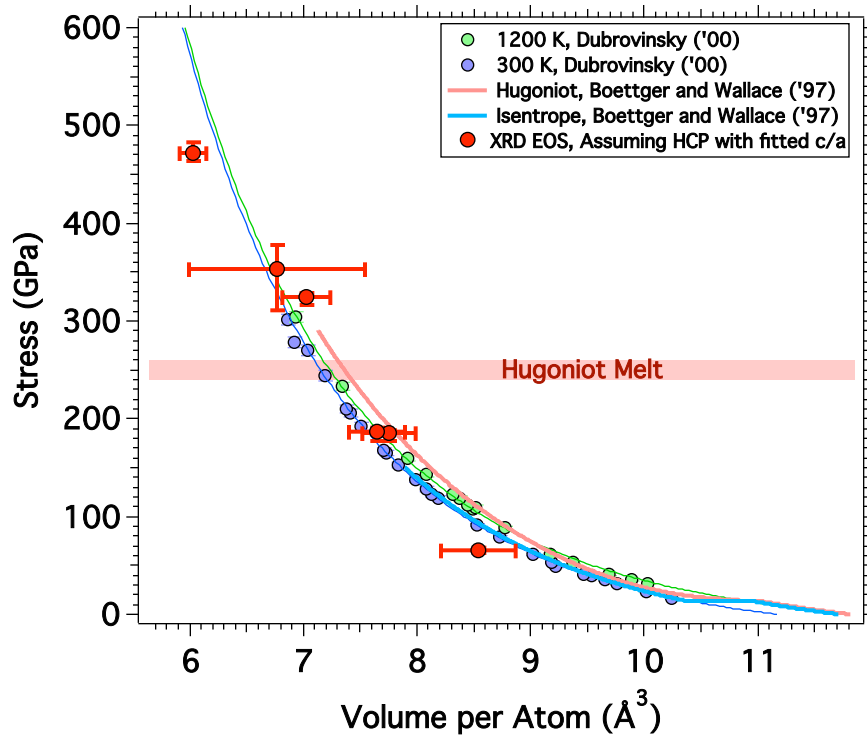
Results and Comparison



Diffraction on *solid* Fe to 472 GPa

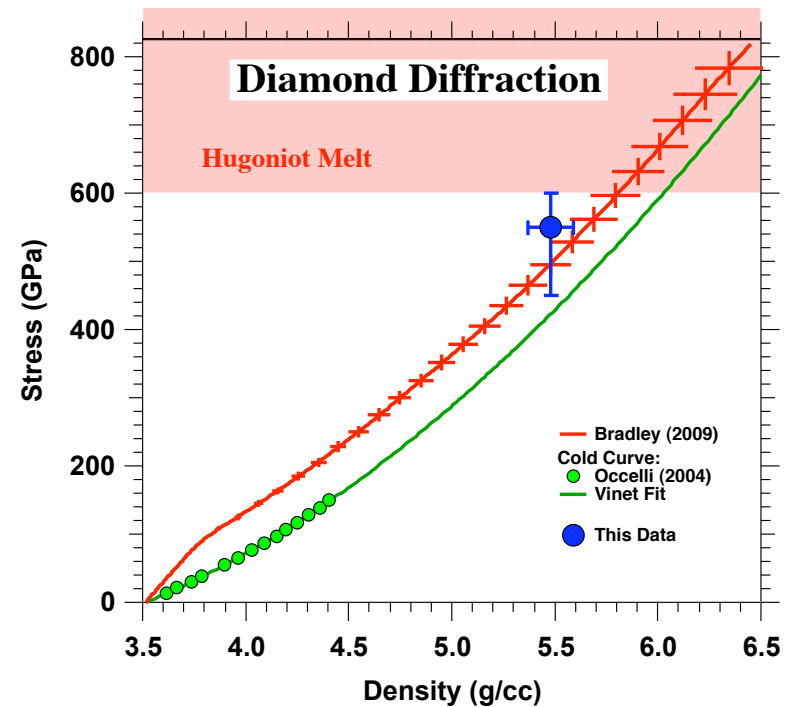
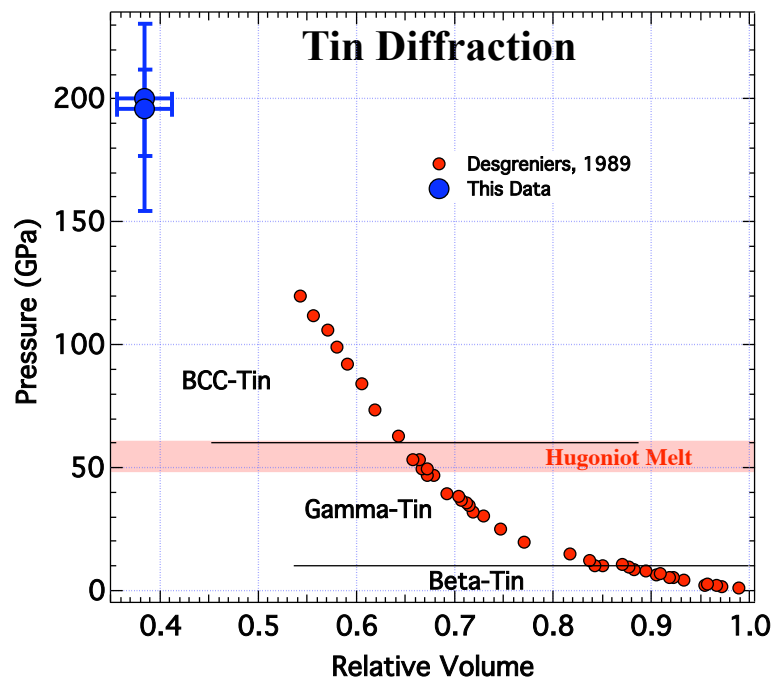
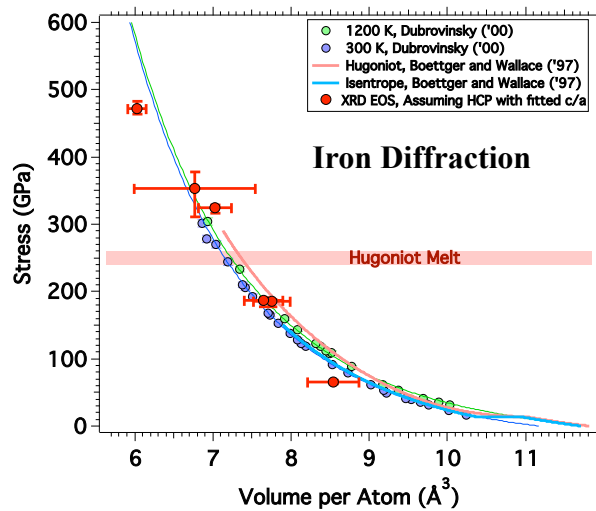
- Highest pressure X-ray diffraction ever.
- Far above Hugoniot melt (~ 250 GPa).
- Structure appears to be HCP with $c/a \sim 1.61$.
- More analyses / experiments still needed.

We can also fit c/a ratio



Our data is in good agreement with previous static data:
 $c/a = 1.61$ (Ma, et al. 2004).

We have also measured Tin and Diamond



X-ray Diffraction



- Highest pressure diffraction data ever recorded.
- Far above Hugoniot melt for Iron (250 GPa).

Future Directions

- Higher pressure.
- More diffraction lines.
- More accurate temperature determination.

DACs in the '80s ↔ Laser Compression in the 00's



DACs	Lasers
Ruby Calibration (Pressure, Temperature)	Quartz Calibration (Pressure, Temperature, Reflectivity)
Raman and Visible Spectroscopy	VISAR
X-ray Diffraction (energy dispersive)	X-ray Diffraction (angle dispersive)

The last 20 years have seen fantastic advances in DAC techniques, measurements, and diagnostics.

Our biggest challenge is to make similar progress in the next 20 years on laser-compression experiments.

The most important experimental advance will be the ability to produce a uniform sample state and perform in-situ measurements.

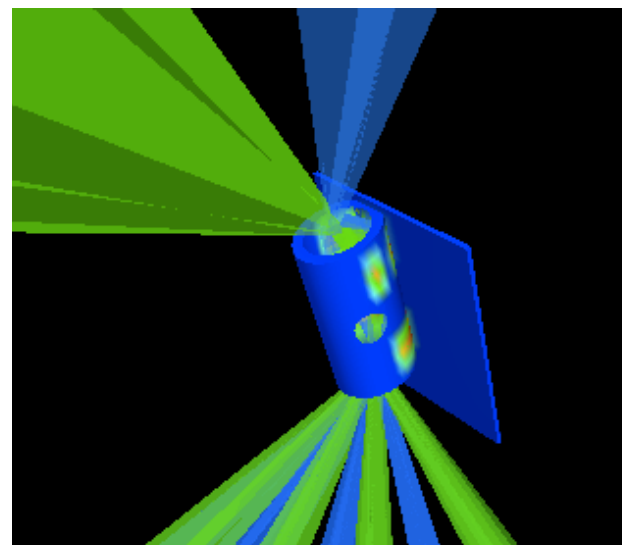
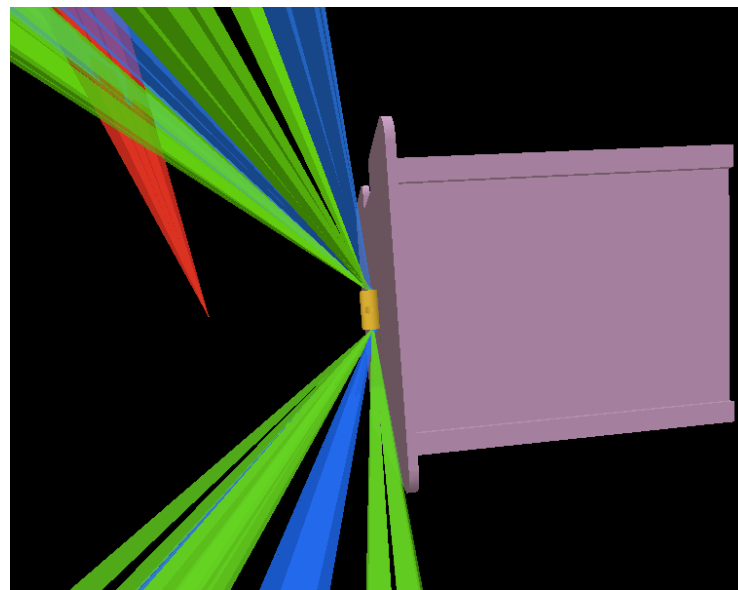
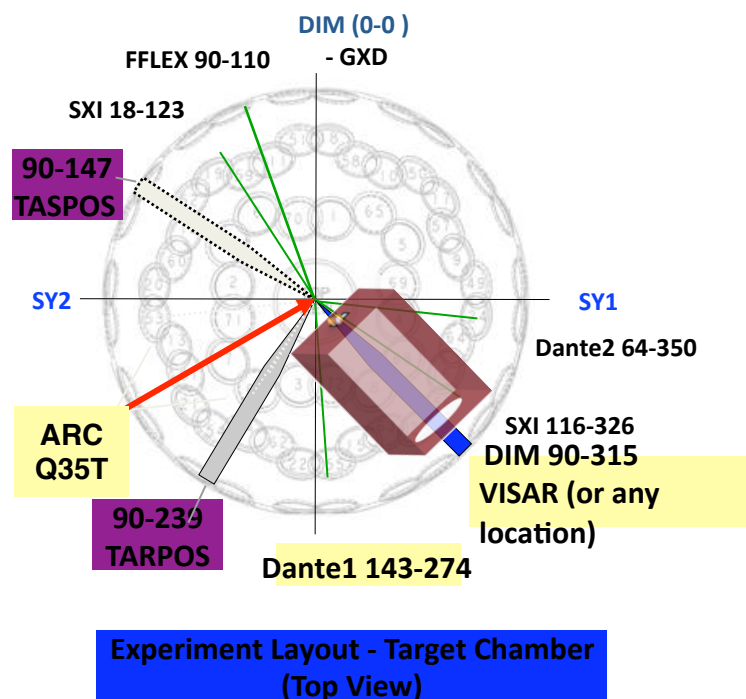
Unfortunately, transparent windows are needed (although LiF is transparent to at least 900 GPa under ramp compression).

Temperature diagnostics are critically needed (EXAFS?).

On to the NIF



We Have a Concept for Xray Diffraction on the NIF



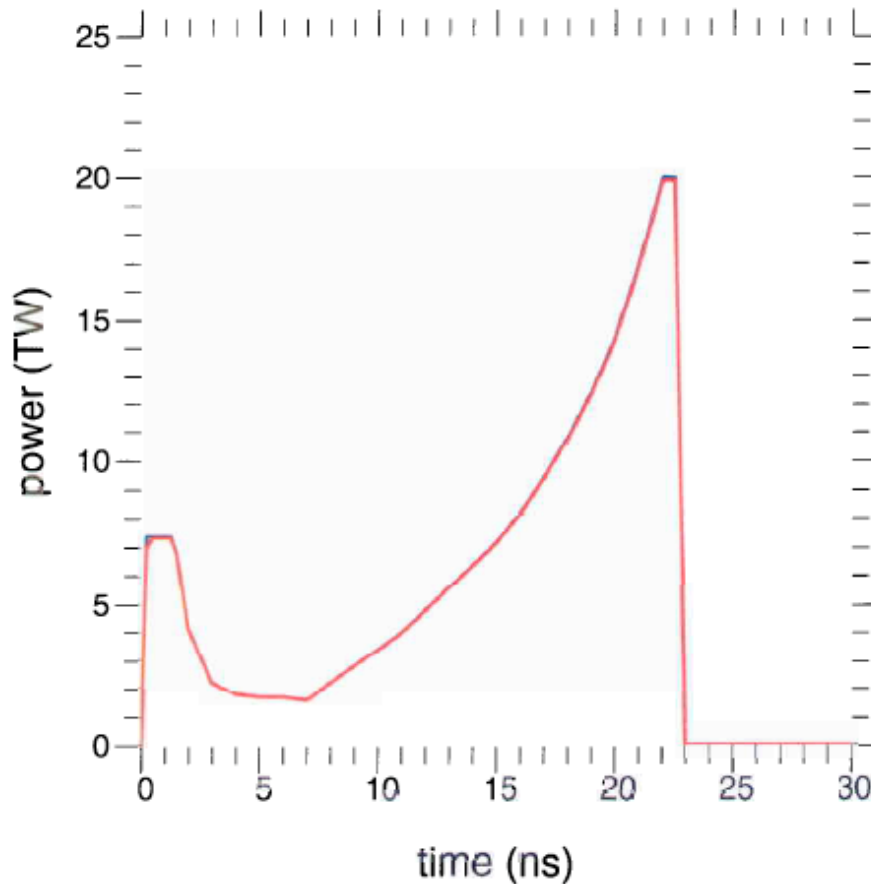
Hohlraum: 60 beams from top and bottom using quads, Q12T, Q16T, Q34T, Q43T, Q44T, Q45T, Q46T, Q11B, Q12B, Q35B, Q36B, Q41B, Q43B, Q45B, Q46B.

Plus ARC, Q35T

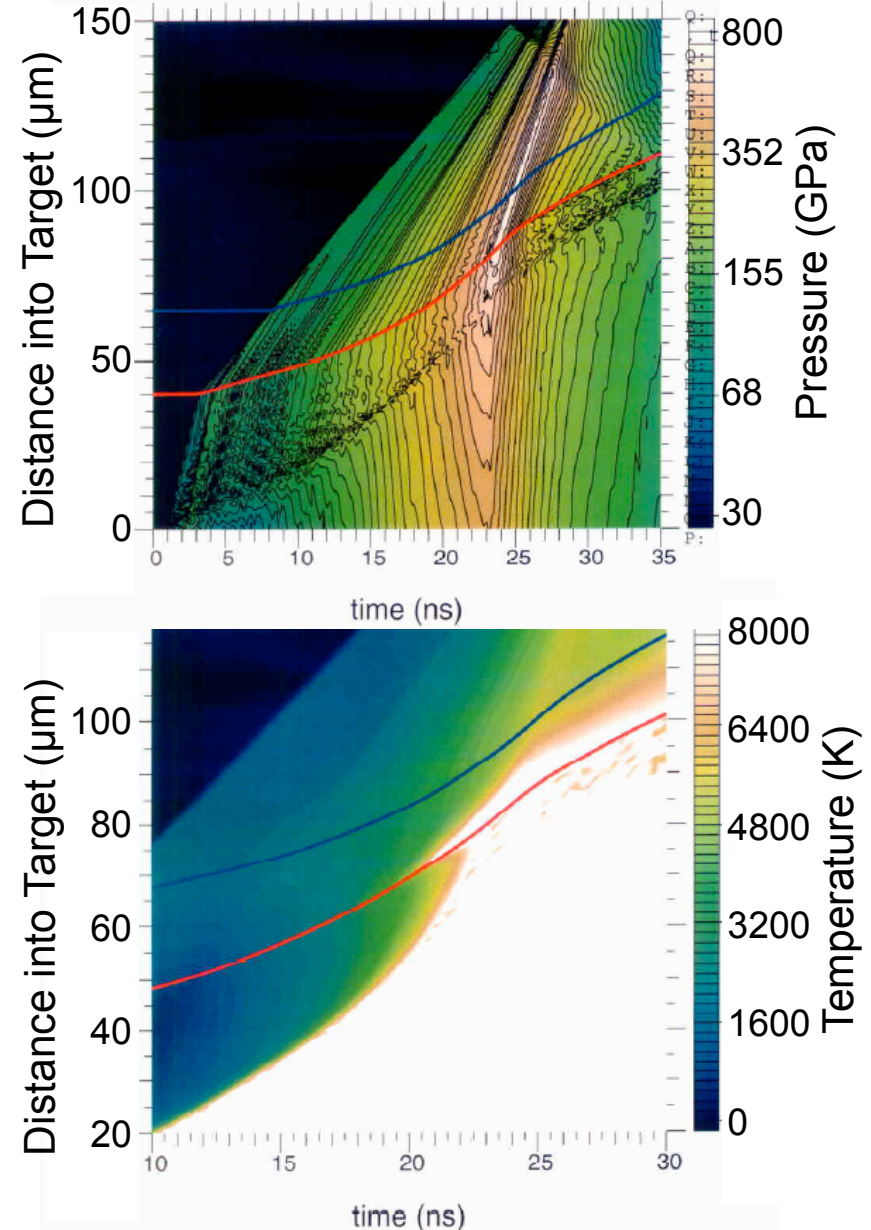
Visar is pointed at TCC.

8 Mbar Ta EOS Point Design for the NIF

Designer: Dave Braun

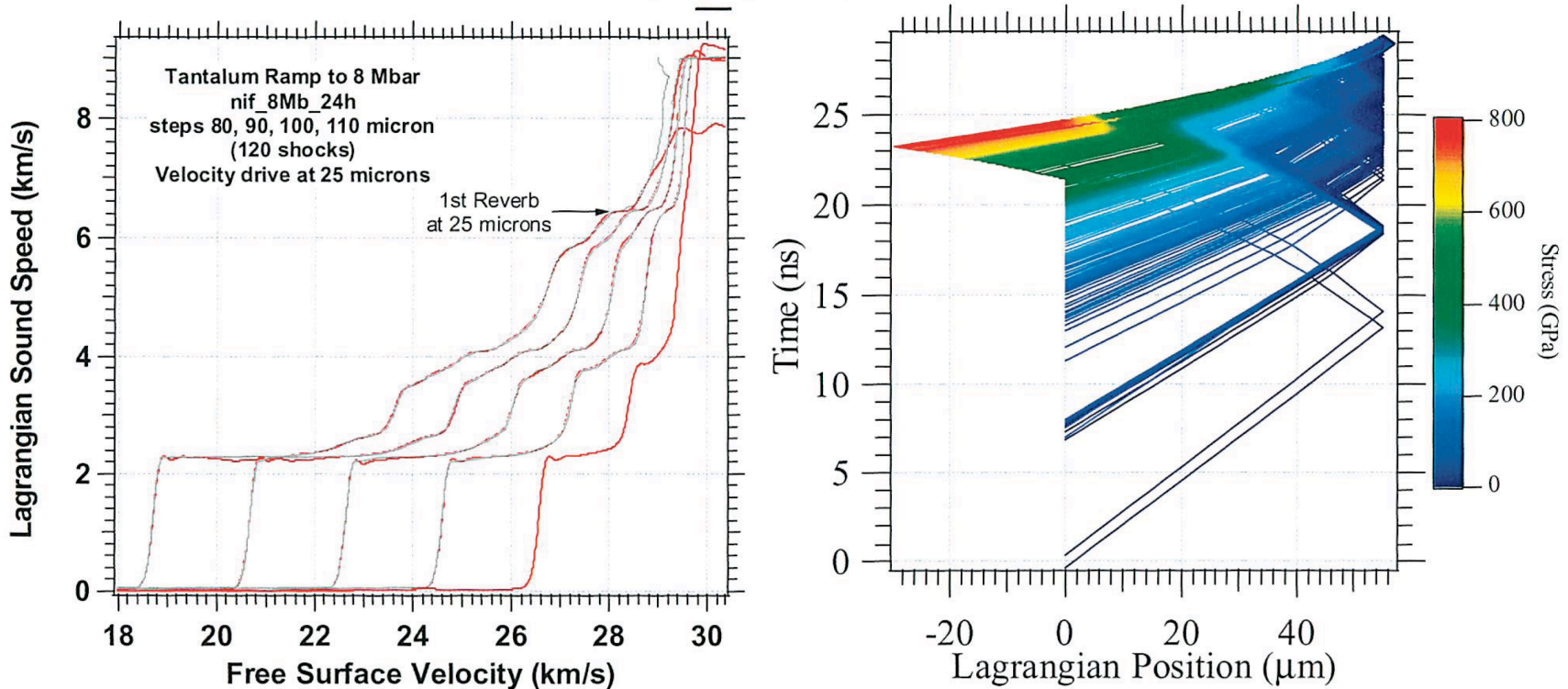


We have a design for an 8Mbar drive for tantalum on NIF using less than 200 kJ of power. We will use this design this spring.



Tantalum Ramp to 8 Mbar

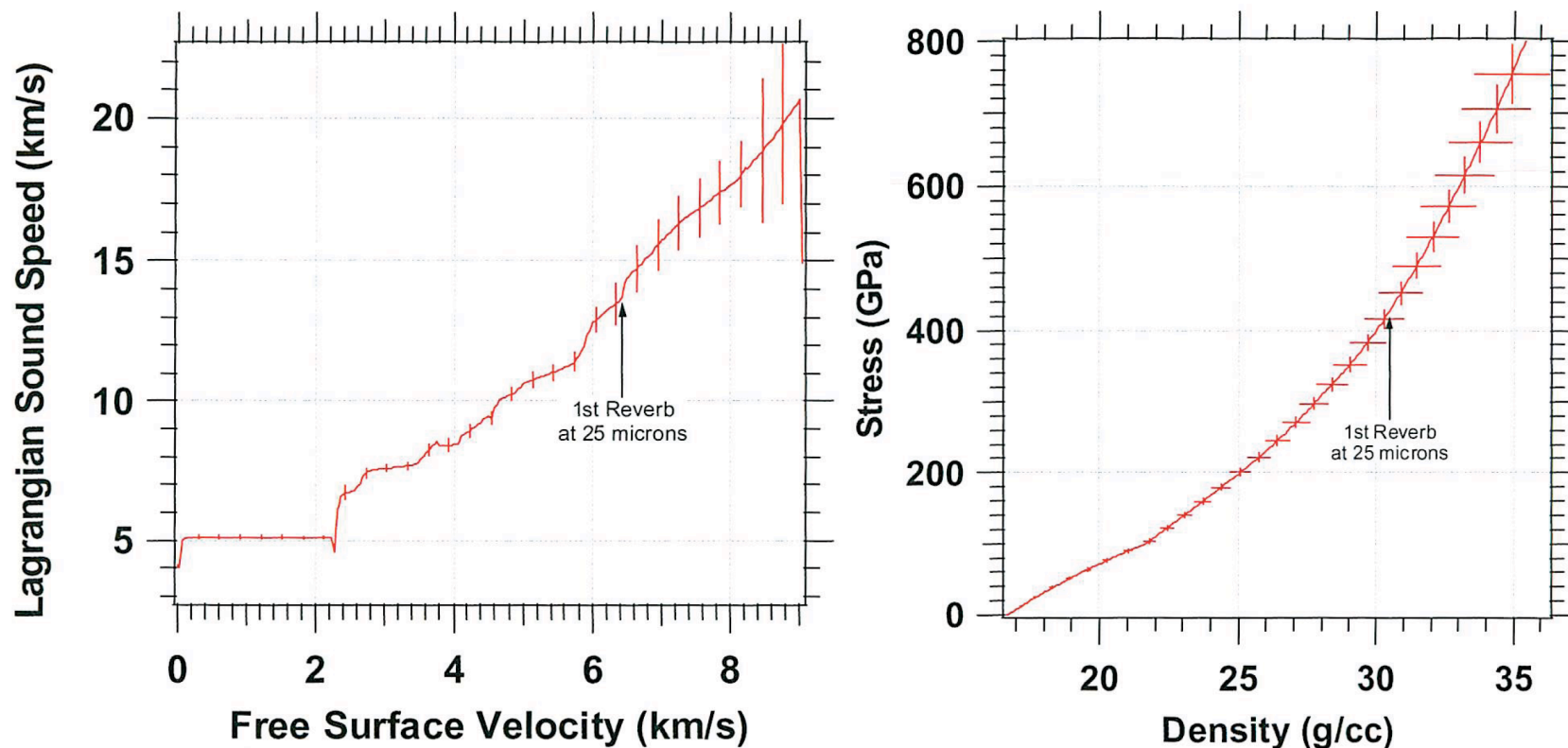
nif_8Mb24h



Velocity drive is at 25 microns so 80 micron step has reverb at 55. Note that the 80 reverb goes back to -25 microns so that only the 90 micron thick step will avoid reverbs.

Thus, we should use this drive with 80, 90, 100, and 110 micron steps. These are the steps I used in the analysis.

Tantalum Ramp to 8 Mbar nif_8Mb24h



Red curve is this analysis using errors of 0.03 km/s, 50 ps, and 100 nm. Reverberations are marked at the 25 micron position, Steps used are 80, 90, 100, and 110 microns.

We believe that we can achieve better than 6% uncertainty in a single NIF shot to 800 GPa.

Conclusions



Ramp Compression Tantalum Equation of State

- Stress-density on 8 shots to over 300 GPa.
- Very consistent with previous Z shots.

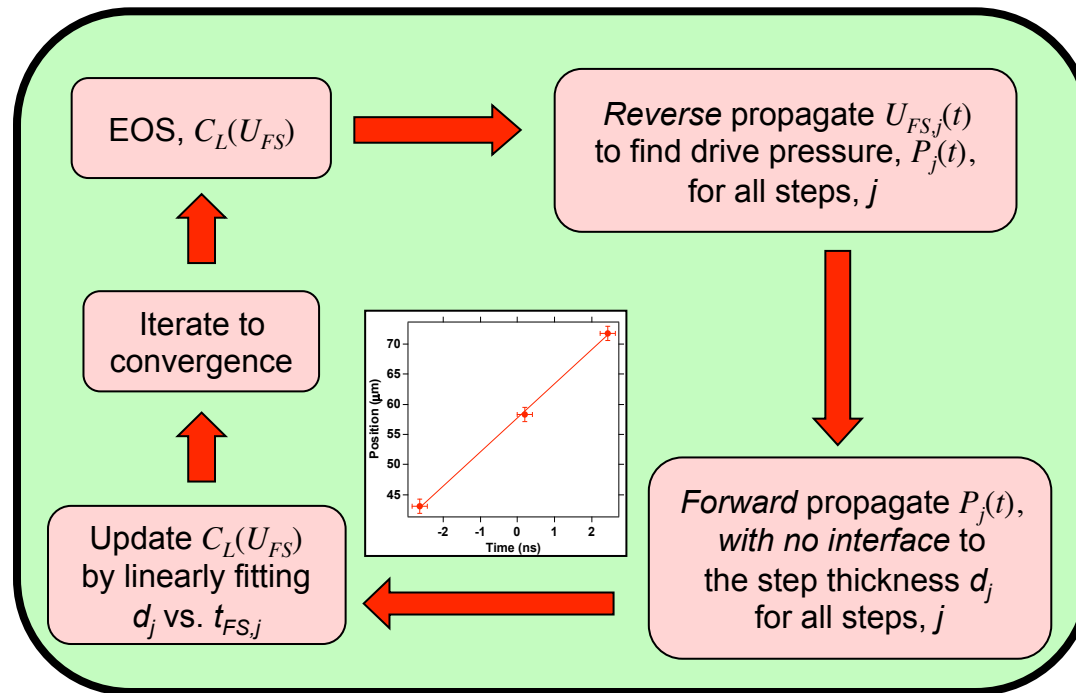
Next Year: NIF experiments to 500 GPa and more . . .

Diffraction on *solid* Fe to 470 GPa

- Highest pressure X-ray diffraction ever.
- Far above Hugoniot melt (~250 GPa).
- Structure appears to be HCP.
- More analyses / experiments still needed.

No obvious limit on pressure

Shortcomings of current analyses



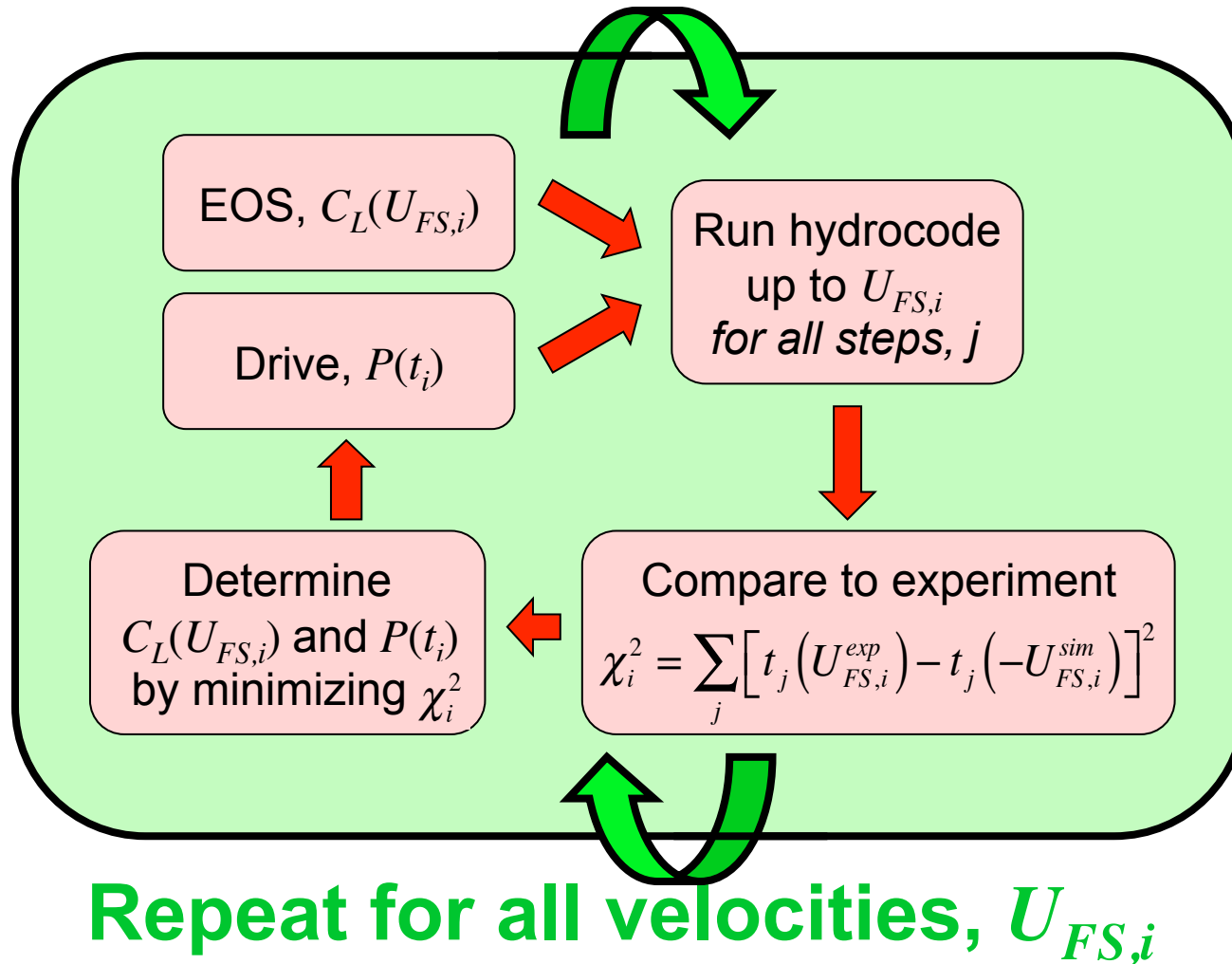
Current method requires *both* reverse and forward propagation steps.

Shocks are created by phase transitions.

Phase transitions and EP transitions both require time-dependent analysis.

We need to develop a forward only analysis method

We are developing a Forward-Only Analysis Method

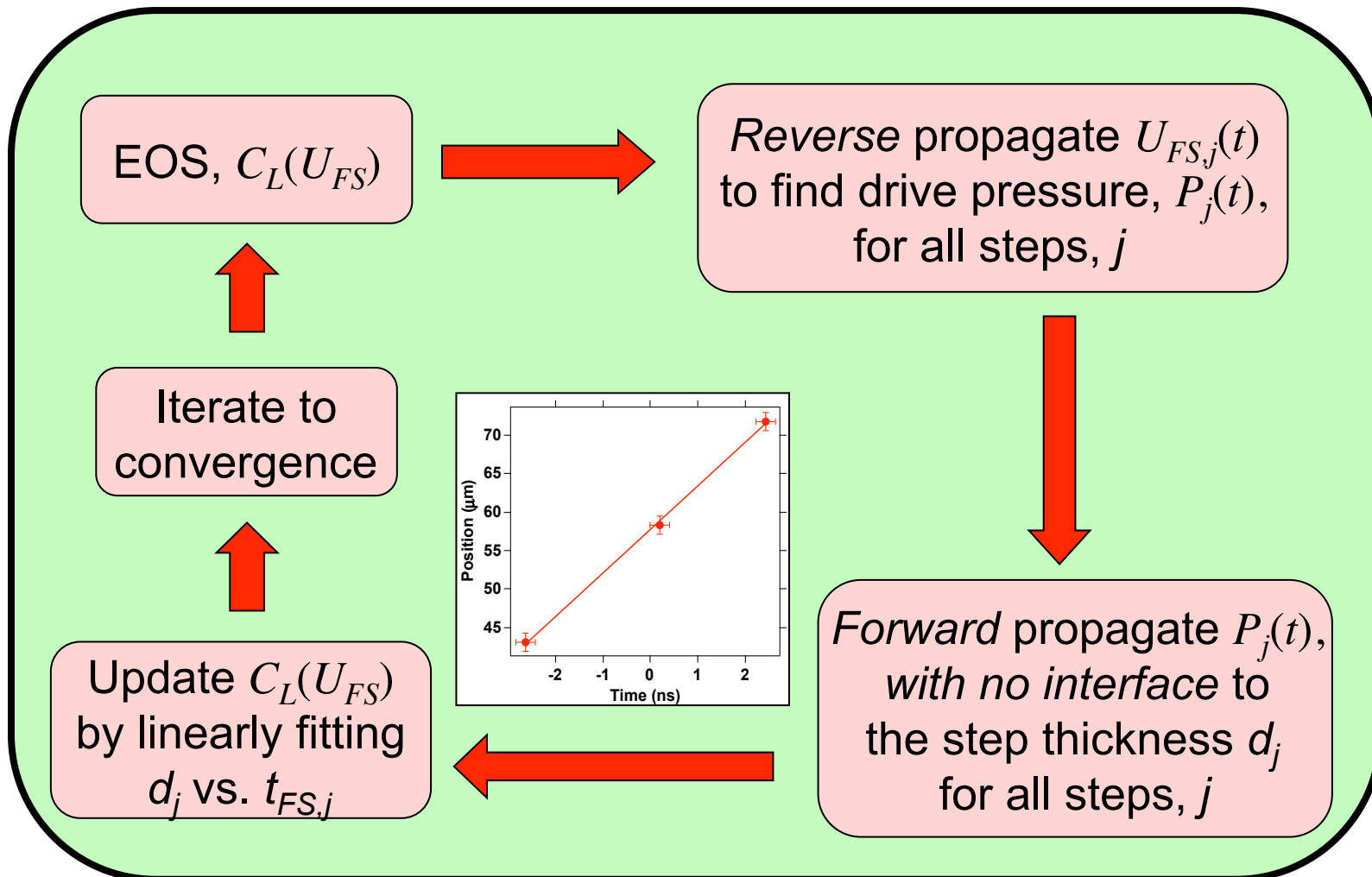


- This method still requires a model for time-dependent phase transitions.
- Exact methods being developed by Evan Reed and by Bryan Reed potentially offer a very attractive alternative.

Iterative Analysis: Correction for free-surface wave interactions.



Rothman, et al. J. Phys. D (2005)



Absolute Stress-Density Measurement



EoS and Spall Data for Ta-2.5%W

Matthew Cotton

matthew.cotton@awe.co.uk

- Introduction
- Material
- Diagnostics
- Setup
- Results
 - EoS
 - Spall
- Conclusions
- Future Work





Introduction

- Hugoniot and release isentrope data to be supplied for Ta-2.5%W
- Data supplied to assist validation of hydrocode models
- Experimental geometry chosen to provide additional information on spall parameters



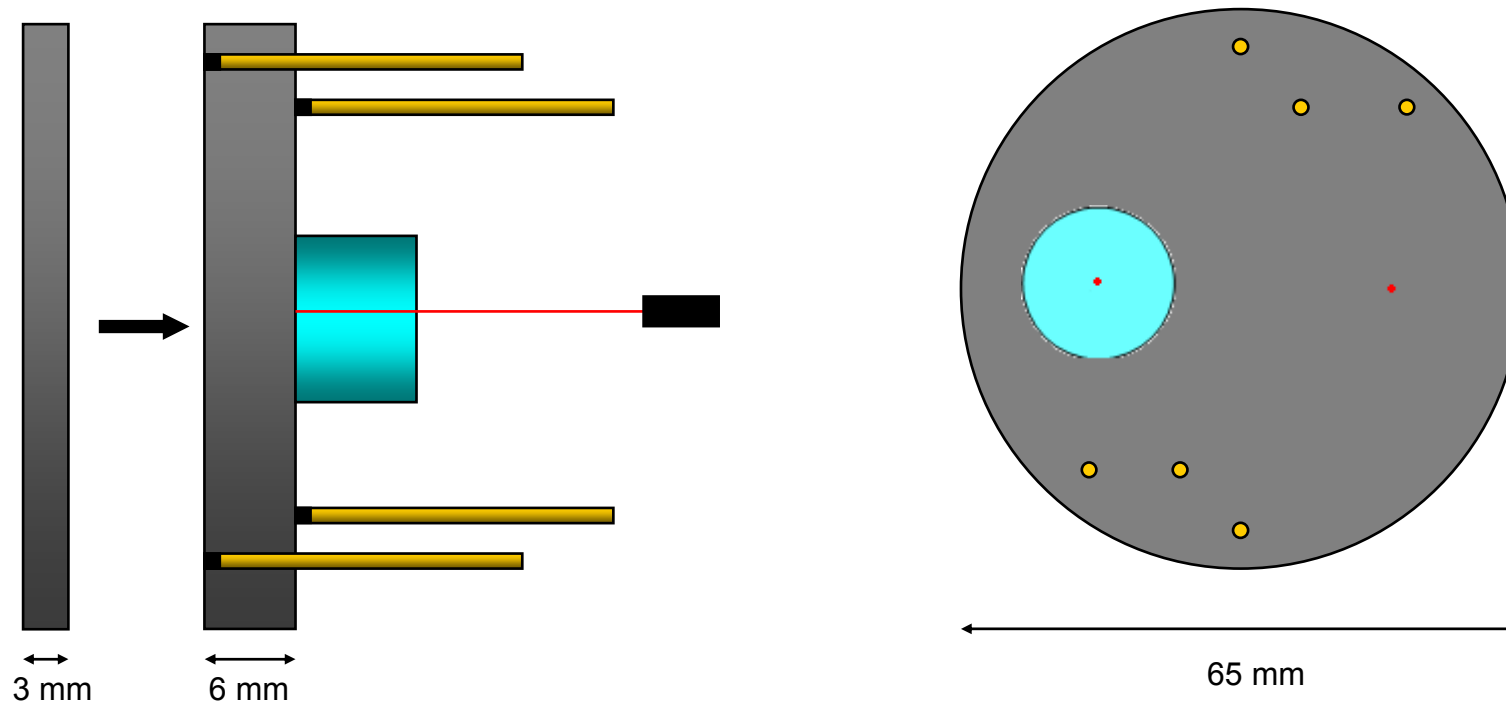
UK UNCLASSIFIED

Material

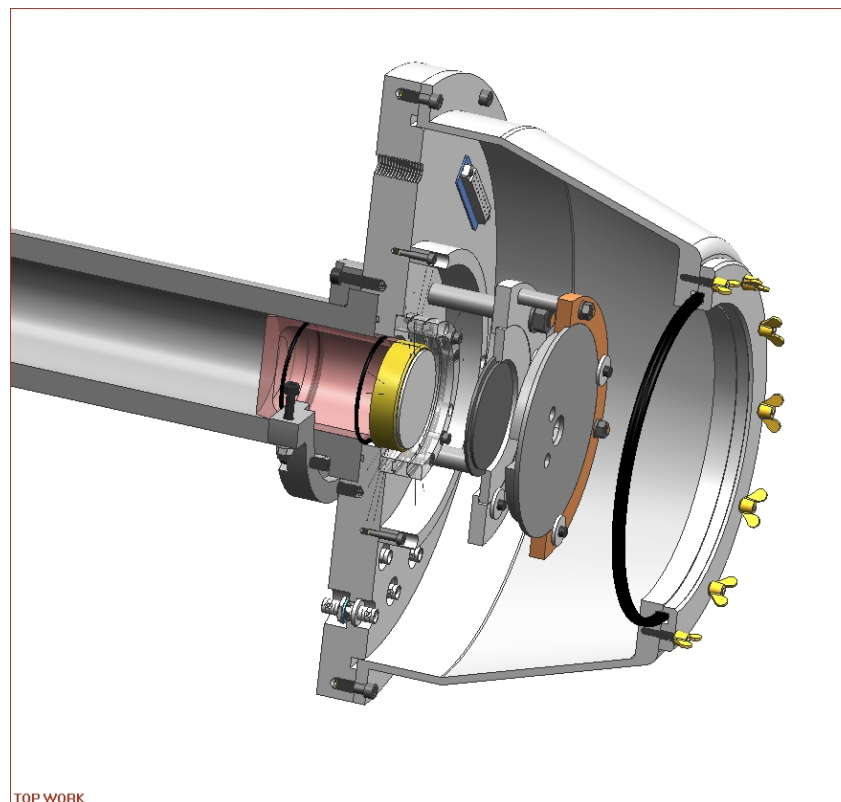
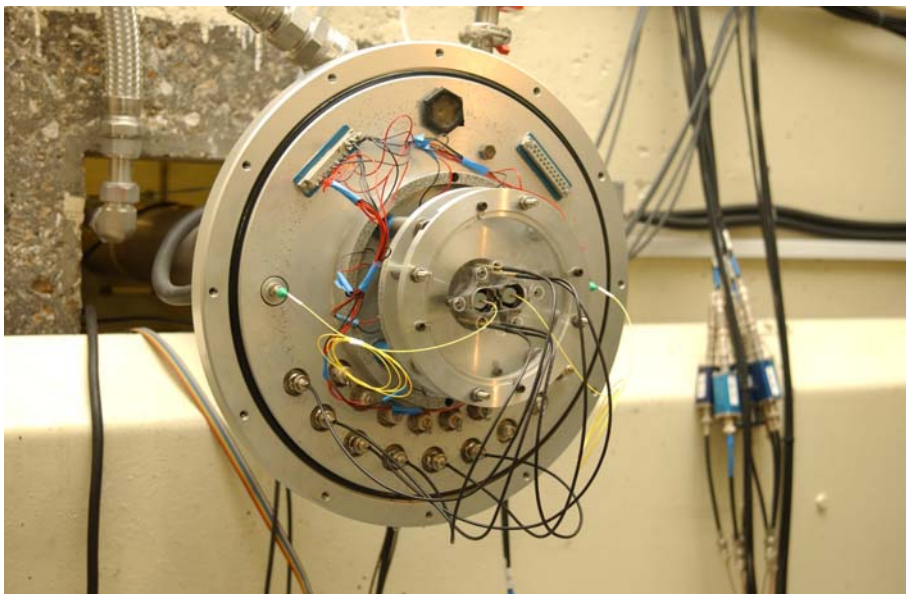
- Unalloyed Ta displays high strain rate and temperature dependence, features seen in other bcc metals
- Sensitive to impurities (embrittlement) and alloying
- Commercial use in defence-related applications due to material response at high strain rates
- W alloying leads to increased yield strength and flow stress

Diagnostics

- Het V diagnostics used to study velocity-time profile
- Quartz windows affixed to rear surface of Ta-2.5%W to allow partial release of shocked target
- Piezo pins provide time-of-arrival and shock transit time

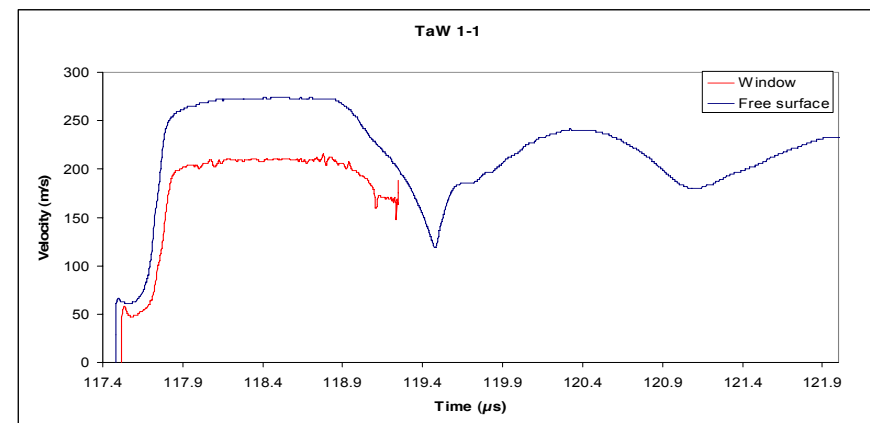
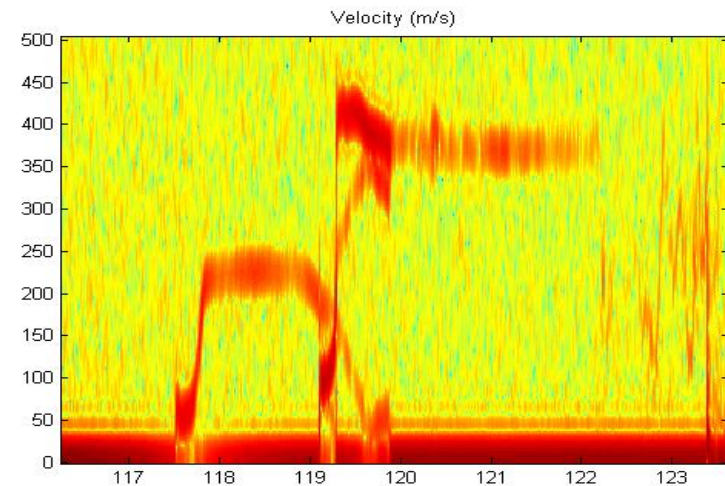


Setup



- He driven, single stage
- 150-800 ms⁻¹ velocity range
- Recently introduced class IV laser capability

- Two channels of HetV provide data from the free surface and target-window interface
- Each shot provides three points on the release isentrope
- Seven shots fired in total, six provided good data

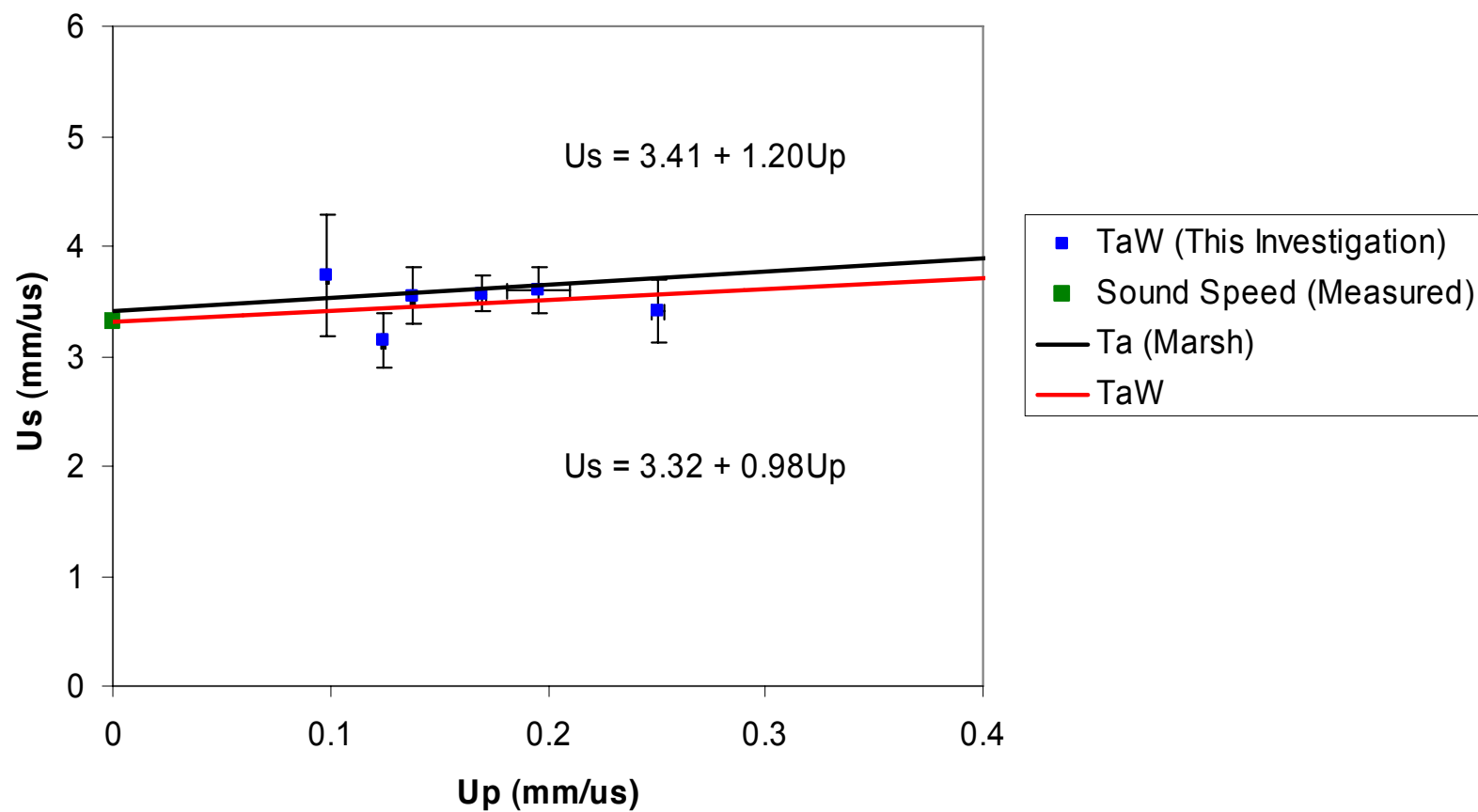




UK UNCLASSIFIED

EoS

•Us-Up Comparison



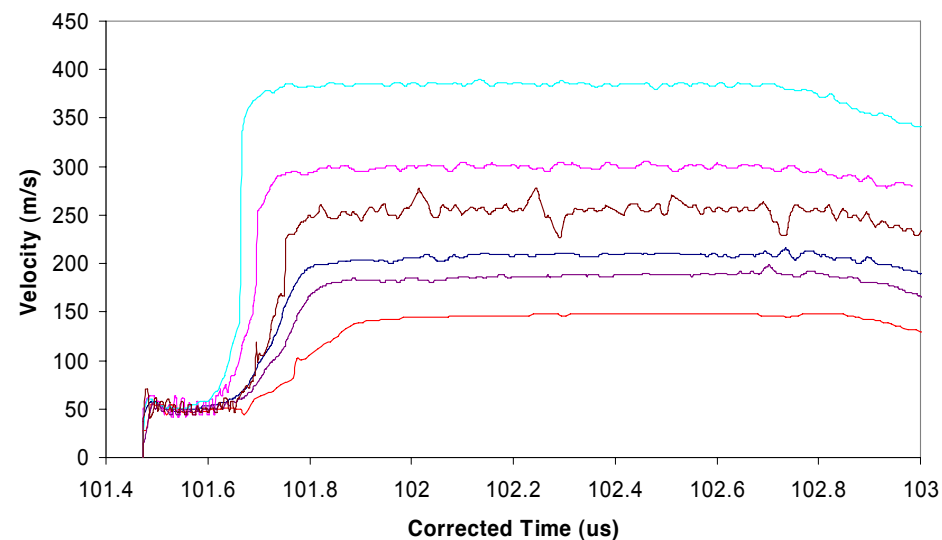
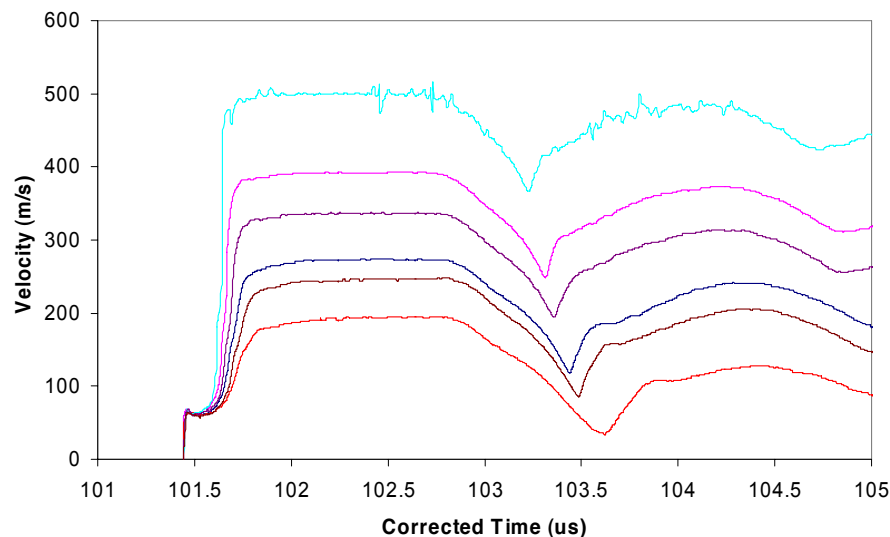
UK UNCLASSIFIED

Slide 8



UK UNCLASSIFIED

EoS



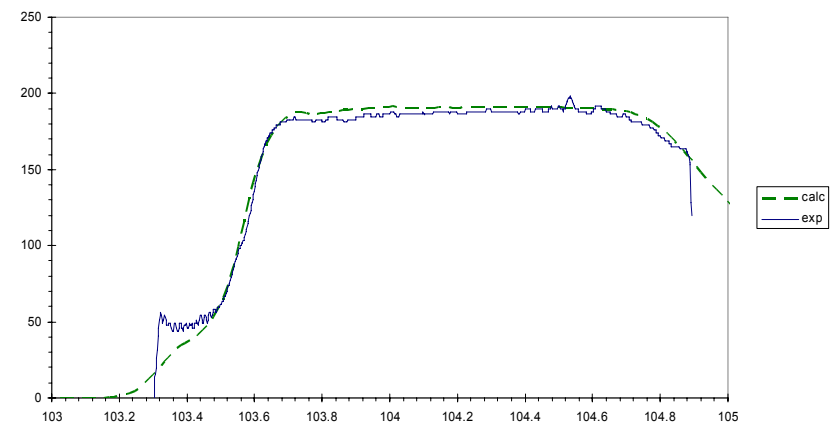
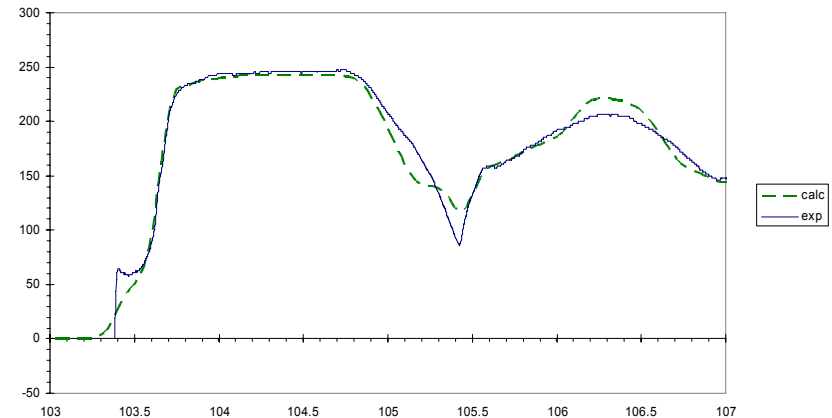
- High degree of shot to shot reproducibility
- Features visible on shock rise and release portion of trace which are common to all shots

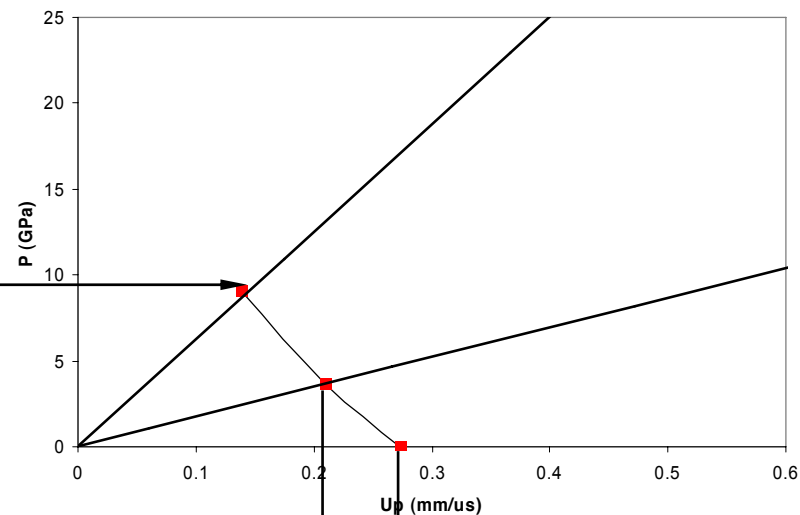
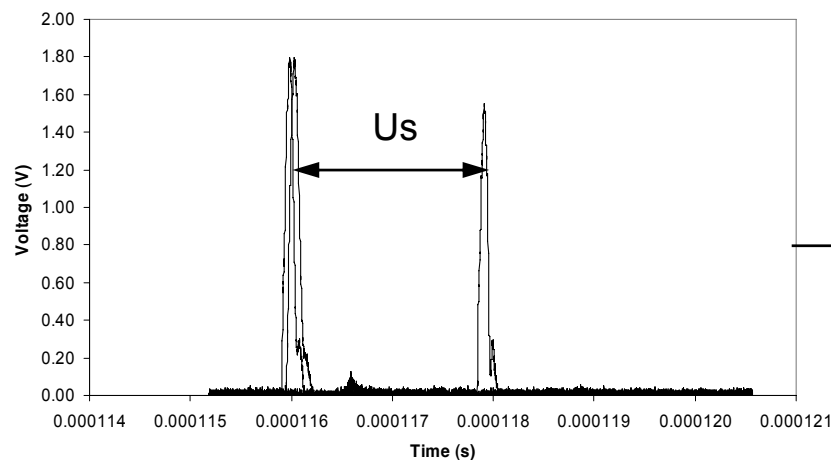
UK UNCLASSIFIED

Slide 9

EoS

- Calculations run with unalloyed Ta for comparison with Het V traces
- Accurately reproduces plastic rise and plateau, some ramping on elastic shock
- Suggests W alloying has a negligible effect on EoS.

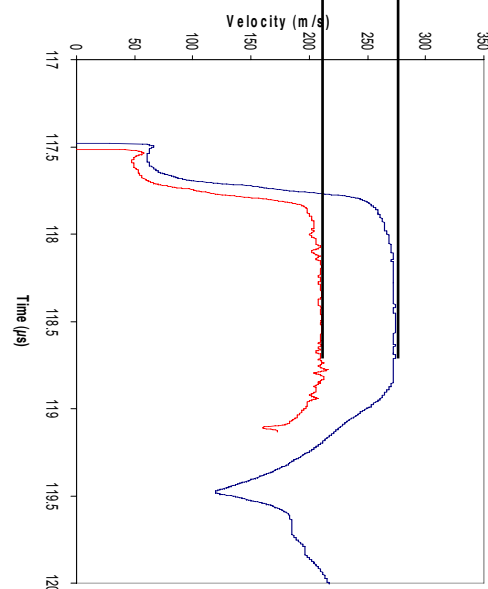




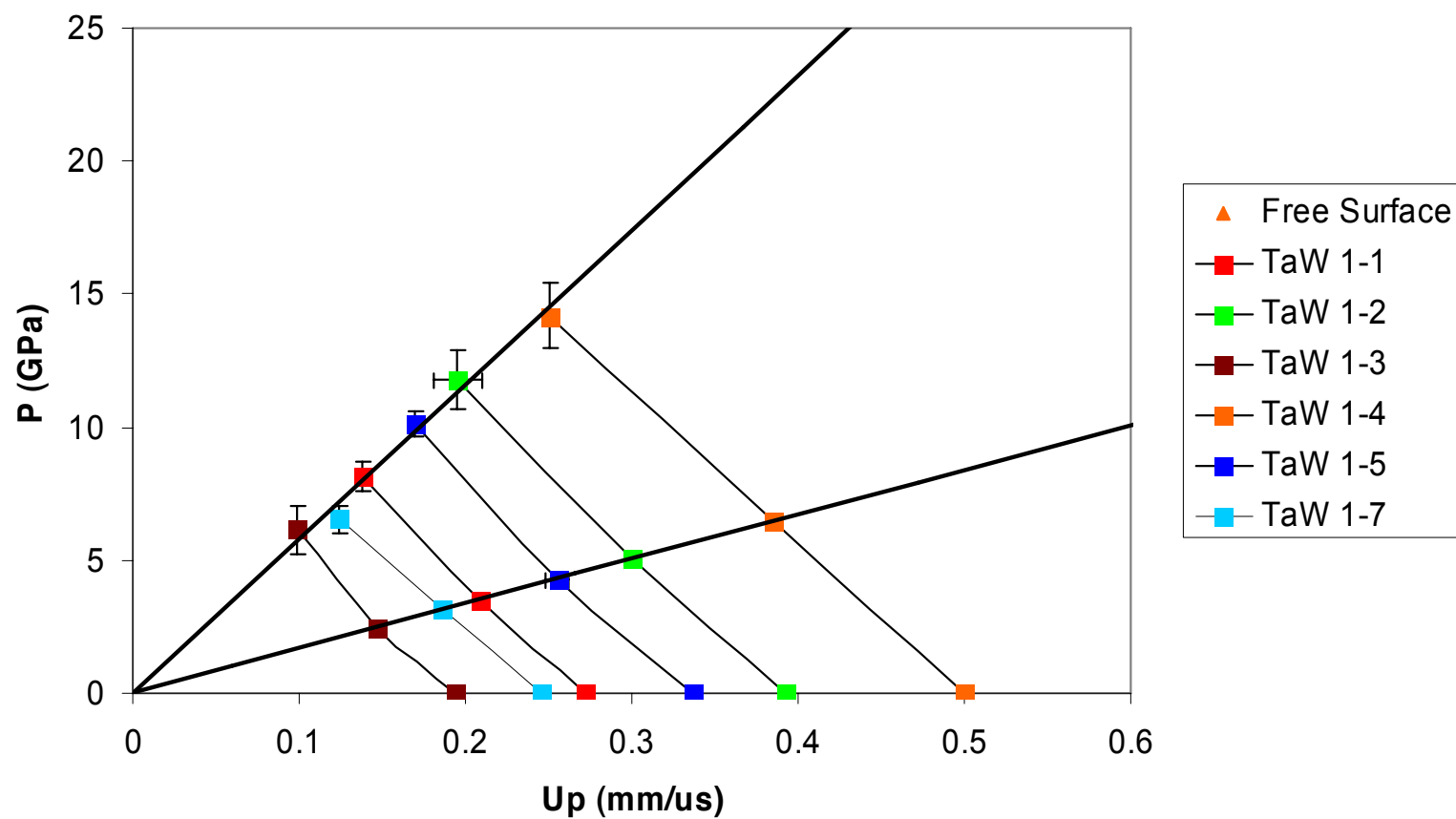
- U_p measured from plateau of Het V trace

- TaW Hugoniot point from velocity pin and piezo pin timings

$$P = \rho_0 U_p U_s$$

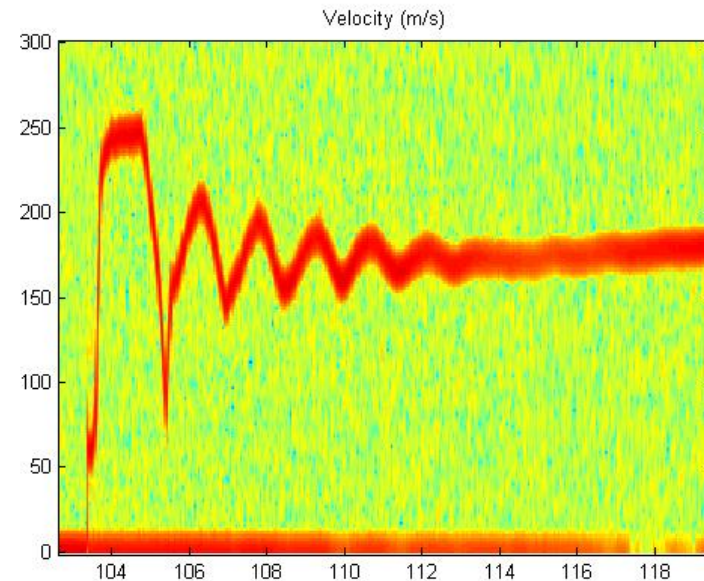


•P-Up Release Isentropes



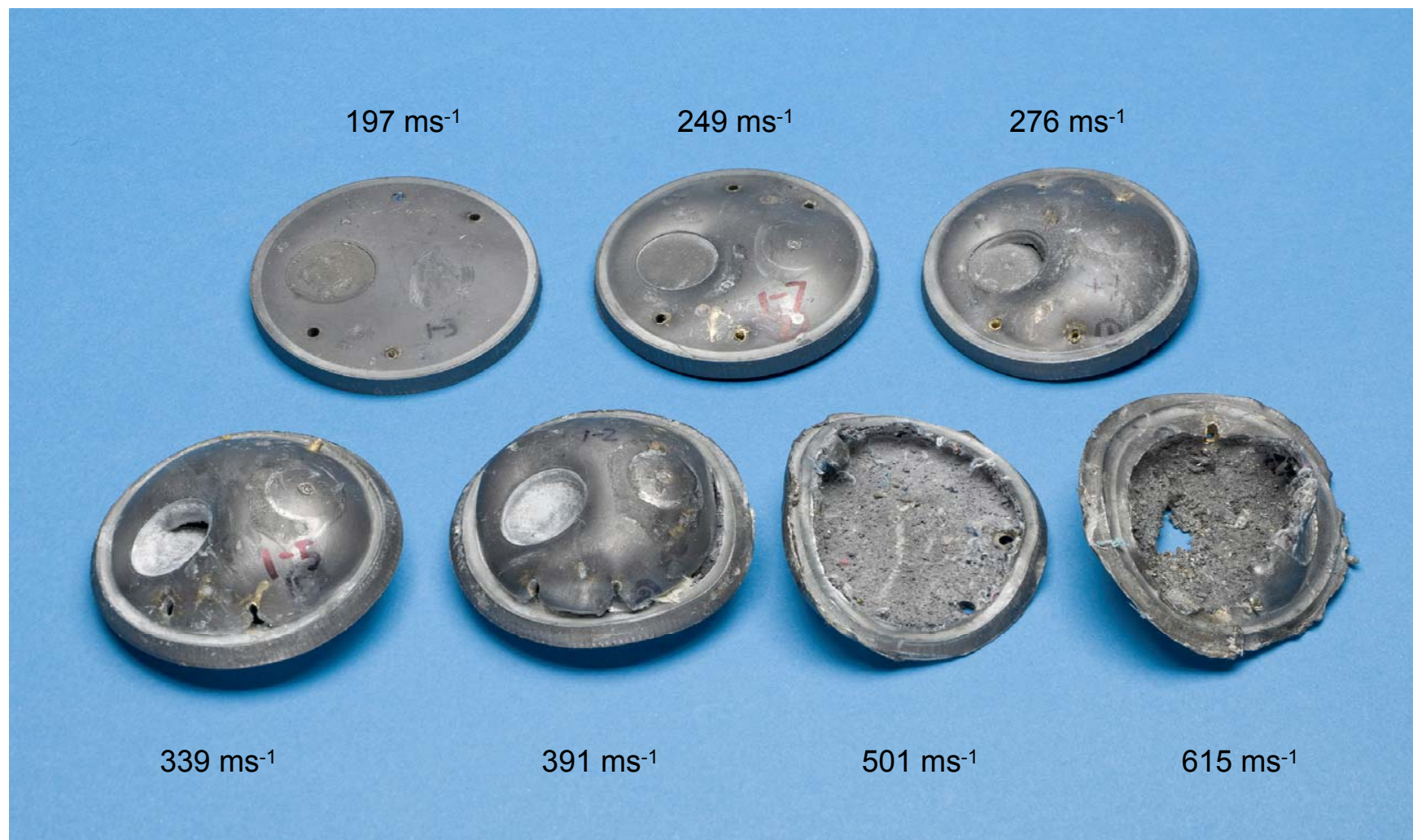
Spall

- Evidence of spall in free surface Het V traces
- Recovered targets also exhibited clear spall separation
- Comparison with pure Ta should help to quantify the effect of W alloying



Spall

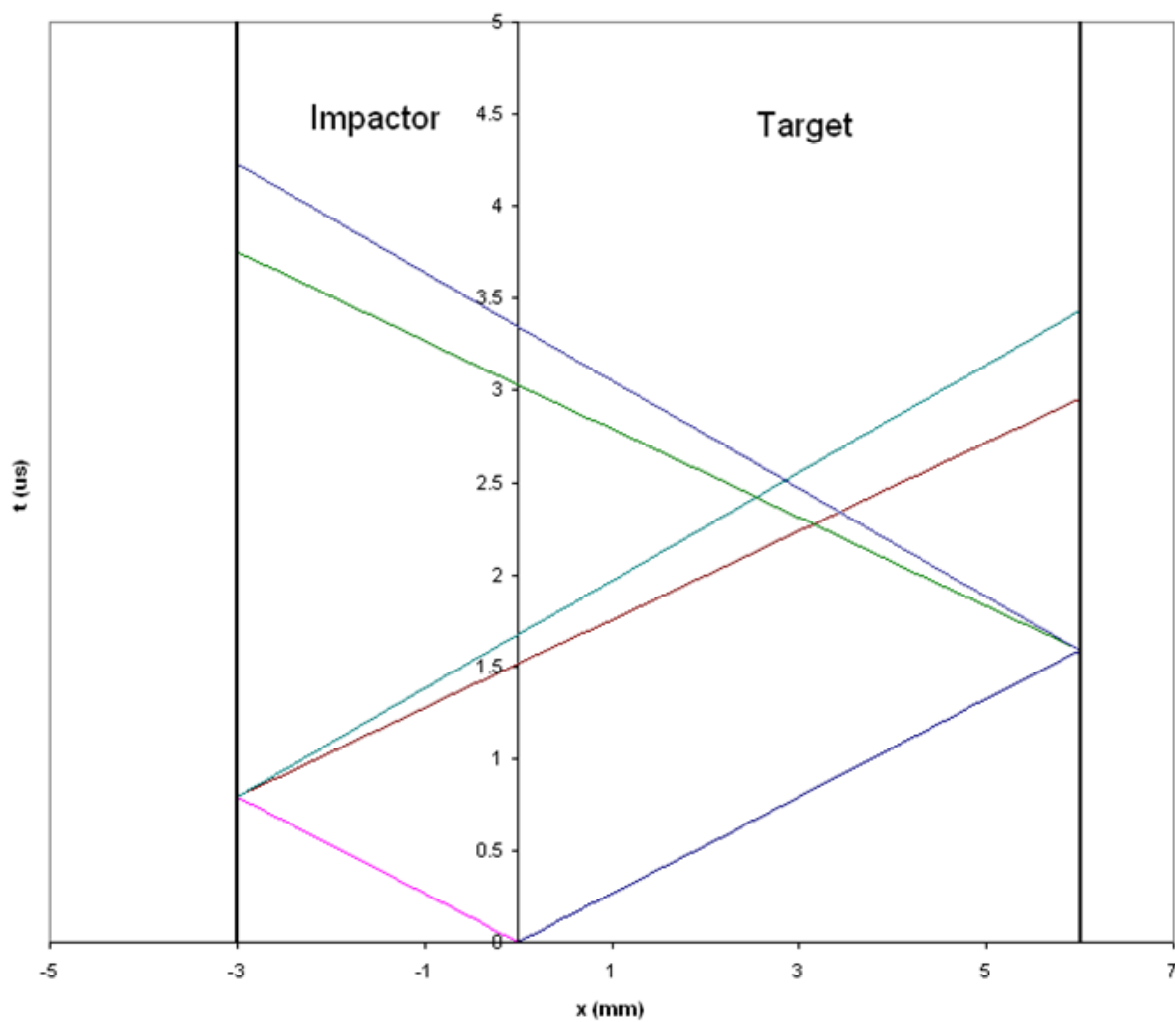
- Recovered Targets





UK UNCLASSIFIED

Spall



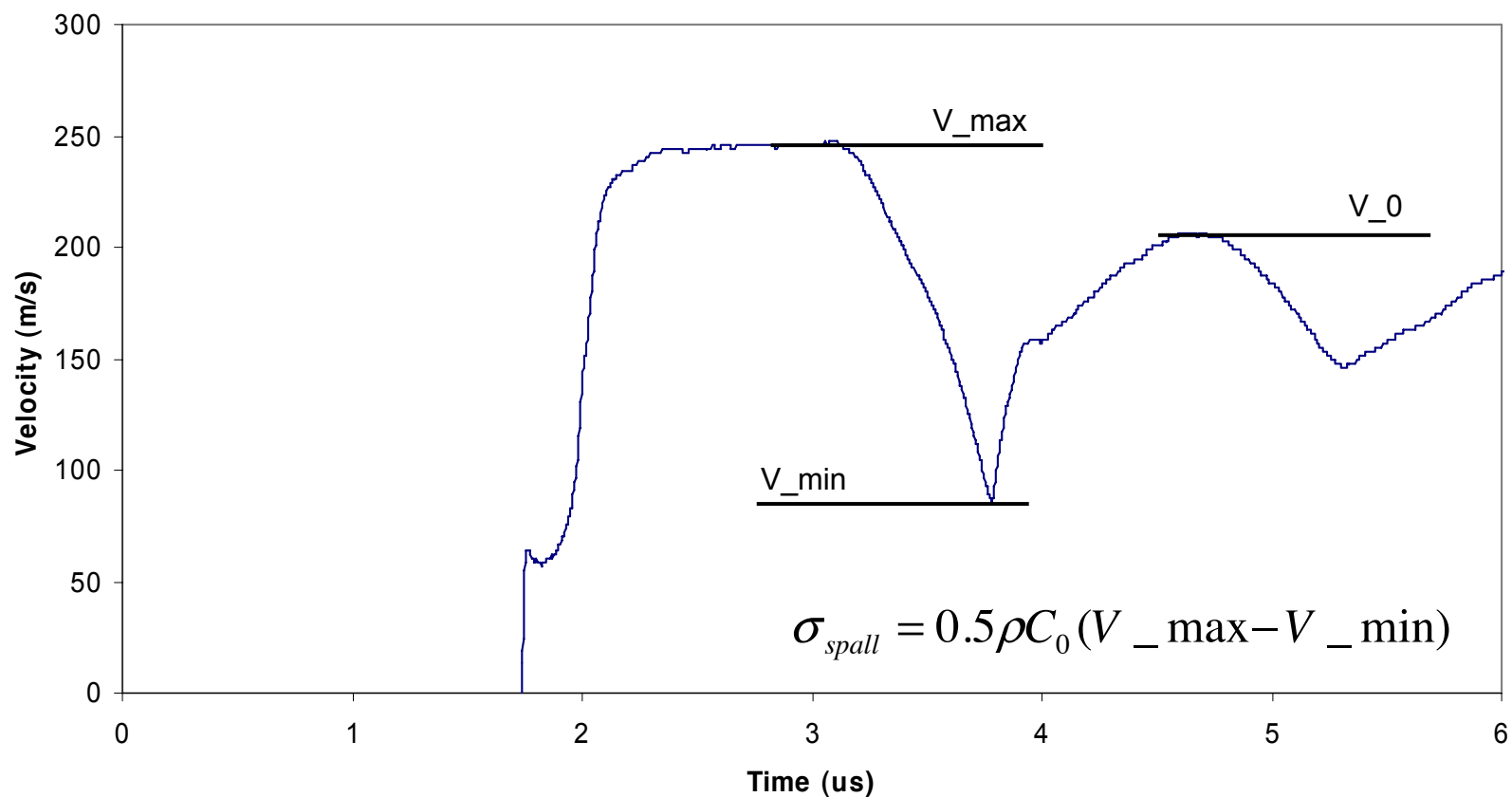
UK UNCLASSIFIED



UK UNCLASSIFIED

Spall

- Calculating Spall Strength

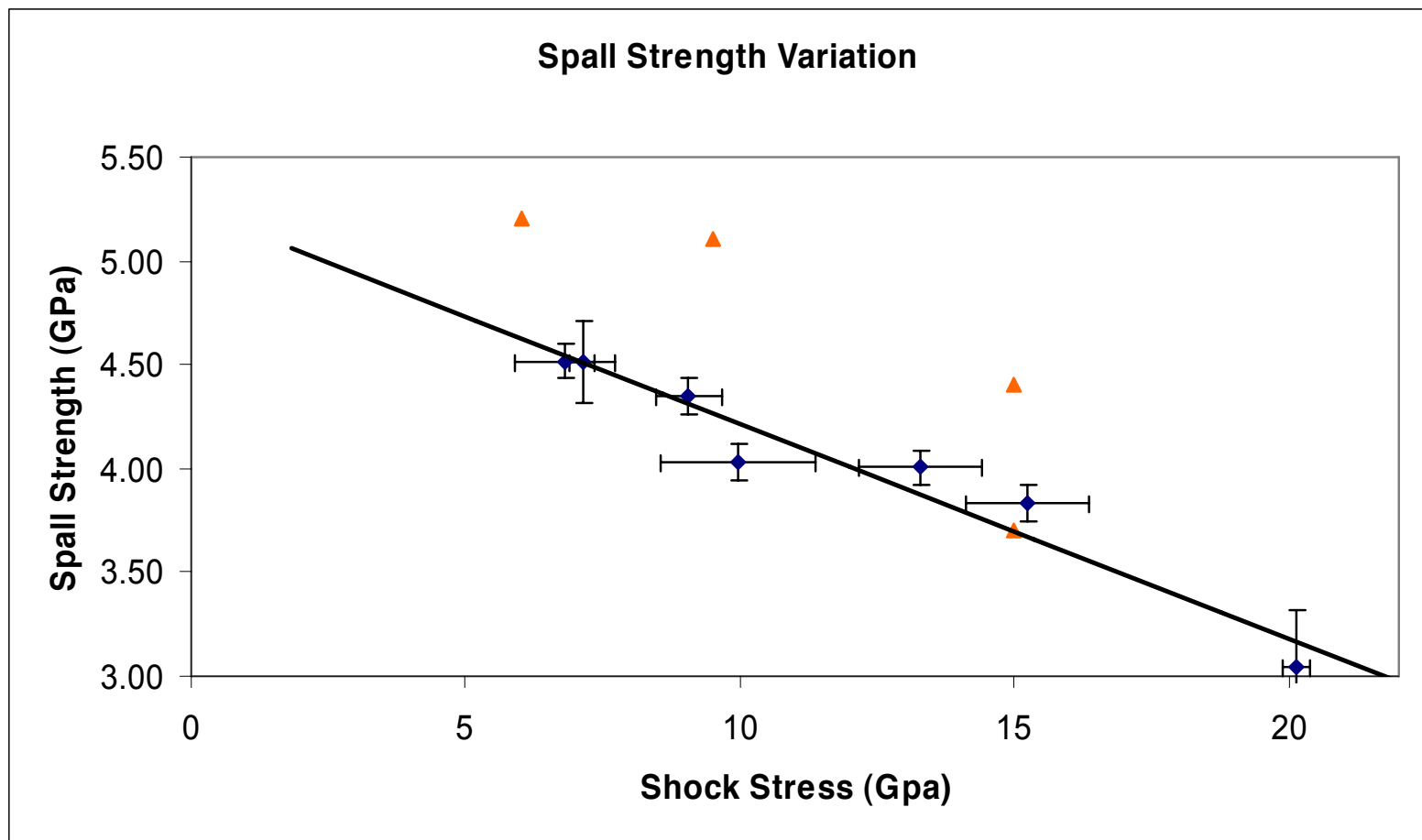


UK UNCLASSIFIED



UK UNCLASSIFIED

Spall



UK UNCLASSIFIED



Conclusions

- Seven gas gun shots performed to provide material properties information for Ta-2.5%W
- Us-Up data produced on D16 gas gun shows little variation from unalloyed Ta Hugoniot
- Release isentropes generated to provide an additional comparison for hydrocodes
- Spall strength calculated over a range of velocities, indicating a decrease in spall strength with increasing impact stress
- Comparison with pure Ta indicates spall strength decreases with W alloying



Future Work

- Further experiments planned to study spall in more detail
 - Impact stresses chosen to induce incipient spall in TaW
 - Post-shock sectioning and imaging of targets to provide information on spall plane formation
 - Varying impactor thickness to look at the effect of altering pulse width
- Side-by-side comparison of Ta and TaW also being considered



Acknowledgments

- Pete Keightley
- Mike Lowe
- Nathan Routley
- Jeremy Millett
- Jayesh Meghani
- Vince Durrant
- Jim Eliot



Questions



The Behaviour of Body Centred Cubic Metals During Shock Loading

Jeremy Millett, Glenn Whiteman, Nigel Park, Neil Bourne,
Stewart Stirk

Jeremy.millett@awe.co.uk

www.awe.co.uk



Introduction

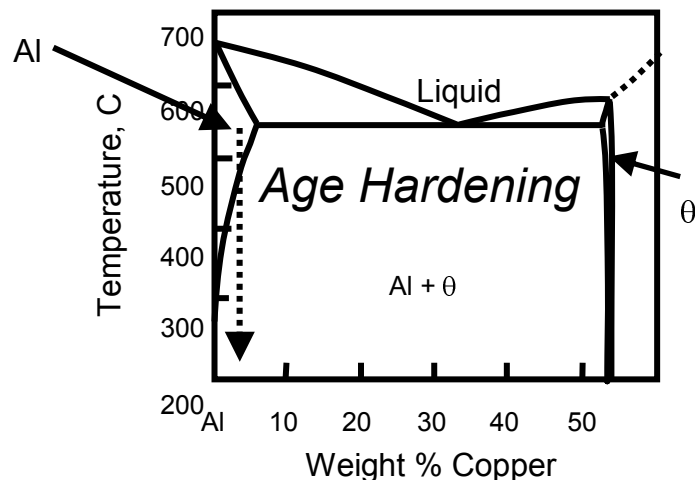
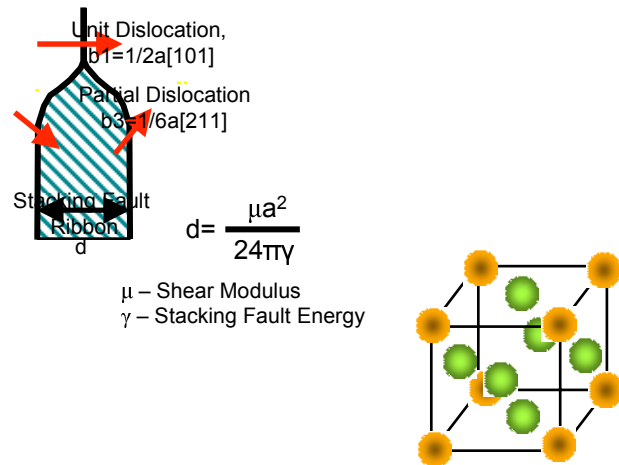
- AWE has interest in a wide range of metals and alloys
 - Cu, SS, Ti-6Al-4V, Ta, Al...
- Fundamental requirement to understand deformation mechanisms to derive and validate physics based models
- Body Centred Cubics of particular interest
 - Ta, W, Mo, Nb and alloys



Shock Loading Experiments

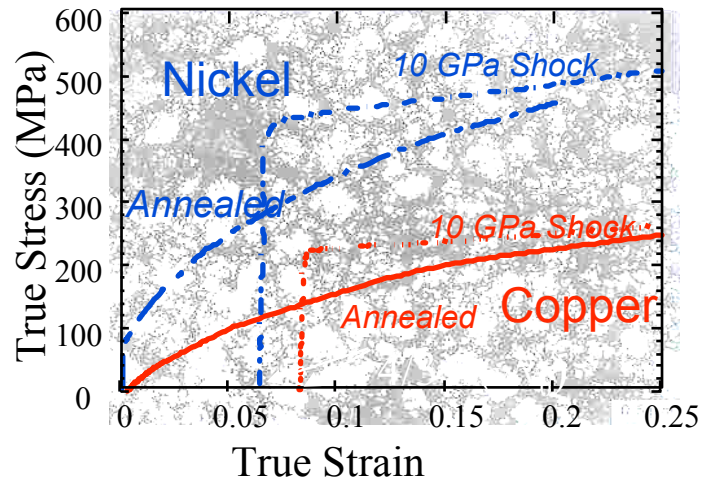
- Time resolved
 - Measurement of shock profiles (stress, velocity *etc*)
 - Observation of waves via high-speed photography, flash x-ray, proton radiography *etc*
- Time integrated
 - Post-mortem analysis of shocked samples
 - Microstructure, chemistry, mechanical properties
 - Loading + Pulse Duration + Release
- Major assumption
 - Sample is semi-infinite
- Both time resolved and time integrated experiments needed to understand materials during shock loading

So Far in FCCs...

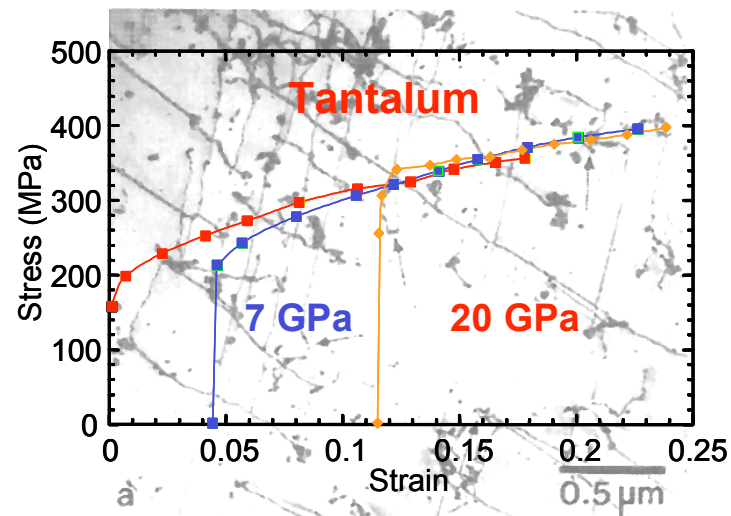


- Stacking fault energies
 - Ni, Ni-60Co, SS304L
 - Shift from dislocation generation to twin formation
 - Reduction in post shock hardening
- Lattice Ordering
 - Ni, Ni₃Al
 - Dislocation cells to planar arrays and twins
- Effects of precipitation hardening
 - Al6061, Cu-2%Be
 - Dislocation cells to randomised distributions
 - Reduction in post shock hardening
 - More details in session 6

Post Shock Properties



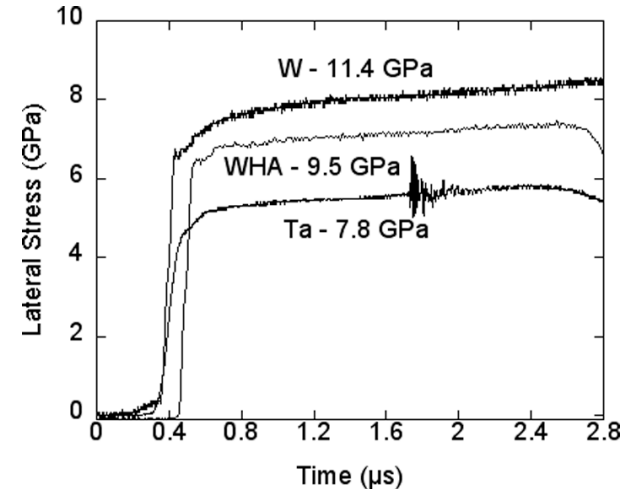
- High stacking fault FCCs show hardening behind shock front. Recovered samples show greater hardness compared to as-received material – dislocation generation – cells



- BCCs show softening behind shock front. No hardening in recovered samples compared to as-received material – motion of existing dislocations

Data on BCCs Limited...

- Large body of data on tantalum and alloys
 - EoS, spall, shear strength, recovery
- Iron and ferritic steels
 - α - ϵ phase transformation, recovery
- Tungsten and heavy alloys
 - EoS, shear strength, recovery
- Less detail on V, Cr, Nb, Mo
- So far assumed Ta and W 'typical' of BCCs



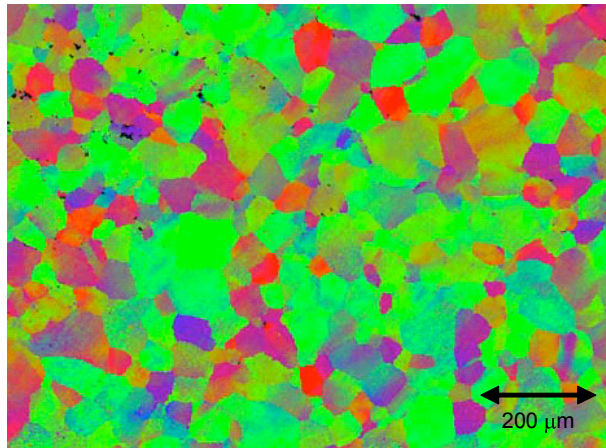
22	23	24	25	26	
87	50.94	52.00	54.94	55.85	5
40	41	42	43	44	
22	92.91	95.94	(98)	101.07	10
72	73	74	75	76	
149	180.95	183.84	186.21	190.23	19
104	105	106	107	108	



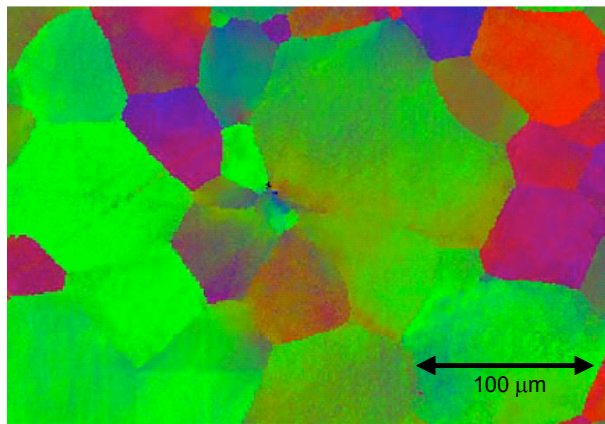
Cannot View Shock in Isolation...

- Microstructural information
 - Grain size, phase balance and distribution
 - Preferred orientations (texture)
- Quasi-static and intermediate mechanical properties
 - Tension and compression
 - SHPD
- Post shock behaviour
 - Microstructure, post shock mechanical response
- Elastic response
 - c_L , c_S , ρ_0 , ν

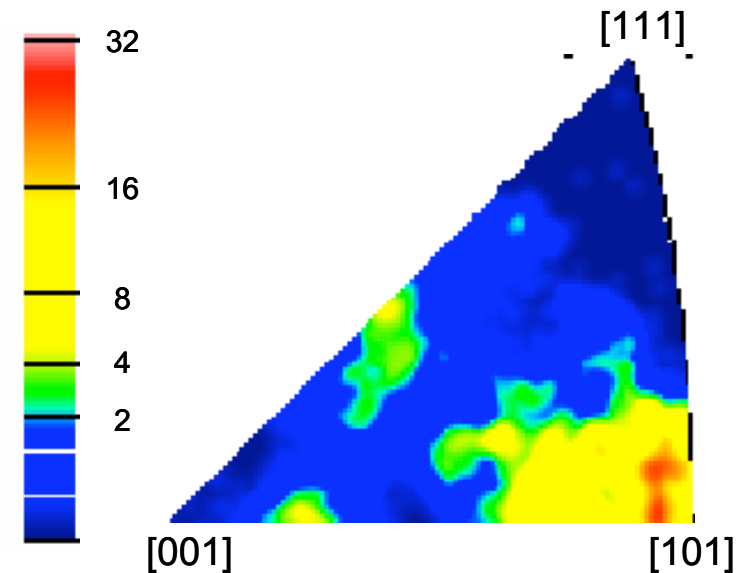
Nb – Microstructure and Inverse Pole Figure



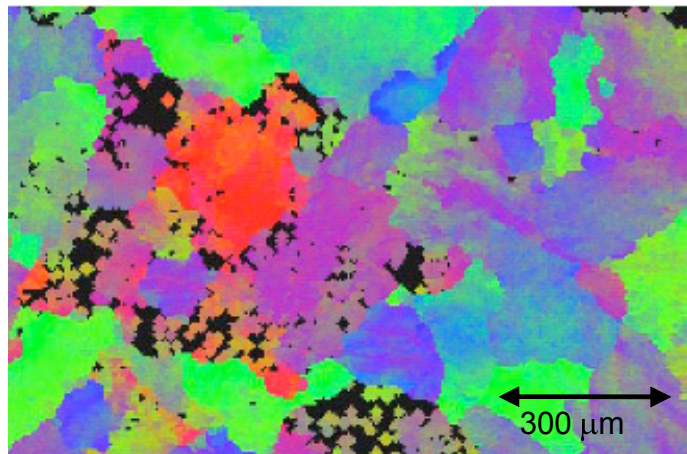
Normal



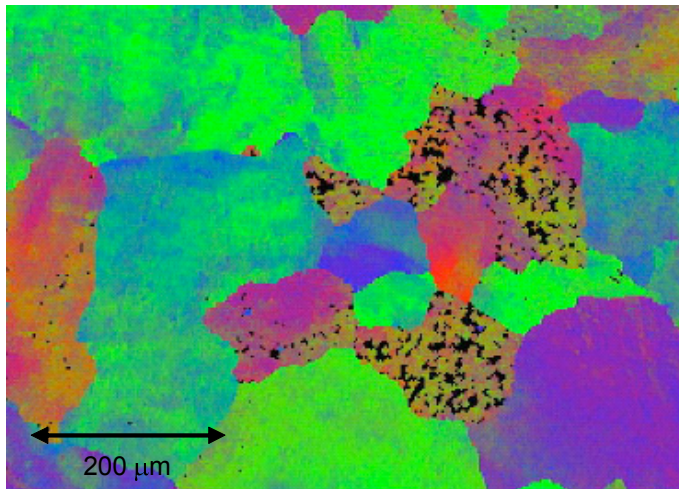
Radial



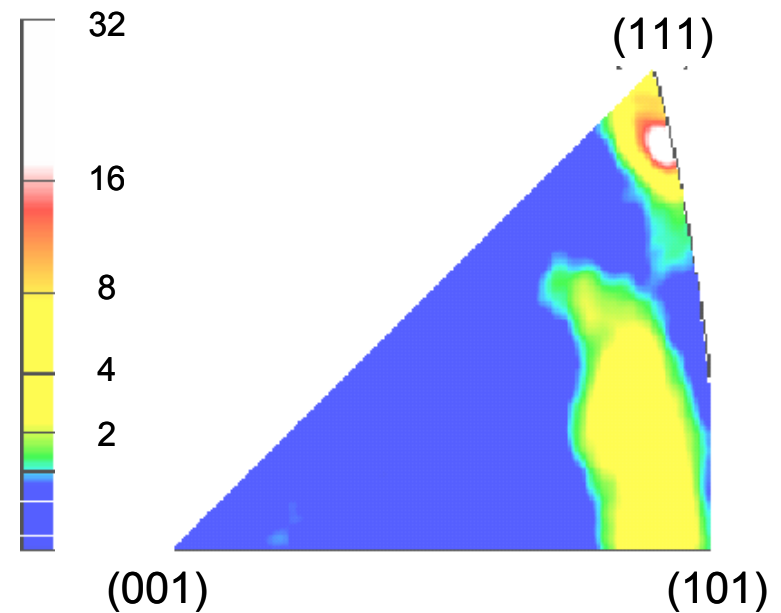
Mo – Microstructure and Inverse Pole Figure



Normal



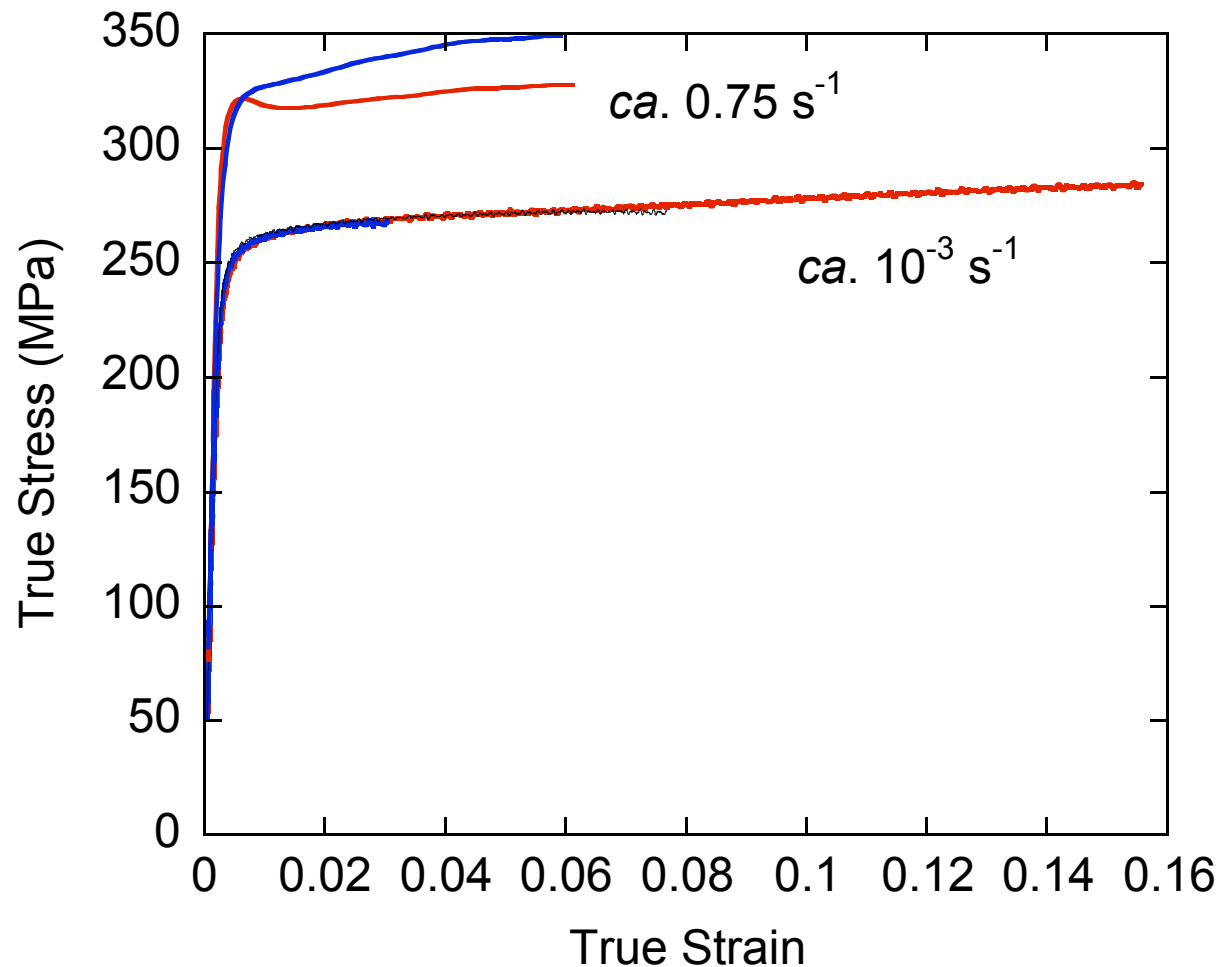
Radial





UNCLASSIFIED

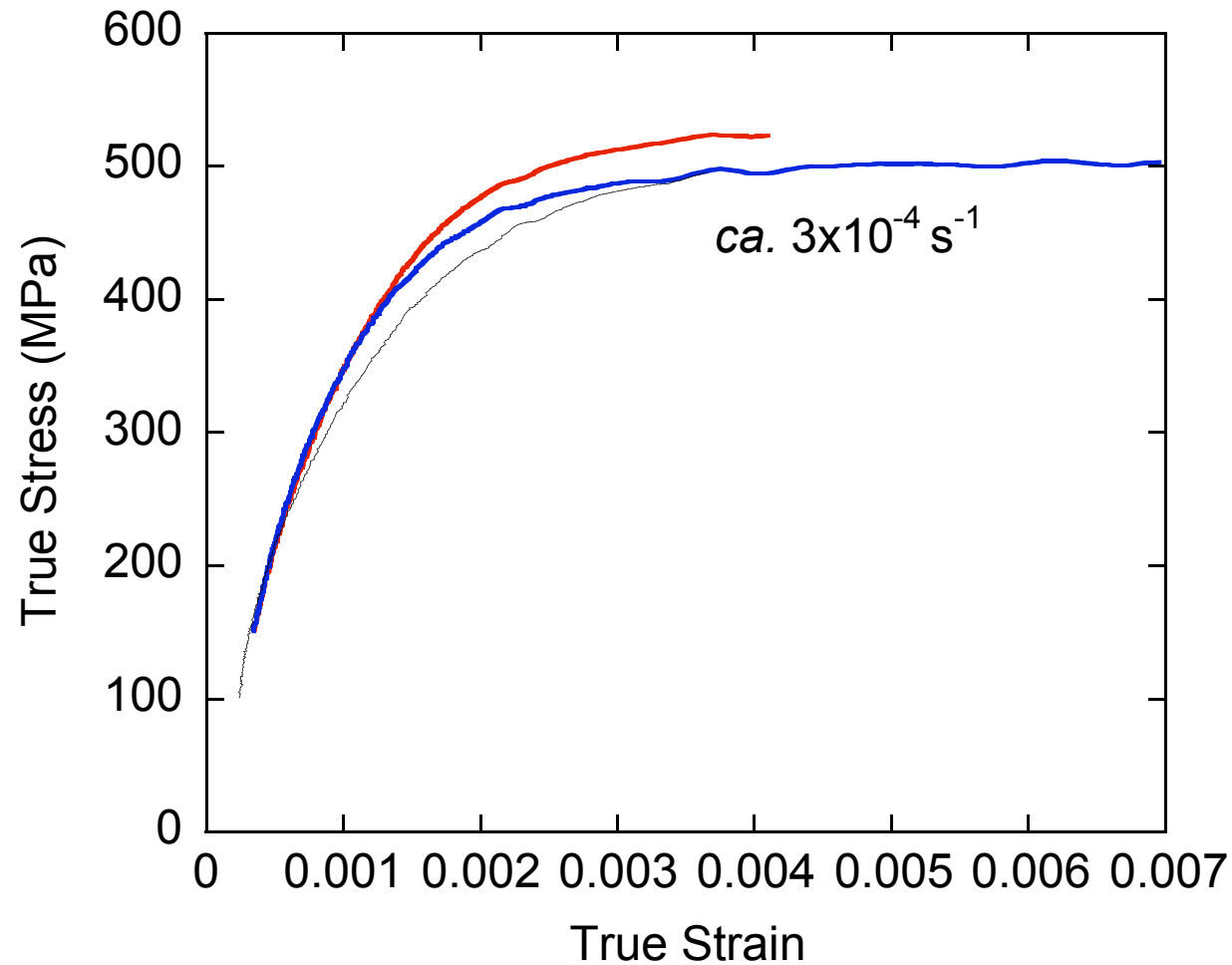
Niobium – Quasi-static Tensile Tests





UNCLASSIFIED

Molybdenum Quasi-Static Tensile Tests





Materials Properties – Quasi-Static

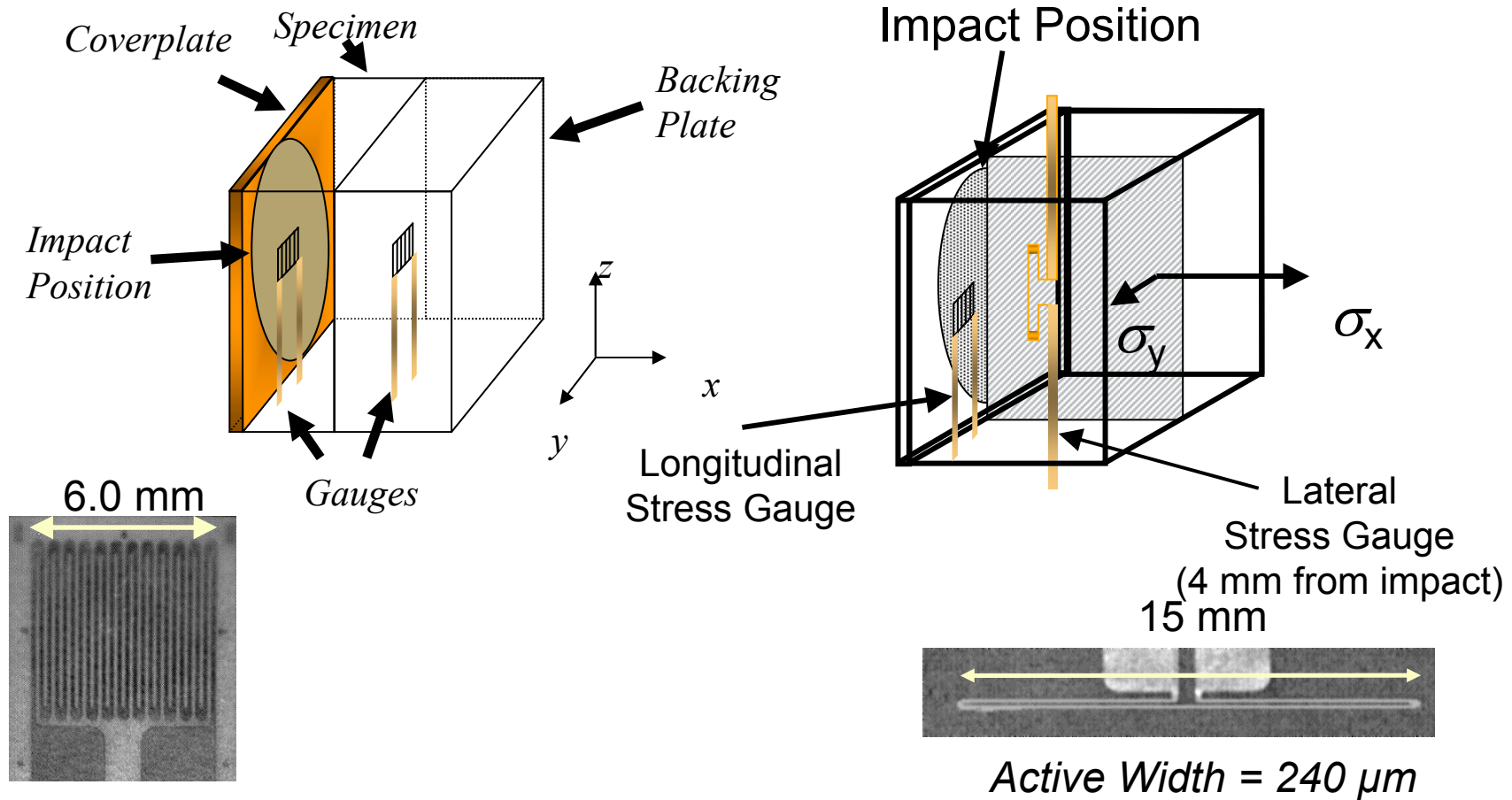
	Nb (10^{-3} s^{-1})	Nb (0.75 s^{-1})	Mo (10^{-4} s^{-1})
.2% PS (MPa)	250	315	496
UTS (MPa)	262	326	506
Strain to failure	0.18	.09	.009
Loading Modulus (GPa)	104	129	443



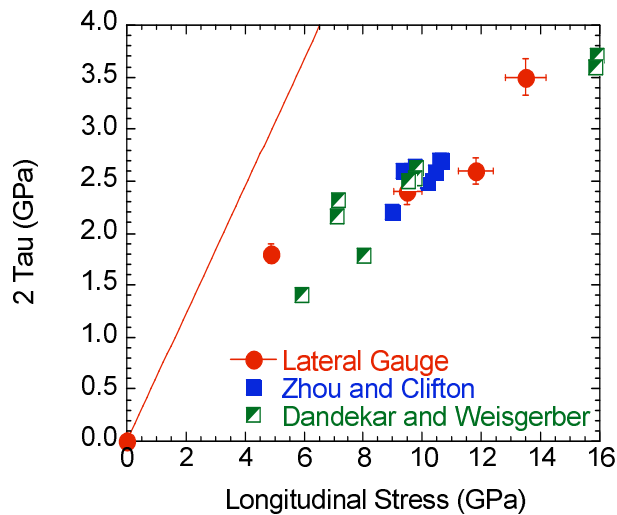
Materials Properties - Ultrasonic

	Niobium	Molybdenum
c_L (mm μs^{-1})	5.12	6.48
c_S (mm μs^{-1})	1.92	3.49
c_B (mm μs^{-1})	4.62	5.07
ρ_0 (g cm^{-3})	8.56	10.15
K (GPa)	183	261
G (GPa)	36	122
E (GPa)	89	320
ν	0.403	0.296

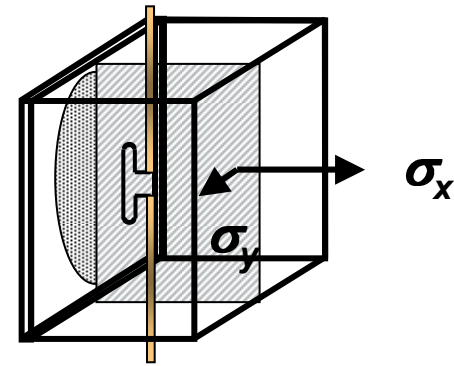
Specimens and Gauges



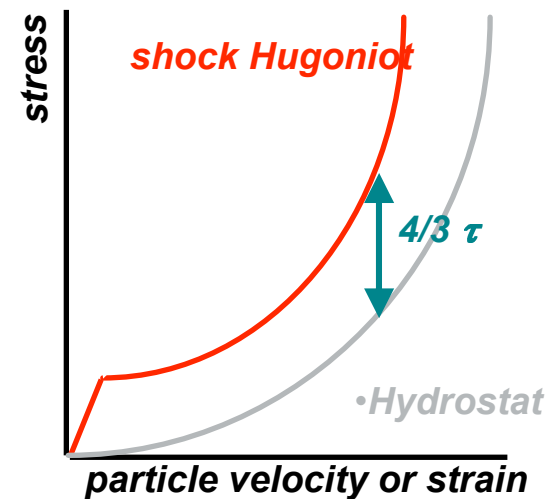
Agreement with Other Techniques ?



Inclined Impact (Pressure Shear)
Zhou and Clifton

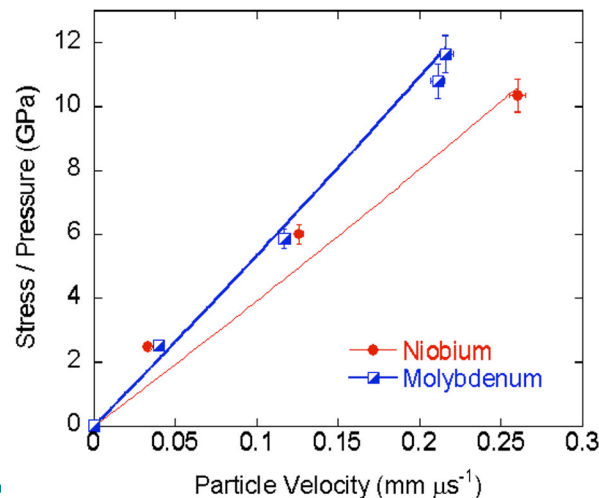
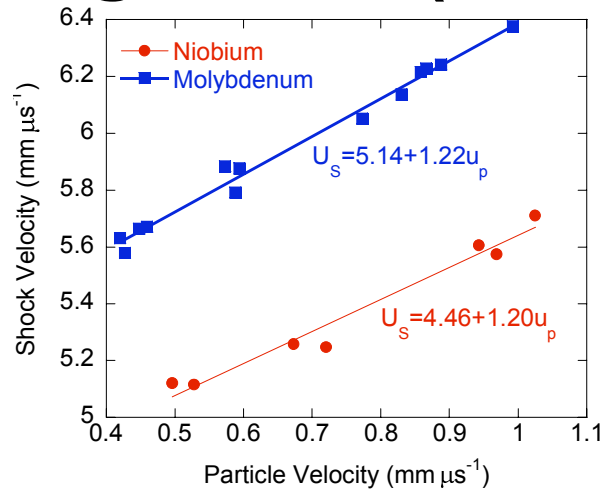


J. Appl. Phys. 86 (1999) 6702



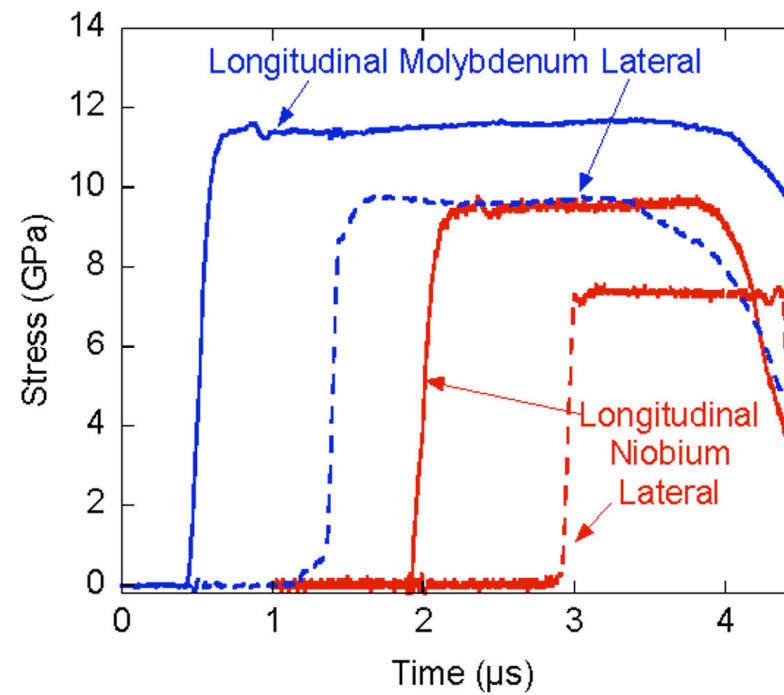
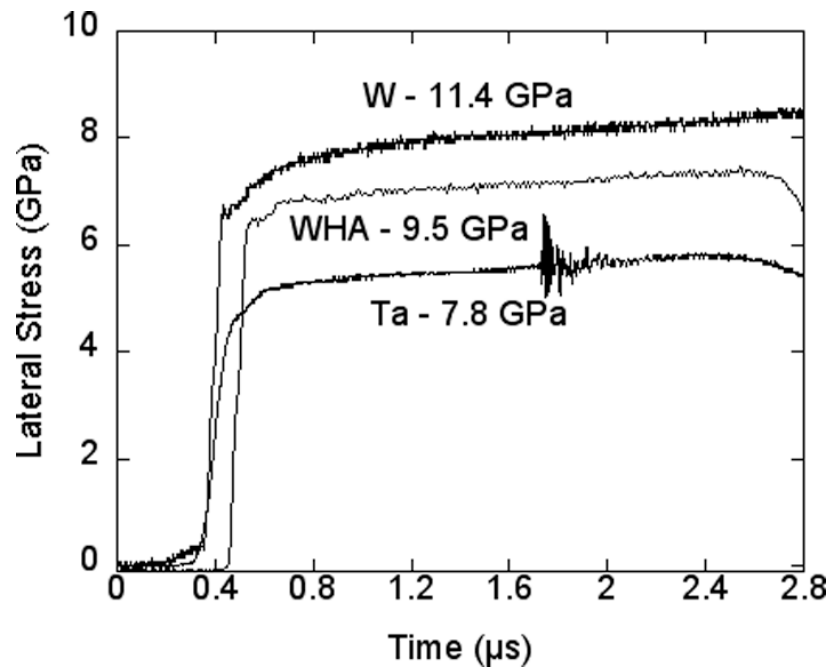
Offset of Hugoniot from Hydrostat
Dandekar and Weisgerber

Hugoniot (Marsh)



- Little available data below 20 GPa
- Molybdenum data suggests linear response extends into regime of interest
- Niobium data less certain.
 - Non linear behaviour?
 - Relatively high shear strengths?

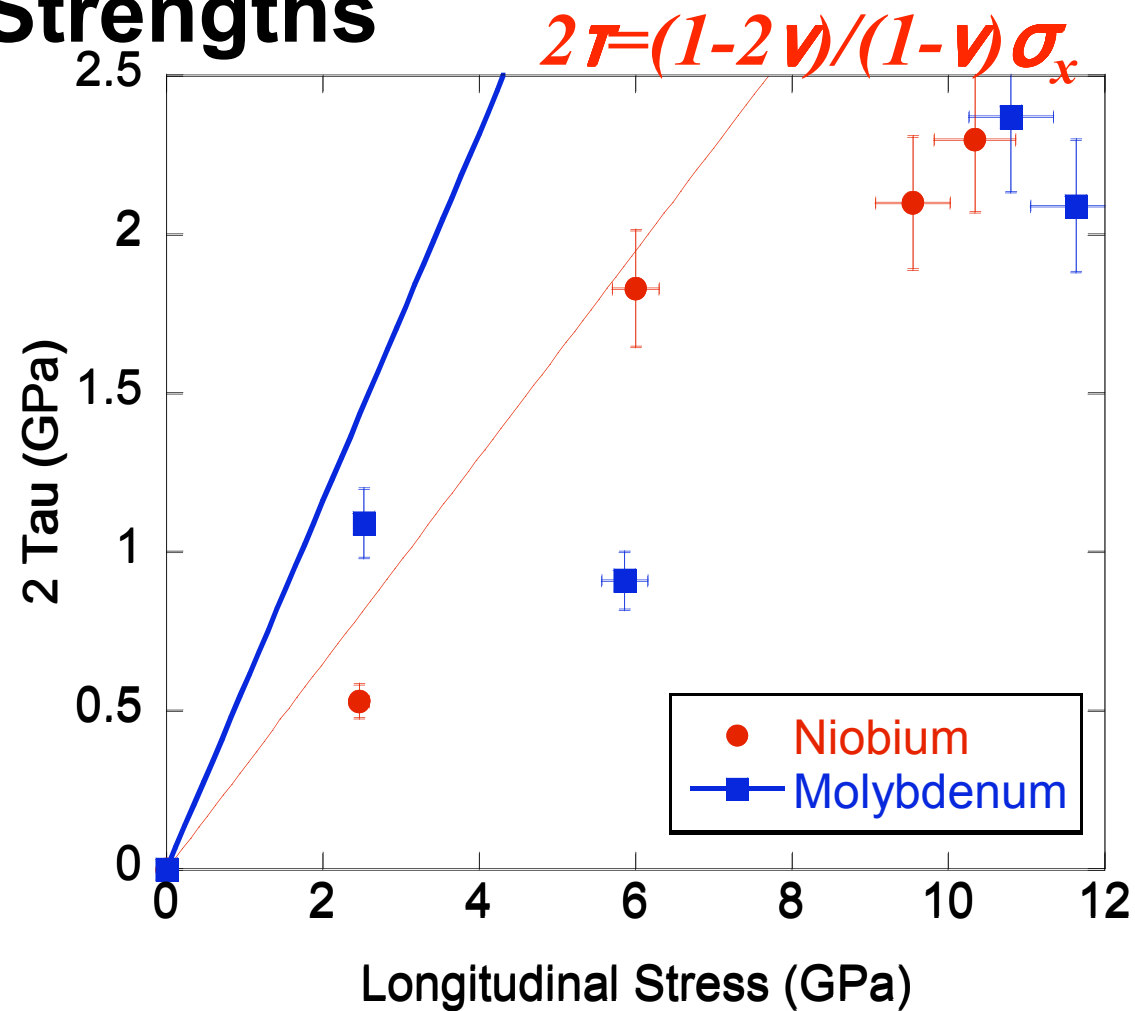
Lateral Gauge Traces



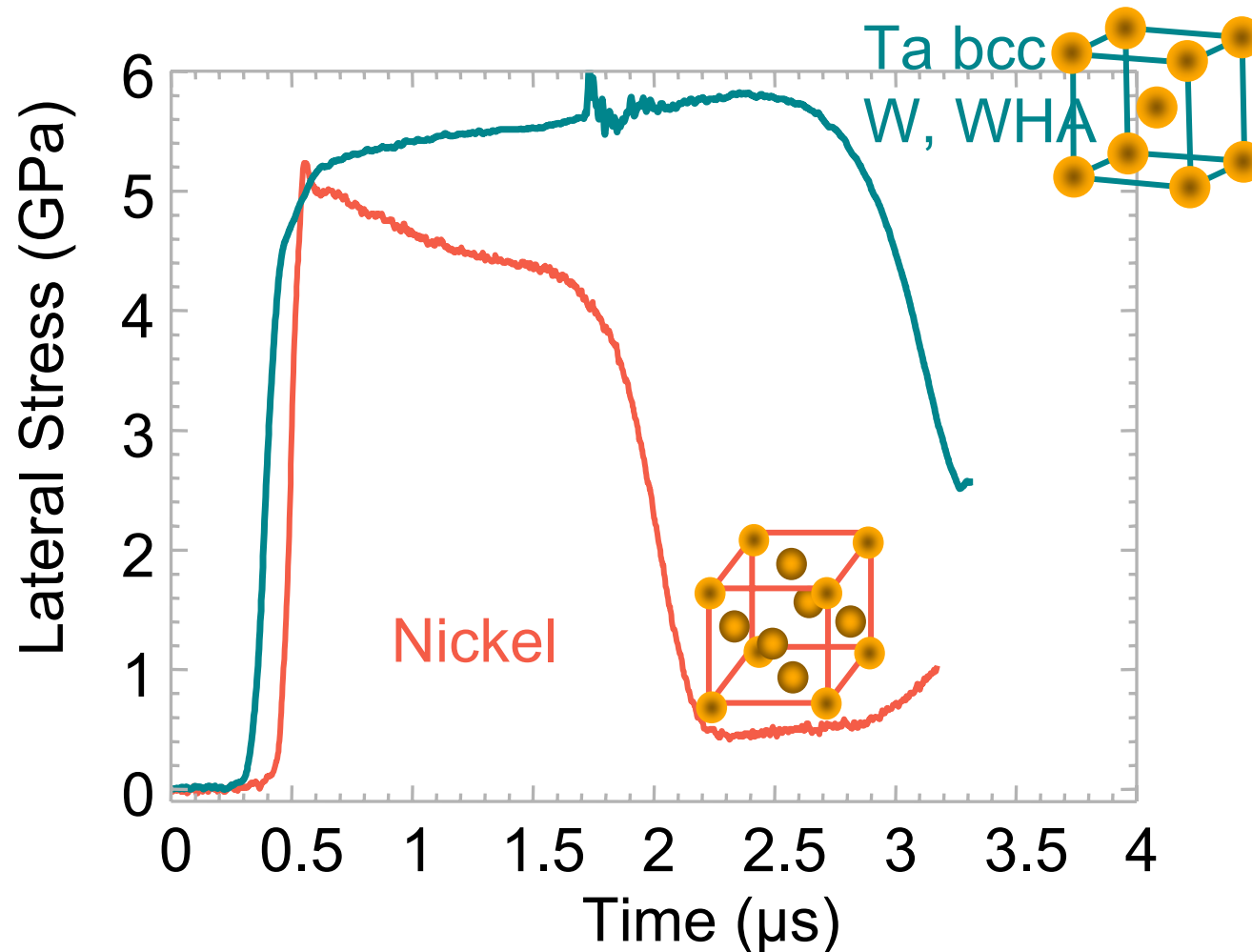


UNCLASSIFIED

Shear Strengths



“Typical” Response





Peierls Stresses

$$\tau_{PN} = \frac{2G}{1-\nu} \exp\left(\frac{-2\pi w}{b}\right); w = \frac{a}{1-\nu}$$

G – Shear modulus; b lattice parameter; w – dislocation width; a – interplane spacing; ν – Poisson's ratio

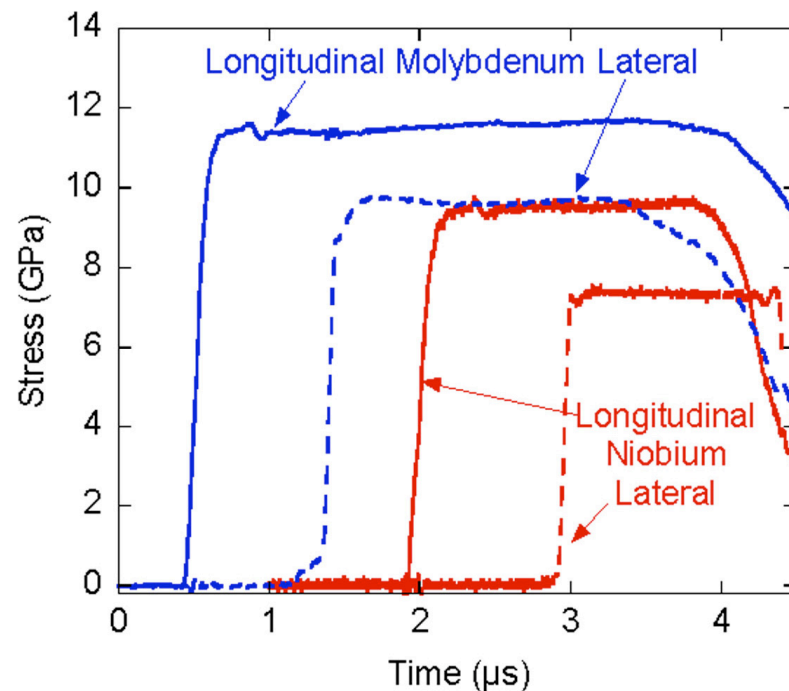
Modern Physical Metallurgy

R.E. Smallman - 1985

- Low Peierls stress in Nb suggests ease of dislocation generation *but*
- G and ν calculated for polycrystalline materials
- Pressure dependence not accounted for
- Order of magnitude calculations only

Metal	G (GPa)	ν	b (nm)	τ (MPa)
Nb	36.3	0.403	0.330	0.04
Mo	121.5	0.296	0.315	2.13
Ta	69	0.339	0.331	0.3
W	160.2	0.279	0.316	1.97
Ni	81.7	0.315	0.352	0.03

Non-Typical Behaviour in Nb and Mo



- Lateral stress trace appears near constant behind shock front in contrast to Ta and W base.
- Suggests different deformation mechanism
- Low Peierls stress in Nb suggests dislocation generation. Tangles and slip bands seen previously
 - Huang and Gray Mat. Sci. Engng 1988
- Twin formation observed in Mo as low as 9 GPa; Dislocation generation enhanced by 6% pre-strain
 - Mahajan and Bartlett Acta. Met 1971

Conclusions

- Programme of work to investigate the shock response of bcc metals Nb and V
 - So far shear strength measurements and quasi-static tensile tests
- Results indicate that neither metals responds in the “typical” BCC way (Ta and W)
- Low Peierl’s stress in Nb appears to promote dislocation generation during shock
- Twinning or pre-strain influenced dislocation generation in Mo possibilities
- The range of behaviours in BCC metals seems a wide as those in FCCs



Further Work

- Hugoniot measurements below 20 GPa
- Spall measurements to compliment existing shear strength data
- Complete quasi-static (compression) and intermediate (SHPB) strain-rate testing
- 1-D recovery experiments to elucidate deformation mechanisms



Acknowledgements

- Andrew Wallwork, Giles Aldrich-Smith, Steve Bailey
 - Quasi-static testing
- Sue Ennaceur
 - EDSB
- Gareth Appleby-Thomas (Cranfield University, Shrivenham)
 - Gas gun shots

JOWOG 32MAT



January 27, 2010
Wednesday

Meeting of the JOWOG 32mat
25-29 January 2010 at LLNL in Livermore, CA, USA

Update on Multi-Megabar Ramp Compression at Z

Jean-Paul Davis

with Marcus D. Knudson, Ray W. Lemke, and others

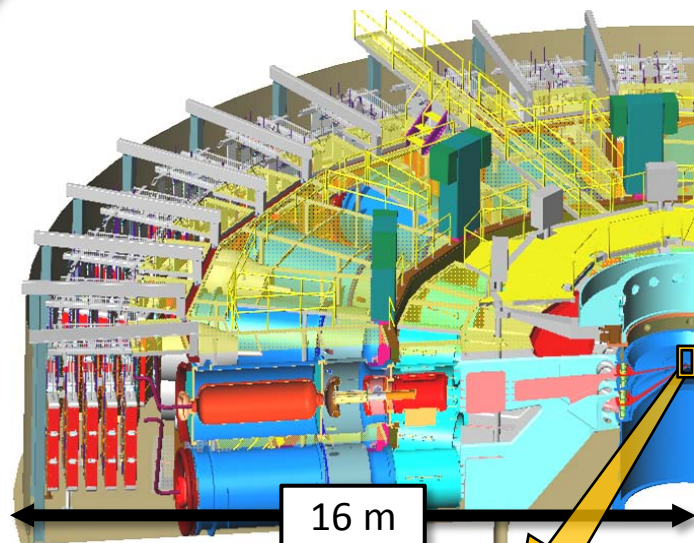
Sandia National Laboratories

Albuquerque, NM 87185-1195 USA

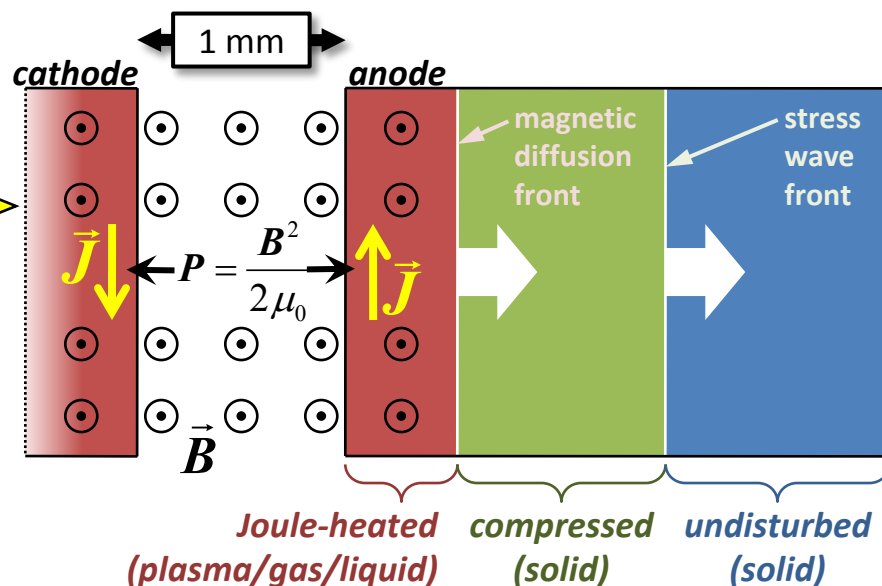
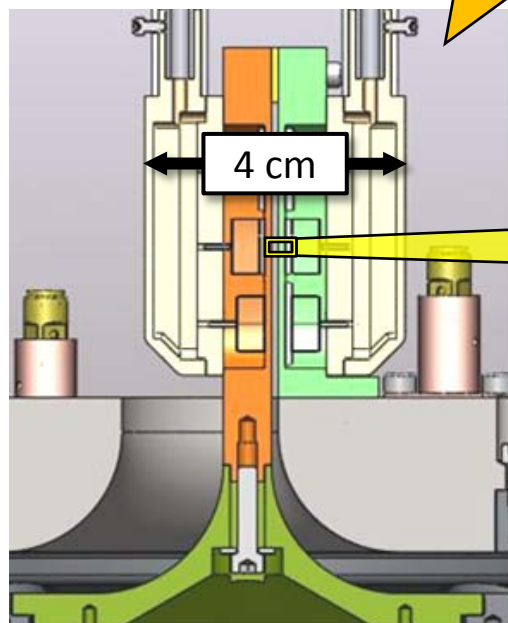


Sandia is a multiprogram laboratory operated by Sandia Corporation, a Lockheed Martin Company, for the United States Department of Energy's National Nuclear Security Administration under contract DE-AC04-94AL85000.

Refurbished Z machine & stripline load enable accurate ramp-compression experiments to > 300 GPa



- current pulse of up to 26 MA delivered to parallel flat-plate electrodes shorted at one end
- magnetic ($\mathbf{J} \times \mathbf{B}$) force induces ramped stress wave in electrode material
- stress wave propagates into ambient material, de-coupled from magnetic drive
- controllable pulse shape, rise time 100-700 ns
- identical magnetic loading of sample pairs





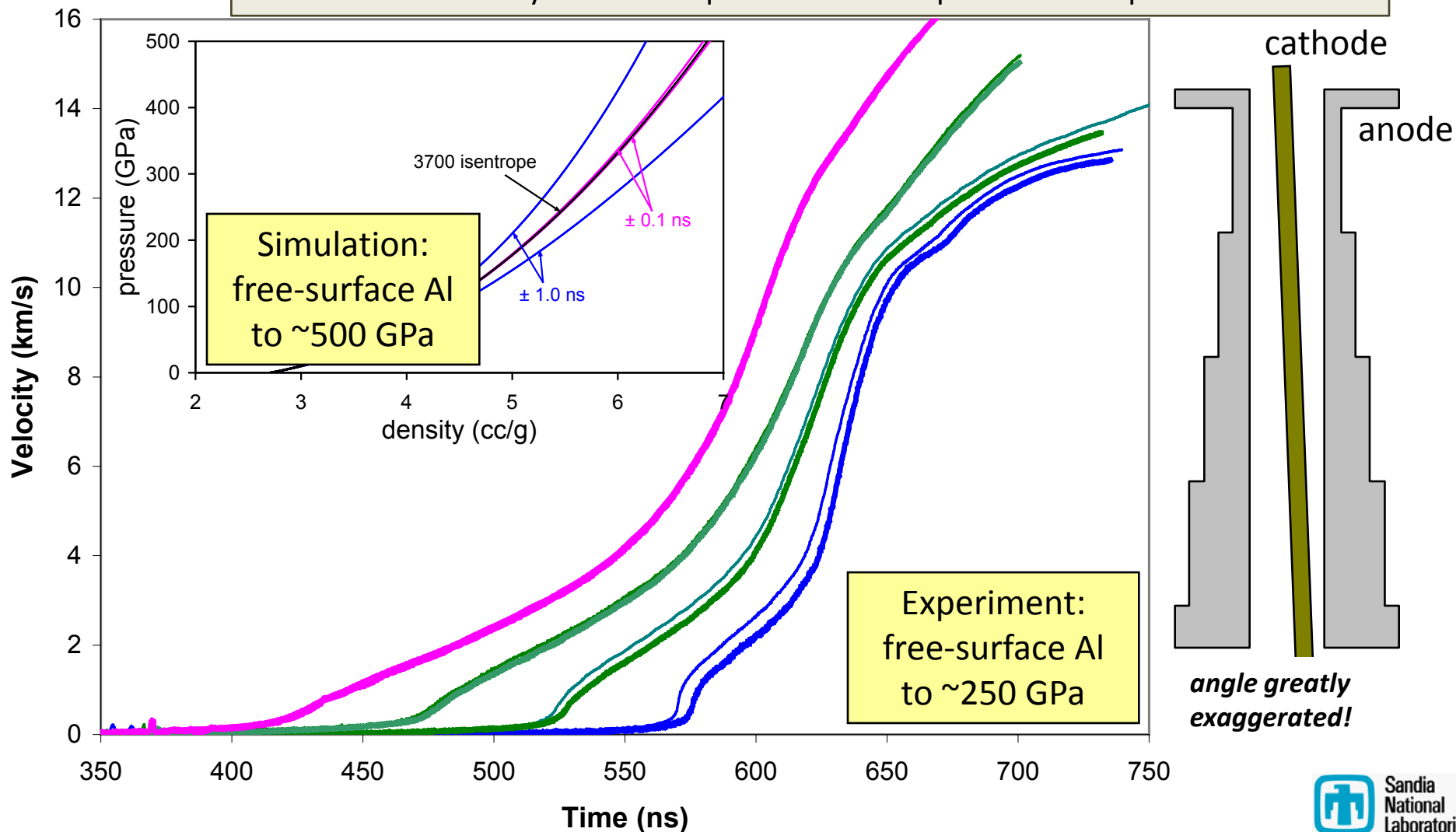
OUTLINE

- 1. Stripline load development (6 slides)**
- 2. Pulse shaping (2 slides)**
- 3. Data analysis (4 slides)**
- 4. Preliminary results on tantalum (2 slides)**

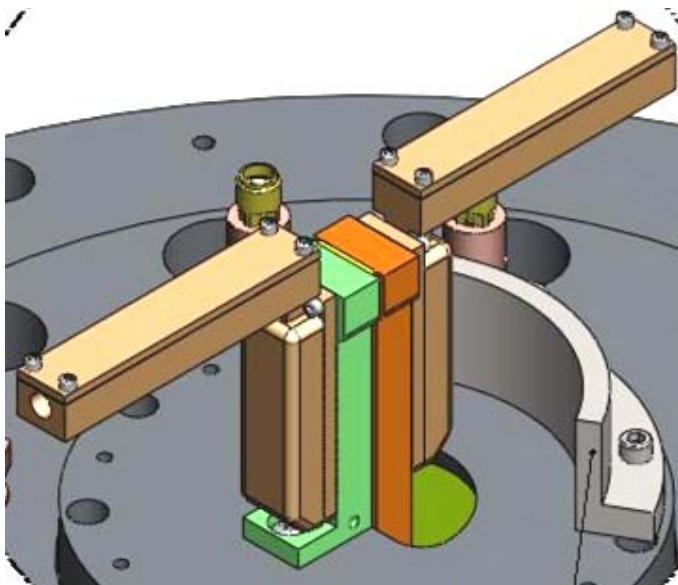
Small misalignments of coaxial anode/cathode geometry can cause significant apparent time shifts

Standard ramp-compression load design on pre-refurbished Z

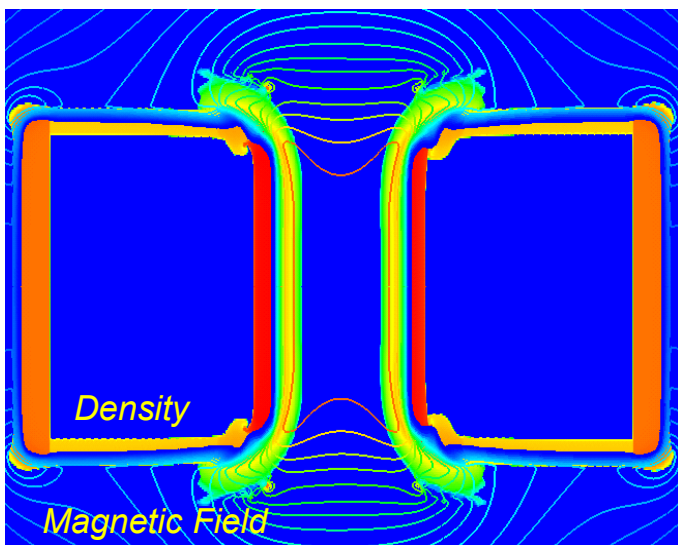
- samples on separate anodes, two coupled A/K gaps
- 1% uncertainty in stress requires electrodes parallel to $< 5 \mu\text{m}$ across 25 mm



New stripline geometry offers several advantages

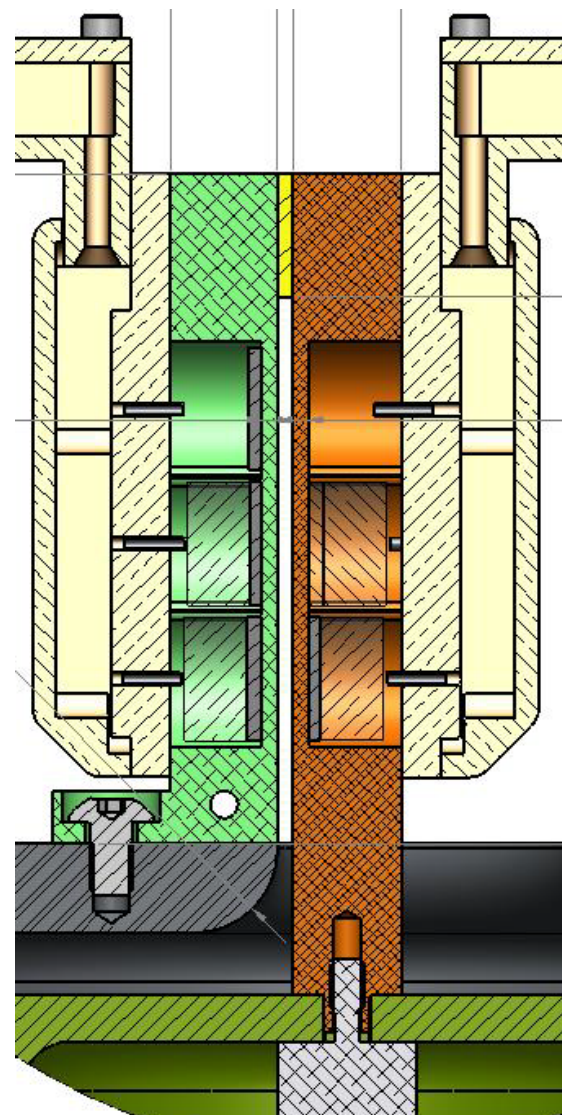


- insensitive to vertical angular misalignment
- single B-field waveform drives two samples
- higher magnetic pressure for given current
- larger lateral extent of uniform 1-D flow

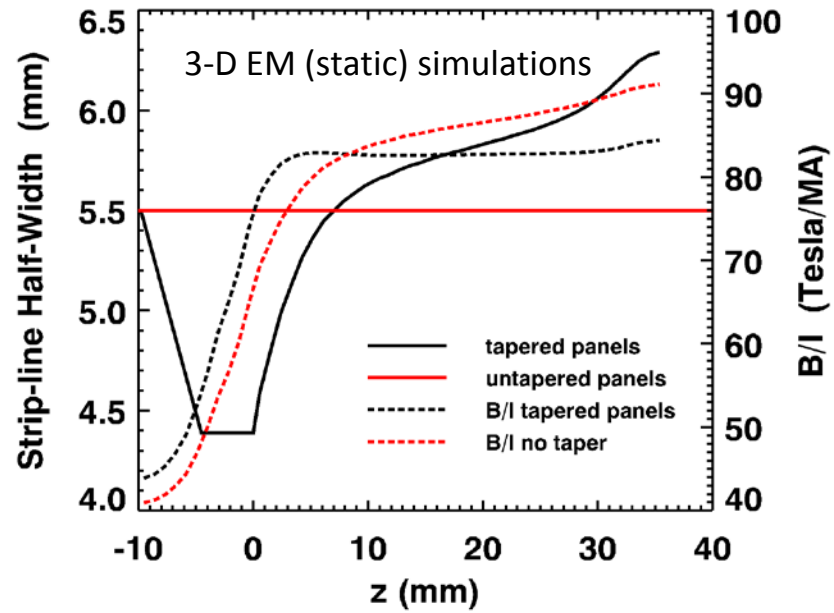
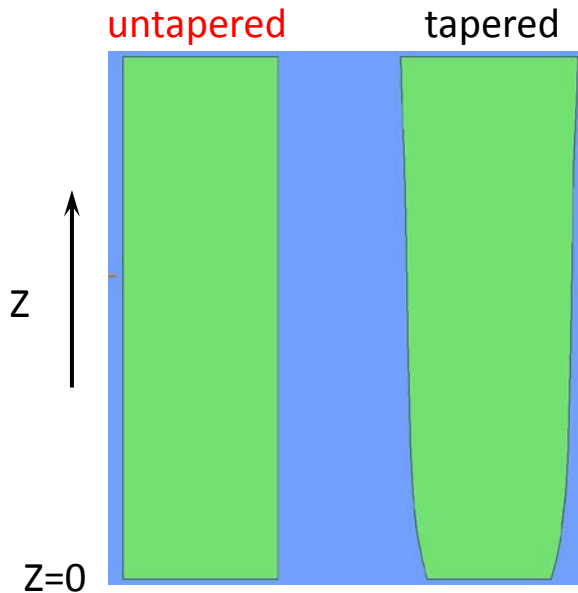
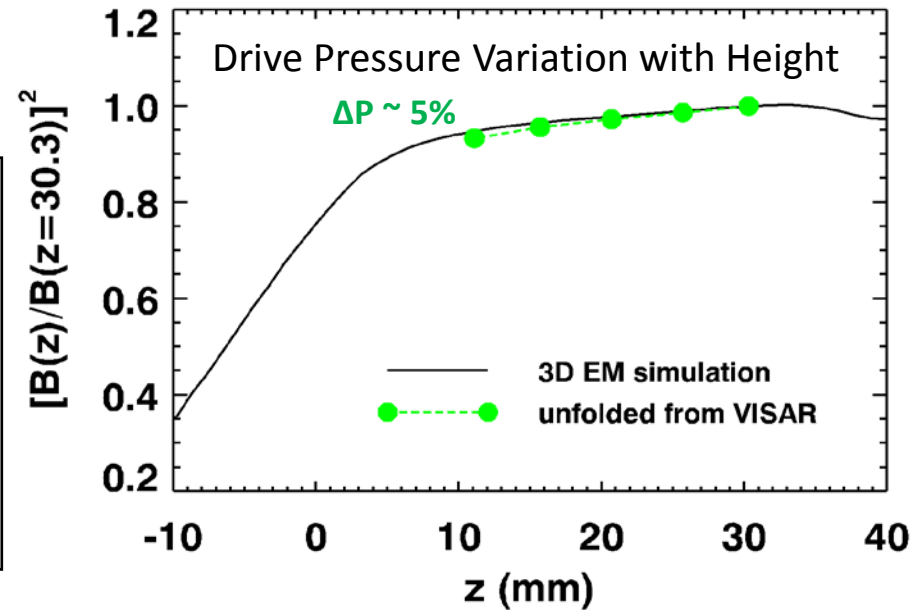
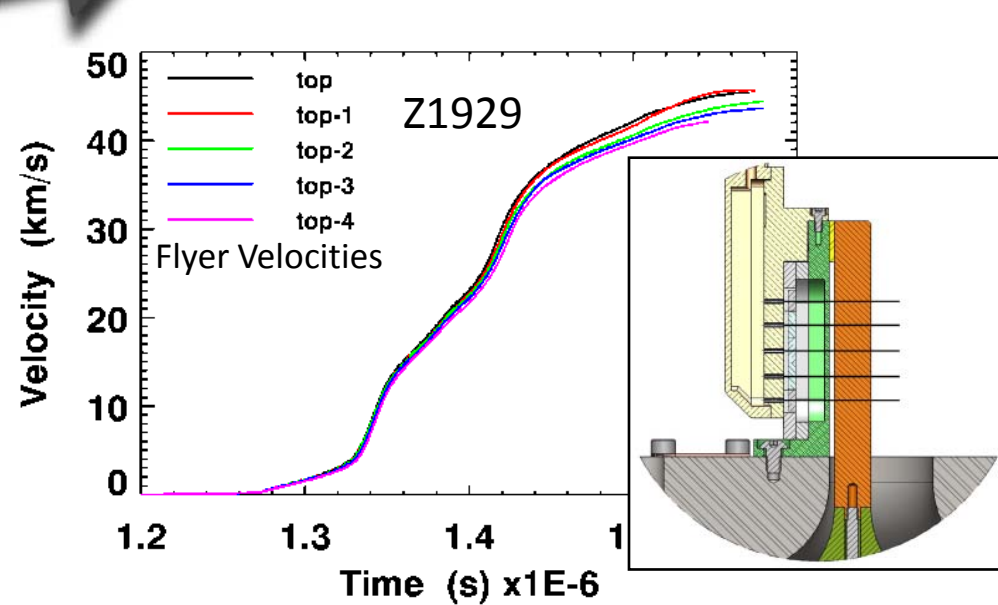


Unconfined B-field:

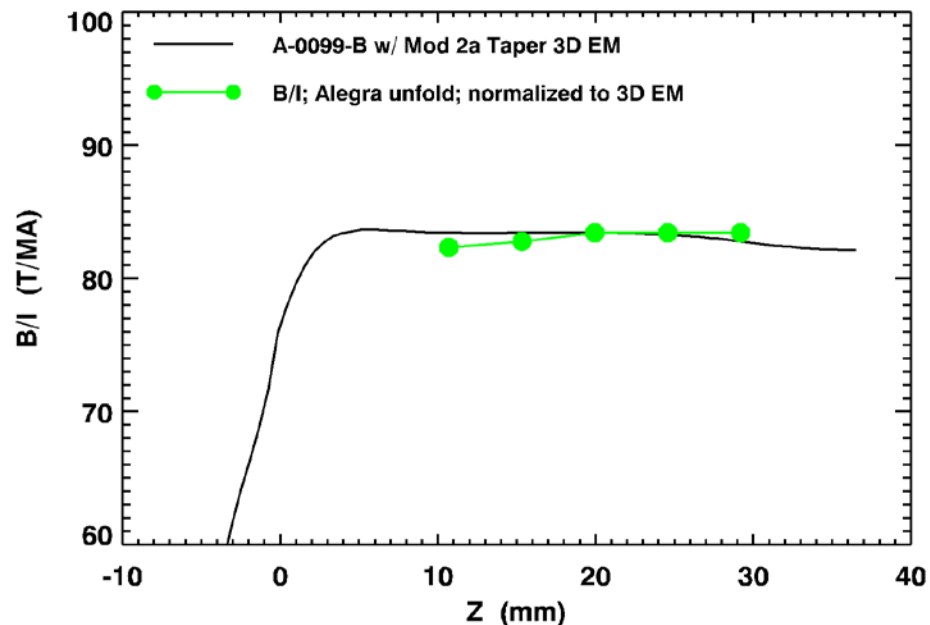
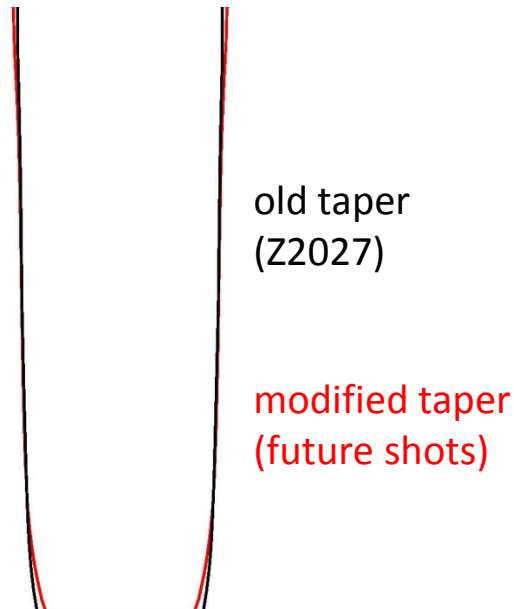
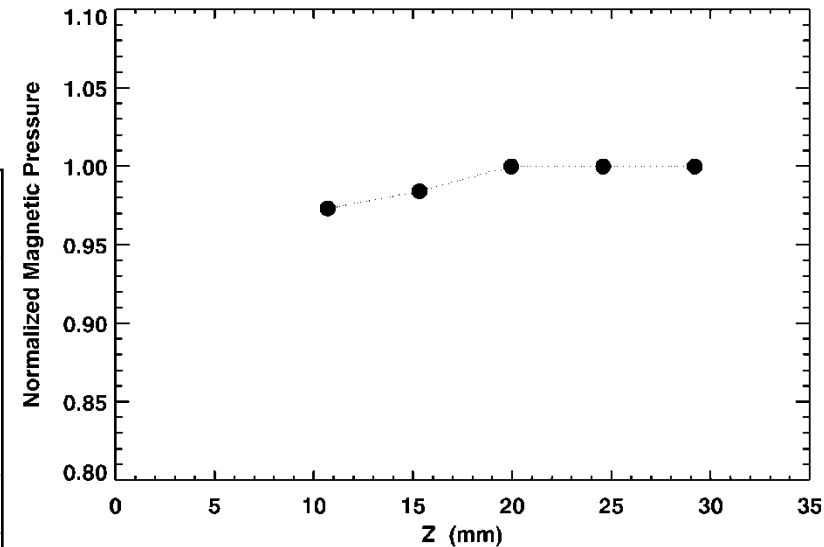
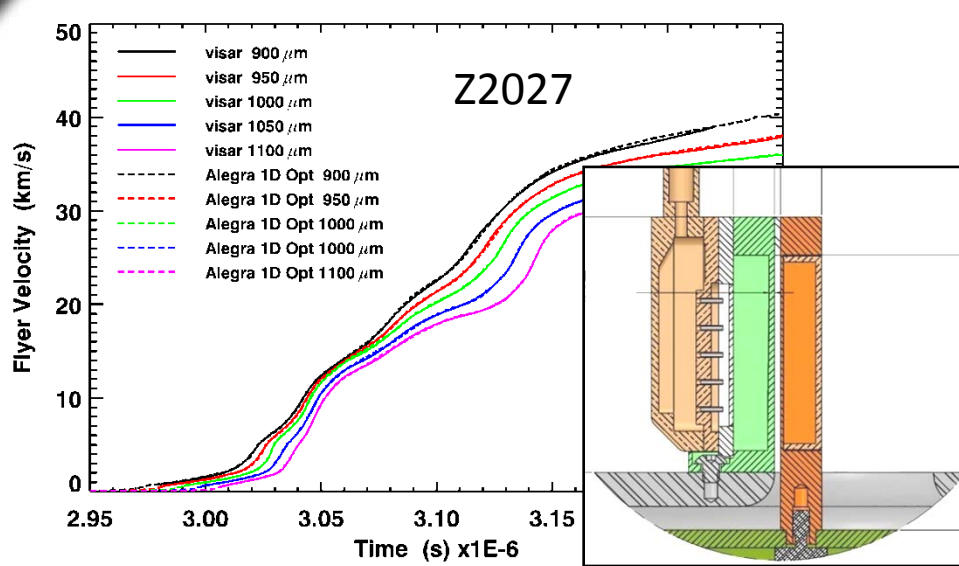
- vertically non-uniform distribution of current inside/outside the gap
- shielding of diagnostics and samples



Measurement of vertical non-uniformity of B-field shows need for functional tapering of stripline width



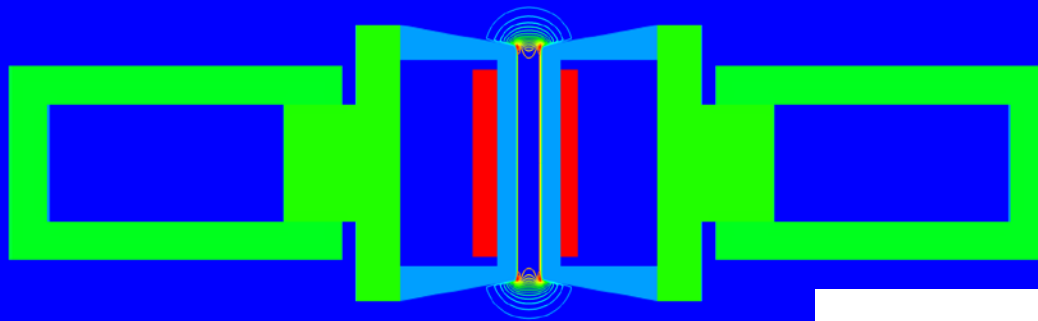
Semi-empirical functional tapering of stripline width should eliminate vertical non-uniformity of B-field



Simulations predict highly uniform B-field in the lateral and normal directions over most of the gap

$t=2.6004e-06$ s

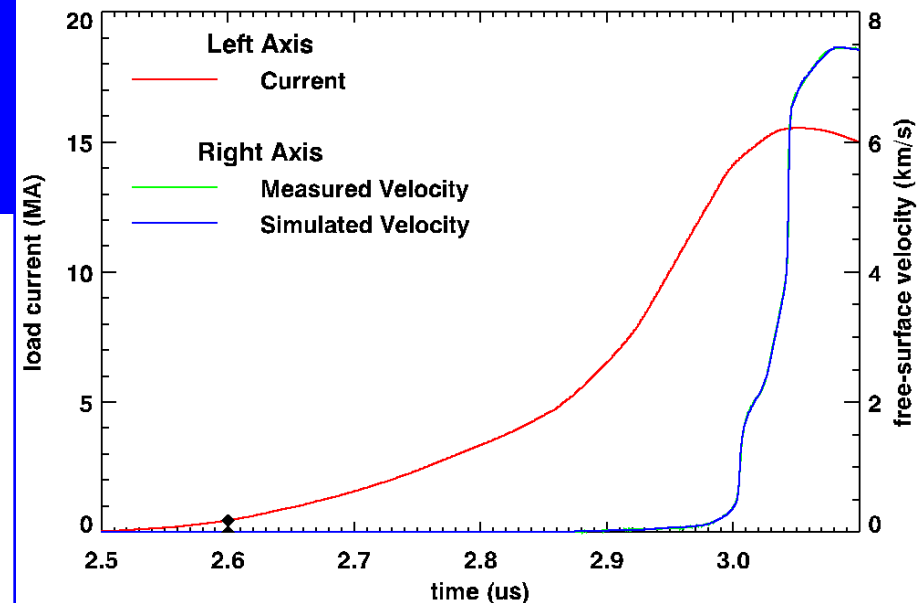
Z1844



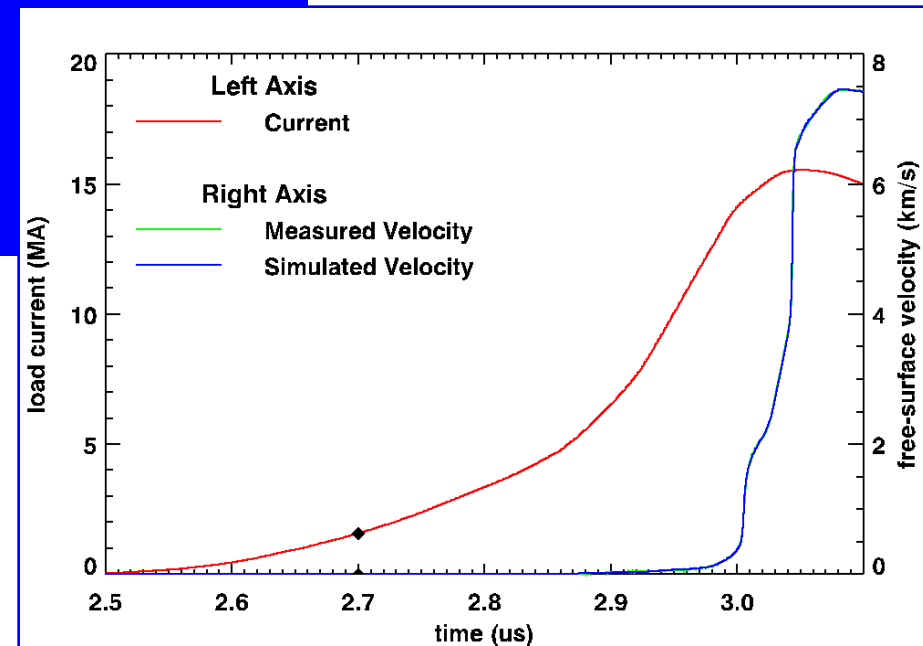
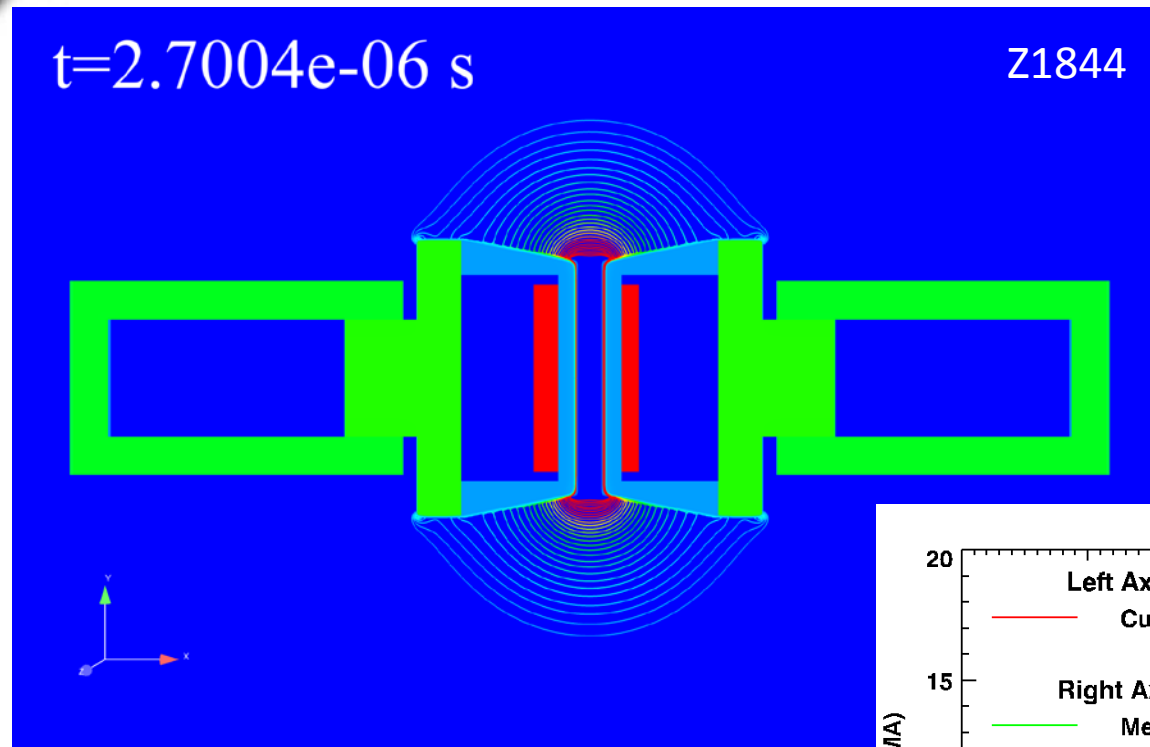
Magnetic Field (line contours)
Density (filled contours)

2-D Alegra-MHD:

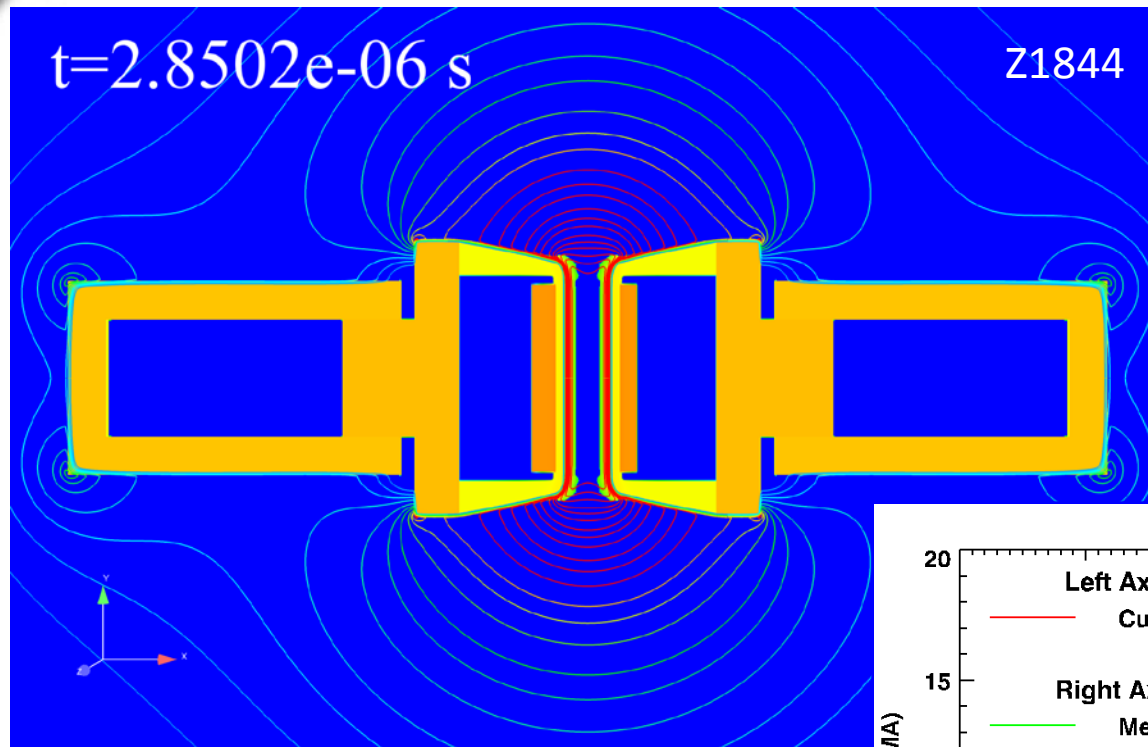
- Resistive MHD
- QMD/LMD conductivity
- Sesame EOS
- Circuit model



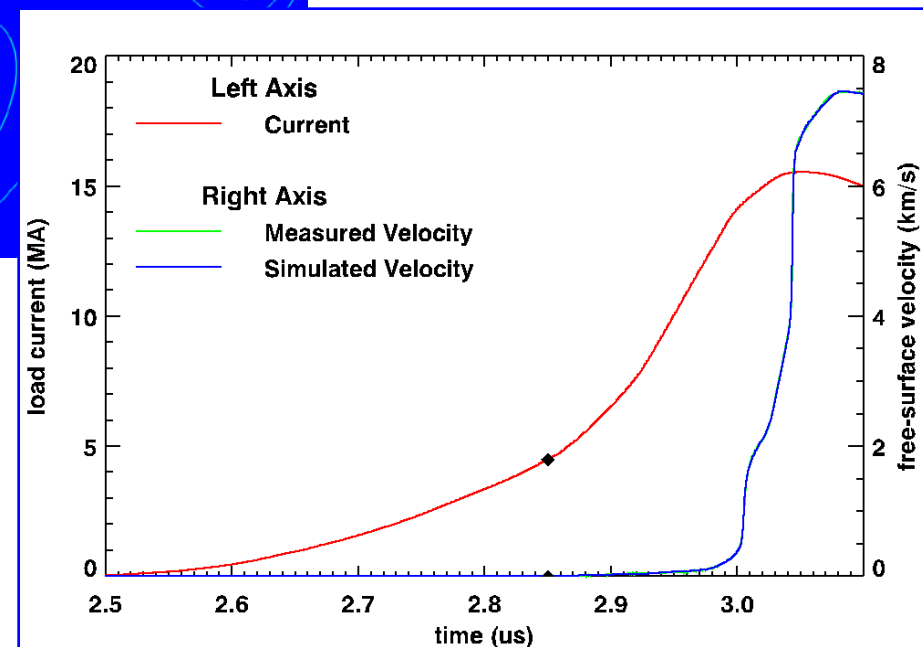
Simulations predict highly uniform B-field in the lateral and normal directions over most of the gap



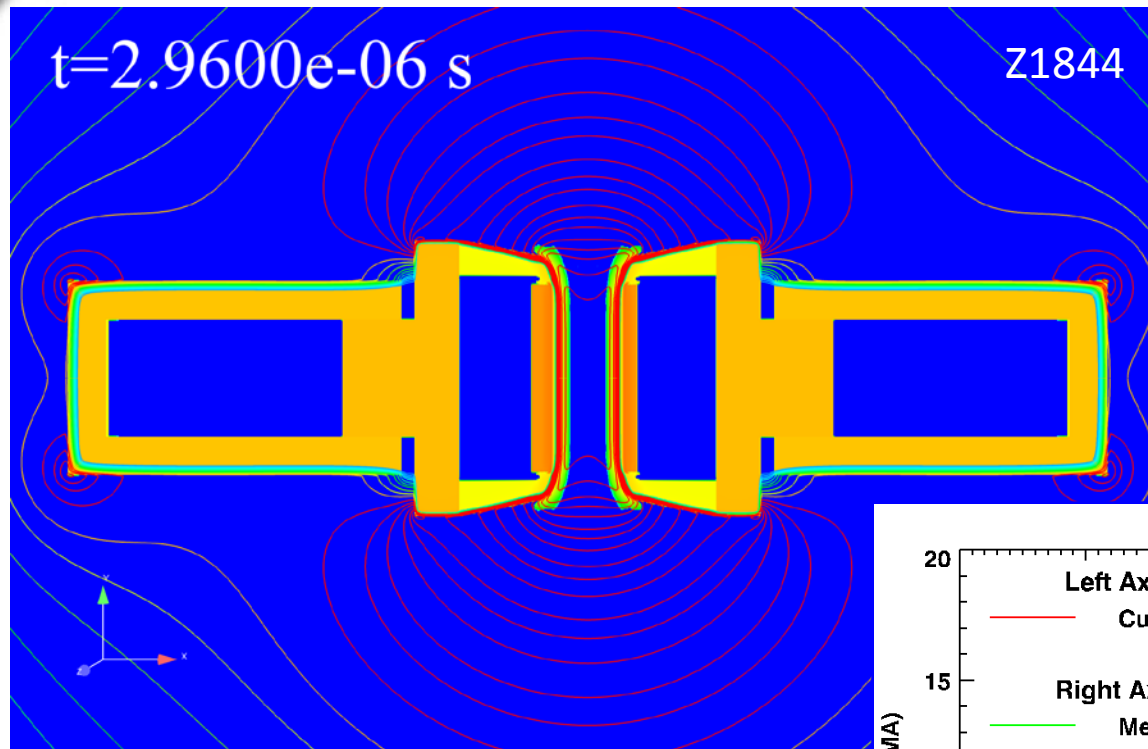
Simulations predict highly uniform B-field in the lateral and normal directions over most of the gap



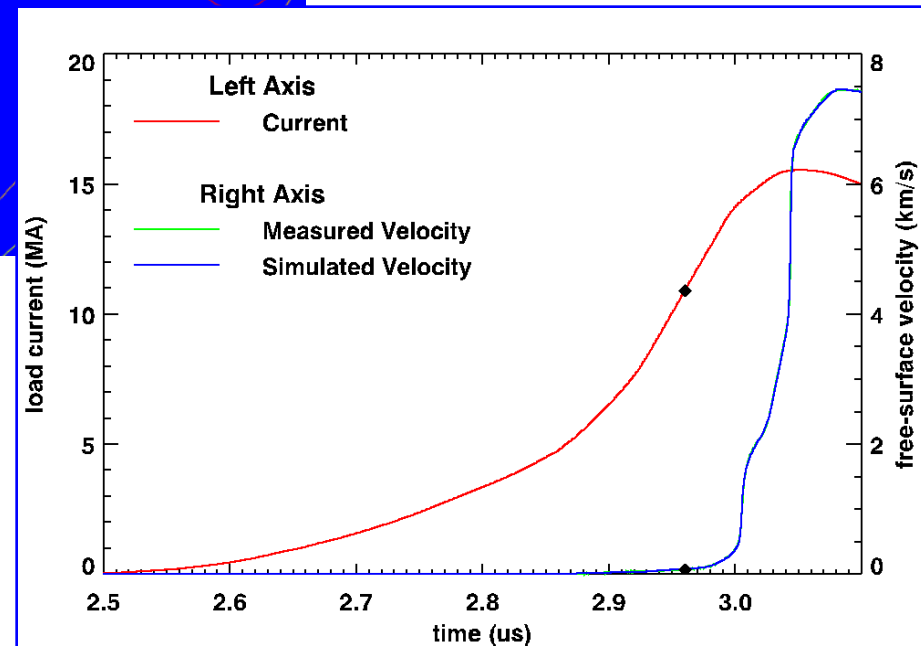
Magnetic Field (line contours)
Density (filled contours)



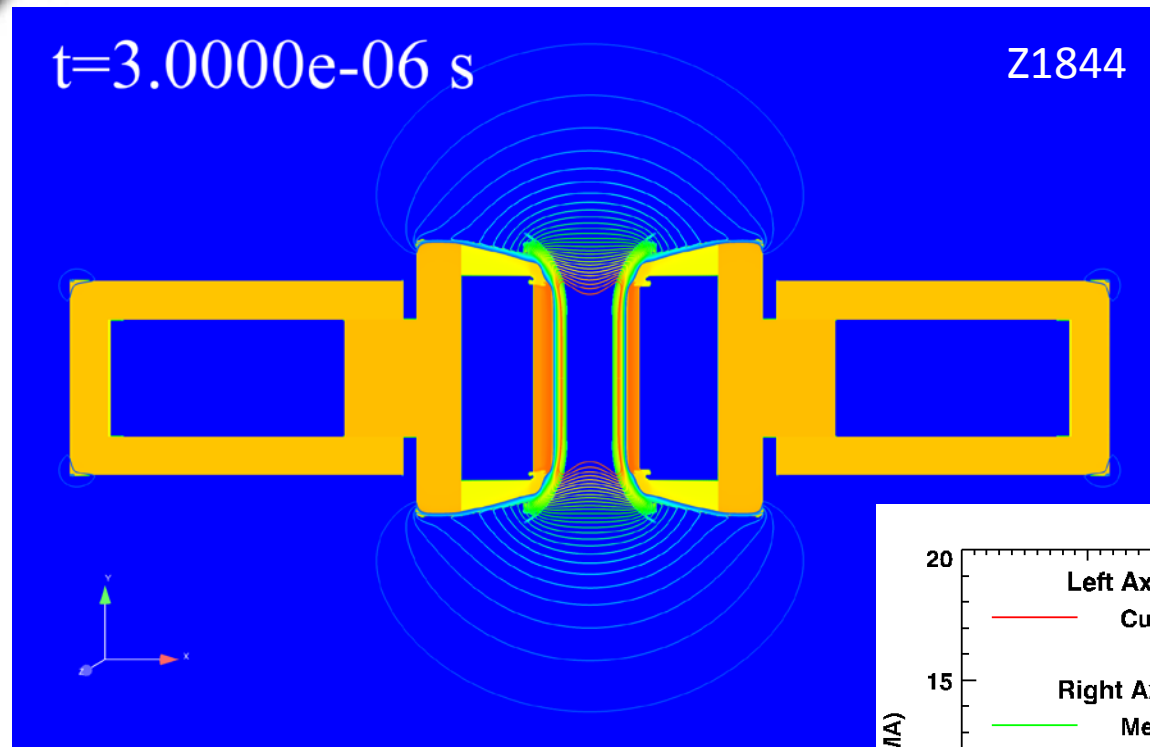
Simulations predict highly uniform B-field in the lateral and normal directions over most of the gap



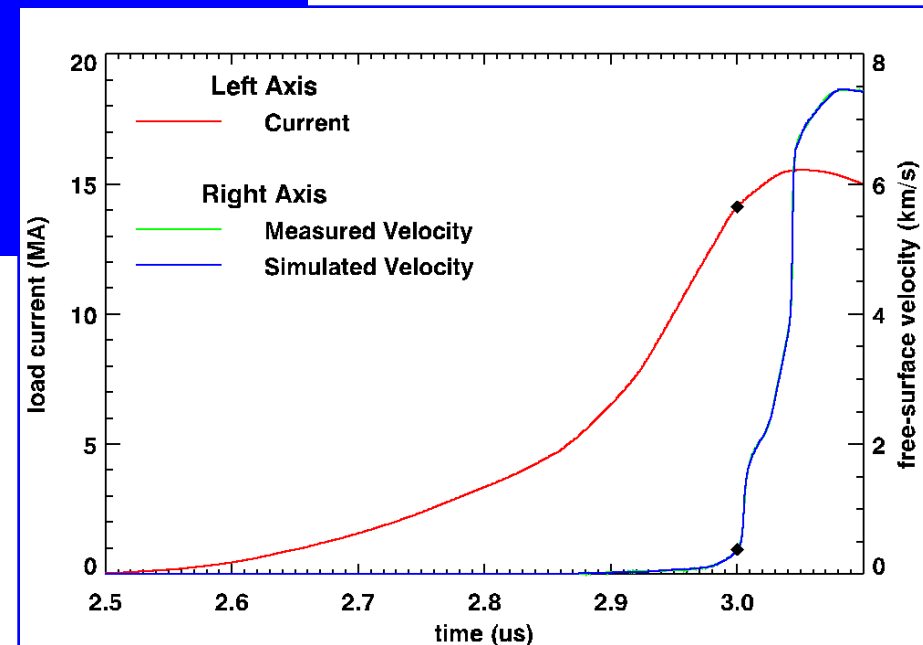
Magnetic Field (line contours)
Density (filled contours)



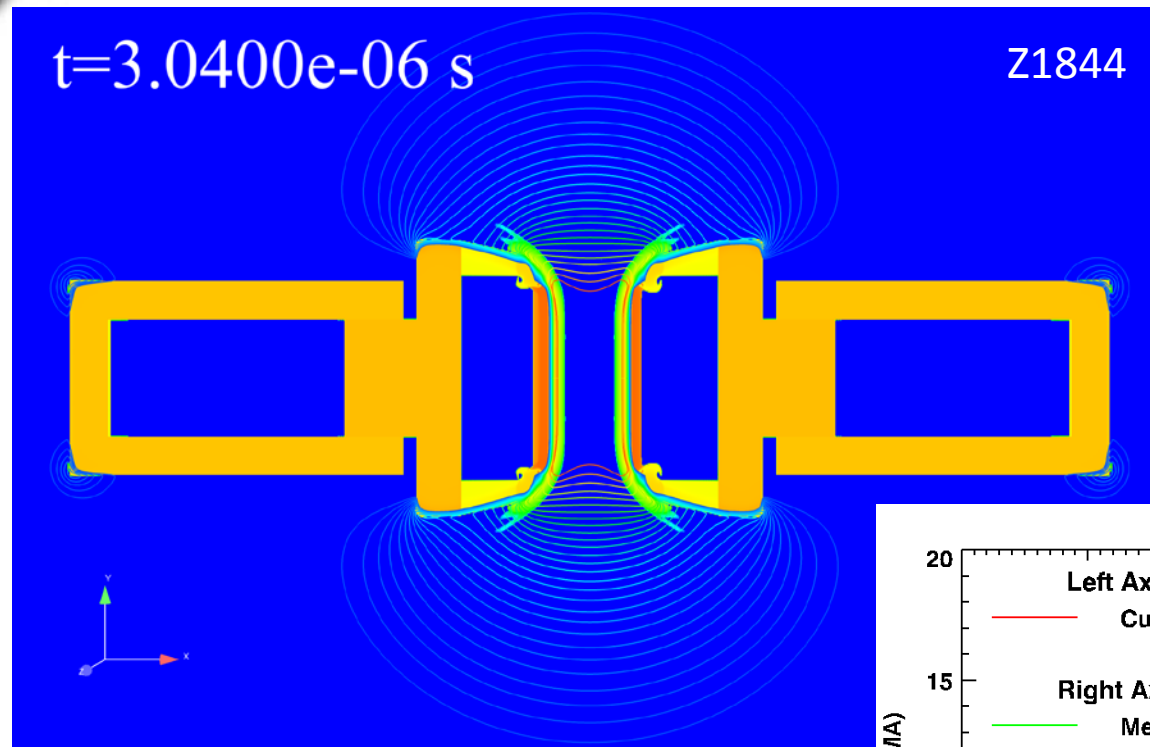
Simulations predict highly uniform B-field in the lateral and normal directions over most of the gap



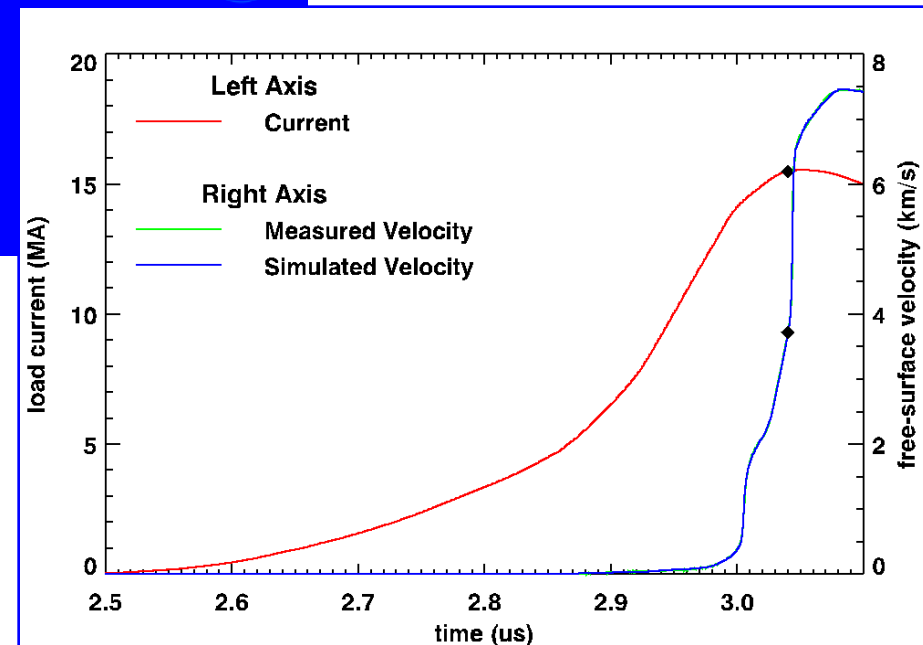
Magnetic Field (line contours)
Density (filled contours)



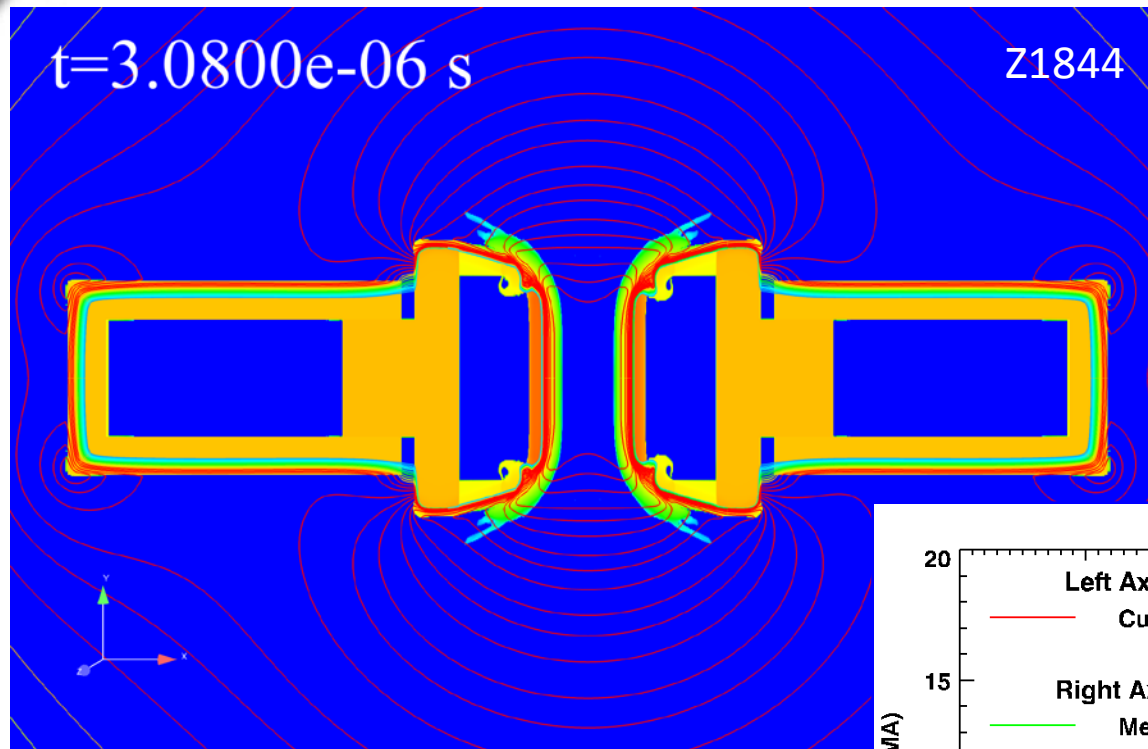
Simulations predict highly uniform B-field in the lateral and normal directions over most of the gap



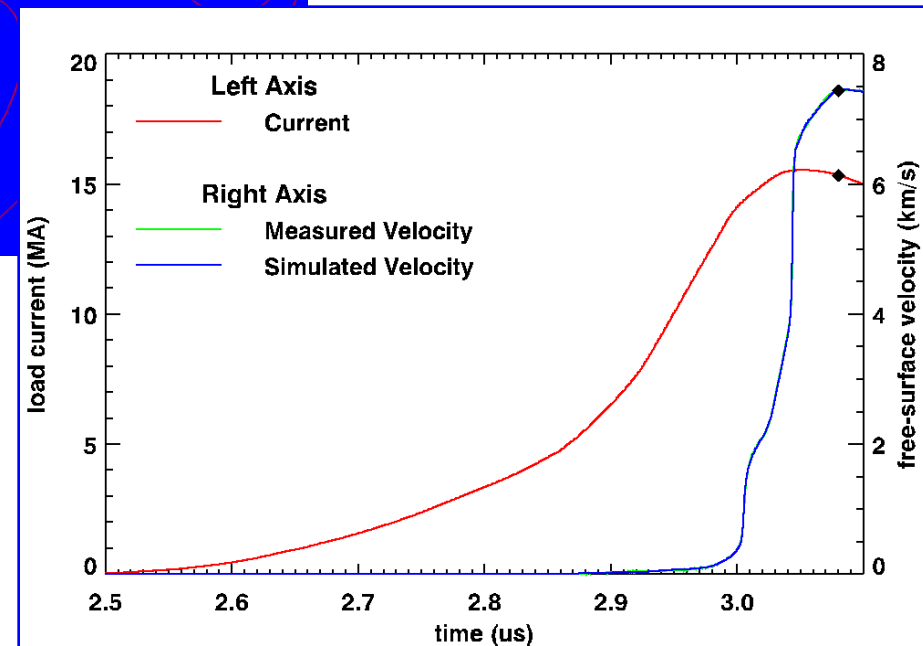
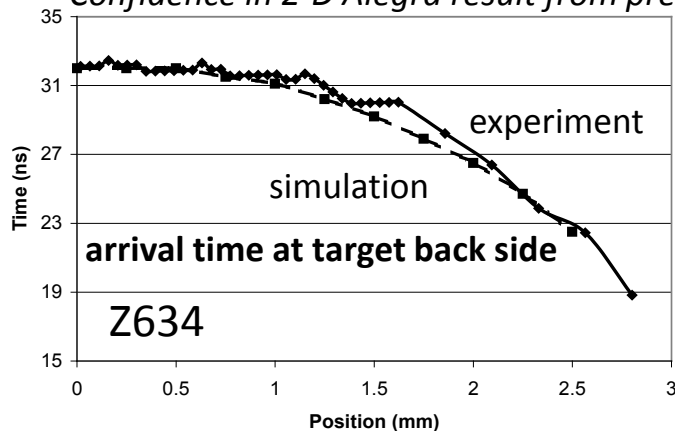
Magnetic Field (line contours)
Density (filled contours)



Simulations predict highly uniform B-field in the lateral and normal directions over most of the gap



Confidence in 2-D Alegra result from pre-ZR coax shots



VISAR fiber darkening issues have been addressed

X-rays generated at corners
inside inner-MITL feed?

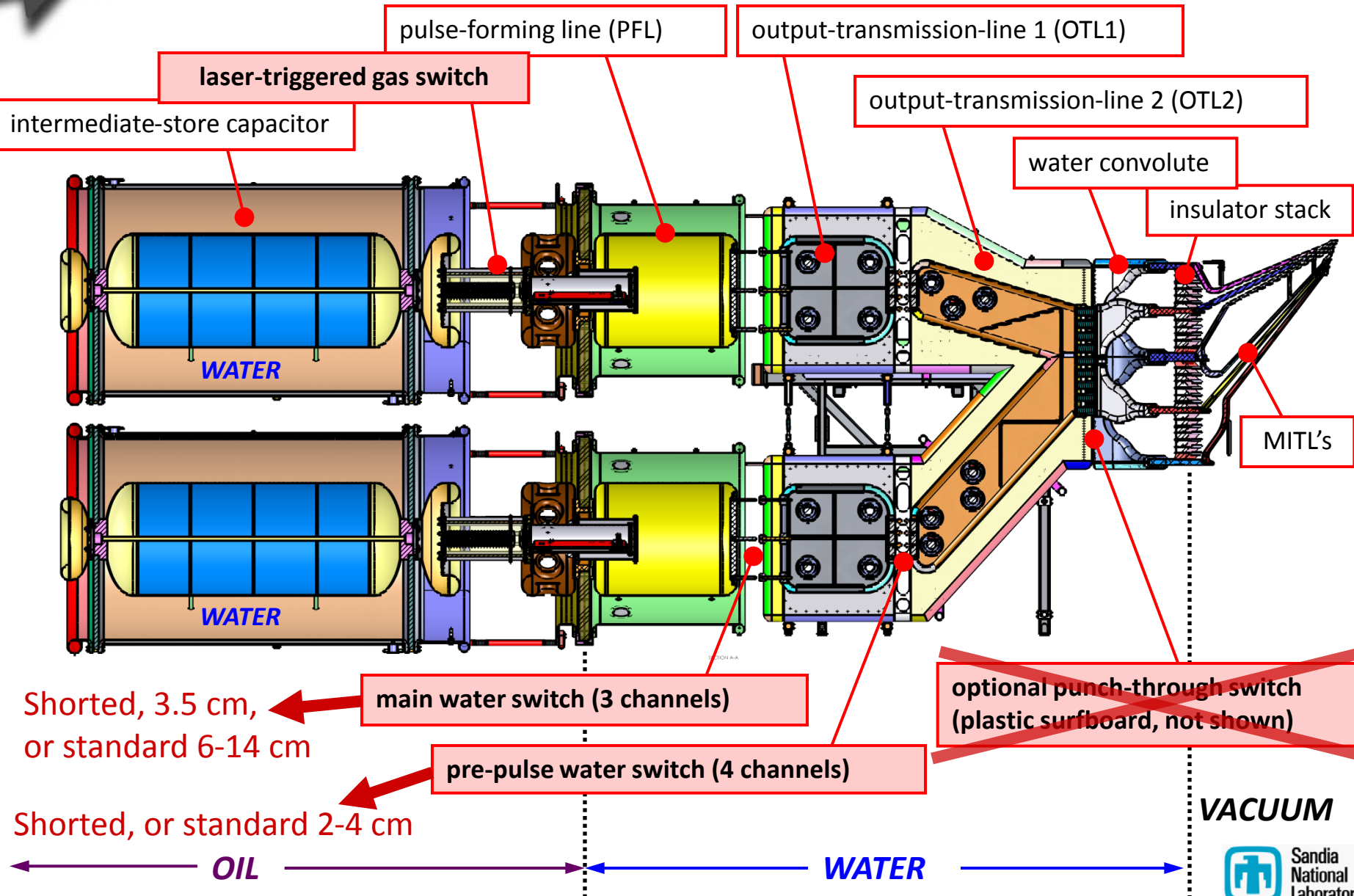
“D-hole” anode opening
decreased to 4-mm
minimum A-K distance



“Radial” feed for
axisymmetric-to-stripline
transition



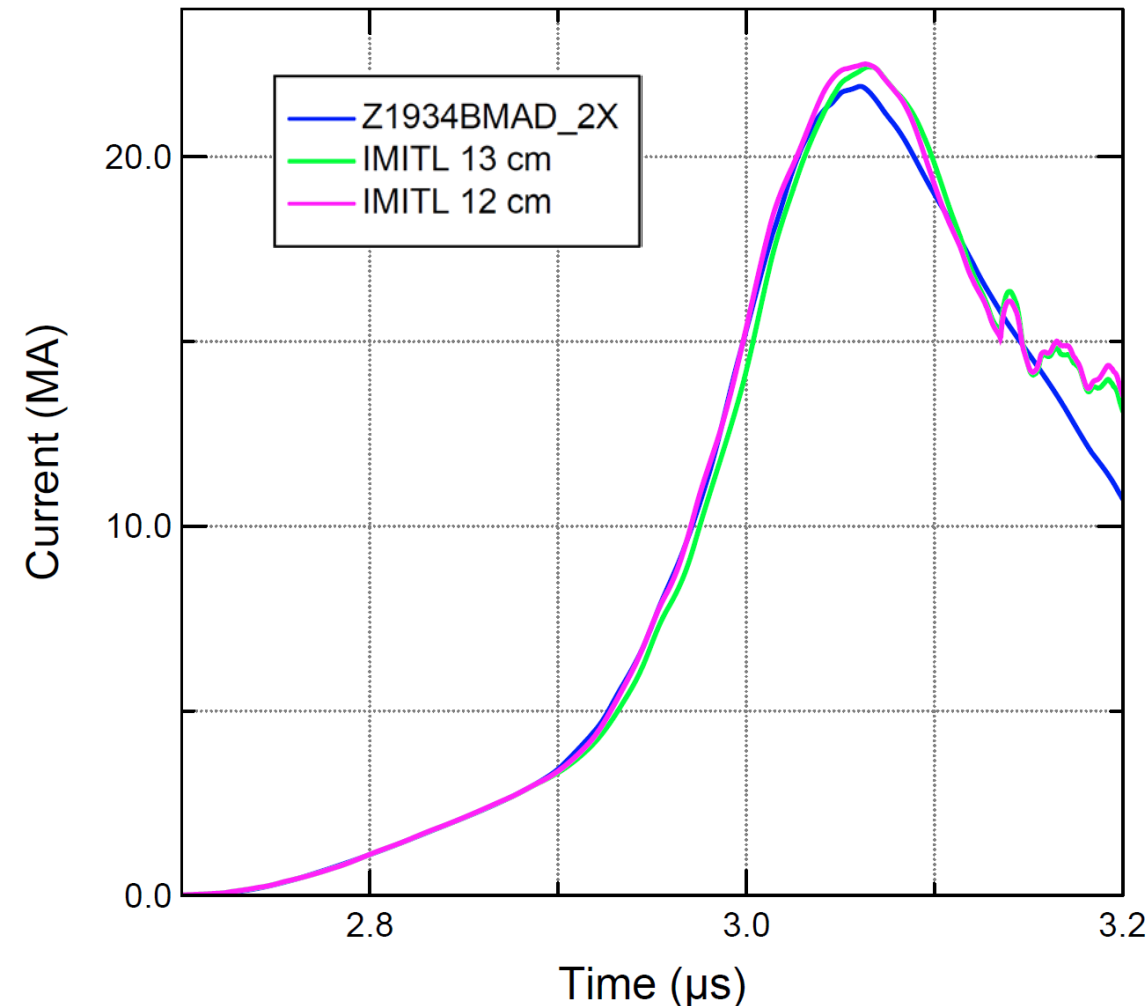
Shaped pulses are obtained by staggering gas-switch times and modifying water switches



Recent improvements to the Bertha circuit model of Z have increased accuracy of predictions

Recovers effect of 1-cm change in main water-switch gaps of 30 short-pulse lines!

85-kV standard = 13cm gap
Z1934 at 12cm instead
(standard for 80-kV on Z1933)



- working with L-3 Communications on final version of model
- calibrate pulse-forming section against flat-MITL shots
- will include 2-D transmission-line sections (OTL2, stack and outer MITLs)

Inverse Lagrangian analysis of velocity from two samples gives quasi-isentropic stress-density response



VISAR

thick sample

electrode

A-K gap

electrode

thin sample

VISAR

Inverse Lagrangian analysis of velocity from two samples gives quasi-isentropic stress-density response

VISAR

thick sample

electrode

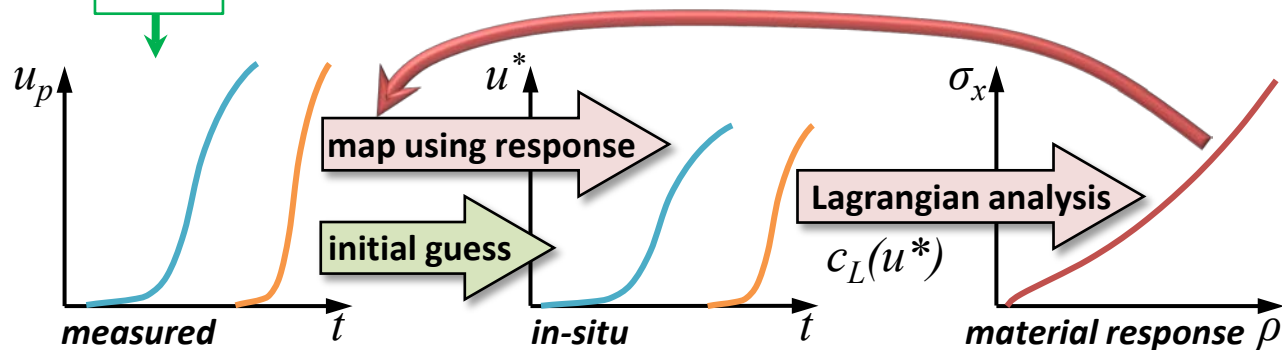
A-K gap

electrode

thin sample

VISAR

1. measure velocity at back faces of two different-thickness samples
2. make initial guess of in-situ $u^*(t)$ at each measurement location
3. determine material response by Lagrangian analysis of in-situ $u^*(t)$
4. use material response to map measured $u_p(t)$ to in-situ $u^*(t)$
5. repeat steps 3-4 until material response converges



- assumes isentropic, simple-wave behavior
- **valid ONLY while electrode/sample interface states identical**

Inverse Lagrangian analysis of velocity from two samples gives quasi-isentropic stress-density response

VISAR

thick sample

electrode

A-K gap

electrode

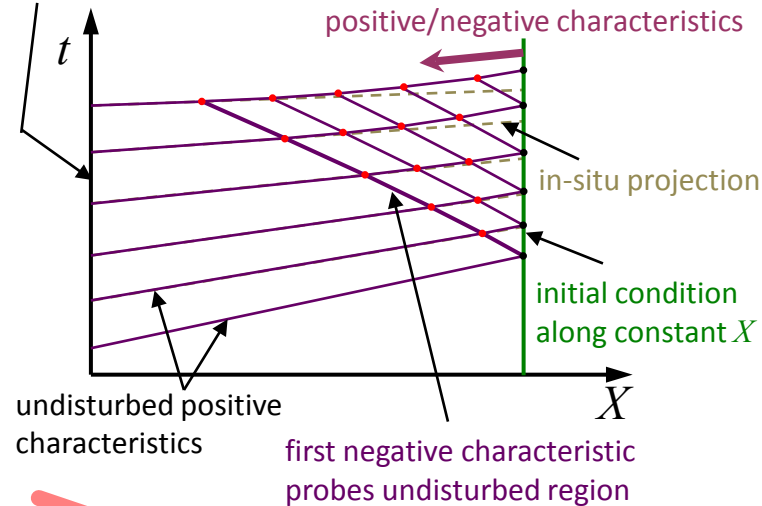
thin sample

VISAR

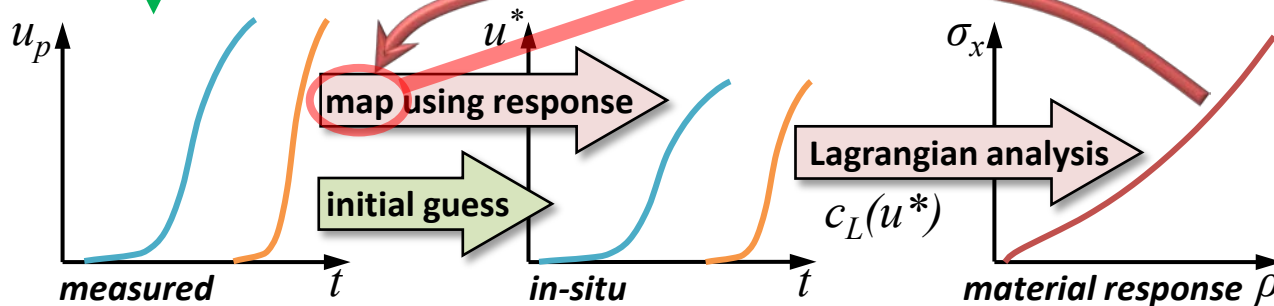
1. measure velocity at back faces of two different-thickness samples
2. make initial guess of in-situ $u^*(t)$ at each measurement location
3. determine material response by Lagrangian analysis of in-situ $u^*(t)$
4. use material response to map measured $u_p(t)$ to in-situ $u^*(t)$
5. repeat steps 3-4 until material response converges

electrode/sample interface
(unknown state)


find intersections between
positive/negative characteristics



- use Riemann invariants to solve intersections between
 1. negative characteristics projected forward in time
 2. positive characteristics projected backward in time
- project points on 1st negative characteristic forward to measurement position

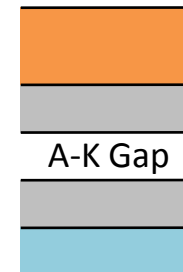


- assumes isentropic, simple-wave behavior
- **valid ONLY while electrode/sample interface states identical**



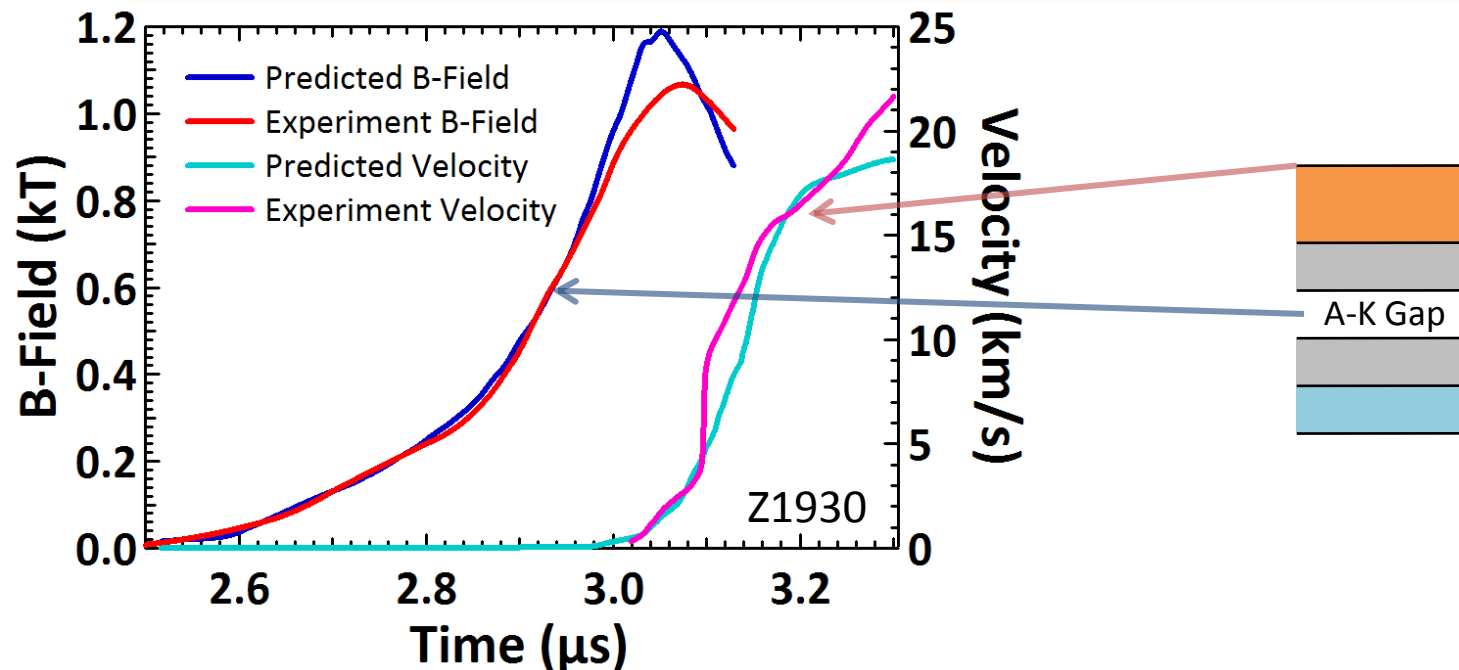
Two-sample approach is limited in accuracy and maximum stress by pulse shape and reverberation

- uncertainty in $c_L = \Delta X / \Delta t$ depends on relative uncertainty in thickness difference
 - must maximize difference in thickness between samples



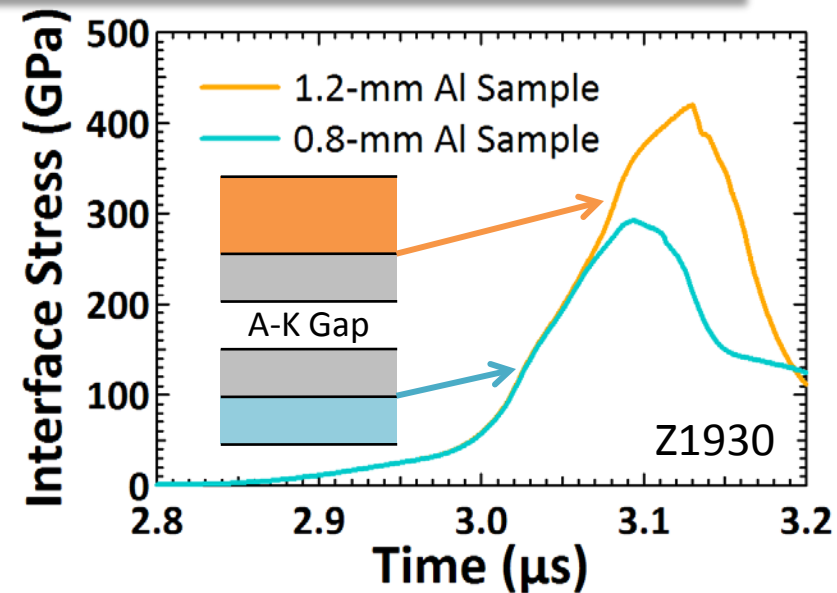
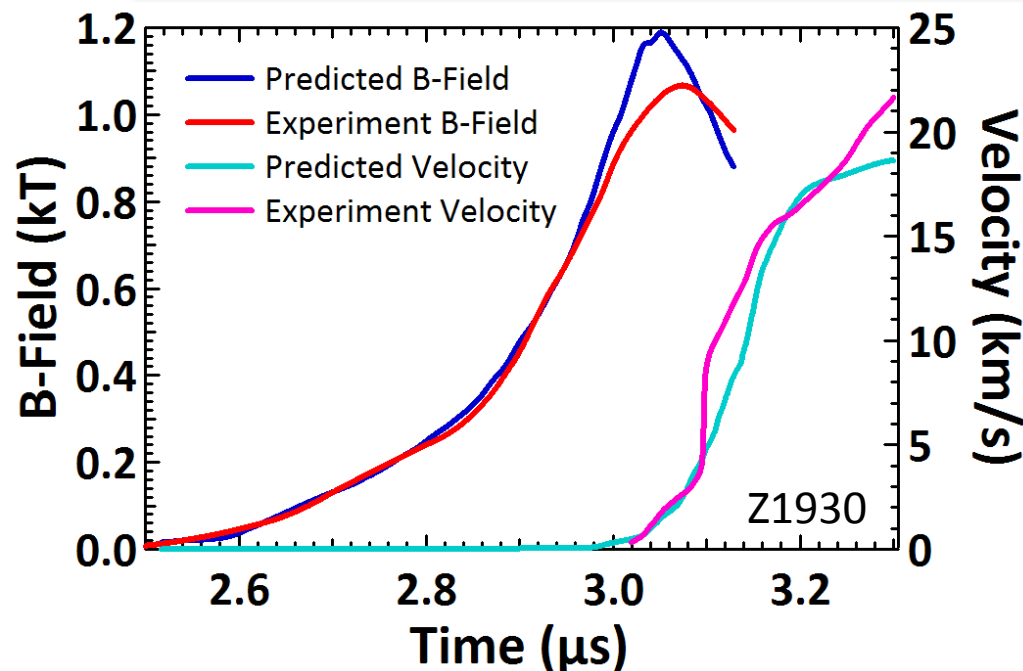
Two-sample approach is limited in accuracy and maximum stress by pulse shape and reverberation

- uncertainty in $c_L = \Delta X / \Delta t$ depends on relative uncertainty in thickness difference
 - must maximize difference in thickness between samples
- requirement for 1-D shock-free loading limits **maximum thickness**
 - imprecision in pulse shaping makes ideal shock-up distance difficult to attain



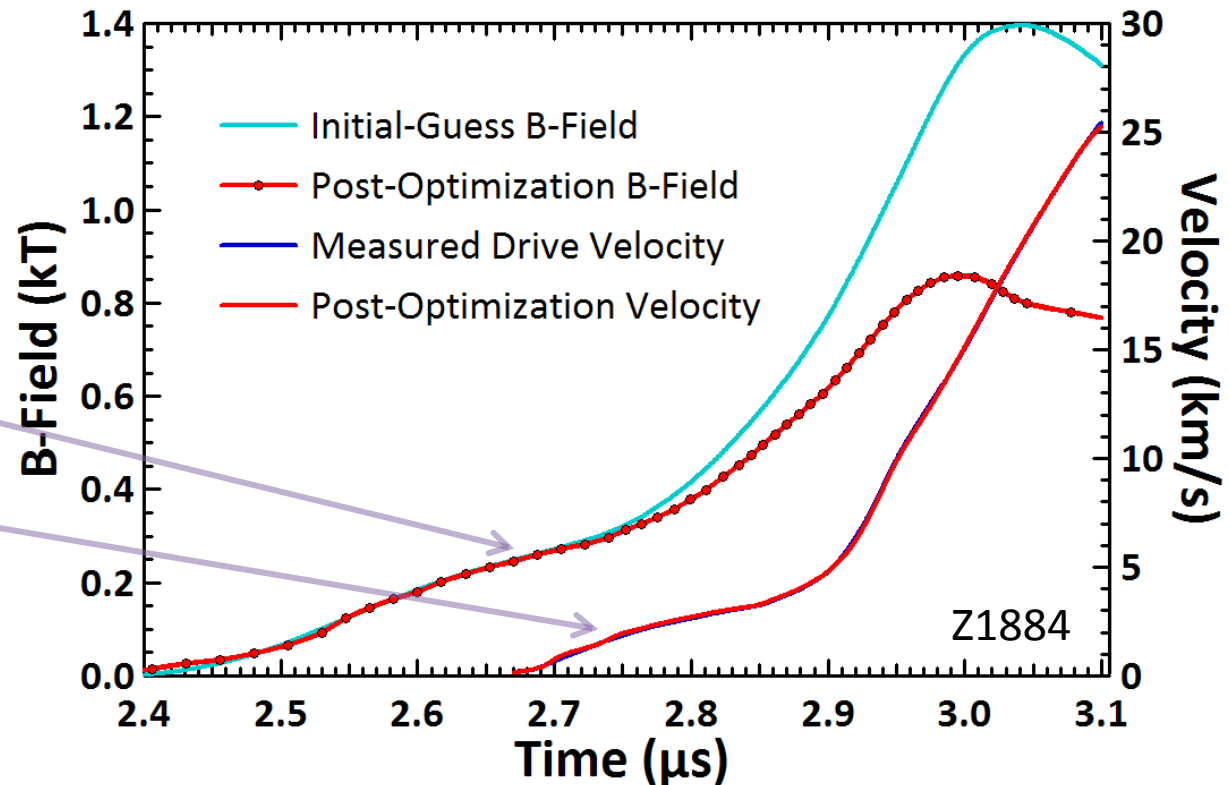
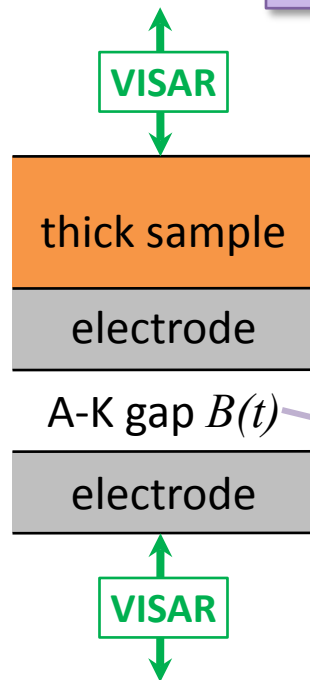
Two-sample approach is limited in accuracy and maximum stress by pulse shape and reverberation

- uncertainty in $c_L = \Delta X / \Delta t$ depends on relative uncertainty in thickness difference
 - must maximize difference in thickness between samples
- requirement for 1-D shock-free loading limits **maximum thickness**
 - imprecision in pulse shaping makes ideal shock-up distance difficult to attain
- arrival of back-surface reflection at sample's front surface (reverberation) limits **minimum thickness** to achieve desired stress state
- increasing rise time to delay shock formation in thick sample reduces peak stress at front surface of thin sample



Optimization technique determines magnetic-field history in A-K gap from electrode “drive” measurement

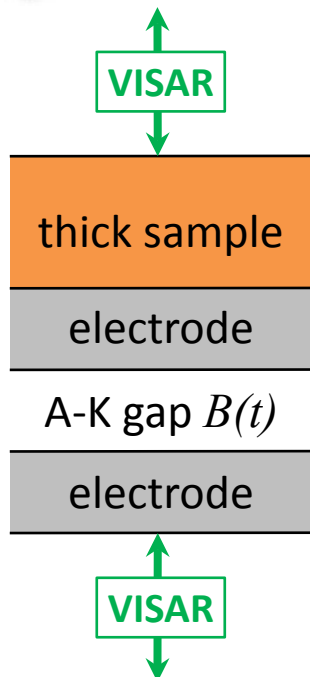
- Dakota optimization framework drives Alegra 1-D MHD simulations
- $B(t)$ represented by constrained cubic spline (25-50 points) with time shift and stretch factors
- objective function is metric of isometry between simulated and experimental velocity history at electrode back surface



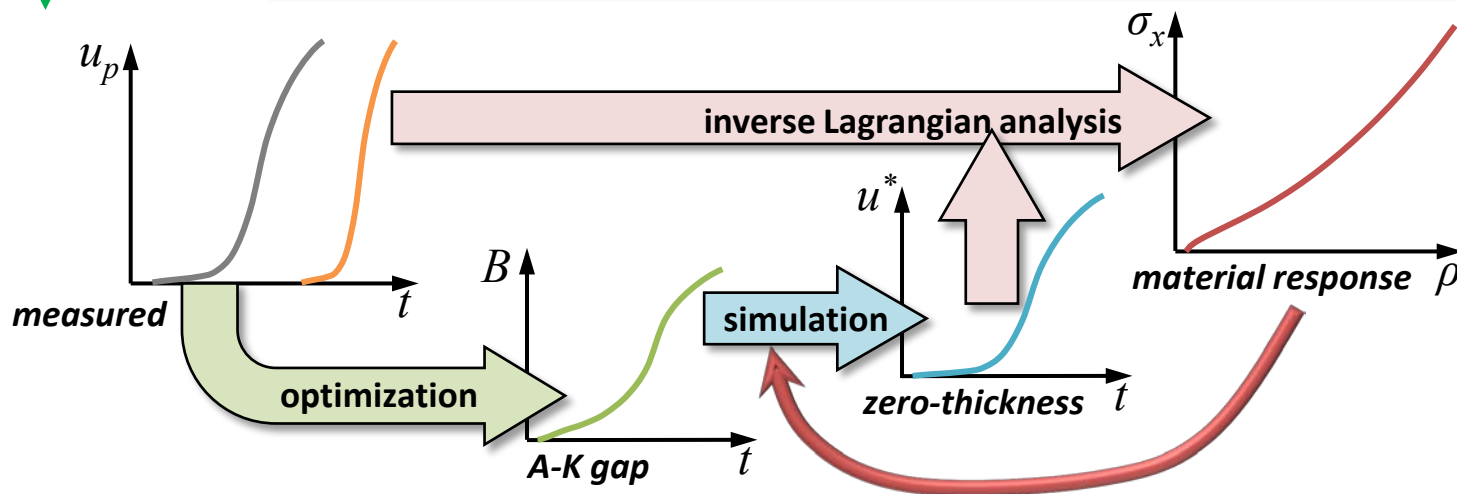
MHD simulations:

- high confidence in aluminum EOS and conductivity models
- high spatial resolution (2.5- μ m cells)

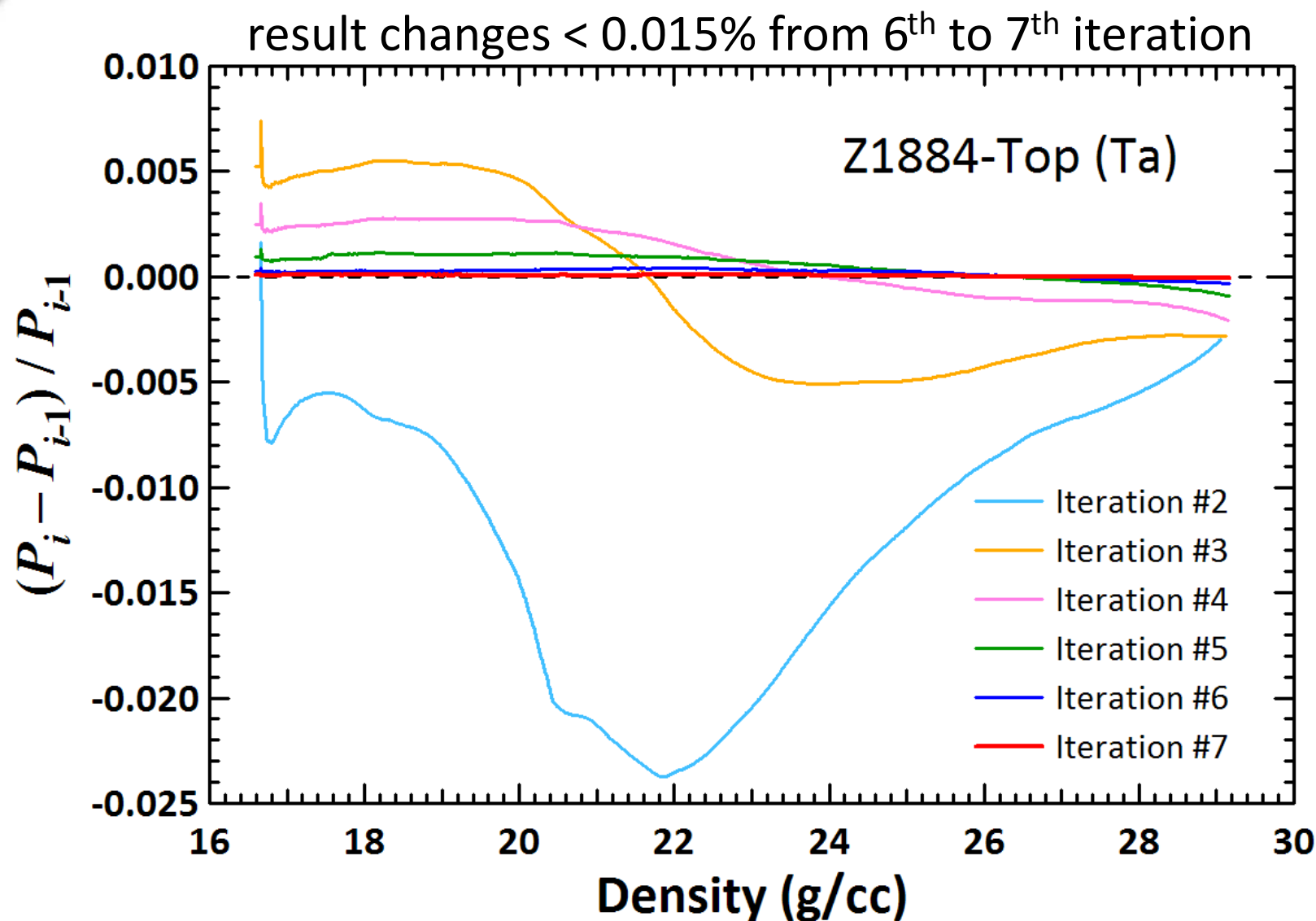
Single sample yields quasi-isentrope by iterating inverse Lagrangian analysis with simulated “zero-thickness” velocity



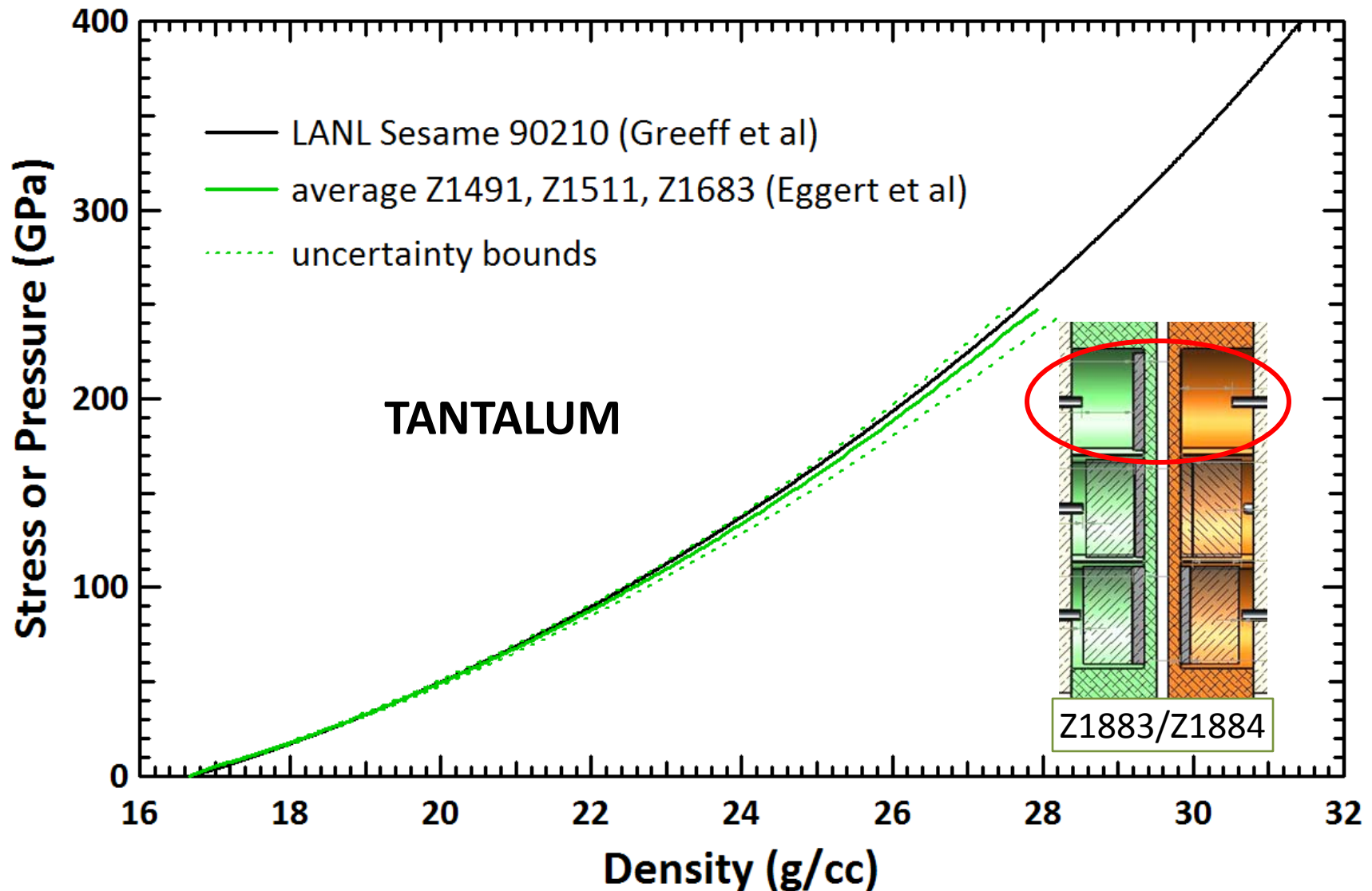
1. measure velocity at back faces of sample and opposite electrode
2. use optimization to determine $B(t)$ from electrode measurement
3. use $B(t)$ and first-guess sample EOS (Sesame table + strength) to simulate electrode/sample interface “zero-thickness” velocity
4. perform inverse Lagrangian analysis on simulated “zero-thickness” velocity and measured back-face velocity of sample
5. convert resulting $\sigma_x(\rho)$ curve to full tabular EOS by assuming constant c_V and Γ/V , equating stress to pressure (strength folded into EOS)
6. use $B(t)$ and new tabular EOS to simulate electrode/sample interface
7. repeat steps 4-6 until material response converges



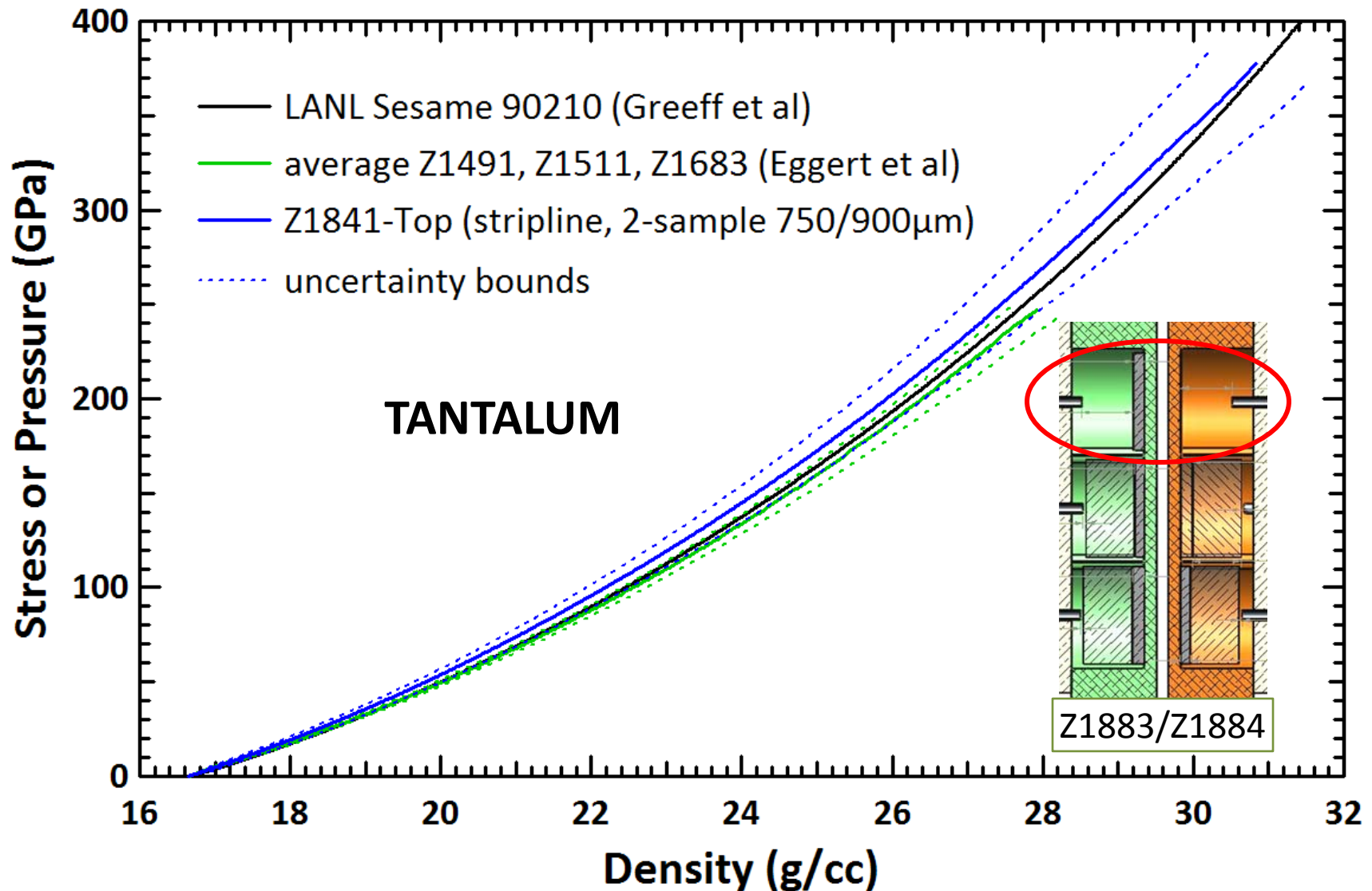
Outer loop of single-sample approach converges



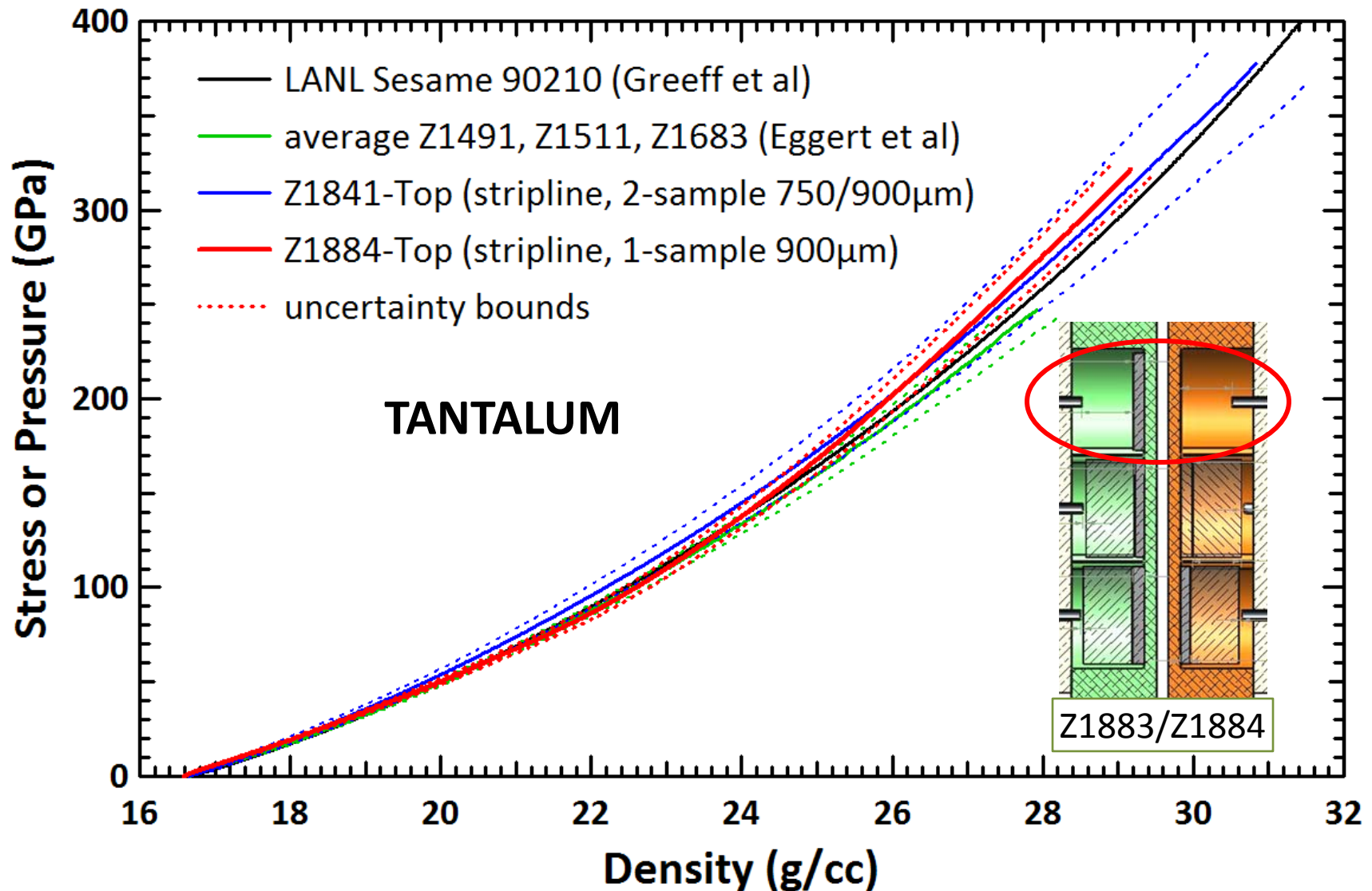
Single-sample measurement of tantalum to 320 GPa decreases uncertainty over two-sample measurement



Single-sample measurement of tantalum to 320 GPa decreases uncertainty over two-sample measurement

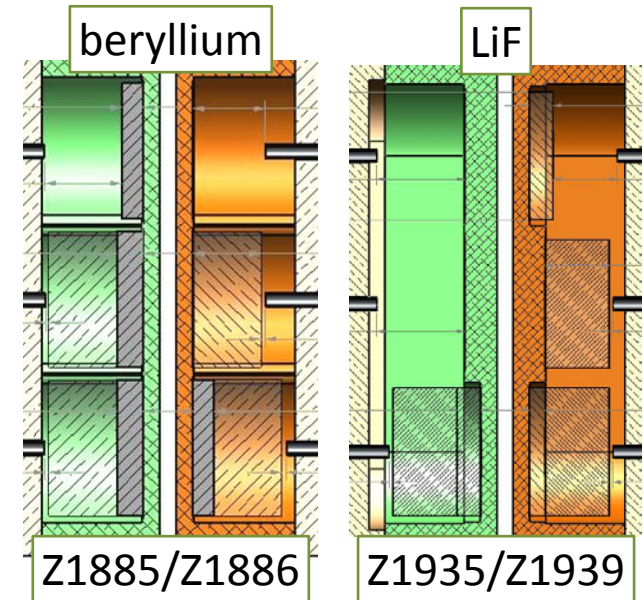


Single-sample measurement of tantalum to 320 GPa decreases uncertainty over two-sample measurement



Further work is planned to fully establish a capability for multi-megabar ramp compression measurements

- Analyze additional single-sample and two-sample data sets on Ta, Be, LiF, Al, Cu, and Au
- Use independently measured strength to correct quasi-isentrope to isentrope
- Extract LiF index-of-refraction window correction
- Quantify sensitivity of results to
 1. aluminum EOS used for B-field optimization
 2. LiF EOS used for windowed samples
 3. B-field gradients across sample diameter



- The stripline load with the single-sample analysis approach has the **potential** to measure quasi-isentropic loading paths to multi-megabar pressures with uncertainties of $\sim 1\%$ in density and $\sim 3\%$ in stress
- Recent design and pulse-shaping improvements suggest measurements to > 5 Mbar are possible on high-Z materials at full machine charge voltage

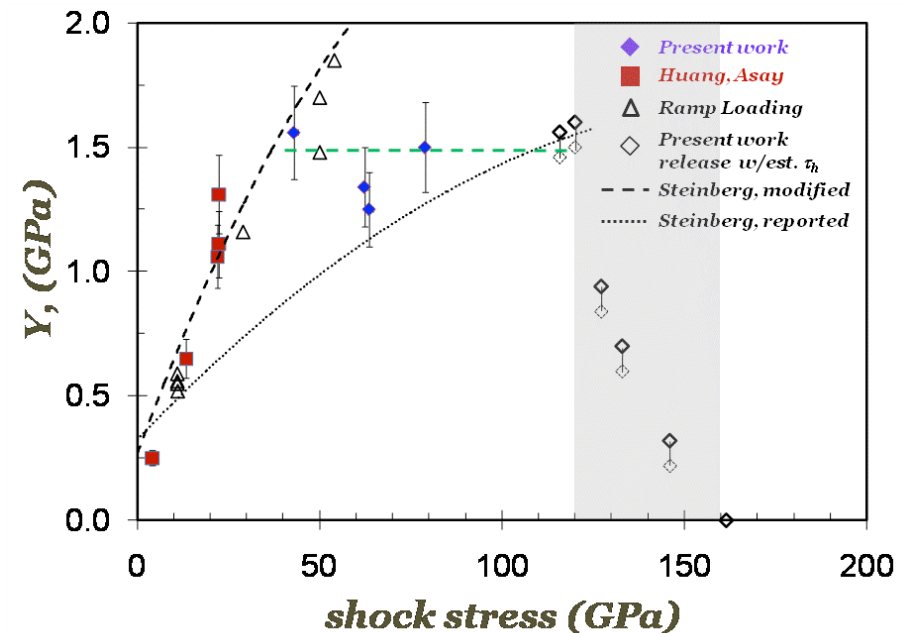


New Strength Data on Aluminum to 160 GPa

C.S. Alexander, W.D. Reinhart,
J.R. Asay, C. Hall

Sandia National Laboratories
Albuquerque, NM

JOWOG 32 Mat
January 25-29, 2010
Livermore, CA



SAND 2010-1616C
Approved for Unlimited Release



Sandia is a multiprogram laboratory operated by Sandia Corporation, a Lockheed Martin Company, for the United States Department of Energy's National Nuclear Security Administration under contract DE-AC04-94AL85000.





Summary of results

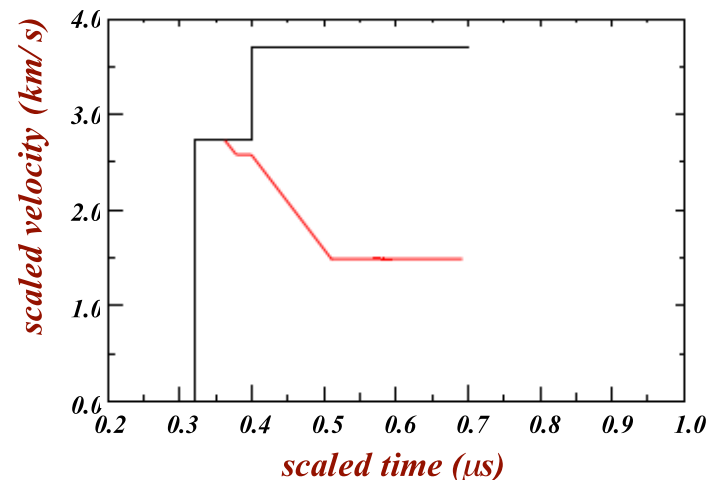
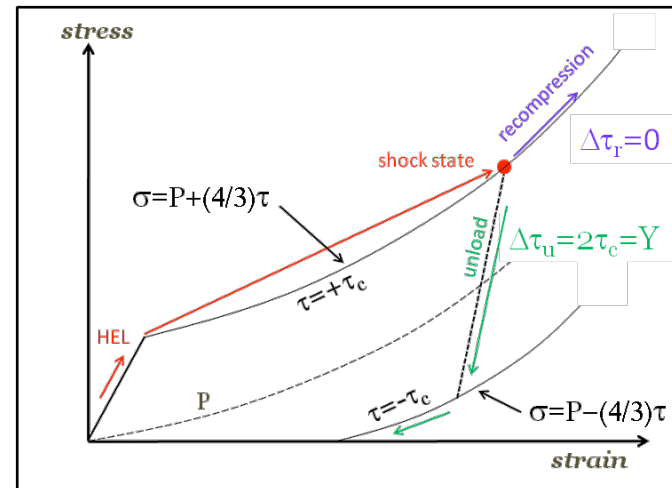
- The shock state of Al does not lie on the yield surface and becomes nearly hydrostatic for shocks exceeding ~ 40 GPa
- There are transitions in Al strength at ~ 40 GPa and at the onset of melting (~ 120 GPa)
- There is a strong alloy dependence of Al strength above ~ 40 GPa

Impact: Existing strength models for Al under predict the strength by nearly a factor of two.



Elastic-plastic theory assumes shock states lie on the upper yield surface

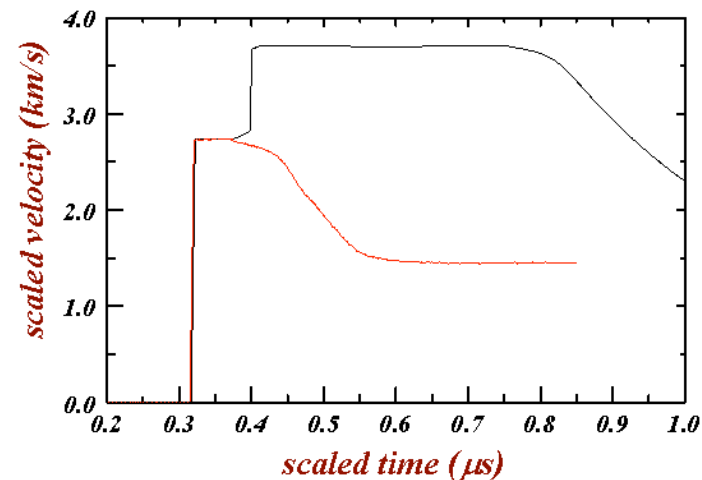
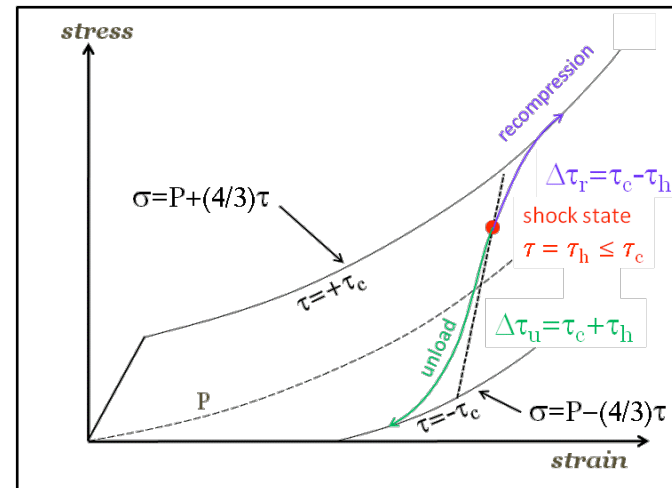
- According to elastic-plastic theory for uniaxial strain:
 - On shock loading, the material first loads elastically to the HEL
 - Shock states lie on a yield surface $\tau = +\tau_c$
 - On release, the material unloads elastically to a yield surface $\tau = -\tau_c$
 - Elastic portion of the release gives $\Delta\tau_u = 2\tau_c = Y$
 - **Key assumption is that the shock state lies on the upper yield surface**
 - $\Delta\tau_r = 0$ on reload
 - » inconsistent with experimental data showing quasi-elastic compression on reloading





Measured strength can be off by up to a factor of two if E-P assumption is invalid

- If the shock state is NOT on the upper yield surface:
 - Evidence suggests that the shock states lie at $\tau = +\tau_H (\leq \tau_c)$
 - On release, the material unloads elastically to a yield surface $\tau = -\tau_c$
 - Elastic portion of the release gives $\Delta\tau_u = \tau_c + \tau_H \leq Y$
 - In order to determine Y must measure both τ_c and τ_H
 - Requires both reload and release data: $Y = 2\tau_c = \Delta\tau_u + \Delta\tau_r$
 - **Measuring release only can lead to errors up to a factor of 2**

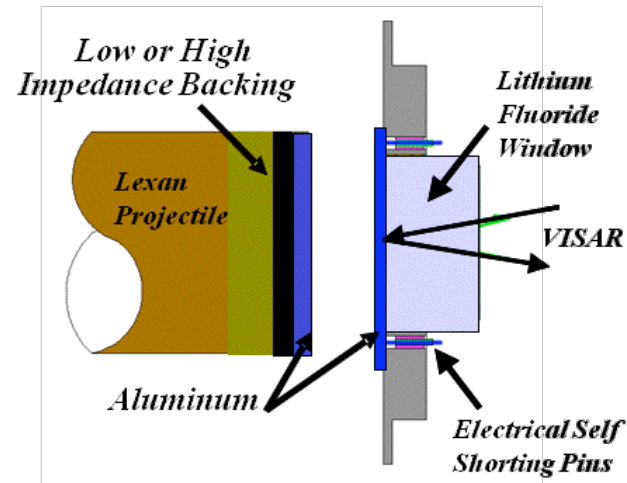




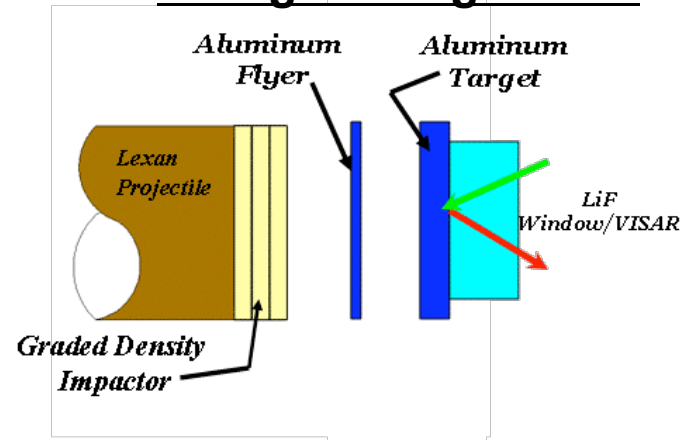
Experimental techniques used for unloading and reloading experiments to 160 GPa

- **Symmetric impact conditions**
 - 3-10 km/s impact velocity
 - Low impedance backing material or free surface generate release
 - High impedance backing generates reload
- **VISAR diagnostics**
 - High sensitivity (0.047 – 1.79 km/s/fr) used to resolve QE recompression
 - Particle velocity uncertainty of 0.1 – 1.0%
- **Previous difficulties**
 - Separation of impactor and backing material compromises reloading data

2-stage configuration



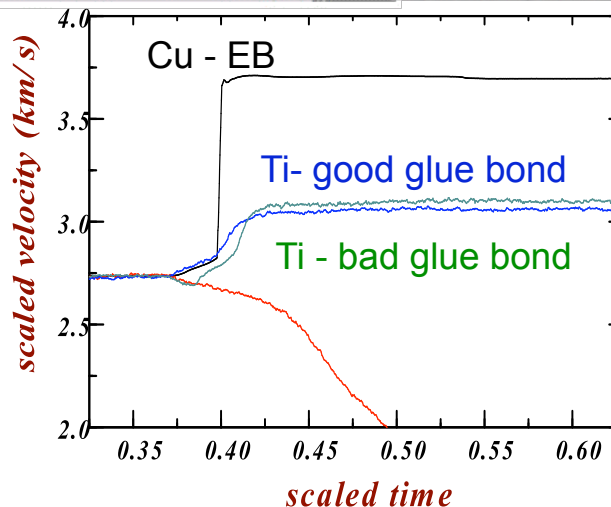
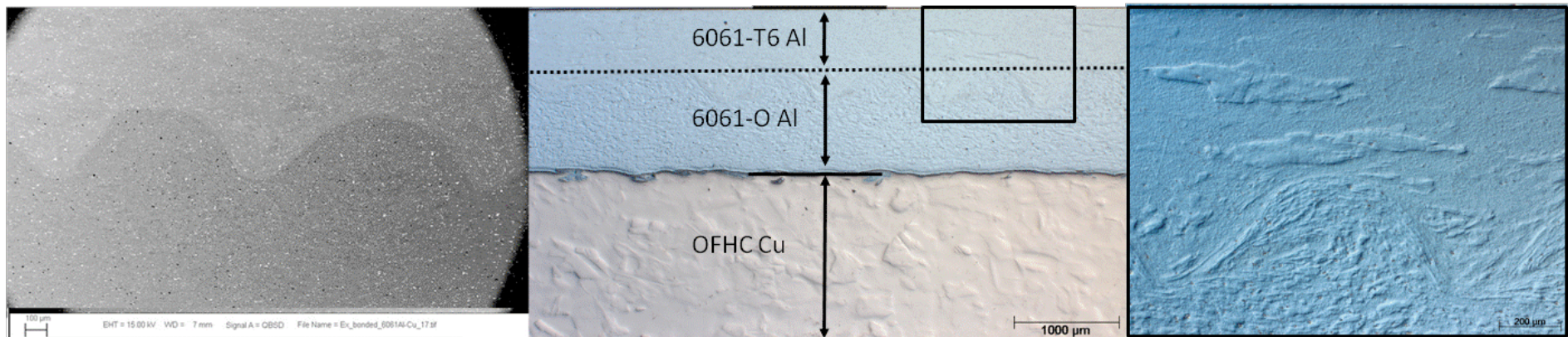
3-stage configuration





Explosively bonded (EB) impactors improve performance over epoxy bonds

- EB Cu backed Al used as impactors in the reload configuration
- No evidence of bond separation as observed previously with epoxy bonding

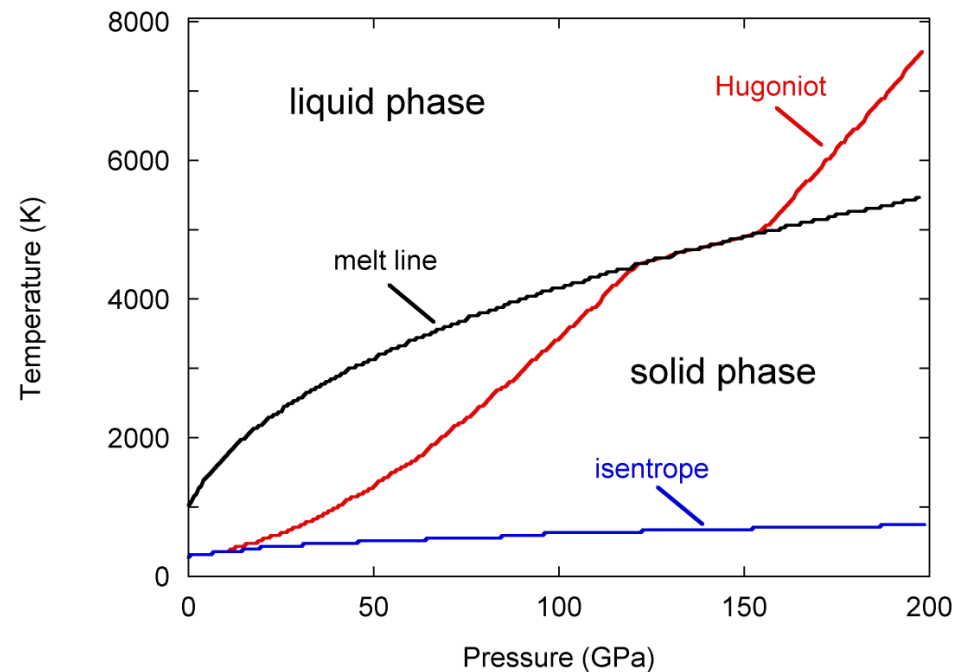


- Material supplied to SNL by B. Jensen (LANL)
- Material fabricated by High Energy Metals, Inc. (Sequim, WA)



Shock loaded aluminum has a mixed phase region between 120-160 GPa

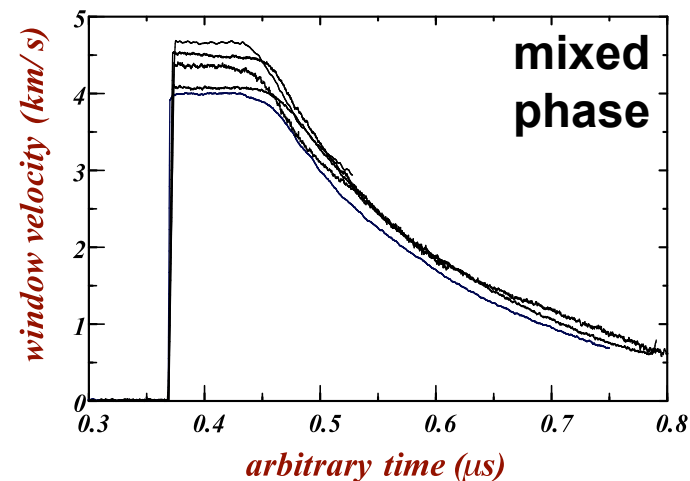
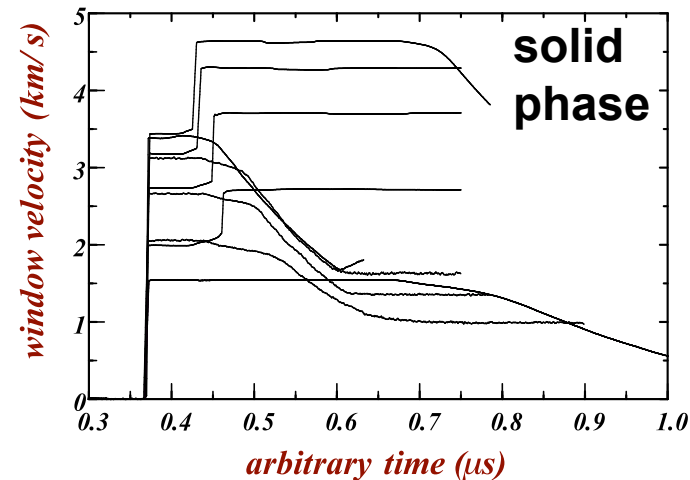
- Material strength in shock induced solid-liquid coexistence regions has not been studied
- Solid-liquid coexistence is expected to influence strength
- Phase boundaries have some uncertainty (~ 5 GPa) depending on theoretical approach used





QE response observed in both unloading and reloading data

- Two-stage shots
 - Unload/reload pairs performed at nearly identical shock conditions
 - QE release (reload) portion of profile provides $\Delta\tau_u$ ($\Delta\tau_r$)
- Three-stage shots
 - Reload has not yet been performed in the three-stage configuration
 - However, release only at high pressures (115 – 161 GPa) provides a good estimate of strength as will be shown





$\Delta\tau$ is determined for unloading (reloading) from the QE portion of each wave profile

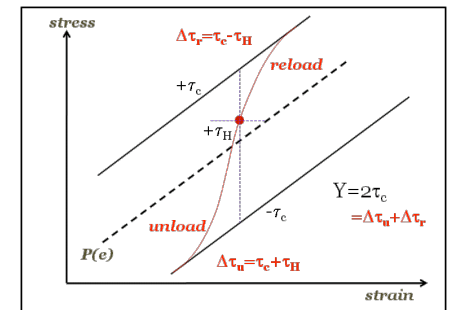
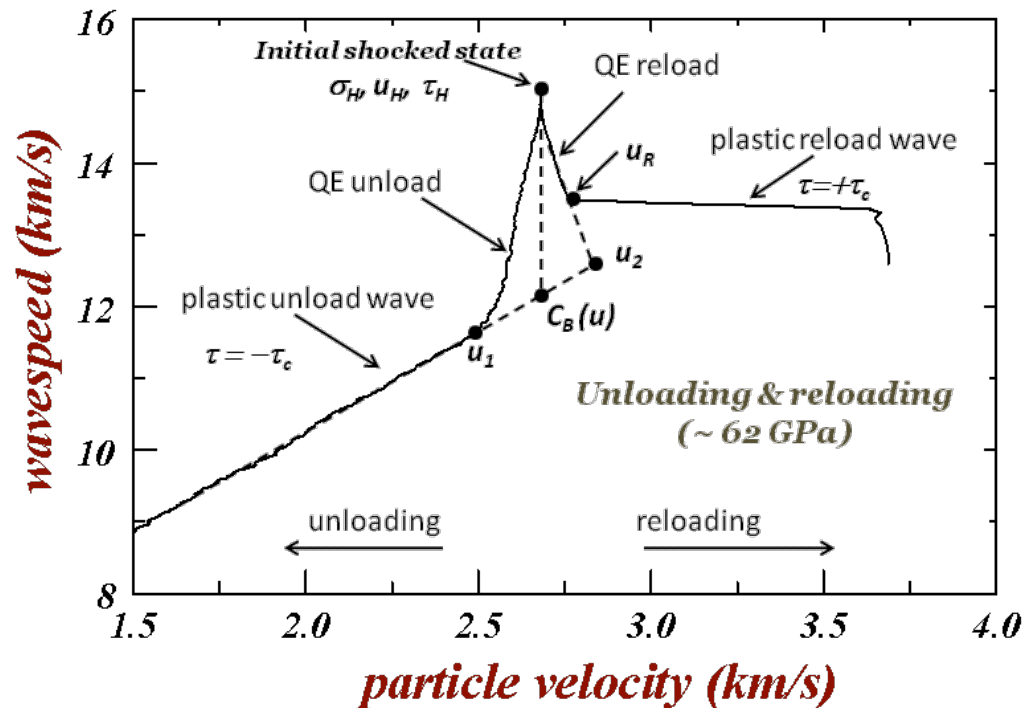
- Wave speed is calculated from the recorded VISAR profiles
- The resolved shear stress is given by

$$d\tau = \frac{3}{4} \rho_0 (c^2 - c_B^2) du$$

- Integrating with respect to u gives:

unload: $\Delta\tau_u = \tau_c + \tau_H = -\frac{3}{4} \rho_0 \int_{u_1}^{u_H} (c^2 - c_B^2) \frac{du}{c_L}$

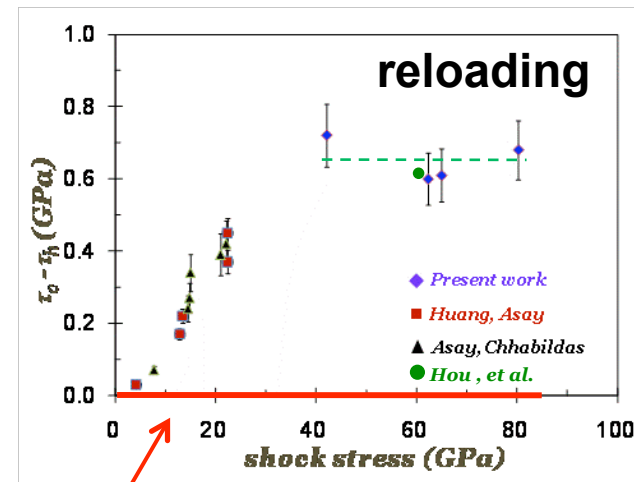
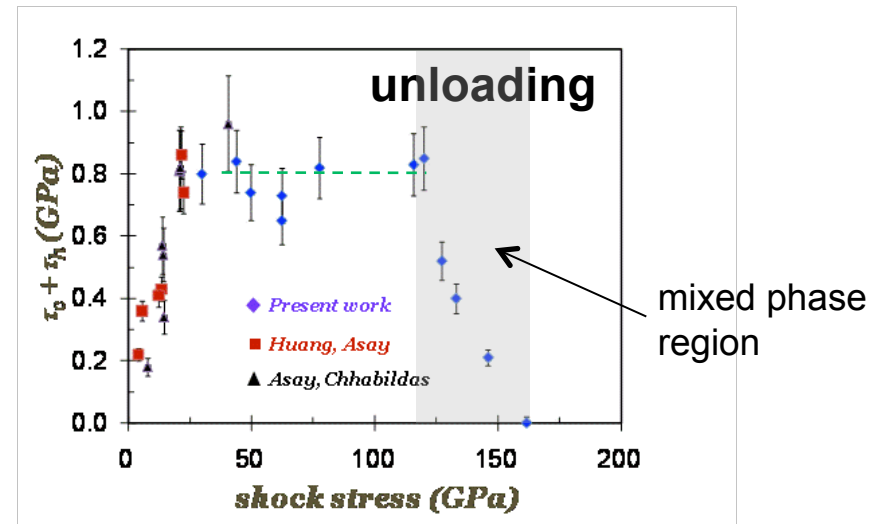
reload: $\Delta\tau_r = \tau_c - \tau_H = \frac{3}{4} \rho_0 \int_{u_H}^{u_2} (c^2 - c_B^2) \frac{du}{c_L}$





Measured $\Delta\tau$ shows a complex response above 40 GPa

- Data is plotted with previous lower stress data
 - Data agree in overlap region (<40 GPa)
 - Essentially constant values seen between 40 GPa and onset of melt (~120 GPa)
 - Steady decline of $\Delta\tau_u$ in the mixed phase region
- Reloading data is not consistent with EP response
- Taking sum and difference gives τ_c and τ_h

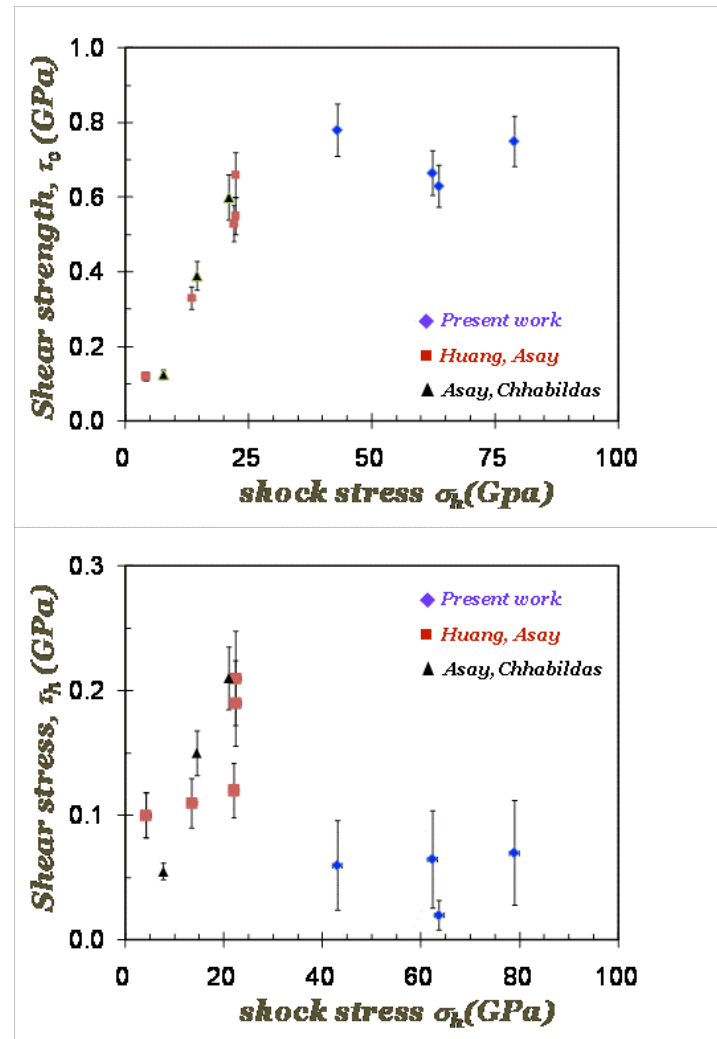


EP response
($\tau_h = \tau_c$)



$\tau_h \neq \tau_c$ indicates failure of EP assumption

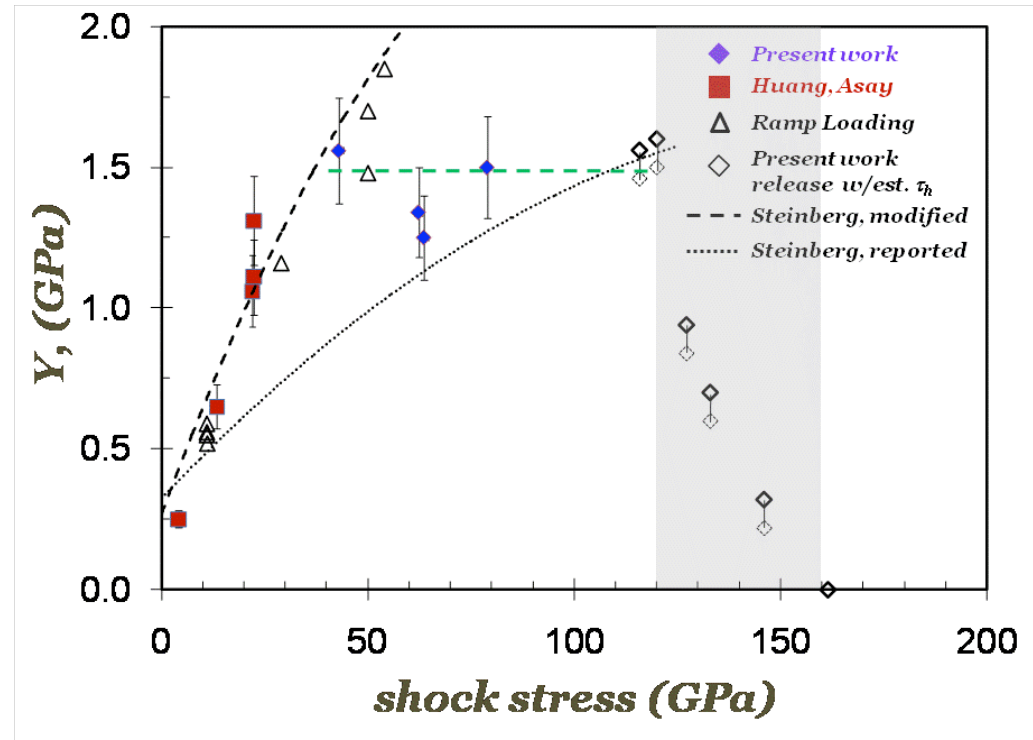
- Clearly the shock state is not on the upper yield surface ($\tau_h = \tau_c$)
- Strength ($Y=2\tau_c$) shows plateau above 40 GPa
- Corresponds to a collapse in τ_h toward the hydrostat
 - Note that while ~75% reduced from the peak value, $\tau_h > 0$
 - τ_h is expected to decay to zero in mixed phase region
 - » Small error in approximating $\Delta\tau_u = \tau_c + \tau_h \approx \tau_c$
 - » Allows release data to approximate strength in the mixed phase region
 - » Different than EP assumption where $\Delta\tau_u = 2\tau_c$





By measuring both τ_c and τ_h strength is determined without the EP assumption

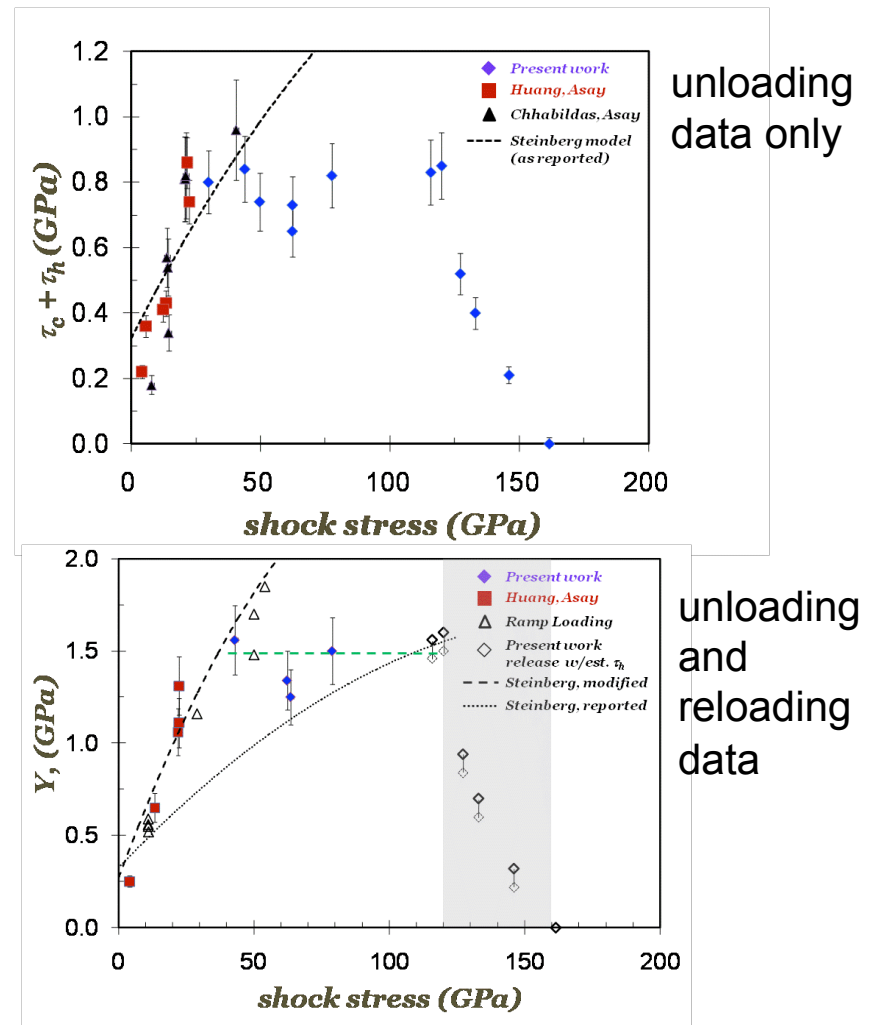
- When reloading data are considered, τ_c and τ_h are determined
- Strength, $Y = 2(\tau_c) \geq (\tau_c + \tau_h)$
- Resulting strength data are not well fit by the reported Steinberg model
- A modified model reported by Huang and Asay is a good fit to 40 GPa
- No strength models predict plateau





Discrepancies in the data have serious implications to existing strength models

- Steinberg model (and others) often based on unloading wave profile data $Y=(\tau_c+\tau_h)$
- Results presented here show that the EP assumptions are invalid in Al (for $\sigma > 40$ GPa)
 - Reloading data must be considered $Y=2(\tau_c)$
- Existing strength models may be off by as much as a factor of two
- New experimental data are required to correct or verify existing models





Strength of aluminum was measured using both reloading and release experiments

- Utilizing reloading and release data, the shear components τ_c and τ_h were measured
- EP assumption that the shock state lies on the upper yield surface shown to be false for aluminum
- Measured strength is almost two times larger than estimates using release data only
- Existing strength models based on release data alone need to be revisited
- Initial properties of aluminum appear to influence high pressure response
 - Accounting for Y_0 insufficient to explain high pressure variation

